

Multi-Carrier CDMA Mobile Radio Systems - Analysis and Optimization of Detection, Decoding, and Channel Estimation*

Stefan Kaiser

Munich, Germany

January 1998

*Ph.D. thesis published with: VDI-Verlag, Dusseldorf, Germany, 1998, ISBN 3-18-353110-0

Address:

Dr. Stefan Kaiser
German Aerospace Center (DLR)
Institute of Communications and Navigation
D-82234 Oberpfaffenhofen
Germany

Tel.: +49 8153 28-2805
Fax: +49 8153 28-1442
E-mail: Stefan.Kaiser@dlr.de
<http://www.dlr.de/KN/KN-S/Kaiser>

Vorwort

Die vorliegende Arbeit entstand während meiner Tätigkeit als wissenschaftlicher Mitarbeiter am Institut für Nachrichtentechnik des Deutschen Zentrums für Luft- und Raumfahrt (DLR) in Oberpfaffenhofen.

Mein besonderer Dank gilt Herrn Prof. Dr.-Ing. P.W. Baier, der diese Arbeit betreut hat und mir den Freiraum für ein kreatives Forschen gewährte. Ich danke ferner Herrn Prof. Dr.-Ing. W. Rupprecht für das Interesse an dieser Arbeit und die Übernahme des Korreferats. Ebenso danke ich dem Vorsitzenden der Promotionskommission, Herrn Prof. Dr.-Ing. R. Zengerle.

An dieser Stelle bedanke ich mich ganz besonders bei meinen Freunden und Kollegen des Instituts für Nachrichtentechnik des DLR für die sehr angenehme Arbeitsatmosphäre und für die in unzähligen Diskussionen gewonnenen Anregungen und Erkenntnisse. Insbesondere bedanke ich mich bei Herrn Dr.-Ing. U.-C. Fiebig für die nachhaltige Unterstützung und Förderung dieser Arbeit und bei Herrn Dr. K. Fazel für die Anregung, dieses interessante Thema anzugehen, und seine stete Diskussionsbereitschaft.

Schließlich danke ich in besonderer Weise meinen Eltern, die mir das Studium der Elektrotechnik ermöglicht und mich immer nach besten Kräften unterstützt haben, sowie meiner Lebensgefährtin Susanna für ihre stete Unterstützung. Ihnen sei diese Arbeit gewidmet.

München, im Januar 1998

Stefan Kaiser

Contents

1	Introduction	1
1.1	Progress in Wireless Communications	1
1.2	Multi-Carrier CDMA for Mobile Communications	4
1.2.1	Principles of DS Spread Spectrum and Multi-Carrier Modulation	4
1.2.2	CDMA Concepts with Multi-Carrier Modulation	6
1.2.3	State of the Art in the Field of MC-CDMA	10
1.3	Goals of the Thesis	13
1.4	Contents and Important Results	14
2	Mobile Radio Channel	16
2.1	Time-Variant Multipath Propagation	16
2.2	Channel Models for Macro-, Micro-, and Picocells	22
2.2.1	CODIT and COST 207 Channel Models	22
2.2.2	Uncorrelated Fading Channel Model for Multi-Carrier Systems	29
3	Multiple Access Scheme MC-CDMA	31
3.1	Multi-Carrier Communications	31
3.1.1	Orthogonal Frequency Division Multiplexing	31
3.1.2	Principle of MC-FDMA, MC-TDMA, and MC-CDMA	38
3.2	MC-CDMA Signal Structure	38
3.3	MC-CDMA Data Detection Techniques	46
3.3.1	Introduction	46
3.3.2	Single-User Detection	49
3.3.3	Interference Cancellation	53
3.3.4	Joint Detection with Maximum Likelihood Criterion	54
3.4	Performance of Uncoded MC-CDMA Systems	56
3.5	Equivalence between MC-CDMA and DS-CDMA	62

4	MC-CDMA with Channel Coding	64
4.1	Introduction	64
4.2	Soft Decision Decoding in MC-CDMA Systems	66
4.2.1	Log-Likelihood Ratio	66
4.2.2	LLR for MC-CDMA Systems with SD	68
4.2.3	LLRs for MC-CDMA Systems with MLSSE and MLSE	71
4.3	Iterative Decoding with Soft Interference Cancellation	71
4.4	Iterative Decoding of Turbo-Codes	74
4.5	Performance of MC-CDMA Systems with Channel Coding	75
4.6	Trade-off between Channel Coding and Spreading	81
5	Channel Estimation for Multi-Carrier Systems	87
5.1	Pilot Symbol Aided Channel Estimation in Two Dimensions	87
5.2	Theory of Two-Dimensional Wiener Filtering	89
5.3	Performance Analysis with Model Mismatch	91
5.3.1	Two-Dimensional FIR Filter	91
5.3.2	Two Cascaded One-Dimensional FIR Filters	92
5.4	Filter Design	94
5.5	Pilot Symbol Grid	95
5.6	Mean Square Error Performance	96
6	MC-CDMA System Evaluation	106
6.1	System Design	106
6.2	Simulation Results	109
6.3	Discussion of the Simulation Results	115
7	Abstract	119
	Kurzfassung (German Summary)	120
A	Analytical Performance Evaluation	126
A.1	SD with MMSE Equalization	126
A.2	JD with MLSSE and MLSE	128
B	Multiple Access Scheme SS-MC-MA	130
B.1	SS-MC-MA Signal Structure	130
B.2	Performance	133

Notations **138**

 Symbols 138

 Abbreviations 143

Bibliography **145**

Chapter 1

Introduction

1.1 Progress in Wireless Communications

The history of wireless communications began in 1886 when H. Hertz generated and, thus, proved the existence of J. C. Maxwell's theoretically predicted electromagnetic waves. In the following years G. Marconi demonstrated the potential of wireless communications, as significantly documented by the words delivered before the Royal Institution in 1897 from the Technical Director of the British Post Office, who supported G. Marconi:

"It is curious that hills and apparent obstructions fail to obstruct... Weather seems to have no influence; rain, fogs, snow and wind, avail nothing... The distance to which signals have been sent is remarkable. On Salisbury Plain Mr. Marconi covered a distance of four miles. In the Bristol Channel this has been extended to over eight miles, and we have by no means reached the limit. It is interesting to read the surmises of others. Half a mile was the wildest dream."

In 1901 G. Marconi established a radio connection over the Atlantic for what he was awarded the Nobel Prize in 1909. Following experimental research and development led to one of the first widely used applications of wireless communications, that of radio broadcasting. Using this medium, G. Marconi in 1937, shortly before his death, said in a radiomessage:

"Radio broadcasting, however, despite the great importance reached and the still unexplored fields open to investigation, is not, in my opinion, the most significant application of modern communications, because it is a one way communication only. Greater importance is related, in my opinion, to the possibility offered by radio of exchanging communications anywhere the correspondents are located, in the middle of the ocean, in the ice pack in the pole, in the desert plains or over the clouds in an airplane."

These words should prove to be true and one hundred years after G. Marconi's first experiments, the market of wireless mobile communications with duplex transmission is one of the fastest expanding of the world. The foundation for a widespread commercial deployment of wireless mobile communications was laid with the standardization of the first generation cellular mobile radio systems in the 1980s. Various standards such as the C-450 in Germany, the Total Access Communications System (TACS) in Europe, the Advanced Mobile Phone Service (AMPS) in the USA, and the Nippon Telephone and Telegraph (NTT) system in Japan were developed

world wide [PGH95, Rap96, Stü96]. Characteristic for systems of the first generation are the analog frequency modulation technique and the allocation of different non-overlapping frequency bands for individual connections. The separation of the user signals in the frequency domain is called frequency division multiple access (FDMA) [Pro95, Rap96, Stü96].

Parallel to the progress in wireless communications significant advances in digital communications took place. The origins of digital communications go back to the work of S. Morse in 1837, demonstrating an electrical telegraphy system. The so-called Morse code represents the letters of the alphabet by sequences of dots and dashes and was the precursor of modern variable-length source coding. The beginnings of modern digital communications stem from the work from H. Nyquist in 1924, who derived the maximum signaling rate that can be sent over a channel of a given bandwidth without intersymbol interference (ISI). Based on Nyquist's work, C.E. Shannon presented the fundamental limits of digital communication systems when he derived the channel capacity in 1948. The channel capacity determines the maximum information rate at which error free transmission is theoretically possible through the channel by appropriate coding. In the following years efficient digital signal processing techniques were developed such as source coding for data compression, encryption for security, and channel coding for error protection.

The rapid development in the area of micro electronics with a continuous increase in device density of integrated circuits and the development of low-rate digital speech coding techniques made completely digital second generation cellular mobile radio systems viable [PGH95]. Various second generation cellular systems were developed in the 1990s. Most of these systems employ time division multiple access (TDMA), such as the Global System for Mobile Communications (GSM) and the Digital Cellular System 1800 (DCS1800) in Europe, the Interim Standard (IS-) 54 in the USA, and the Personal Digital Cellular (PDC) system in Japan [PGH95, Rap96, Stü96]. With TDMA, the time axis is subdivided into different non-overlapping time slots where each user is exclusively assigned its time slots in which this user employs the total available bandwidth. Thus, TDMA separates the users in the time domain [Pro95, Rap96, Stü96]. In practice, TDMA is combined with FDMA to reduce the hardware complexity of an otherwise extremely broadband system and to increase the flexibility of the system.

Parallel to the TDMA based second generation standards, the IS-95 was developed in the USA, employing code division multiple access (CDMA) with direct sequence (DS) spectrum spreading, combined with FDMA [PGH95, Rap96, Vit95, Stü96]. The origins of CDMA go back to the beginnings of spread spectrum communications in the first half of the 20st century [Sch82]. Primary applications of spread spectrum communications lay in the development of secure digital communication systems for military use. Since the second half of the 20st century, spread spectrum communications became of great interest also for commercial applications, including mobile multi-user communications. Spread spectrum signals are characterized by their used bandwidth, which is much greater than the minimum necessary bandwidth for data transmission [Dix94, BGP84]. The spectrum spreading is achieved by using a spreading code that is

independent of the message and is known to the receiver. The receiver uses a synchronized replica of the spreading code to despread the received signal allowing recovery of the message. The large redundancy inherent in spread spectrum signals is required to overcome interference caused by the nature of the channel, by intentional disturbances, and by multiple access of various users. The exploitation of the spread spectrum technique to enable multiple users a simultaneous access to the channel is called CDMA. The separation of the user signals is performed in the code domain by applying user specific matched filtering in the receiver, referred to as despreading. Three principles of user specific spectrum spreading may be distinguished, namely DS, frequency hopped (FH), and time hopped (TH) spreading [Dix94, SOS94]. With FH spreading and TH spreading, the user specific spreading code is used to pseudo randomly hop the carrier frequency through a large bandwidth and to pseudo randomly hop the time slots through a large time duration, respectively. With DS spreading, the user specific spreading code introduces rapid phase transitions into the data stream, expanding the required bandwidth.

Wireless mobile communication systems of the 21st century have to ensure a wide range of multimedia services such as speech, image, and data transmission with different and variable bit rates up to 2 Mbit/s in hierarchical cell structures and in multi-operator scenarios [PGH95, BJK96]. The new services have to be available in indoor and outdoor environments, where the integration of satellite links shall enable world-wide coverage [PGH95, BJK96]. These requirements cannot be completely covered by the second generation systems, which have a relatively low available bit rate in the range of 10 kbit/s per user, primarily designed for speech transmission applications. Research activities concerning the standardization of the third generation mobile radio systems are in progress world-wide [PGH95, BJK96, Jun95]. International investigations run under the generic term Future Public Land Mobile Telecommunications Systems (FPLMTS) or also International Mobile Telecommunications 2000 (IMT-2000), and in Europe they are referred to as Universal Mobile Telecommunications Systems (UMTS) [PGH95, BJK96, Rap96]. An important challenge for UMTS and IMT-2000 is the selection of an appropriate multiple access scheme to meet the demands of third generation mobile radio systems. Within the program Research and Development in Advanced Communications Technologies in Europe, Phase II (RACE II), the two projects referred to as Code Division Testbed (CODIT) [BFG94] and advanced TDMA (ATDMA) [CDE94] can be mentioned as examples for a DS-CDMA and a TDMA concept, respectively, developed for UMTS. Both projects ran from 1992 till 1995 and their results were presented for standardization at the European Telecommunication Standards Institute (ETSI) and at the International Telecommunications Union (ITU).

The pros and cons of FDMA, TDMA, CDMA, or any combination thereof have to be considered carefully. They all perform the same under ideal transmission conditions assuming optimal design. However, under real transmission conditions encountered in mobile communications, the multiple access schemes can perform with significant differences. Essential for a decision is a comparison between CDMA and TDMA since FDMA is a quasi natural component of any multiple access scheme [Bai94]. A multitude of publications addressed to this comparison have shown that no definite winner emerges and further investigations of hybrid multiple ac-

cess schemes have to be carried out to exploit the advantages of the various access schemes [JBS93, Bai94, BJK96, Bai96, Kle96, Agh96]. Furthermore, attention has to be focused on recent developments in wireless communications, such as in the field of multi-carrier (MC) communications [Bin90], which can possibly improve the conventional multiple access schemes. In 1993, various concepts based on a combination of DS-CDMA and MC modulation were proposed [FaP93, YLF93, Van93, KoM93, Faz93, DaS93, CBJ93]. These novel CDMA concepts with MC modulation are described and discussed in the following section.

1.2 Multi-Carrier CDMA for Mobile Communications

1.2.1 Principles of DS Spread Spectrum and Multi-Carrier Modulation

Before introducing the new CDMA concepts based on MC modulation, a brief introduction to the basic elements DS spread spectrum and MC modulation is given in this section. A three-dimensional time/frequency/power density representation, shown in Fig. 1.1, is introduced to illustrate the principles of the various CDMA concepts and of MC modulation. A box indicates

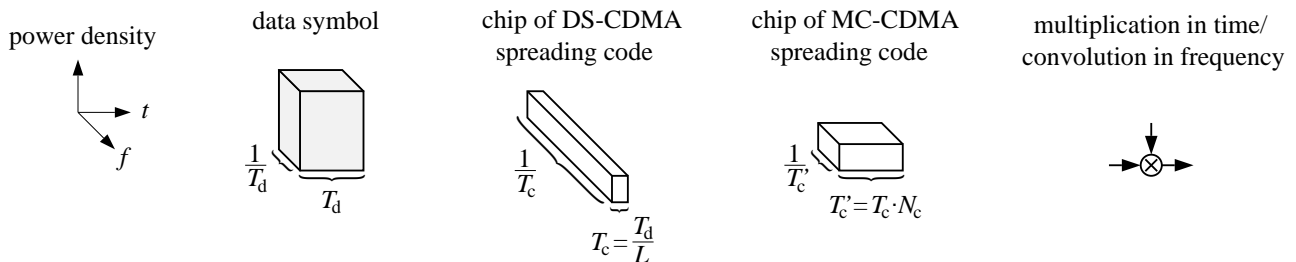


Figure 1.1: Three-dimensional time/frequency/power density representation

the three-dimensional time/frequency/power density range of the signal, in which most of the signal energy is located and does not make any statement about the pulse or spectrum shaping. The representation is normalized on the energy of a data symbol with duration T_d and rate $1/T_d$, respectively. For comparison, a chip of a DS-CDMA spreading code and of an MC-CDMA spreading code, explained in detail in the sequel, are shown.

The principle of DS spreading, comprehensively explained in [Dix94, BGP84, SOS94, Vit95, Pra96, Rap96], is illustrated in Fig. 1.2. The data symbols of a user are spectrally spread before transmission on carrier f_c by multiplying them with a user specific spreading code. The user specific DS-CDMA spreading code consists of L chips, each of duration T_c , cf. Fig. 1.1. The chip rate $1/T_c$ is a factor L larger than the data symbol rate $1/T_d$. The factor L corresponds to the spreading code length and is also referred to as bandwidth spreading factor or processing gain. With DS-CDMA, multiple users simultaneously use the total available bandwidth at the same time, performing the separation of the user signals in the code domain.

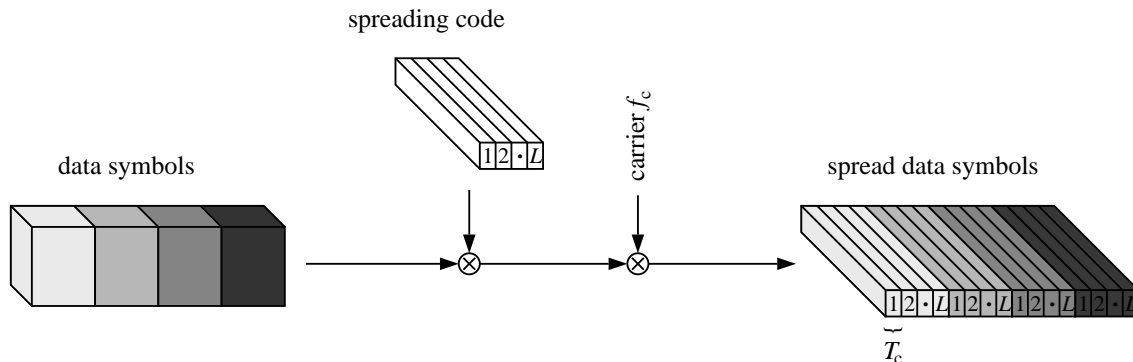


Figure 1.2: Principle of DS spreading of the data of a single user; $T_c = T_d/L$

The progress in wireless communications entails a demand for higher data rates and, thus, shorter symbol durations. However, if the duration of the transmitted symbol becomes smaller than the time dispersion of the multipath channel, the performance of the wireless communication system suffers from ISI. This is a crucial problem since the receiver complexity is related to the amount of ISI. An approach to prevent ISI is offered by parallel data transmission [Cha66, Sal67, WeE71], referred to as MC communications. The principle of MC modulation, depicted in Fig. 1.3, is to convert a high rate data stream into N_c low-rate substreams, where N_c is the number of subcarriers used for data transmission. Each substream is modulated on its

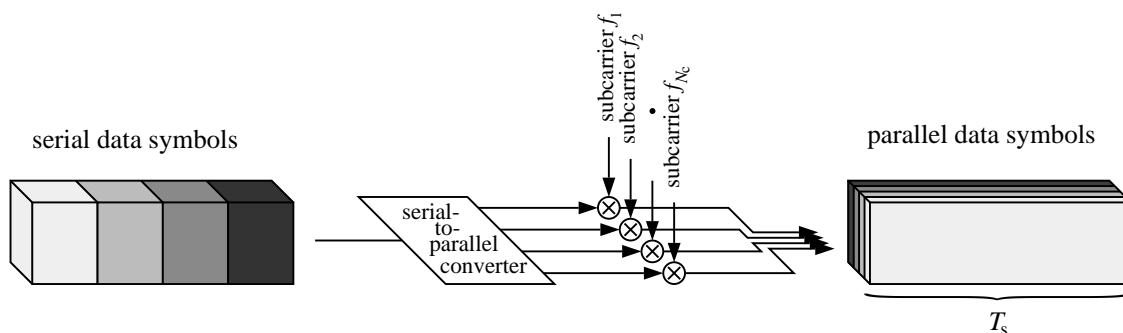


Figure 1.3: Principle of multi-carrier modulation; $T_s = T_d N_c$

assigned subcarrier f_n , $n = 1, \dots, N_c$. Thus, the available channel bandwidth is subdivided into N_c narrow subbands, which ideally appear frequency non-selective. The data symbol rate per subcarrier is reduced by a factor N_c and with that, the ISI is reduced. A common realization of MC communications is conventional frequency division multiplexing where the subbands are completely separated in the frequency domain. However, due to finite steepness of the filter roll-offs, the subchannel spacing has to be greater than the Nyquist bandwidth to avoid inter-subchannel interference (ICI). This inefficient use of the available spectrum can be overcome by permitting spectral overlap between adjacent subchannels [Cha66, Sal67]. ICI can be avoided by guaranteeing orthogonality between the signals on the subcarriers. With rectangular pulse shaping, orthogonality between the signals is obtained by choosing a subcarrier spacing equal to the reciprocal of the symbol duration per subcarrier T_s , known as orthogonal frequency division multiplexing (OFDM) [WeE71, Hir81, Cim85]. The N_c parallel modulated data symbols

of duration T_s equal to $N_c \cdot T_d$ are referred to as an OFDM symbol with the assigned OFDM symbol rate $1/T_s$. By increasing the number of subcarriers, the OFDM spectrum approaches an ideal rectangular shaping within the bandwidth B .

The origins of MC communications go back to the 1950s as one of the earliest MC systems, the so-called Kineplex system with 20 subcarriers, each with a data rate of 150 bit/s, was presented [DHM57]. Since the amount of filters and oscillators is considerable for a larger number of subcarriers, an efficient digital implementation of OFDM was proposed by using the discrete Fourier transform (DFT) or its more computationally efficient implementation, the fast Fourier transform (FFT) [WeE71]. The progress in semiconductor technology enabled the realization of an FFT for a high number of subcarriers up to several thousands whereby OFDM gained much in significance. Residual ISI in MC communications can be avoided completely if a guard interval is added to each OFDM symbol, which has to be chosen larger than the time dispersion of the channel [All87, Bin90]. The breakthrough of MC communications came in the 1990s as OFDM was chosen for the European Digital Audio Broadcasting (DAB) standard [All87] and also for the European terrestrial Digital Video Broadcasting (DVB-T) standard [FKR95]. In broadcast applications, OFDM offers the possibility of operating in single frequency networks with a frequency reuse factor of one. The interference from neighbouring cells is experienced as artificial multipath reception causing additional ISI which can also be combatted by the guard interval [FKR96].

1.2.2 CDMA Concepts with Multi-Carrier Modulation

The success of MC modulation in broadcast applications motivated many researchers to investigate the suitability of MC modulation for wireless mobile communications. First multiple access systems with MC modulation were published in 1993 and were based on DS-CDMA [FaP93, YLF93, Van93, KoM93, Faz93, DaS93, CBJ93]. Two different concepts of combining DS-CDMA with MC modulation were introduced. Concept I is referred to as MC-CDMA, also known as OFDM-CDMA or MC-SSMA, and is the topic of this thesis. Concept II was proposed in two variants, the first one is referred to as MC-DS-CDMA, the second one as multi-tone (MT) CDMA. For both Concept I and Concept II, all users simultaneously share the available bandwidth where the separation of the users signals is carried out in the code domain comparable to DS-CDMA.

Concept I: MC-CDMA is based on a serial concatenation of DS spreading, cf. Fig. 1.2, and MC modulation, cf. Fig. 1.3, [FaP93, YLF93, CBJ93]. The high rate DS spread data stream is MC modulated in such a way, that the L chips of a spread data symbol are transmitted in parallel on different subcarriers. Thus, the assigned data symbol is simultaneously transmitted on L subcarriers. If the number of subcarriers N_c is equal to the spreading code length L , MC-CDMA requires the total bandwidth for the transmission of a single data symbol comparable to DS-CDMA. When choosing L smaller than N_c and introducing an appropriate frequency interleaving, the flexibility of an MC-CDMA system can be increased and the complexity of

the data detector can be reduced [FaP93, Faz93]. Fig. 1.4 shows the principle of an equivalent realization of the serial concatenation of DS spreading, cf. Fig. 1.2, and MC modulation, cf. Fig. 1.3. Each data symbol is copied onto L substreams before multiplication with one chip

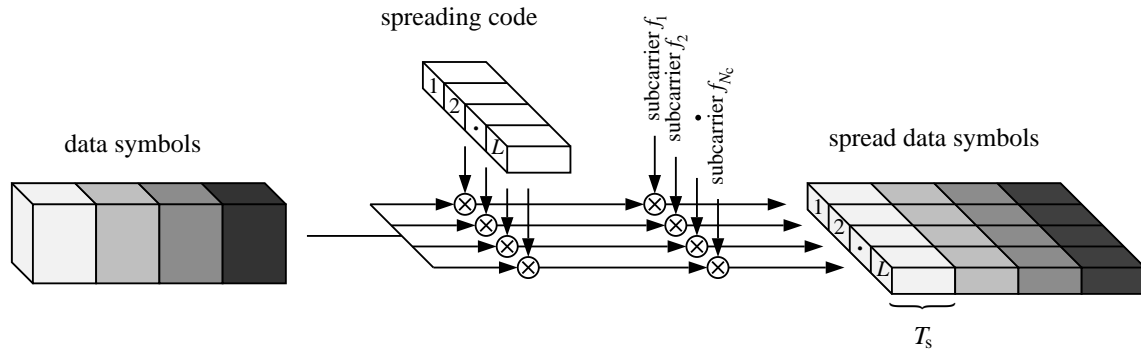


Figure 1.4: Principle of spreading of the data of a single user by MC-CDMA for the case $N_c = L$, i.e., $T_s = T_d$ and $T'_c = T_d$

of the spreading code per substream. A chip of the MC-CDMA spreading code grouped in the frequency domain has the duration T'_c , cf. Fig. 1.1, which is by a factor of N_c greater than the duration T_c of a chip of the DS-CDMA spreading code. The case of N_c equal to L is illustrated in Fig. 1.4, yielding that the data symbol duration T_d , the chip duration T'_c , and the OFDM symbol duration T_s are identical. Fig. 1.4 reflects the fact that MC-CDMA has a spreading code grouped in the frequency domain. Comparing the spread data symbols of DS-CDMA, cf. Fig. 1.2, with those of MC-CDMA, cf. Fig. 1.4, it can be seen that MC-CDMA offers an additional flexibility in the frequency domain, which results in simple methods for signal reconstruction in the frequency domain. MC-CDMA was introduced with OFDM for optimum use of the available bandwidth [FaP93, YLF93, CBJ93]. Most MC-CDMA systems were proposed for the downlink from a base station (BS) to a mobile station (MS) where powerful mobile receivers with low complexity are required [FaP93, YLF93, CBJ93]. The time/frequency synchronism between the users in the downlink allows a simple realization of an efficient channel estimation required for coherent detection.

An approach to mitigate the effect of ISI in mobile radio environments without the exploitation of a guard interval implies more complex receivers with joint detection (JD), however, overcomes the loss in data rate due to the guard interval [JBP96a, JBP96b]. This approach was considered for the uplink from an MS to a BS where more complex receivers can be applied in the fixed BS. Since MC-CDMA can be implemented as DS-CDMA with a spreading code structure in the time domain [JBP96a, NaS96], this approach can employ JD techniques which have been primarily developed for DS-CDMA in the uplink [KIB93, KKB94, JuB95, Kle96].

Concept II: With Concept II, the serial data stream is first converted into parallel low-rate substreams before applying DS spreading on each substream, see Fig. 1.5 [DaS94, CSP95a, SoN96, Van95]. When setting the number of subcarriers N_c to one, Concept II becomes identical to DS-CDMA. Concept II was proposed in the two variants MC-DS-CDMA and MT-CDMA.

MC-DS-CDMA modulates the substreams on subcarriers with a spacing of the reciprocal of the chip duration to guarantee orthogonality between the signals of the substreams after DS spreading [DaS94, CSP95a, SoN96]. A chip of the MC-DS-CDMA spreading code has the same duration T'_c as a chip of the MC-CDMA spreading code, cf. Fig. 1.1. Comparable with MC-CDMA, the OFDM symbol duration T_s is equal to the chip duration T'_c . If the spreading code length L is equal to the number of subcarriers N_c , as illustrated in Fig. 1.5, or less than N_c , a single data symbol is not spread in bandwidth with MC-DS-CDMA, instead, it is extended in the time. The design of MC-DS-CDMA systems with a high number of subchannels, where

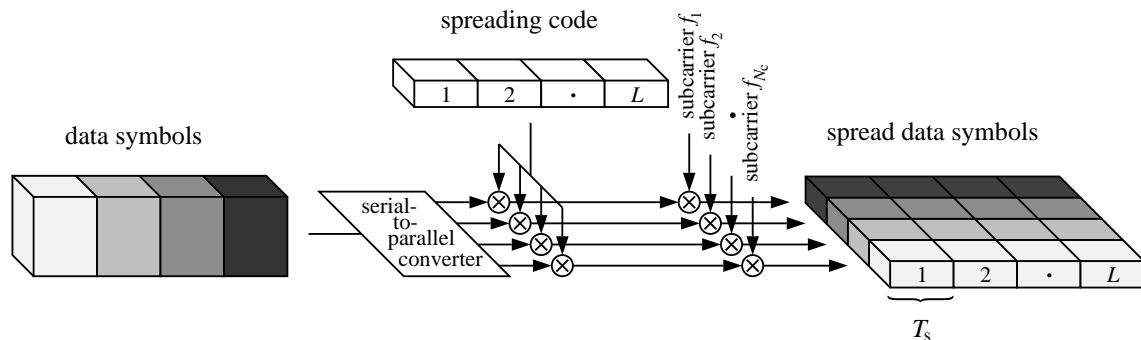


Figure 1.5: Principle of spreading of the data of a single user by MC-DS-CDMA for the case $N_c = L$, i.e., $T_s = T_d$ and $T'_c = T_d$

each subchannel can be considered as frequency non-selective, is advantageous in the sense of exploiting time diversity. However, due to the frequency non-selective fading per subchannel, frequency diversity can only be exploited if channel coding with appropriate interleaving [CSP95a] or subcarrier hopping [CSP95b] is used, or if the same information is transmitted in parallel on several subcarriers [SoN96]. This could be extended to the case where the same information is transmitted on all subcarriers [KoM93, KoM96]. The latter approach implies a repetition coding, reducing the data rate by a factor of N_c . The MC-DS-CDMA system investigated in [KoM96] chooses a subcarrier spacing which is larger than the reciprocal of the chip duration with the intention to increase the frequency diversity of the system. The system considered in [KoM96] is primarily designed as a CDMA system overlaid onto existing narrow-band systems. MC-DS-CDMA uses N_c coherent non-RAKE receivers for data detection and was investigated for the quasi-synchronous and also for the asynchronous uplink.

MT-CDMA applies the same data mapping and spreading as MC-DS-CDMA. However, in contrast to MC-DS-CDMA, the subcarrier spacing is a factor of N_c smaller than the reciprocal of the chip duration [Van93, Van95]. Thus, the N_c parallel converted data symbols before DS spreading fulfill the orthogonality requirements [Van93, Van95]. The DS spreading per subcarrier violates the orthogonality requirements, hence, introducing ICI. However, tight subcarrier spacing enables the use of spreading codes which are longer by a factor of approximately N_c compared to the spreading codes of DS-CDMA, assuming the same total available bandwidth. Therefore, the system may be able to supply more users than with DS-CDMA at the expense

of ICI [HaP96]. Since each subchannel is affected by frequency selective fading in a multipath channel, a RAKE receiver or more complex multi-user detectors can be applied per subchannel as investigated in [Van93, Van95, Van97] and therein included references. MT-CDMA was investigated for the asynchronous uplink.

A multitude of research activities was addressed to performance comparisons between MC-CDMA, DS-CDMA, MC-DS-CDMA, and MT-CDMA [CBJ93, Kai95a, HLP95, Kai95b, FKS95, HaP96, PrH96, JBP96b, Pra96]. The bit error rate (BER) P_b and the bandwidth efficiency β of a mobile radio system with perfect channel estimation and without channel coding were chosen as decision criterion. The bandwidth efficiency is defined as [Pra96]

$$\beta = \frac{K_{\text{sys}} R_b}{B}, \quad (1.1)$$

where K_{sys} is the user capacity of the mobile radio system in a single cell, R_b is the bit rate per user, and B is the total used bandwidth. The user capacity K_{sys} is the maximum possible number of simultaneously active users at a certain signal-to-noise ratio (SNR) for which the BER is less or equal to a predefined threshold. The bandwidth efficiency is a measure for the maximum achievable bit rate at a given bandwidth of an isolated cell with the dimension bit/s/Hz [Pra96]. The bandwidth efficiency has to be distinguished from the cellular spectrum efficiency [BKN94, Ste96]. The cellular spectrum efficiency is a measure for the maximum achievable bit rate at a given bandwidth per cell while maintaining a required service quality within a cellular system and has the dimension bit/s/Hz/cell [BKN94, Ste96].

First comparisons were carried out between MC-CDMA and DS-CDMA with RAKE receiver, applied in the downlink of a mobile radio system [Kai95a, HLP95, Kai95b, FKS95]. It was demonstrated that MC-CDMA can outperform DS-CDMA with RAKE receiver significantly with respect to the BER for a high number of active users and can achieve an about four times higher bandwidth efficiency β . Advantageous for MC-CDMA is the application of orthogonal spreading codes by guaranteeing optimal code synchronization in the receiver due to the spreading code structure in the frequency domain. Furthermore, the absence of ISI enables an efficient utilization of the total received energy for signal detection with low complexity. Other performance comparisons for the downlink include MC-DS-CDMA and MT-CDMA and confirm that only MC-CDMA, but not MC-DS-CDMA and MT-CDMA, can significantly outperform DS-CDMA with a RAKE receiver [HaP96, PrH96]. MC-DS-CDMA and MT-CDMA systems provide results similar to those obtained with DS-CDMA. Moreover, a BER performance comparison between MC-CDMA with JD and DS-CDMA with JD for the uplink shows a slightly better performance with MC-CDMA [JBP96b].

Finally, a performance comparison of MC-CDMA with the recently proposed MC-FDMA and MC-TDMA [ReR94, RoG96a, RoG96b, HaP96, Kai96] reveals in the uncoded and the coded case of a downlink mobile radio system advantages for MC-CDMA [Kai96]. Since the performance of MC-FDMA and MC-TDMA is used as a reference throughout the thesis, both multiple access schemes will be briefly introduced.

The combination of FDMA and TDMA, respectively, with MC modulation employing OFDM is referred to as MC-FDMA and MC-TDMA, respectively, in the sequel. Other references also use the names OFDM-FDMA and OFDM-TDMA. In an MC-FDMA system, the data symbols for different users are transmitted on different subcarriers. One or several subcarriers are exclusively allocated to a user for transmission [ReR94, HaP96, Kai96]. An advantage of MC-FDMA compared to conventional FDMA is that with OFDM an optimal bandwidth utilization of the available bandwidth is guaranteed without ICI. However, the performance of an uncoded MC-FDMA system is poor in a mobile radio channel since the frequency non-selectivity per subchannel causes dominant performance degradations if a subcarrier is located in a deep fade. Channel coding is necessary for MC-FDMA systems to enable the exploitation of diversity. In the case of MC-TDMA, the whole bandwidth is allocated to a single user for a certain number of OFDM symbols [RoG96a, RoG96b, Kai96]. The complexity of conventional TDMA systems is determined by the amount of ISI caused by the mobile radio channel. In MC-TDMA systems, the long OFDM symbol duration drastically can reduce the amount of ISI which can completely be avoided by the used of a guard interval. MC-TDMA needs channel coding in the same way as MC-FDMA to enable the exploitation of diversity.

1.2.3 State of the Art in the Field of MC-CDMA

The employment of MC-CDMA for mobile multi-user communications has become an active field of research since 1993. Up to now, the majority of publications in the field of MC-CDMA was devoted to the investigation of data detection techniques suitable for mobile radio systems in the downlink. Due to the novelty of the subject, investigations including the potential of channel coding with code bit interleaving or the influence of non-perfect channel estimation were scarcely carried out. This section gives an overview on the state of the art concerning the topics data detection, channel coding, and channel estimation applied in MC-CDMA mobile radio systems. Contributions to these topics made by the author of the thesis are not included in this overview. These contributions will be presented in the Chapters 3 to 6.

Important contributions to the field of MC-CDMA data detection techniques are summarized in Table 1.1 and can be classified as either single-user detection (SD) or multi-user detection (MD). The conventional approach with SD detects the user signal of interest by not taking into account any information about the multiple access interference (MAI). In MC-CDMA mobile radio systems, SD is realized by one tap equalization to compensate for the distortion due to flat fading on each subcarrier, followed by user specific despreading [Faz93, YLF93, CBJ93]. The one tap equalizer is simply one complex-valued multiplication per subcarrier. Under ideal transmission conditions, SD performs optimally in MC-CDMA mobile radio systems, since synchronous transmission with orthogonal spreading codes is applied. However, in non-ideal channels with frequency selective fading due to multipath propagation, the orthogonality between the signals of the different users is lost and MAI occurs. A multitude of SD techniques was proposed to combat the channel fading and, thus, the MAI, cf. Table 1.1. Basic SD techniques investigated and evaluated for MC-CDMA mobile radio systems are equal gain combining

Table 1.1: Contributions to the field of data detection for MC-CDMA mobile radio systems

classification	references	detection technique
SD	[Faz93][YLF93]	EGC
	[Faz93][CBJ93]	ZF equalization
	[YLF93][DeK97]	MRC
	[CBJ93][YeL94b]	MMSE equalization
	[FBA94]	RAKE in the frequency domain
	[YeL94a][RoB96]	controlled equalization
	[NaS96]	EGC, MRC, ZF equalization, and MMSE equalization in the time domain
	[NaF97]	RAKE in the time domain
MD	[Faz93][HLP95] [KaP96b][MaO97a] [StP97b]	IC
	[FaP93][Faz93]	JD with MLSE
	[JBP96b]	JD with ZF equalization and MMSE equalization, both with and without decision feedback
	[TER97]	JD with recurrent neural network structure

(EGC) [Faz93, YLF93], zero-forcing (ZF) equalization [Faz93, CBJ93], maximum ratio combining (MRC) [YLF93], and minimum mean square error (MMSE) equalization [CBJ93]. Further SD techniques are classified in Table 1.1.

As long as the spreading code structure of the interfering signals is known, the MAI is not noise-like, yielding SD to be suboptimal. The suboptimality of SD can be overcome with MD where the a priori knowledge about the spreading codes of the interfering users is exploited in the detection process [Kle96, Pro95]. The performance improvements with MD compared to SD are achieved at the expense of higher receiver complexity. The methods of MD can be divided into interference cancellation (IC) and JD [Kle96]. The principle of IC is to detect the information of the interfering users with SD and to reconstruct the interfering contribution in the received signal before subtracting, i.e., cancelling the interfering contribution from the received signal and detecting the information of the desired user. The iterative application of IC leads to a multistage detection scheme [VaA90]. IC can be carried out parallel for all interfering users when the amount of interference from each user is similar, first investigated for MC-CDMA mobile radio systems in [Faz93]. Another method of IC would be successive IC where per iteration the contribution of the strongest interferer remaining after the previous IC stage is cancelled. Successive IC is especially well suited in the case of users, interfering with different signal strength. The optimal detector applies JD with maximum likelihood

sequence estimation (MLSE) or maximum likelihood symbol-by-symbol estimation (MLSSE), respectively [Pro95]. Since the complexity of MLSE and of MLSSE grows exponentially with the number of users, their use is limited in practice to applications with a small number of users. By applying a hybrid MC-CDMA system with an integrated FDMA structure on subcarrier level, this requirement can be fulfilled and JD can be realizable in MC-CDMA mobile radio systems with low complexity [FaP93]. Further JD techniques are classified in Table 1.1.

MC modulated systems with flat fading per subchannel require either the use of spread spectrum techniques or of channel coding to exploit diversity. Interleaving further improves the diversity gain achievable with both approaches. MC systems with channel coding such as DAB and DVB-T systems [All87, FKR95] and coded MC-FDMA and coded MC-TDMA mobile radio systems [Kai96] yield promising results. Channel coding also considerably improves the performance of MC-CDMA systems which already exploit diversity due to the spread spectrum technique [FaP93, JBB97]. Binary convolutional codes were chosen as channel codes in the MC-CDMA mobile radio systems [FaP93, StP97a]. Investigations of MC-CDMA mobile radio systems with channel coding are summarized in Table 1.2. The combination of spreading and

Table 1.2: Contributions to the field of channel coding for MC-CDMA mobile radio systems

references	coding technique & <i>comments</i>
[FaP93][MaO97a] [StP97a][StP97b] [JBB97]	convolutional coding
[MaO96][StP97a]	low rate orthogonal convolutional coding; <i>used for spreading also</i>

channel coding by applying a low-rate orthogonal convolutional code [Vit90] for both spreading and coding in MC-CDMA systems [MaO96, StP97a] show that this approach achieves only a low bandwidth efficiency [StP97a].

Coherent data detection as well as channel decoding exploiting reliability information require knowledge about the channel and, thus, channel estimation. MC systems with OFDM allow channel estimation by exploiting the correlation of the fading process in frequency and time. Pilot symbol aided channel estimation realized by a two-dimensional filter or two one-dimensional filters working sequentially [Höh91] is a promising concept for MC-CDMA receivers operating in mobile radio environments [MBR96]. Various principles of channel estimation concepts proposed for the down- and the uplink of MC-CDMA mobile radio systems are summarized in Table 1.3.

Finally, the suitability of MC-CDMA systems was, for instance, investigated for cellular mobile radio applications in [TCC97, JBB97] and for wireless local area networks in [CFR96, BCF96].

The overview of research activities in the field of data detection, channel coding, and channel estimation for MC-CDMA mobile radio systems in Tables 1.1 to 1.3 reflects that a multitude of

Table 1.3: Contributions to the field of channel estimation for MC-CDMA mobile radio systems

link	references	principle of channel estimation & <i>comments</i>
downlink	[CFG95]	reference OFDM symbols; <i>indoor</i>
	[MRG95]	pilot symbols with filtering in two dimensions
	[ToK96c]	least-squares algorithm with training symbols; <i>indoor</i>
uplink	[CFG95]	reference OFDM symbols; <i>indoor</i>
	[Ste97a][Ste97b]	pilot tones
	[JBB97][BJP97]	single-carrier modulated midamble

research activities were carried out in the last years. However, the overview also demonstrates that, especially when looking at the beginning of the research for this thesis in 1994, many problems were open and are still open, which form the motivation for this thesis presented in the following section.

1.3 Goals of the Thesis

Proceeding from the state of the art and from emerging, still uncovered fields, the thesis has two main objectives. The first objective is to find and optimize appropriate concepts for the single components data detection, channel decoding, and channel estimation applied in MC-CDMA mobile radio systems. The second objective is to analyze the performance of a complete MC-CDMA mobile radio system in various mobile radio environments in the downlink. To reach these objectives, in particular, the following goals are pursued:

- CDMA concepts with MC modulation known from literature shall be put together and shall be classified. This has already been accomplished in Section 1.2.2.
- The MC-CDMA signal structure shall be mathematically described. By introducing appropriate modifications, the flexibility of MC-CDMA mobile radio systems shall be pointed out. Techniques for SD and MD applied in MC-CDMA mobile radio systems shall be developed, evaluated, and as far as possible, analyzed theoretically. A comparative overview of the performance of novel and known SD and MD techniques for MC-CDMA mobile radio systems shall be given.
- Table 1.2 shows that MC-CDMA mobile radio systems with channel coding and code bit interleaving were rarely investigated. MC-CDMA systems have to be considered with various channel coding schemes applying hard and soft decision decoding. Furthermore, recent developments in the field of iterative channel decoding have to be taken into account. Since decoders based on the Viterbi algorithm should exploit log-likelihood ratios (LLRs) as soft inputs with optimum reliability information, the LLRs for coded

MC-CDMA systems with soft decision decoding applying SD as well as MD have to be derived. The iterative concatenation of data detection and decoding for IC with reliability information shall be investigated. The trade-off between coding and spreading in MC-CDMA mobile radio systems shall be found.

- A powerful channel estimation concept is required for MC-CDMA systems to guarantee efficient coherent data detection and soft decision channel decoding. Channel estimation concepts with filtering in two dimensions shall be developed and analyzed generally for MC modulated systems operating in mobile radio channels with fast time variation and large time dispersion, typical for large cells.
- Future cellular mobile radio systems have to operate in hierarchical cell structures with cells of various size, adapted to the specific environment and requirement. Three typical cell classifications can be distinguished, macro-, micro-, and picocells, where each class has its characteristic signal propagation. To the best of the author's knowledge, no complete system analysis of a coded MC-CDMA mobile radio system with non-perfect channel estimation for all three propagation scenarios typical for future cellular concepts is available. An extensive system analysis of an MC-CDMA system in the downlink with channel coding and non-perfect channel estimation shall be carried out for mobile radio channels, typical for macro-, micro-, and picocell propagation scenarios. This analysis shall prove the suitability of an MC-CDMA system as a potential candidate for future mobile radio systems.

1.4 Contents and Important Results

The thesis consists of 7 chapters, where the contents of the Chapters 3 to 6 correspond to the goals mentioned in Section 1.3.

The fundamentals of time variant multipath propagation, which characterize the demands on a mobile radio system, are summarized in Chapter 2. After describing the mobile radio channel and its statistical modelling, channel models typical for future cellular mobile radio systems are classified for macro-, micro-, and picocells.

In Chapter 3, the MC-CDMA concept under investigation is presented. After an introduction into MC modulation with OFDM, the MC-CDMA signal structure is explained and its flexibility is pointed out by introducing the M -, the Q -, and the $M&Q$ -Modification. A discrete-time and -frequency MC-CDMA transmission model is mathematically described using the vector-matrix notation. Low-complex SD techniques, a multistage detection technique with IC, where the detection stages are adapted to the residual MAI, and the optimum JD with MLSSE are developed and analyzed for MC-CDMA systems. Their performance is demonstrated and compared to known SD and MD techniques based on Monte Carlo simulations. The principle of MC-FDMA and MC-TDMA is briefly introduced and the performance of MC-CDMA, MC-FDMA, and MC-TDMA systems is compared to each other. Finally, the equivalence between MC-CDMA and DS-CDMA is pointed out in Chapter 3.

The adaptation of channel coding with soft decision decoding and code bit interleaving to MC-CDMA systems is treated in Chapter 4. Convolutional encoding with conventional and different iterative decoding strategies employing the Viterbi algorithm are investigated. To guarantee an optimum concatenation of data detection and soft decision channel decoding, the optimum soft decided values which can be delivered to a Viterbi decoder, are derived for MC-CDMA receivers with SD and with MD. Exploiting the optimum soft decided values, an iterative detection and decoding scheme referred to as soft IC is introduced. With soft IC, reliability information about the reconstructed interference is taken into account in the iterative IC scheme, reducing error propagation. An important result is that IC based on soft decided values from the channel decoder significantly outperforms JD with MLSSE followed by soft decision channel decoding. In Chapter 4, also the suitability of the recently proposed Turbo codes as channel codes for MC-CDMA systems is investigated. However, it is shown that Turbo codes are only of limited use in MC-CDMA systems when considering speech transmission applications. Iterative Turbo decoding outperforms simpler conventional Viterbi decoding only when applying large Turbo code interleaver sizes, resulting in large delays which are not permitted in speech transmission applications. The trade-off between spreading and coding in MC-CDMA systems is determined and a bandwidth efficiency plan for MC-CDMA, MC-FDMA, and MC-TDMA systems is presented. It can be concluded that the performance of coded MC-CDMA systems with SD and MD, respectively, applying code rates R less than $2/3$ improves with spreading codes of increasing length up to L equal to 8. A further increase of the spreading code length results in no relevant performance gain.

In Chapter 5, a pilot symbol aided channel estimation for MC systems with filtering of the fading process in time and frequency is analyzed and optimized. Model mismatch between the correlation functions of the channel and those used for the filter design is taken into account in the analysis. An appropriate arrangement of the pilot symbols in an OFDM frame based on the two-dimensional sampling theorem is presented, where the redundancy due to pilot symbols is less than 6%. It is shown that the performance of the presented low-complex channel estimation with two one-dimensional FIR filters working sequentially closely approximates the performance of a channel estimation with an optimum two-dimensional Wiener filter.

A complete MC-CDMA system is designed and analyzed in the downlink of a mobile radio system in Chapter 6. The system evaluation takes into account channel coding, non-perfect channel estimation, and propagation scenarios typical for macro, micro, and picocells. The suitability of the developed MC-CDMA system for mobile radio environments with high Doppler frequencies of 400Hz and with large time dispersion of $20 \mu s$ is demonstrated. Guaranteeing a good transmission quality with a coded BER P_b equal to 10^{-3} , the presented MC-CDMA mobile radio system achieves the remarkable bandwidth efficiency of 0.81 bit/s/Hz at an SNR per bit between 8 dB and 12 dB on the average.

Chapter 7 contains an abstract and a German summary of the thesis.

Chapter 2

Mobile Radio Channel

2.1 Time-Variant Multipath Propagation

Splitting the service area of a mobile radio system into multiple geographically separated cells enables the reuse of the same frequency band in different cells. Besides the frequency reuse which considerably increases the number of simultaneously communicating users within the service area, cell splitting reduces the required transmission power with decreasing cell size. Within a cell, a BS serves a number of roaming MSs. The cells in mobile radio communications vary substantially in size and shape and are, for instance, adapted to areas with low density fast moving vehicular MSs and areas with high density low speed portable MSs. Three typical cell classifications can be distinguished [COD95, FIL96]:

- **Macrocells** have a radius of 1 km to 35 km. The basic categories of macrocells are urban, suburban, rural, and hilly environments. The BS antenna is elevated well above the local terrain. Rarely a direct line of sight (LOS) path between the BS and the MS antennas exists because of the natural and man-made objects that are in immediate vicinity of the MS. Due to the large size of macrocells, they are suited for the support of MSs with high velocities due to the lower handoff rate compared to smaller cells.
- **Microcells** typically have a radius of 20 m to 300 m and are found in urban areas and city centers. The determining characteristic is that the BS antenna height is under the mean level of the surrounding roof tops. In microcells, LOS is the situation often found. Microcells with a radius up to 1 km have the BS antenna situated above the mean surrounding roof tops. The velocity of the MSs is mainly the speed of pedestrians and city traffic.
- **Picocells** have a radius up to 100 m and are typically applicable to indoor like environments. LOS between the BS and the MS antenna is mostly present if both antennas are inside the same room. The velocity of the MSs in picocells is typically on the order of a few km/h.

The link between a BS and an MS is given by the mobile radio channel. In the mobile radio channel, the transmitted signal suffers from three nearly independent effects which are characterized as follows:

- **Multipath propagation** occurs as a consequence of reflections, scattering, and diffraction of the transmitted electromagnetic wave at natural and man-made objects. Thus, at the receiver antenna, a multitude of waves arrives from many different directions with different delays, attenuations, and phases. The superposition of the waves results in amplitude and phase variations of the composite received wave. Due to the mobility of the MS and moving objects in the mobile radio channel, changes in the phases and amplitudes of the arriving waves occur, resulting in time-variant multipath propagation. Even small movements on the order of the wavelength may result in a totally different wave superposition. The varying signal strength due to time-variant multipath propagation is referred to as fast fading.
- **Shadowing** is caused by obstruction of the transmitted waves by hills, buildings, walls, etc., resulting in more or less strong attenuation of the signal strength. Compared to fast fading, longer distances have to be covered to significantly change the shadowing constellation. The varying signal strength due to shadowing is called slow fading and can be described by a log-normal distribution [Par92].
- **Path loss** predicts how the mean signal power decays with distance from the BS. In free space, the mean signal power decreases with the square of the distance from the BS. In a mobile radio channel, where often no direct LOS path exists between the BS and the MS antennas, the signal power typically decreases with a power higher than two and is typically in the order of three to five [Rap96].

Variations of the received power due to shadowing and path loss can be counteracted by power control and are not considered further in this thesis. In this section, the mobile radio channel is described with respect to its fast fading characteristic. A statistical description of the multipath channel is chosen [Bel63], since a deterministic description appears impossible in practice. Throughout the thesis, all bandpass signals and channels are replaced by equivalent lowpass signals and channels for mathematical convenience but with no loss of generality [Pro95, Rup93]. The lowpass representation is in general complex-valued. In the sequel, complex values are marked by underlining. The symbol $(\cdot)^*$ denotes the complex conjugation.

The mobile radio channel is given by the time-variant channel impulse response $\underline{h}(\tau, t)$ or by the time-variant channel transfer function $\underline{H}(f, t)$, which is the Fourier transform of $\underline{h}(\tau, t)$. The channel impulse response represents the response of the channel at time t due to an impulse applied at time $t - \tau$. The mobile radio channel is assumed as a wide-sense stationary (WSS) random process, i.e., the channel has a fading statistic that remains constant over short periods of time or small spatial distances. In environments with multipath propagation, the channel impulse response is composed of a large number of scattered impulses received over N_p different paths,

$$\underline{h}(\tau, t) = \sum_{p=1}^{N_p} a_p e^{j(2\pi f_{D,p} t + \varphi_p)} \delta(\tau - \tau_p), \quad (2.1)$$

where a_p , $f_{D,p}$, φ_p , and τ_p are the amplitude, the Doppler frequency, the phase, and the propagation delay, respectively, associated with the p th path. The Doppler frequency

$$f_{D,p} = \frac{v f_c}{c} \cos \alpha_p \quad (2.2)$$

depends on the velocity v of the MS, the speed of light c , the carrier frequency f_c , and the angle of incidence α_p of a wave assigned to the p th path.

The description of the correlation functions of the channel impulse response $\underline{h}(\tau, t)$ is sufficient to characterize the fast fading of the mobile radio channel [Bel63]. The autocorrelation function of $\underline{h}(\tau, t)$ is defined as

$$\underline{R}(\tau_1, \tau_2, \Delta t) = \frac{1}{2} \text{E}\{\underline{h}(\tau_1, t) \underline{h}^*(\tau_2, t + \Delta t)\}. \quad (2.3)$$

Under the presumption that the WSS random processes $\underline{h}(\tau_1, t)$ and $\underline{h}(\tau_2, t)$ are uncorrelated for τ_1 not equal to τ_2 , called uncorrelated scattering (US), the autocorrelation function (2.3) simplifies to

$$\underline{R}(\tau_1, \tau_2, \Delta t) = \underline{\rho}(\tau_1, \Delta t) \delta(\tau_1 - \tau_2), \quad (2.4)$$

where $\underline{\rho}(\tau, \Delta t)$ is the delay cross-power spectral density [Bel63]. The mobile radio channel characterized by (2.4) is referred to as WSSUS channel. The Fourier transform of $\underline{\rho}(\tau, \Delta t)$ in Δt yields the scattering function [Bel63]

$$S(\tau, f_D) = \int_{-\infty}^{\infty} \underline{\rho}(\tau, \Delta t) e^{-j2\pi f_D \Delta t} d(\Delta t). \quad (2.5)$$

The scattering function is real-valued and provides a measure of the average power output of the channel as a function of the delay τ and the Doppler frequency f_D .

By integrating the scattering function $S(\tau, f_D)$ over the Doppler frequency f_D , the delay power density spectrum

$$\rho(\tau) = \int_{-\infty}^{\infty} S(\tau, f_D) df_D, \quad (2.6)$$

is obtained, which is identical to the delay cross-power spectral density $\underline{\rho}(\tau, \Delta t)$ at Δt equal to 0. The delay power density spectrum gives the average power of the channel output as a function of the delay τ and can be viewed as a scattering function averaged over all Doppler shifts. The mean delay $\bar{\tau}$, the delay spread σ_τ , and the maximum delay τ_{\max} are characteristic parameters of a multipath channel and can be determined from the delay power density spectrum. If the duration T_s of the transmitted symbol is significantly larger than the maximum delay τ_{\max} , the channel produces a negligible amount of ISI. This effect is exploited with MC transmission where the duration per transmitted symbol increases with the number of subcarriers and, hence, the amount of ISI decreases. Residual ISI can be eliminated by the use of a guard interval, cf. Section 1.2.1. The time dispersive properties of multipath channels are most commonly

quantified by their mean delay and the delay spread [Par92]. The mean delay is the first moment of the delay power density spectrum resulting in

$$\bar{\tau} = \frac{\int_0^{\infty} \tau \rho(\tau) d\tau}{\int_0^{\infty} \rho(\tau) d\tau}. \quad (2.7)$$

The normalization with $\int_0^{\infty} \rho(\tau) d\tau$ is applied because $\rho(\tau)$ is not a probability density function. The delays are measured relative to the first detectable path at the receiver. The delay spread is the standard deviation of the delay power density spectrum and is given by

$$\sigma_{\tau} = \sqrt{\frac{\int_0^{\infty} (\tau - \bar{\tau})^2 \rho(\tau) d\tau}{\int_0^{\infty} \rho(\tau) d\tau}}. \quad (2.8)$$

The coherence bandwidth $(\Delta f)_c$ of a mobile radio channel is the bandwidth over which the signal propagation characteristics are correlated and is proportional to the reciprocal of the delay spread σ_{τ} . The coherence bandwidth can be defined as the bandwidth over which the frequency correlation function is above 0.5 and, thus, can be approximated by [Rap96, Skl97a]

$$(\Delta f)_c \approx \frac{1}{5\sigma_{\tau}}. \quad (2.9)$$

The frequency correlation function is the Fourier transform of the delay power density spectrum $\rho(\tau)$, i.e.,

$$\underline{\theta}(\Delta f) = \int_{-\infty}^{\infty} \rho(\tau) e^{-j2\pi\tau\Delta f} d\tau. \quad (2.10)$$

The channel is said to be frequency selective if the signal bandwidth B is larger than the coherence bandwidth $(\Delta f)_c$. On the other hand, if B is smaller than $(\Delta f)_c$, the channel is said to be frequency non-selective or flat. The coherence bandwidth of the channel is of importance for evaluating the performance of spreading and frequency interleaving techniques that try to exploit the inherent frequency diversity D_f of the mobile radio channel. In the case of MC transmission, frequency diversity is exploited if the separation of subcarriers transmitting the same information exceeds the coherence bandwidth. The maximum achievable frequency diversity is approximated by the ratio between the signal bandwidth B and the coherence bandwidth $(\Delta f)_c$,

$$D_f \approx \frac{B}{(\Delta f)_c}, \quad (2.11)$$

and, consequently, depends on the delay spread σ_{τ} of the channel, cf. (2.9).

By integrating the scattering function $S(\tau, f_D)$ over the delay τ , the Doppler power density spectrum

$$S_{f_D}(f_D) = \int_{-\infty}^{\infty} S(\tau, f_D) d\tau \quad (2.12)$$

is obtained. The Doppler power density spectrum gives the average power of the channel output as a function of the Doppler frequency f_D and can be viewed as a scattering function averaged over all delays. The frequency dispersive properties of multipath channels are most commonly quantified by the maximum occurring Doppler frequency $f_{D_{\max}}$. If in the case of MC transmission the subchannel spacing is significantly larger than the maximum Doppler frequency $f_{D_{\max}}$, the channel produces a negligible amount of ICI. The coherence time of the channel $(\Delta t)_c$ is the duration over which the channel characteristics can be considered as time-invariant and is proportional to the reciprocal of the maximum Doppler frequency. The coherence time can be defined as the time over which the time correlation function is above 0.5 and, thus, can be approximated by [Ste94, Rap96]

$$(\Delta t)_c \approx \frac{9}{16\pi f_{D_{\max}}}. \quad (2.13)$$

The time correlation function is the inverse Fourier transform of the Doppler power density spectrum $S_{f_D}(f_D)$, i.e.,

$$\varrho(\Delta t) = \int_{-\infty}^{\infty} S_{f_D}(f_D) e^{j2\pi f_D \Delta t} df_D. \quad (2.14)$$

If the duration T_s of the transmitted symbol is larger than the coherence time $(\Delta t)_c$, the channel is said to be time selective. On the other hand, if T_s is smaller than $(\Delta t)_c$, the channel is said to be time non-selective. The coherence time of the channel is of importance for evaluating the performance of coding and interleaving techniques that try to exploit the inherent time diversity D_t of the mobile radio channel. Time diversity can be exploited if the separation between successive time slots carrying the same information exceeds the coherence time. A number of N_s successive time slots create a time frame of duration T_{fr} . The maximum time diversity achievable in one time frame is approximated by the ratio between the duration T_{fr} of a time frame and the coherence time $(\Delta t)_c$,

$$D_t \approx \frac{T_{fr}}{(\Delta t)_c}, \quad (2.15)$$

which, consequently, depends on the maximum Doppler frequency $f_{D_{\max}}$ of the channel, cf. (2.13).

A system exploiting frequency and time diversity can achieve the overall diversity

$$D = D_f \cdot D_t. \quad (2.16)$$

The system design should allow one to optimally exploit the available diversity D . For instance, in systems with MC transmission the same information should be transmitted on different subcarriers and in different time slots, achieving uncorrelated fading in both dimensions. In MC systems, a time slot corresponds to an OFDM symbol. Further diversity schemes like space, angle, or polarization diversity which are not within the scope of this thesis can additionally increase the overall diversity and are described in [Jak74, Lee93, Rap96, Stü96]. It should be noted that space diversity, also known as antenna diversity, is a popular form of diversity used in wireless systems [BBS97].

Several probability distributions can be considered in attempting to model the statistical characteristics of the fading process. A simple and often used approach is obtained from the assumption that there is a large number of scatterers in the channel that contribute to the signal at the receiver. The application of the central limit theorem leads to a complex-valued Gaussian process for the channel impulse response. In the absence of a LOS or a dominant component, the process is zero-mean. The magnitude of the corresponding channel transfer function

$$a(f, t) = |\underline{H}(f, t)| \quad (2.17)$$

is a random variable, for brevity denoted by a , with a Rayleigh distribution given by [Pro95]

$$p(a) = \frac{2a}{\Omega} e^{-a^2/\Omega}, \quad a \geq 0, \quad (2.18)$$

where

$$\Omega = E\{|\underline{H}(f, t)|^2\} \quad (2.19)$$

is the average power. The phase is uniformly distributed in the interval $[0, 2\pi[$. This channel is said to be a Rayleigh fading channel and best agrees with the propagation characteristic of macrocells.

In the case that the multipath channel contains a LOS or dominant component in addition to the randomly moving scatterers, the channel impulse response can no longer be modeled as zero-mean. Under the assumption of a complex-valued Gaussian process for the channel impulse response, the magnitude of the channel transfer function has a Rice distribution given by [Pro95]

$$p(a) = \frac{2a(K_{\text{Rice}} + 1)}{\Omega} e^{-K_{\text{Rice}} - a^2(K_{\text{Rice}} + 1)/\Omega} I_0\left(2a\sqrt{\frac{K_{\text{Rice}}(K_{\text{Rice}} + 1)}{\Omega}}\right), \quad a \geq 0. \quad (2.20)$$

The Rice factor K_{Rice} is determined by the ratio of the power of the dominant path to the power of the scattered paths at the receiver. The average power Ω is given according to (2.19) and $I_0(\cdot)$ is the zero-order modified Bessel function of first kind. The phase is uniformly distributed in the interval $[0, 2\pi[$. This channel is said to be a Ricean fading channel and best agrees with the propagation characteristic of micro- and picocells.

An alternative, more empirical approach to statistically model the magnitude $|\underline{H}(f, t)|$ distribution of the channel transfer function, by providing a closer match to some experimental data than either the Rayleigh or Rice distribution, is given by the Nakagami- m distribution, introduced by Nakagami in the early 1940's [Nak60]. The Nakagami- m distribution describes the magnitude $|\underline{H}(f, t)|$ distribution by a central chi-square distribution with m , not necessarily integer, degrees of freedom and is defined as [Nak60, Stü96]

$$p(a) = \frac{2a^{2m-1}}{\Gamma(m)} \left(\frac{m}{\Omega}\right)^m e^{-ma^2/\Omega}, \quad a \geq 0, \quad (2.21)$$

where

$$m = \frac{\Omega^2}{E\{(a^2 - \Omega)^2\}}, \quad m \geq \frac{1}{2}. \quad (2.22)$$

The average power Ω over all paths is given according to (2.19) and $\Gamma(\cdot)$ is the Gamma function. The parameter m is related to the fading strength and can be used to model fading conditions that are more or less severe than those modelled according to the Rayleigh distribution. In the case of a dominant path, the Nakagami- m distribution can closely approximate the Rice distribution by using the following relations between the Rice factor K_{Rice} and the Nakagami parameter m [Nak60, Stü96],

$$K_{\text{Rice}} = \frac{\sqrt{m^2 - m}}{m - \sqrt{m^2 - m}}, \quad m \geq 1, \quad (2.23)$$

and

$$m = \frac{(K_{\text{Rice}} + 1)^2}{(2K_{\text{Rice}} + 1)}. \quad (2.24)$$

A statistical description of the fading process based on the Nakagami- m distribution often leads to closed analytical expressions, while the Rice distribution due to the Bessel function does not. If m and, thus, K_{Rice} approach infinity, the Nakagami- m distribution and the Rice distribution become an impulse, corresponding to an ideal channel. If m is equal to 1 and, thus, K_{Rice} is equal to 0, the Nakagami- m distribution and the Rice distribution become a Rayleigh distribution. If m is in the interval $[1/2, 1[$, the fading conditions become more severe than Rayleigh fading and the distribution reduces for m equal to 1/2 to a one-sided Gaussian distribution. Thus, the Nakagami- m distribution is the most flexible of the three presented distributions. Moreover, the simple algebraic form of m and Ω allows a straightforward extraction of these parameters from measured data [BrD91], as applied for the definition of macro-, micro-, and picocell propagation models in the CODIT study [COD95]. The channel models defined in the CODIT study are described in the following section.

2.2 Channel Models for Macro-, Micro-, and Picocells

2.2.1 CODIT and COST 207 Channel Models

The investigations of the MC-CDMA mobile radio system proposed in this thesis should be carried out on a basis which takes into account the requirements of future mobile radio systems. Thus, different channel models typical for macro-, micro-, and picocells are required. The channel models of two different studies are chosen for the investigations in this thesis. Namely, the propagation models of the CODIT study [COD95, FIL96], defined for macro-, micro-, and picocell scenarios, and the propagation models of the COST 207 study [COS89, FIL96], defined for macrocell scenarios only. Throughout the thesis, these two types of channel models are referred to as CODIT channel models and COST 207 channel models. The use of both types of channel models for the investigations should, besides the evaluation of the MC-CDMA system, enable a comparison between the CODIT and the COST 207 channel models. Furthermore, performance comparisons with other mobile radio systems which take into account any of these

channel models should be enabled. In the following, the different philosophies behind the CODIT and the COST 207 channel models are pointed out and the implementation of the channel models of both studies is described.

The philosophy of modelling the mobile radio channel with the CODIT and COST 207 approach is related to the physical description of the channel and is based on the implementation of a discrete multipath scenario. This type of channel modelling enables the reconstruction of a scattering function $S(\tau, f_D)$ obtained from measured mobile radio channels. The channel impulse response corresponds to (2.1), where the N_p discrete paths may differ in the amplitudes, Doppler frequencies, phases, and propagation delays. The assigned channel transfer function becomes

$$\underline{H}(f, t) = \sum_{p=1}^{N_p} a_p e^{j(2\pi f_{D,p} t + \varphi_p)} e^{-j2\pi f \tau_p} \quad (2.25)$$

and is chosen for the implementation of the CODIT and COST 207 channel models in this thesis, since channels with MC transmission can be simulated computationally efficiently in the frequency domain. Preconditions for the frequency domain implementation are the absence of ISI and ICI, the frequency non-selective fading per subcarrier, and the time-invariance during one OFDM symbol. The investigated MC-CDMA mobile radio systems are designed to fulfill these preconditions. Thus, a discrete representation of the channel transfer function is enabled according to

$$\underline{H}_{n,i} = \underline{H}(nF_s, iT'_s) = \sum_{p=1}^{N_p} a_p e^{j(2\pi f_{D,p} iT'_s + \varphi_p)} e^{-j2\pi nF_s \tau_p}, \quad (2.26)$$

where $\underline{H}(f, t)$ is sampled in time at OFDM symbol rate $1/T'_s$ and in frequency at subcarrier spacing F_s . The OFDM symbol duration T'_s includes the guard interval duration. The basic differences between the CODIT channel models and the COST 207 channel models originate in the defined amplitude, Doppler frequency, and propagation delay distributions.

The **CODIT channel models** describe the fading characteristics of the various propagation environments by the parameters of the Nakagami- m distribution. Every environment is defined in terms of a number of scatterers which can take on values up to 20. The number of scatterers is equal to the number of paths N_p . Each scatterer p , $p = 1, \dots, N_p$, is characterized by a path delay τ_p , an angle of incidence α_p , a Nakagami parameter m_p , and an average power Ω_p . The approach of the CODIT channel models is based on a wave interference problem and assumes that the signal strength produced by one scatterer is caused by the sum of a sufficiently large number of waves, superimposed at the receiver. Each scatterer is composed of a number of N_w waves which is equal to 100, and, if existent, of one dominant component. The spatial scatterer model used in the CODIT channel models is illustrated in Fig. 2.1. The spatial scatterer model is applied for macro-, micro-, and picocell scenarios. The propagation delay τ_p and the average power Ω_p of the p th scatterer are taken from a uniform distribution within the interval $[\tau_{p,\min}, \tau_{p,\max}]$ and $[\Omega_{p,\min}, \Omega_{p,\max}]$, respectively, independently for each scatterer. The channel is

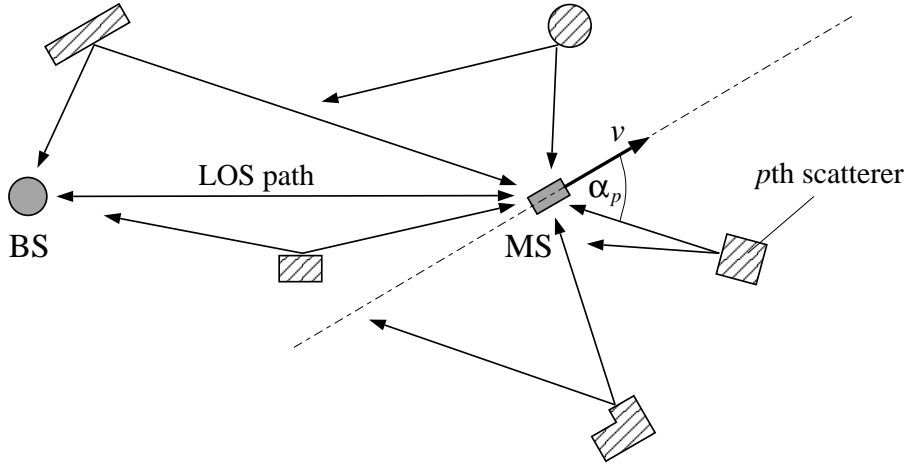


Figure 2.1: Spatial scatterer model used in the CODIT channel models

power normalized, so that

$$\Omega = \sum_{p=1}^{N_p} \Omega_p = 1. \quad (2.27)$$

The Nakagami parameter m_p of each scatterer p , $p = 1, \dots, N_p$, is explicitly indicated, except for one channel model where an interval of a uniform distribution is defined. In the sequel, the joint index p, w indicates a variable assigned to the w th wave of the p th scatterer, with $p = 1, \dots, N_p$ and $w = 1, \dots, N_w$. The index $p, 0$ indicates a variable assigned to the, if existent, dominant component of the p th path. The wave amplitudes $a_{p,w}$, $p = 1, \dots, N_p$, $w = 1, \dots, N_w$, are obtained from a zero-mean Gaussian distribution with variance

$$\sigma_{a_{p,w}}^2 = \frac{\Omega_p}{N_w} \left(1 - \sqrt{1 - \frac{1}{m_p}} \right), \quad p = 1, \dots, N_p, \quad w = 1, \dots, N_w. \quad (2.28)$$

If a dominant component exists, its amplitude $a_{p,0}$ is given by

$$a_{p,0} = \sqrt{\Omega_p \sqrt{1 - \frac{1}{m_p}}}, \quad p = 1, \dots, N_p. \quad (2.29)$$

The Doppler power density spectrum is defined by the spatial scatterer distribution and the mobile velocity according to (2.2). The angle of incidence α_p per scatterer is taken from a uniform distribution within the interval $[\alpha_{p,\min}, \alpha_{p,\max}]$ or is predefined by the location of other scatterers assuming correlation between these scatterers. Correlation between the angles of incidence is given in propagation scenarios like in streets or corridors where the signal propagation is concentrated in a certain direction. Thus, the N_p angles of incidence of the scatterers are not necessarily uniformly distributed within the whole interval $[0, 2\pi[$. However, if an isotropic distribution of the scatterers is chosen, a classical Doppler power density spectrum according to Clarke is obtained [Par92]. The angle of incidence of the, if existent, dominant component $\alpha_{p,0}$ is equal to α_p and the angles of the waves $\alpha_{p,w}$, $w = 1, \dots, N_w$, are obtained from a Gaussian distribution with standard deviation of 0.15 radians and mean α_p . Each wave has a phase $\varphi_{p,w}$,

Table 2.1: CODIT channel model parameters; each scatterer is composed of $N_w = 100$ waves and, if existent, one dominant component; the angle of incidence per wave is taken from a Gaussian distribution with mean α_p and standard deviation of 0.15 radians; values between brackets $[a, b]$ mean that the value is taken from a uniform distribution within a and b

cell type	environment	N_p	p	Ω'_p	m_p	α_p	τ_p in μs
macro	suburban (SU)	6	1	1	15	$[0, 2\pi]$	0
			2-6	$[0.1, 0.4]$	$[1, 5]$	$[0, 2\pi]$	$[0.1, 15]$
	urban (U)	20	1-20	$[0.5, 1.5]$	1	$[0, 2\pi]$	$[0, 2]$
	rural (R)	1	1	1	25	$[0, 2\pi]$	0
micro	urban 1 (Mic1)	20	1	1	3	$[0, 2\pi]$	0
			2-20	$[0.1, 0.4]$	1	$[0, 2\pi]$	$[0, 1]$
	urban 2 (Mic2)	20	1-20	$[0.5, 1.5]$	1	$[0, 2\pi]$	$[0, 1]$
pico	indoor 1 (Pic1)	12	1	1	8	$\alpha_0 \in [0, 2\pi]$	0
			2-7	$[0.03, 0.5]$	4	$\alpha_0 \pm [0, \pi/3]$	$[0.01, 0.05]$
			8-12	$[0.001, 0.03]$	1	$[0, 2\pi]$	$[0.025, 0.125]$
	indoor 2 (Pic2)	20	1	1	3	$[0, 2\pi]$	0
			2-10	$[0.1, 1]$	2	$[0, 2\pi]$	$[0.01, 0.1]$
			11-20	$[0.001, 0.1]$	1	$[0, 2\pi]$	$[0.1, 0.5]$

$w = 0, \dots, N_w$, chosen randomly within the interval $[0, 2\pi[$, so that the superposition of the waves corresponds to a random phase interference situation.

The channel transfer function implemented by the CODIT channel models can be written as

$$H_{n,i} = \sum_{p=1}^{N_p} \left(a_{p,0} e^{j(2\pi \frac{v f_c}{c} i T'_s \cos(\alpha_{p,0}) + \varphi_{p,0})} + \sum_{w=1}^{N_w} a_{p,w} e^{j(2\pi \frac{v f_c}{c} i T'_s \cos(\alpha_{p,w}) + \varphi_{p,w})} \right) e^{-j2\pi n F_s \tau_p}. \quad (2.30)$$

Table 2.1 shows the basic macro-, micro-, and picocell environments defined in the CODIT study and used for the investigations in this thesis. Further propagation scenarios for specific micro- and picocell scenarios are given in [COD95]. It has to be mentioned that the power of the scatterers Ω'_p defined in Table 2.1 is not normalized according to (2.27). Therefore, the power of each scatterer has to be normalized by

$$\Omega_p = \frac{\Omega'_p}{\sum_{p=1}^{N_p} \Omega'_p}, \quad p = 1, \dots, N_p. \quad (2.31)$$

Exemplary, a scattering function $S(\tau, f_D)$ typical for the urban environment defined in the CODIT study is plotted in Fig. 2.2. Each impulse train of the scattering function represents

the contribution of one scatterer of the total of 20 scatterers and consists of 100 waves, where the angles of incidence of the waves are Gaussian distributed around the mean α_p of the assigned scatterer. The angles of incidence of the scatterers in the urban environment are uniformly distributed in the interval $[0, 2\pi[$, resulting in a classical Doppler power density spectrum according to Clarke [Par92].

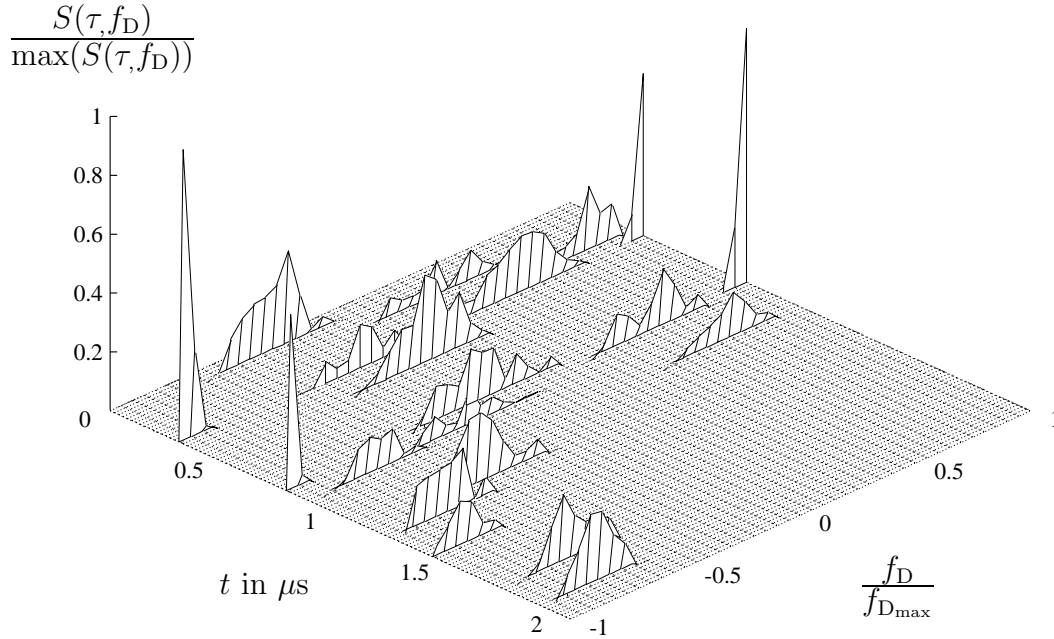


Figure 2.2: Scattering function of the urban environment defined in the CODIT study

The **COST 207 channel models** basically determine the various propagation scenarios by continuous, exponentially decreasing delay power density spectra $\rho(\tau)$. Every environment can be modeled by a number of N_p discrete paths, where each path has the same amplitude and is specified by its propagation delay τ_p [Sch89]. Each propagation delay is chosen according to the probability density function of τ within the given interval $[\tau_{p,\min}, \tau_{p,\max}]$. The probability density function of τ is proportional to the delay power density spectrum $\rho(\tau)$ [Höh92]. The average power Ω_p per path is chosen to be $1/N_p$, normalizing the power of the channel according to (2.27). The N_p paths are modelled with isotropic scattering, i.e., the angles of incidence α_p are taken from a uniform distribution in the interval $[0, 2\pi[$. Hence, a classical Doppler power density spectrum according to Clarke is obtained [Par92]. Each path has a phase φ_p uniformly distributed over the interval $[0, 2\pi[$.

The channel transfer function implemented by the COST 207 channel models can be written as

$$\underline{H}_{n,i} = \frac{1}{\sqrt{N_p}} \sum_{p=1}^{N_p} e^{j(2\pi \frac{v f_c}{c} i T'_s \cos(\alpha_p) + \varphi_p)} e^{-j2\pi n F_s \tau_p}. \quad (2.32)$$

Table 2.2: COST 207 channel model parameters; the power per path is normalized to $\Omega_p = 1/N_p$; the angles of incidence α_p are taken from a uniform distribution in the interval $[0, 2\pi[$; the propagation delays τ_p are chosen within the given interval $[\tau_{p,\min}, \tau_{p,\max}]$ proportional to the assigned delay power density function $\rho(\tau)$

cell type	environment	N_p	p	Ω_p	m_p	α_p	τ_p in μs	$\rho(\tau)$
macro	hilly terrain (HT)	100	1-74	0.01	1	$[0, 2\pi]$	$[0, 2]$	$\propto e^{-3.5\tau_p/\mu s}$
			75-100	0.01	1	$[0, 2\pi]$	$[15, 20]$	$\propto 0.1 e^{15-\tau_p/\mu s}$
	bad urban (BU)	100	1-68	0.01	1	$[0, 2\pi]$	$[0, 5]$	$\propto e^{-\tau_p/\mu s}$
			69-100	0.01	1	$[0, 2\pi]$	$[5, 10]$	$\propto 0.5 e^{5-\tau_p/\mu s}$
	typical urban (TU)	100	1-100	0.01	1	$[0, 2\pi]$	$[0, 7]$	$\propto e^{-\tau_p/\mu s}$
	rural area (RA)	100	1-100	0.01	1	$[0, 2\pi]$	$[0, 0.7]$	$\propto e^{-9.2\tau_p/\mu s}$

Table 2.2 shows the macrocell environments defined in the COST 207 study, which are used for the investigations within this thesis. As mentioned before, the propagation environments defined within the COST 207 study are only valid for macrocell environments, and are not suitable for investigations with smaller cells, typical for future cellular systems.

When comparing the CODIT and the COST 207 channel models, the following statements can be made:

- The CODIT channel models are more flexible compared to the COST 207 channel models due to higher degrees of freedom given by the definition of the parameters Ω_p , m_p , α_p , and τ_p individually for each path p , $p = 1, \dots, N_p$. This enables one to implement a scattering function $S(\tau, f_D)$ of a mobile radio channel which well approximates a measured scattering function.
- Compared to the COST 207 channel models, only the CODIT channel models define propagation scenarios for micro- and picocells which are especially of interest for the analysis of future mobile radio systems.
- Higher implementation efforts and simulation times have to be taken into account when using the CODIT channel models as opposed to the simple COST 207 channel models. This is the price to pay for increased flexibility and modelling accuracy.
- The COST 207 channel models are more popular than the CODIT channel models and, thus, more often enable comparisons to existing systems evaluated with the popular COST 207 channel models.

Generally, the CODIT channel models seems to be of higher relevance for investigations related closely to the propagation situations in real life and are of main interest in the MC-CDMA mobile radio system evaluation presented in Chapter 6. However, since the COST 207 channel models are more popular than the CODIT channel models, performance results of the MC-CDMA system with the COST 207 channel models are included also in Chapter 6. In the sequel, the propagation scenarios are referred to by the abbreviations given in brackets in Tables 2.1 and 2.2.

A comparison between the different CODIT and COST 207 channel models with respect to the mean delay, the delay spread, and the coherence bandwidth is presented in Table 2.3. The

Table 2.3: Characteristic values for the CODIT and COST 207 channel models

channel model	cell type	environment	$\bar{\tau}$ in μs	σ_{τ} in μs	$(\Delta f)_c$ in kHz
CODIT	macro	suburban (SU)	4.17	4.70	42.6
		urban (U)	1.00	0.58	344.8
		rural (R)	0	0	∞
	micro	urban 1 (Mic1)	0.39	0.32	625.0
		urban 2 (Mic2)	0.50	0.29	689.7
	pico	indoor 1 (Pic1)	0.02	0.02	10000.0
indoor 2 (Pic2)		0.06	0.07	2857.1	
COST 207	macro	hilly terrain (HT)	4.36	6.90	29.0
		bad urban (BU)	2.62	2.52	79.4
		typical urban (TU)	0.99	0.98	204.1
		rural area (RA)	0.11	0.11	1818.2

coherence bandwidth $(\Delta f)_c$ is obtained according to (2.9). The achievable frequency diversity D_f can be approximated with (2.11). It has to be mentioned that the COST 207 channel model HT offers less frequency diversity as obtained with (2.11), since the delay power density spectrum is non-zero only on a fraction of the interval $[0, \tau_{\max}]$. Hence, the achievable frequency diversity is approximately reduced by the ratio of the time over which the delay power density spectrum is non-zero to the maximum delay.

The time variability of mobile radio channels depends on the velocity v of the MSs. Each cell type has its typically occurring velocities of the MSs. Table 2.4 gives an overview on the velocities of the MS used in this thesis for the different cell types. Additionally, the Doppler frequency occurring at a carrier frequency of f_c equal to 1.8 GHz and the assigned coherence time according to (2.13) is given.

Table 2.4: Velocities of the MS, chosen for the different cell types; a choice is indicated by the symbol X

v in km/h	$f_{D_{\max}}$ in Hz		cell type		
	$f_c = 1.8$ GHz	$(\Delta t)_c$ in ms $f_c = 1.8$ GHz	macro	micro	pico
3	5.0	35.8	X	X	X
30	50.0	3.6	X	X	-
150	250.0	0.7	X	-	-
250	416.7	0.4	X	-	-

2.2.2 Uncorrelated Fading Channel Model for Multi-Carrier Systems

The main disadvantage of channel models which are based on the implementation of a discrete multipath scenarios like the CODIT or COST 207 channel models are in general the high simulation times, because for each data symbol the contribution of each of the N_p paths must be calculated. When simulating broadband MC systems, this disadvantage can be overcome by fulfilling the following conditions:

- The MC system is provided with a frequency interleaver which guarantees that neighbouring symbols in the data stream fade independently, i.e., the interleaving depth exceeds the coherence bandwidth.
- An appropriate time interleaver, e.g., code bit interleaver, ensures that the fading in adjacent OFDM symbols can be modelled as independent.
- Frequency non-selective fading per subcarrier and time-invariance during one OFDM symbol have to be guaranteed, i.e., the subchannel bandwidth has to be smaller than the coherence bandwidth $(\Delta f)_c$ and the symbol duration has to be smaller than the coherence time $(\Delta t)_c$.
- The absence of ISI and ICI has to be guaranteed by the use of a guard interval equal to or longer than the maximum delay of the channel τ_{\max} .

These conditions enable one to model the fading channel computationally efficiently in the frequency domain. A symbol transmitted on the n th subchannel of the i th OFDM symbol is multiplied by a fading amplitude $a_{n,i}$ chosen from a distribution $p(a)$ according to the considered cell type, cf. Section 2.1, and a random phase $\varphi_{n,i}$, uniformly distributed over the interval $[0, 2\pi[$. The resulting complex-valued channel fading coefficient

$$\underline{H}_{n,i} = a_{n,i} e^{j\varphi_{n,i}} \quad (2.33)$$

is thus generated independently for each subcarrier and OFDM symbol. For a propagation scenario in a macrocell without LOS, the fading amplitude is generated by a Rayleigh distribution and the channel model is referred to as an uncorrelated Rayleigh fading channel. Analogously, for smaller cells where often a dominant propagation component occurs, the fading amplitude is chosen from a Rice distribution or Nakagami- m distribution. The advantages of the uncorrelated fading channel model are the simple implementation, which can be observed when comparing (2.33) with (2.32) and (2.30), the computationally efficient system simulation, and the simple reproduction of the simulation results. These advantages are the reason for the often use of the uncorrelated fading channel models for the evaluation of MC modulated systems in multipath channels.

For the evaluation of MC-CDMA data detection techniques presented in Chapter 3 and the channel encoding and decoding strategies investigated in Chapter 4, the uncorrelated Rayleigh fading channel model is used with the intention of presenting the results as reference curves for further investigations. For the design of a channel estimation with filtering in time and frequency direction in Chapter 5 and its application in the complete MC-CDMA system evaluation in Chapter 6, the CODIT and COST 207 channel models are used, since correlated fading in time and frequency is required. Furthermore, the performance degradation due to a finite interleaver size can be shown with correlated fading.

Chapter 3

Multiple Access Scheme MC-CDMA

3.1 Multi-Carrier Communications

3.1.1 Orthogonal Frequency Division Multiplexing

The principle of MC modulation is to map a serial high rate source stream onto multiple parallel low rate substreams and to modulate each substream on another subcarrier. Since the symbol rate on each subcarrier is much less than the serial source symbol rate, the effects of delay spread significantly decrease, reducing the complexity of the equalizer. OFDM is a low-complex technique to bandwidth-efficiently modulate multiple subcarriers by using the digital signal processing as introduced in Section 1.2.1. In the sequel, MC modulation based on OFDM is described and forms the basis for the introduction of the MC-CDMA signal structure in Section 3.2. One of the main design goals for an MC transmission scheme based on OFDM in a mobile radio channel is that the channel can be considered as time-invariant during one OFDM symbol and that the fading per subcarrier can be considered as flat. Thus, the OFDM symbol duration should be smaller than the coherence time $(\Delta t)_c$ of the channel, cf. (2.13), and the subcarrier spacing should be smaller than the coherence bandwidth $(\Delta f)_c$ of the channel, cf. (2.9). By fulfilling these conditions, the realization of low-complex receivers is possible.

A communication system with MC modulation transmits a sequence $\{\underline{S}_n\}$ consisting of N_c complex-valued source symbols \underline{S}_n , $n = 1, \dots, N_c$, in parallel on N_c subcarriers. Throughout the thesis, variables which can be interpreted as values in the frequency domain like the source symbols \underline{S}_n , $n = 1, \dots, N_c$, each modulating another subcarrier frequency, are written with capital letters. The source symbols may, for instance, be obtained after source and channel coding, interleaving, and symbol mapping. For brevity, but without loss of generality, the transmission of a single but arbitrary sequence $\{\underline{S}_n\}$ is considered in this chapter, so that no additional time index is required. The isolated consideration of $\{\underline{S}_n\}$ is valid since ISI and ICI can be avoided with OFDM.

The MC modulator maps a sequence $\{\underline{S}_n\}$ of N_c serial source symbols of rate $1/T$ onto N_c parallel substreams, cf. Fig. 1.3. The source symbol rate per substream reduces to

$$\frac{1}{T_s} = \frac{1}{N_c T}. \quad (3.1)$$

According to OFDM, the N_c substreams are modulated on subcarriers with a spacing of

$$F_s = \frac{1}{T_s} \quad (3.2)$$

to achieve orthogonality between the signals on the N_c subcarriers, presuming a rectangular pulse shaping. The N_c parallel modulated source symbols S_n , $n = 1, \dots, N_c$, are referred to as an OFDM symbol of duration T_s . The complex envelope of an OFDM symbol with rectangular pulse shaping has the form

$$\underline{x}(t) = \frac{1}{\sqrt{N_c}} \sum_{n=1}^{N_c} S_n \operatorname{rect}\left(\frac{t}{T_s} - \frac{1}{2}\right) e^{j2\pi f_n t}. \quad (3.3)$$

In (3.3), the factor $1/\sqrt{N_c}$ normalizes the energy. The N_c subcarrier frequencies are located at

$$f_n = \frac{n-1}{T_s}, \quad n = 1, \dots, N_c, \quad (3.4)$$

where the center of the frequency spectrum is located at $(N_c - 1)/(2T_s)$. This definition of f_n , $n = 1, \dots, N_c$, facilitates a simple mathematical modelling. The carrier frequency f_c determining the location of the signal in the bandpass domain is neglected in (3.4), since the equivalent lowpass domain is considered. The energy density spectrum $|\underline{X}(f)|^2$ of an OFDM symbol is the sum of the energy density spectra of N_c independently modulated subcarriers and results in

$$|\underline{X}(f)|^2 = \frac{1}{N_c} \sum_{n=1}^{N_c} \left| S_n T_s \frac{\sin(\pi(f - f_n)T_s)}{\pi(f - f_n)T_s} \right|^2. \quad (3.5)$$

The normalized energy density spectrum of an OFDM symbol with N_c equal to 16 subcarriers versus the normalized frequency fT is depicted as a solid curve in Fig. 3.1. The OFDM spectrum is shown for the case where the symbols S_n , $n = 1, \dots, N_c$, are transmitted with equal energy. The dotted curve illustrates the energy density spectrum of the first modulated subcarrier f_1 and indicates the construction of the overall energy density spectrum as the sum of N_c , each by $1/T_s$ shifted, individual energy density spectra. For large values of N_c , the energy density spectrum becomes more flat in the normalized frequency range of $fT \in [-0.5, 0.5]$ containing the subcarriers. Only subcarriers near the band edges contribute to the out-of-band power. Therefore, as N_c becomes large, the energy density spectrum approaches that of single carrier modulation with ideal Nyquist filtering. As a reference, the normalized energy density spectrum of binary phase shift keying (BPSK) [Pro95] is plotted as a dashed curve.

A key advantage of using OFDM is that the MC modulation can be implemented in the discrete domain by using an IDFT, or a more computationally efficient IFFT [WeE71]. When sampling the complex envelope $\underline{x}(t)$ of an OFDM symbol at time instances t equal to $(\nu - 1)T_s/N_c$, $\nu = 1, \dots, N_c$, the samples are

$$\underline{x}_\nu = \frac{1}{\sqrt{N_c}} \sum_{n=1}^{N_c} S_n e^{j2\pi(n-1)(\nu-1)/N_c}, \quad \nu = 1, \dots, N_c, \quad (3.6)$$

and the sampling rate is N_c/T_s . The important result is that the sampled sequence $\{\underline{x}_\nu\}$, $\nu = 1, \dots, N_c$, is the IDFT of the source symbol sequence $\{S_n\}$, $n = 1, \dots, N_c$. The block

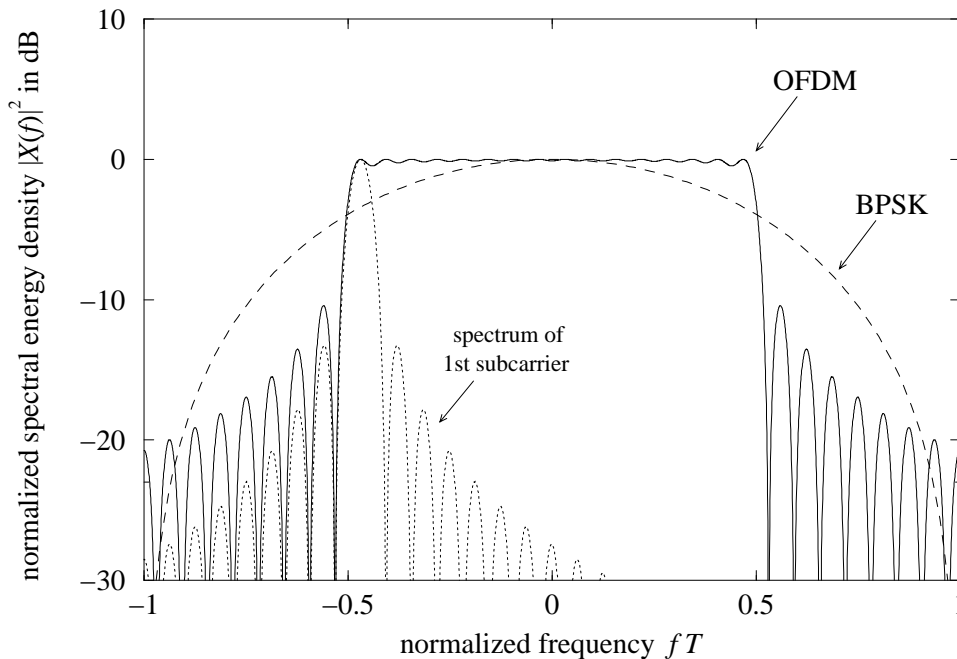


Figure 3.1: Normalized energy density spectrum versus normalized frequency fT of an OFDM symbol with $N_c = 16$ subcarriers, of the first subcarrier, and of BPSK

diagram of an MC modulator employing OFDM based on an IDFT and MC demodulator employing inverse OFDM based on a DFT is illustrated in Fig. 3.2.

When the number of subcarriers increases, the OFDM symbol duration T_s becomes large compared to the duration of the impulse response τ_{\max} of the channel and the amount of ISI reduces. However, to completely avoid the effect of ISI and, thus, to maintain the orthogonality between the signals on the N_c subcarriers, i.e., also to avoid ICI, a guard interval of duration

$$T_g \geq \tau_{\max} \quad (3.7)$$

has to be inserted between adjacent OFDM symbols [All87, Bin90, Pro95]. The guard interval is a cyclic prefix added to each OFDM symbol which is obtained by extending the duration of an OFDM symbol to

$$T'_s = T_g + T_s. \quad (3.8)$$

The discrete length of the guard interval has to be

$$L_g \geq \left\lceil \frac{\tau_{\max} N_c}{T_s} \right\rceil \quad (3.9)$$

samples to prevent ISI. The sampled sequence $\{x_\nu\}$ with cyclic extended guard interval results in

$$x_\nu = \frac{1}{\sqrt{N_c}} \sum_{n=1}^{N_c} S_n e^{j2\pi(n-1)(\nu-1)/N_c}, \quad \nu = 1 - L_g, \dots, N_c. \quad (3.10)$$

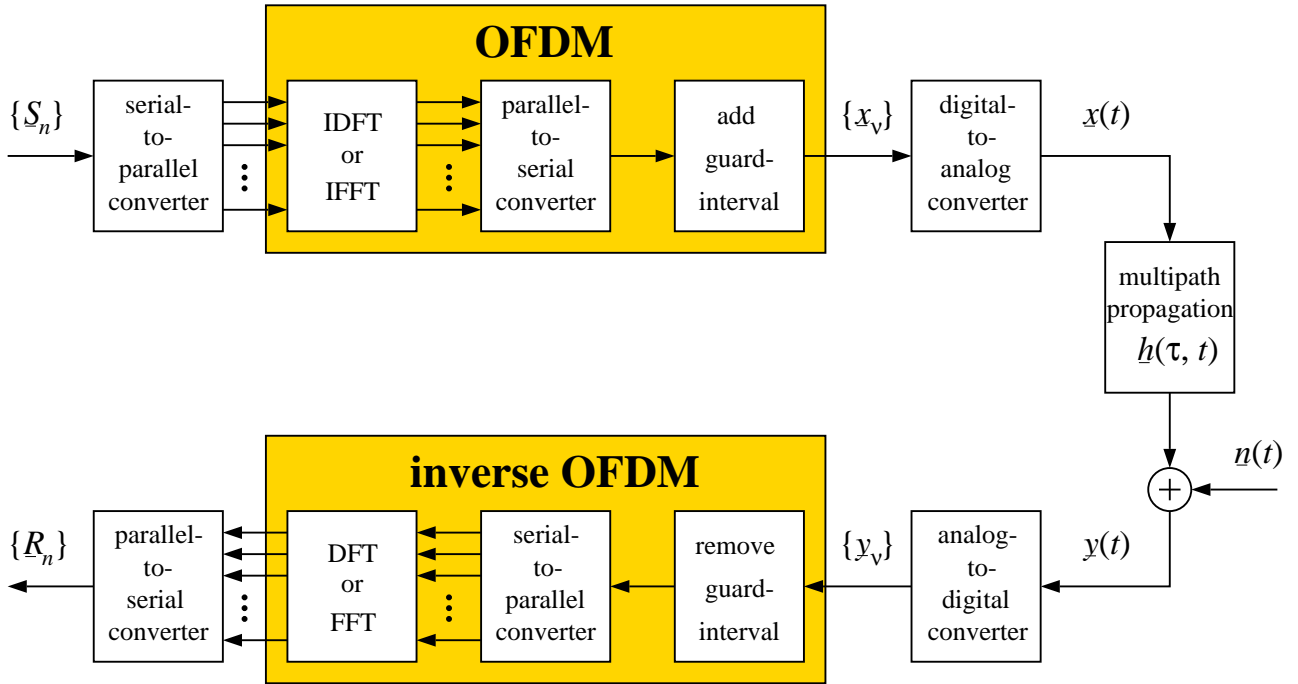


Figure 3.2: MC transmission system with OFDM

In practice, the sampled sequence $\{\underline{x}_\nu\}$, $\nu = 1 - L_g, \dots, N_c$, is passed through a digital-to-analog converter whose output ideally would be the signal waveform $\underline{x}(t)$ given in (3.3) with increased duration T'_s .

The output of the channel is the signal waveform $\underline{y}(t)$ obtained from convolution of $\underline{x}(t)$ with the channel impulse response $\underline{h}(\tau, t)$ and addition of a noise signal $\underline{n}(t)$, i.e.,

$$\underline{y}(t) = \int_0^{\tau_{\max}} \underline{x}(t - \tau) \underline{h}(\tau, t) d\tau + \underline{n}(t). \quad (3.11)$$

The noise signal $\underline{n}(t)$ contains the inherent disturbances of the transmission system, which are, motivated by the central limit theorem, modelled as additive white Gaussian noise (AWGN). The received signal $\underline{y}(t)$ is passed through an analog-to-digital converter, whose output sequence $\{\underline{y}_\nu\}$, $\nu = 1 - L_g, \dots, N_c$, is the received signal $\underline{y}(t)$ sampled at rate N_c/T_s . Since ISI is only present in the first L_g samples of the received sequence, these L_g samples are removed before MC demodulation. The ISI-free part $\nu = 1, \dots, N_c$ of $\{\underline{y}_\nu\}$ is MC demodulated by inverse OFDM exploiting a DFT. The output of the DFT is the MC demodulated sequence $\{\underline{R}_n\}$, $n = 1, \dots, N_c$, consisting of N_c complex-valued symbols

$$\underline{R}_n = \frac{1}{\sqrt{N_c}} \sum_{\nu=1}^{N_c} \underline{y}_\nu e^{-j2\pi(n-1)(\nu-1)/N_c}, \quad n = 1, \dots, N_c. \quad (3.12)$$

Since ICI can be avoided due to the guard interval, each subchannel can be considered separately. When, furthermore, assuming that the fading on each subchannel is flat and ISI is

removed, a received symbol \underline{R}_n is obtained from the frequency domain representation according to

$$\underline{R}_n = \underline{H}_n \underline{S}_n + \underline{N}_n, \quad n = 1, \dots, N_c, \quad (3.13)$$

where \underline{H}_n is the flat fading factor of the n th subcarrier and \underline{N}_n represents the AWGN of the n th subcarrier. The flat fading factor \underline{H}_n is the sample of the channel transfer function $\underline{H}_{n,i}$ according to (2.26) at the n th subcarrier. The time index i is omitted for simplicity, as mentioned at the beginning of this section. The real and the imaginary parts of the noise components \underline{N}_n , $n = 1, \dots, N_c$, are assumed to be statistically independent, Gaussian distributed random variables with zero-mean and equal variance. The variance of the noise is given by

$$\sigma^2 = E\{|\underline{N}_n|^2\}, \quad n = 1, \dots, N_c. \quad (3.14)$$

With the assumptions made in (3.13), the MC transmission system shown in Fig. 3.2 can be viewed as a discrete-time and -frequency transmission system with a set of N_c parallel Gaussian channels with different complex-valued attenuations according to Fig. 3.3.

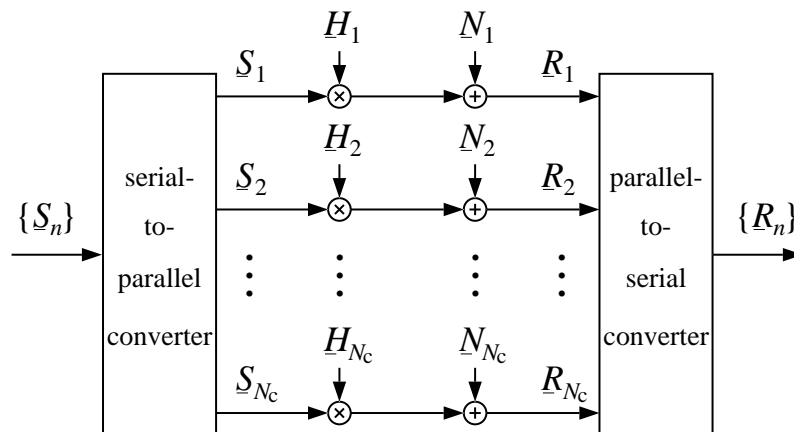


Figure 3.3: Simplified MC transmission system based on OFDM

The time/frequency representation of an OFDM symbol used in this thesis is shown in Fig. 3.4 a). A block of subsequent OFDM symbols, where the information transmitted within this OFDM symbols belongs together, e.g., due to coding and/or spreading in time and frequency direction, is referred to as an OFDM frame. An OFDM frame consisting of N_s OFDM symbols with frame duration

$$T_{\text{fr}} = N_s T'_s \quad (3.15)$$

is illustrated in Fig. 3.4 b). The time/frequency representation in Fig. 3.4 is obtained from the three-dimensional time/frequency/power density representation introduced in Section 1.2 by omitting the dimension of the power density.

In order to concisely describe OFDM and later on MC-CDMA, a matrix-vector notation is introduced. Vectors are represented by boldface small letters and matrices by boldface capital

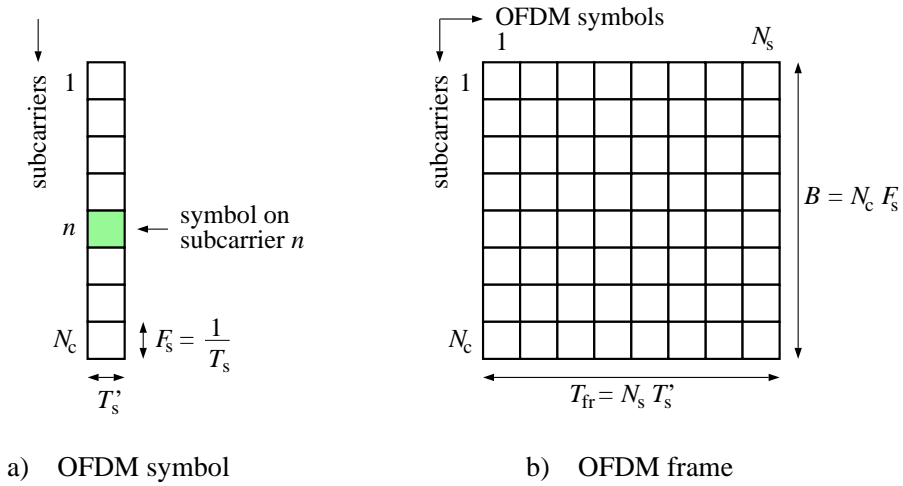


Figure 3.4: Time/frequency representation of an OFDM symbol and an OFDM frame

letters. The symbol $(\cdot)^T$ denotes the transposition of a vector or a matrix. The sequence $\{\underline{S}_n\}$, $n = 1, \dots, N_c$, of N_c source symbols transmitted in one OFDM symbol is represented by the vector

$$\underline{\mathbf{s}} = (\underline{S}_1, \underline{S}_2, \dots, \underline{S}_{N_c})^T \quad (3.16)$$

and the assigned received sequence $\{\underline{R}_n\}$, $n = 1, \dots, N_c$, obtained after inverse OFDM is given by the vector

$$\underline{\mathbf{r}} = (\underline{R}_1, \underline{R}_2, \dots, \underline{R}_{N_c})^T. \quad (3.17)$$

With these notations, the received vector $\underline{\mathbf{r}}$ is obtained from

$$\underline{\mathbf{r}} = \underline{\mathbf{H}}\underline{\mathbf{s}} + \underline{\mathbf{n}}, \quad (3.18)$$

where the $N_c \times N_c$ channel matrix

$$\underline{\mathbf{H}} = \begin{pmatrix} \underline{H}_1 & 0 & \cdots & 0 \\ 0 & \underline{H}_2 & & 0 \\ \vdots & & \ddots & \vdots \\ 0 & 0 & \cdots & \underline{H}_{N_c} \end{pmatrix} \quad (3.19)$$

is of diagonal type due to the absence of ICI. The diagonal components of $\underline{\mathbf{H}}$ are the complex-valued flat fading coefficients \underline{H}_n , $n = 1, \dots, N_c$. The vector

$$\underline{\mathbf{n}} = (\underline{N}_1, \underline{N}_2, \dots, \underline{N}_{N_c})^T \quad (3.20)$$

represents the AWGN on the N_c subcarriers. Furthermore, the sequence $\{\underline{x}_\nu\}$, $\nu = 1 - L_g, \dots, N_c$, of an OFDM symbol including the guard interval at the output of the MC modulator is given by the vector

$$\underline{\mathbf{x}} = (\underline{x}_{1-L_g}, \underline{x}_{2-L_g}, \dots, \underline{x}_{N_c})^T \quad (3.21)$$

and is the IDFT of the vector $\underline{\mathbf{s}}$, cf. (3.10). The received sequence $\{y_\nu\}$, $\nu = 1 - L_g, \dots, N_c$, at the input of the MC demodulator including the guard interval is represented by the vector

$$\underline{\mathbf{y}} = (y_{1-L_g}, y_{2-L_g}, \dots, y_{N_c})^T. \quad (3.22)$$

The vector $\underline{\mathbf{r}}$ given by (3.18) is the DFT of the vector $\underline{\mathbf{y}}$ without guard interval, cf. (3.12).

The motivation for the use of OFDM in mobile radio applications is the possibility of realizing bandwidth-efficient systems with simple receivers. The necessary equalization in multipath channels can simply be realized by one complex-valued multiplication per subcarrier, treated in detail in Section 3.3. However, the following effects which may more or less degrade the system performance have to be taken into account when applying OFDM:

- The energy of a transmitted OFDM symbol increases due to the cyclically extended guard interval. The loss in energy in dB due to the guard interval is

$$V_{\text{guard}} = 10 \log_{10} \left(\frac{T_g}{T_s} + 1 \right). \quad (3.23)$$

Even if the guard interval is in the order of 20% of the total OFDM symbol duration T'_s , the loss V_{guard} is less than 1 dB. In this case, the loss in data rate due to the guard interval is 20%. However, single carrier systems have a similar loss in data rate due to pulse shaping with filter roll-offs of finite steepness. Thus, with respect to the ICI- and ISI-free data detection, the guard interval seems to be a good investment [ViF95, OrM97].

- An accurate frequency and time synchronization is required in MC systems [CIM94, PoM95, Rob97]. The investigation of synchronization errors in MC-CDMA mobile radio systems is not part of this work and the reader is referred to [ToK96a, ToK96b]. Time and frequency synchronization are assumed to be perfect within this thesis.
- The effect of phase noise caused by the imperfections of the transmitter and receiver oscillators substantially influence the system performance [RoK95, SSR95]. The influence of phase noise on the performance of MC-CDMA mobile radio systems is investigated in [ToK96a, StM97] and is not in the scope of this thesis.
- An OFDM symbol $\underline{x}(t)$ is the sum of many independently modulated sinewaves and its envelope has an almost Gaussian distribution. This yields high peak-to-average power ratios and high demands on linear amplifiers. Nonlinearities in the amplifiers may cause ICI and if the amplifiers are not adapted with proper output backoff, the clipping distortion may cause severe performance degradations [SSR95, BCF96]. Possible counter-measures are predistortion of the transmitted signal with a complementary nonlinearity [Bin90] or, when considering MC-CDMA systems, an approach is to design spreading codes resulting in reduced dynamic ranges [AuF96]. Within this thesis, the amplifiers in the MC-CDMA mobile radio system are assumed to be linear and adapted with appropriate output backoff.

3.1.2 Principle of MC-FDMA, MC-TDMA, and MC-CDMA

The advantages of combining the multiple access schemes FDMA, TDMA, and DS-CDMA with MC modulation were discussed in Section 1.2.2. The principle of the arising MC-FDMA, MC-TDMA, and MC-CDMA schemes is depicted in Fig. 3.5 a), b), and c), respectively, for the case of two active users. In the case of MC-FDMA, one or several subcarriers are exclusively

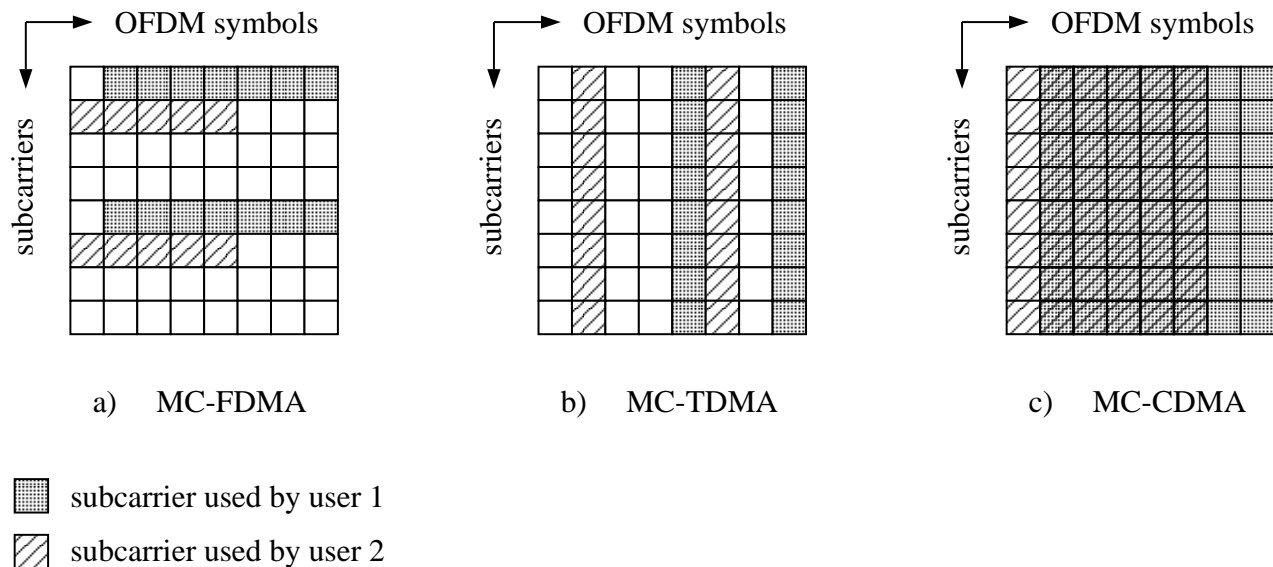


Figure 3.5: Multiple access schemes based on MC modulation; two active users

allocated to a user for transmission. In the case of MC-TDMA, the whole transmission bandwidth is exclusively allocated to a single user for a certain number of OFDM symbols. Thus, MC-FDMA and MC-TDMA can completely avoid MAI, ISI, and ICI. Assuming that adjacent source symbols are affected by fading independently to each other due to perfect interleaving, the performance of MC-FDMA and MC-TDMA systems or any hybrid combination of both is similar [Kai96]. With MC-CDMA different users share the same frequency band, i.e., the same subcarriers, at the same time. Hence, an MC-CDMA system has to cope with MAI and, thus, may perform quite differently from MC-FDMA and MC-TDMA systems. The performance of an uncoded and coded MC-FDMA and MC-TDMA system, respectively, with perfect interleaving is chosen as reference for the evaluation of the presented MC-CDMA system. In the next section the signal structure of MC-CDMA is introduced in detail.

3.2 MC-CDMA Signal Structure

The fundamentals of data symbol spreading with MC-CDMA introduced in Section 1.2.2 are pointed out in the three-dimensional time/frequency/power density representation of Fig. 1.4. The essential difference of data symbol spreading with MC-CDMA and data symbol spreading

with DS-CDMA is visualized in the comparison of Figs. 1.2 and 1.4. DS-CDMA signals are characterized by their multiple repetition of each data symbol due to the multiplication with the high rate spreading code in the time domain, where, in contrast, MC-CDMA signals are characterized by their multiple repetition of each data symbol due to the multiplication with a high rate spreading code in the frequency domain. Moreover, a DS-CDMA signal is typically designed to transmit the data modulated chips of a spreading code on adjacent time slots, whereas, an MC-CDMA signal transmits the data modulated chips of a spreading code on not necessarily neighbouring subcarriers, increasing the flexibility of the system. In this section, the MC-CDMA signal structure is described and the flexibility due to the spreading code structure in the frequency domain is pointed out. The number of simultaneously active users in the MC-CDMA mobile radio system is K . Values and functions related to the k th user, where k may take on the values $1, \dots, K$, are marked by an index (k) . All statements for values and functions with the index (k) are valid for each $k, k = 1, \dots, K$.

The generation of an MC spread spectrum signal is illustrated in Fig. 3.6 and is applicable on the transmitter side in both the up- and the down-link. The serial concatenation of DS

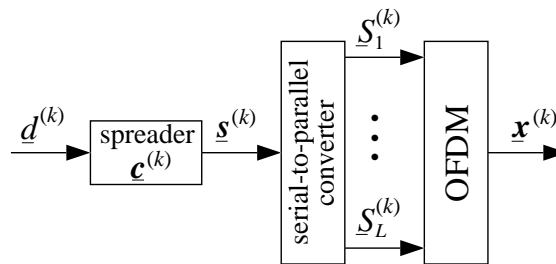


Figure 3.6: MC spread spectrum signal generation

spreading, cf. Fig. 1.2, and MC modulation, cf. Fig. 1.3, is shown, however, the equivalent realization illustrated in Fig. 1.4 is also applicable. The transmission of a complex-valued data symbol $\underline{d}^{(k)}$ of the k th user is shown in Fig. 3.6. The data symbol $\underline{d}^{(k)}$ to be transmitted over the radio channel is taken from the complex data symbol alphabet

$$V_d = \{v_{d,1}, v_{d,2}, \dots, v_{d,M_d}\} \quad (3.24)$$

of size M_d . The data symbol $\underline{d}^{(k)}$ is obtained after symbol mapping, where $\log_2(M_d)$ data bits are mapped into a complex-valued data symbol $\underline{d}^{(k)}$ [Pro95]. The data symbol rate is $1/T_d$. For brevity, but without loss of generality, the MC-CDMA signal generation is described for a single data symbol per user as far as possible, by omitting an otherwise necessary data symbol index. In the transmitter, the data symbol $\underline{d}^{(k)}$ is multiplied and, thus, marked with the user specific spreading code

$$\underline{\mathbf{c}}^{(k)} = (\underline{C}_1^{(k)}, \underline{C}_2^{(k)}, \dots, \underline{C}_L^{(k)})^T \quad (3.25)$$

of the k th user. The chips $\underline{C}_l^{(k)}, l = 1, \dots, L$, are taken from the complex chip alphabet

$$V_c = \{v_{c,1}, v_{c,2}, \dots, v_{c,M_s}\} \quad (3.26)$$

of size M_s , where M_s is not necessarily equal to M_d . The chip rate of the serial spreading code $\mathbf{c}^{(k)}$ before serial-to-parallel conversion is

$$\frac{1}{T_c} = \frac{L}{T_d} \quad (3.27)$$

and is L times higher than the data symbol rate $1/T_d$. The complex-valued sequence obtained from the multiplication of a data symbol $\underline{d}^{(k)} \in \mathcal{V}_d$, cf. (3.24), with the assigned spreading code $\mathbf{c}^{(k)}$ is given by the vector

$$\mathbf{s}^{(k)} = \underline{d}^{(k)} \mathbf{c}^{(k)} = (\underline{S}_1^{(k)}, \underline{S}_2^{(k)}, \dots, \underline{S}_L^{(k)})^T. \quad (3.28)$$

The rate of the components $\underline{S}_l^{(k)}$, $l = 1, \dots, L$, before serial-to-parallel conversion is $1/T_c$. It should be noted that the transmission of $\mathbf{s}^{(k)}$ with single-carrier modulation conforms with the principle of DS spread spectrum according to Fig. 1.2. An MC-CDMA signal is obtained after modulating the components $\underline{S}_l^{(k)}$, $l = 1, \dots, L$, in parallel onto L subcarriers according to (3.10) [FaP93, YLF93, CBJ93]. Thus, each data symbol $\underline{d}^{(k)}$ is spread over L subcarriers. The duration of an MC modulated component $\underline{S}_l^{(k)}$, $l = 1, \dots, L$, is equal to the OFDM symbol duration, which, including the guard interval, is

$$T'_s = T_g + N_c T_c. \quad (3.29)$$

The transmission of one data symbol per user per OFDM symbol requires

$$N_c = L \quad (3.30)$$

subcarriers. In this case, the OFDM symbol duration including the guard interval is

$$T'_s = T_g + T_d. \quad (3.31)$$

An MC-CDMA system designed for the transmission of one data symbol per user per OFDM symbol is referred to as a basic MC-CDMA system in the following. When applying orthogonal spreading codes $\mathbf{c}^{(k)}$ like Walsh-Hadamard codes, the maximum number of active users K_{\max} in the basic MC-CDMA system corresponds to the spreading code length L , i.e.,

$$K_{\max} = L. \quad (3.32)$$

With fully loaded basic MC-CDMA system according to (3.32) and taking into account that K_{\max} is upper bounded by the receiver complexity, the number of subcarriers N_c is also upper bounded by K_{\max} , cf. (3.32) and (3.30). To support large numbers of users while having a low receiver complexity and, furthermore, to use MC-CDMA systems with a sufficiently large number of subcarriers to guarantee flat fading per subchannel, modifications of the basic MC-CDMA system are necessary [FaP93, Faz93]. In the following, appropriate modifications of the basic MC-CDMA system are introduced and explained for the downlink of a mobile radio system. The downlink is chosen, since this scenario enables a better illustration of the modifications than the uplink. It has to be mentioned that this modifications are also suitable in the uplink of an MC-CDMA mobile radio system.

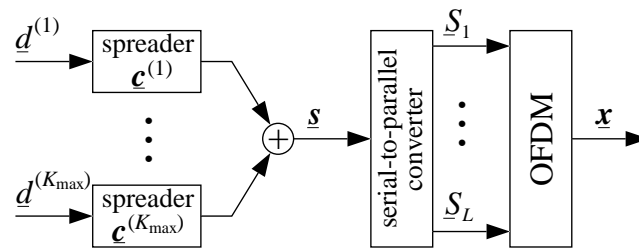


Figure 3.7: Basic MC-CDMA transmitter for the downlink; BS with $K_{\max} = L$ active users and $N_c = L$ subcarriers

Generally, when considering the downlink of an MC-CDMA system, it is computationally efficient to add the signals of the K users in the transmitter before serial-to-parallel conversion, as depicted in Fig. 3.7 for a basic MC-CDMA transmitter. Thus, OFDM has to be carried out only once per OFDM symbol for all users. The case with the maximum number of active users, i.e., with a fully loaded system, is shown with the intention to straightforwardly derive the MC-CDMA system modifications. The data symbol and, thus, chip synchronous superposition of the K_{\max} vectors $\underline{s}^{(k)}$, $k = 1, \dots, K_{\max}$, yields the vector

$$\underline{s} = \sum_{k=1}^{K_{\max}} \underline{s}^{(k)} = (S_1, S_2, \dots, S_L)^T. \quad (3.33)$$

The three MC-CDMA system modifications presented in the following are in this thesis referred to as M -Modification, Q -Modification, and $M\&Q$ -Modification. The M -Modification and the Q -Modification are introduced as basic components of the $M\&Q$ -Modification. An MC-CDMA system with $M\&Q$ -Modification correspond to the MC-CDMA system concept considered in [FaP93, Faz93]. Since the M -Modification and the Q -Modification are independent from each other, they can be applied individually also.

M -Modification: The intention of the M -Modification is to increase the number of subcarriers while maintaining constant the spreading code length and the maximum number of active users. Consequently, the OFDM symbol duration increases and the loss in bandwidth efficiency due to the guard interval decreases. Moreover, the tighter subcarrier spacing enables one to guarantee flat fading per subchannel in propagation scenarios with decreased coherence bandwidth. With the M -Modification, each user transmits simultaneously M greater than 1 data symbols per OFDM symbol. The total number of subcarriers of the modified MC-CDMA system is

$$N_c = ML. \quad (3.34)$$

Each user exploits the total of N_c subcarriers for data transmission. The OFDM symbol duration including the guard interval increases to

$$T'_s = T_g + MLT_c, \quad (3.35)$$

where it can be observed that the loss in bandwidth efficiency due to the guard interval decreases with increasing M . The maximum number of active users is still defined according to

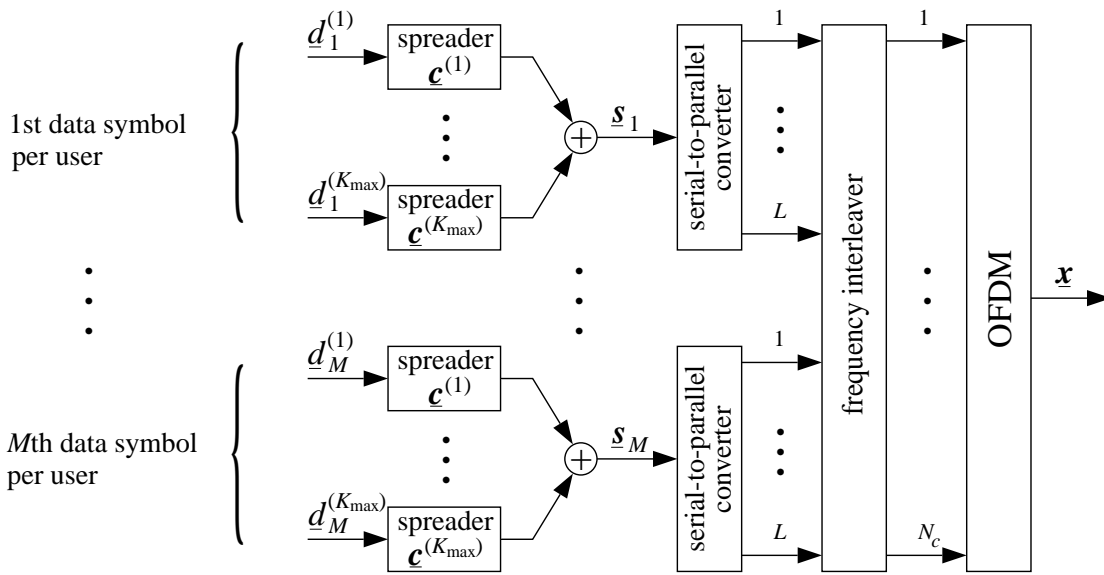


Figure 3.8: *M*-Modification: MC-CDMA transmitter with simultaneous transmission of *M* data symbols per user and OFDM symbol; BS with $K_{\max} = L$ active users and $N_c = ML$ subcarriers

(3.32). The assigned MC-CDMA transmitter is shown in Fig. 3.8. The data symbol index m , $m = 1, \dots, M$, is introduced in Fig. 3.8 to distinguish the M simultaneously transmitted data symbols $d_m^{(k)}$, $m = 1, \dots, M$, of the k th user. The number M is upper limited by the coherence time $(\Delta t)_c$ of the channel, cf. (2.13), since the symbol duration T'_s , which increases with increasing M , has to be smaller than $(\Delta t)_c$ to guarantee that the channel is time-invariant during one OFDM symbol duration.

To optimally exploit frequency diversity, the components of the sequences \mathbf{s}_m , $m = 1, \dots, M$, transmitted in the same OFDM symbol are interleaved over the frequency. Subcarriers used for the transmission of \mathbf{s}_m should have a spacing greater than the coherence bandwidth of the channel. Thus, the components of one sequence \mathbf{s}_m are affected independently, reducing the probability that \mathbf{s}_m is completely located in a deep fade. The interleaving is carried out prior to OFDM. The frequency interleaver can be a block interleaver which guarantees the maximum frequency separation between the components of \mathbf{s}_m . However, due to a possible periodicity of the fading process in frequency, the block interleaver can fail if the periodicity is similar to the frequency separation between adjacent components. This effect can be reduced if a pseudo-random frequency interleaver is used.

Q-Modification: The intention of the *Q*-Modification is to reduce the receiver complexity by reducing the spreading code length per user, while maintaining constant the maximum number of active users and the number of subcarriers. The complexity of an MC-CDMA receiver with SD increases with increasing spreading code length L . In the case of MD, the complexity of an MC-CDMA receiver increases with both increasing spreading code length L and increasing number of active users K . If, for instance, JD with MLSE should be applied in the receiver,

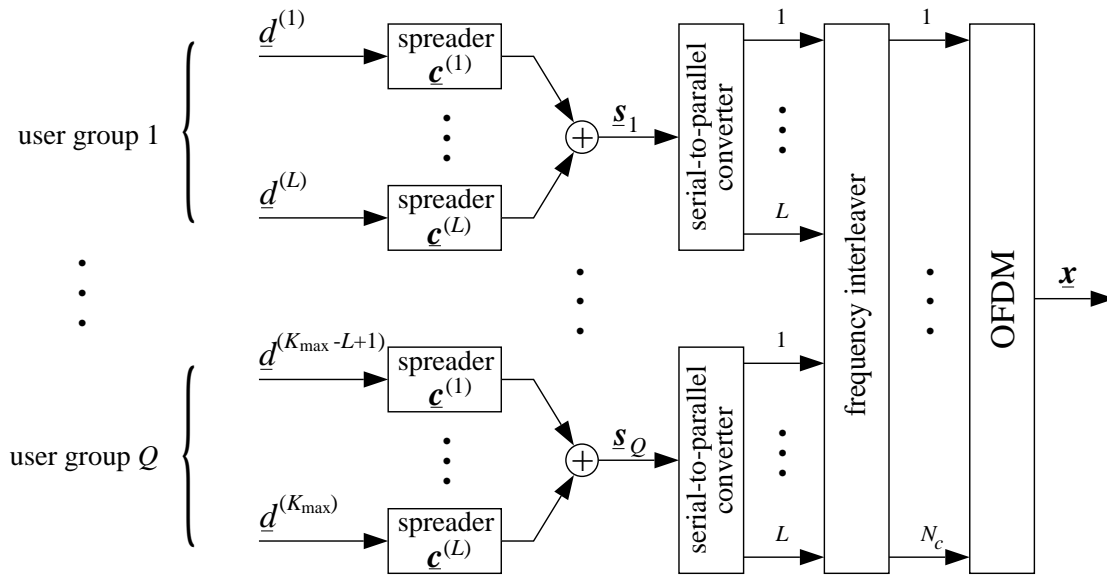


Figure 3.9: Q -Modification: MC-CDMA transmitter with Q independent user groups; BS with $K_{\max} = QL$ active users and $N_c = QL$ subcarriers

the number of simultaneously active users is limited to K less than 10 due to computational complexity [Pro95]. To keep the complexity of the receiver to an acceptable level by nevertheless allowing large numbers of active users, the basic MC-CDMA transmitter has to be modified as depicted in Fig. 3.9. The users are subdivided in Q independent user groups, where each user group q , $q = 1, \dots, Q$, exploits its own L subcarriers within its subsystem. The Q -Modification introduces an additional FDMA component on subcarrier level in the transmission scheme, resulting in a hybrid MC-CDMA mobile radio system. A single subsystem is comparable to the basic MC-CDMA transmitter illustrated in Fig. 3.7. The number of active users in the q th subsystem is K_q and the maximum number of active users in the q th subsystem is

$$K_{q,\max} = L \quad (3.36)$$

The total number of simultaneously active users in the MC-CDMA system is

$$K = \sum_{q=1}^Q K_q, \quad (3.37)$$

and the maximum number of active users results in

$$K_{\max} = \sum_{q=1}^Q K_{q,\max} = QL. \quad (3.38)$$

While maintaining the maximum number of supplied users constant, the required spreading code length decreases proportional to Q . This enables a significant reduction of the receiver complexity, since in the receiver, only the data symbols of the assigned subsystem have to be detected. The number of subcarriers of the modified scheme is

$$N_c = QL, \quad (3.39)$$

where each user only exploits a subset of L subcarriers for data transmission due to the FDMA component introduced by the Q -Modification. To nevertheless optimally exploit the frequency diversity of the channel, the components of the spread sequences \mathbf{s}_q , $q = 1, \dots, Q$, are interleaved over the frequency, comparable to the frequency interleaving applied with the M -Modification. The OFDM symbol duration including the guard interval is

$$T'_s = T_g + QLT_c. \quad (3.40)$$

It has to be mentioned that only one set of L orthogonal spreading codes of length L is required within the whole MC-CDMA system. This set of spreading codes is used in each subsystem, cf. Fig. 3.9.

$M\&Q$ -Modification: The $M\&Q$ -Modification is a combination of the M - and the Q -Modification, resulting in an MC-CDMA system with adjustable number of subcarriers and receiver complexity, keeping constant the maximum number of active users. The transmission of M data symbols per user and, additionally, the splitting of the users in Q independent user groups according to the $M\&Q$ -Modification is illustrated in Fig. 3.10. The total number of subcarriers used by the MC-CDMA system with $M\&Q$ -Modification is

$$N_c = QML, \quad (3.41)$$

where each user only exploits a subset of ML subcarriers for data transmission due to the FDMA component introduced by the Q -Modification. The maximum number of active users is given by (3.38). The total OFDM symbol duration including the guard interval results with the $M\&Q$ -Modification in

$$T'_s = T_g + QMLT_c. \quad (3.42)$$

A frequency interleaver scrambles the information of all subsystems prior OFDM to guarantee an optimum exploitation of the frequency diversity offered by the mobile radio channel.

As mentioned before, the Q -, the M -, and the $M\&Q$ -Modifications are also suitable for the uplink of an MC-CDMA mobile radio system. For the Q - and $M\&Q$ -Modification in the uplink only the inputs of the frequency interleaver of the user group of interest are connected in the transmitter, all other inputs are set to zero.

Finally, it has to be noted that an MC-CDMA system with its basic implementation or with any of the three modifications presented in this section supports an additional TDMA component in the up- and in the downlink, since the transmission is synchronized on OFDM symbols [KaH97a]. The additional flexibility due to a TDMA component in an MC-CDMA system is exploited in the system design presented in Chapter 6.

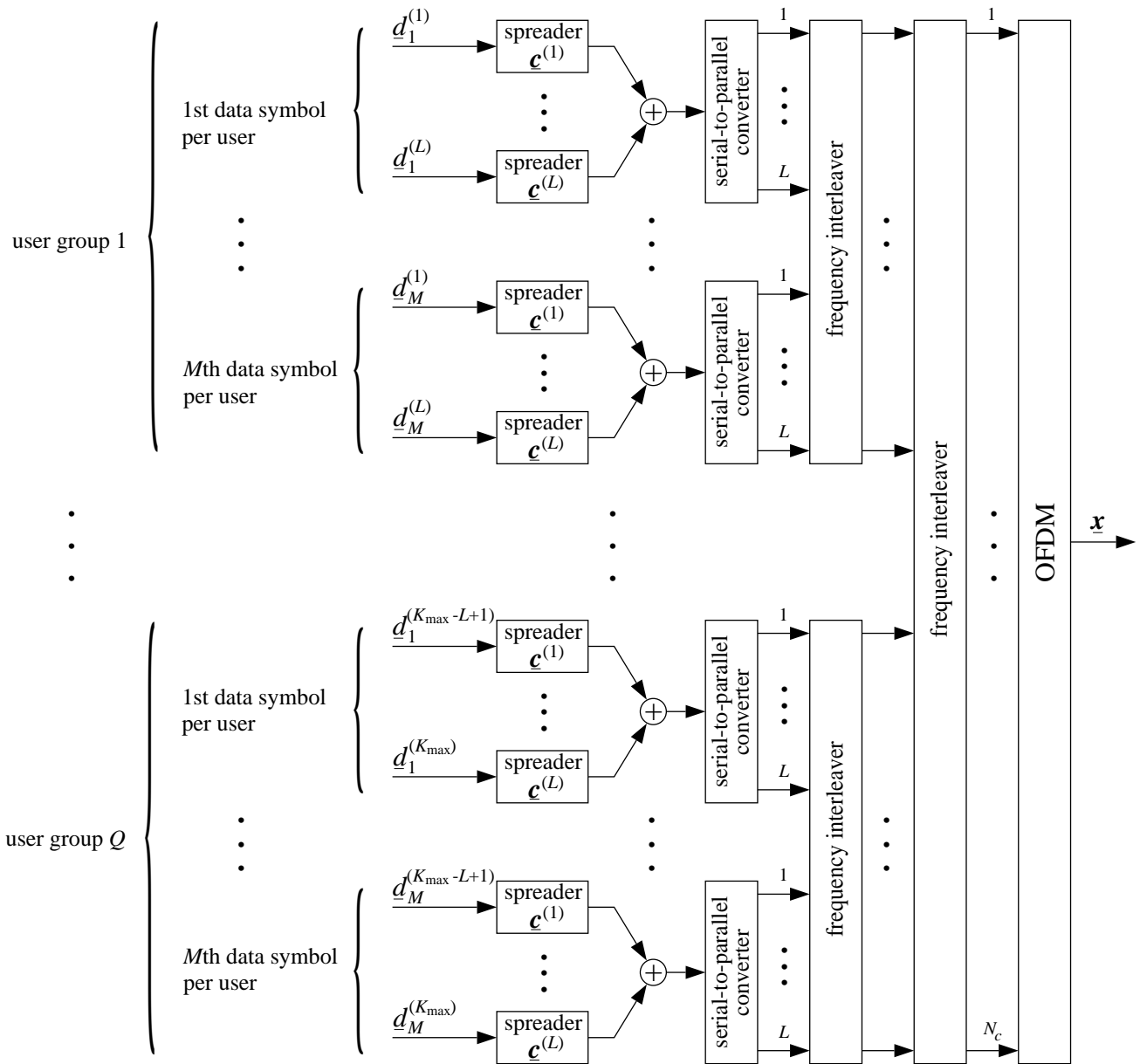


Figure 3.10: $M \& Q$ -Modification: MC-CDMA transmitter with Q independent user groups and simultaneous transmission of M data symbols per user and OFDM symbol; BS with $K_{\max} = QL$ active users and $N_c = QML$ subcarriers

3.3 MC-CDMA Data Detection Techniques

3.3.1 Introduction

The MC-CDMA signal structure introduced in the previous section enables the realization of powerful receivers with low complexity due to the avoidance of ISI and ICI in the detection process. This advantage can be exploited in the up- and in the downlink of a mobile radio system. However, especially in the downlink, the requirements with respect to weight, size, and cost and, therefore, to low complexity while still guaranteeing high bandwidth and power efficiency are more severe for the mobile receiver than for the BS. In the BS more complex receivers are tolerable. This thesis mainly focuses on the high demands on the mobile receiver in the downlink and presents in this section data detection techniques especially designed for the downlink. An appropriate uplink concept employing MC modulation in combination with the spread spectrum technique is presented and investigated in Appendix B.

The data detection considered in the sequel includes all components such as equalizer, quantizer, etc., which are necessary to get a hard or a soft decided value about the transmitted data symbol. The investigated combining techniques MRC and EGC, which combine the received signal components but not try to equalize the received signal, are also part of the data detection. The data detection techniques analyzed in this section are suitable for MC-CDMA mobile radio systems with any of the modifications presented in the previous section. Since the data detection between the different subsystems is independent from each other and since due to frequency interleaving the performance in all subsystems is similar, it is sufficient to focus on the data detection in one arbitrary subsystem. The mobile MC-CDMA receiver with SD or MD, respectively, for the data of the k th user transmitted in one subsystem is depicted in Fig. 3.11.

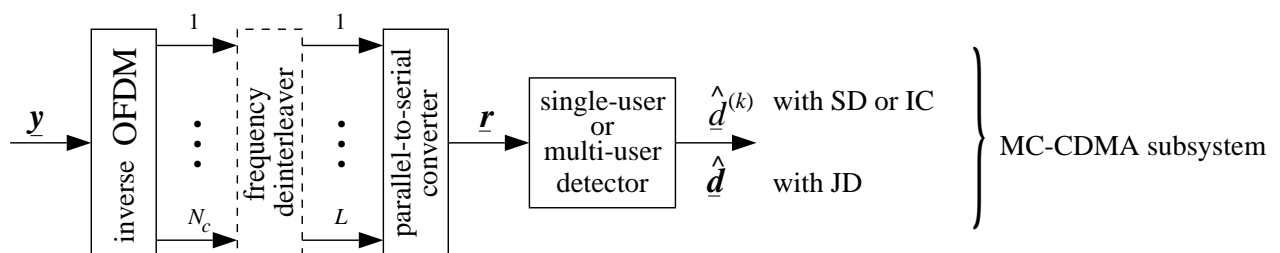


Figure 3.11: MC-CDMA receiver with data detection of the k th user in one subsystem

The relation between the number of subcarriers N_c and the spreading code length L depends on whether the basic MC-CDMA system, cf. (3.30), or a modified MC-CDMA system, cf. (3.34), (3.39), and (3.41), respectively, is considered.

In the following, the data symbol and user group indices m , $m = 1, \dots, M$, and q , $q = 1, \dots, Q$, respectively, are omitted for brevity. Only the notation of the number of users in a subsystem

K_q and $K_{q,\max}$, respectively, is further used with the purpose of emphasizing that the total number of users K and K_{\max} , respectively, of the whole MC-CDMA system is in general much higher than K_q and $K_{q,\max}$, respectively. Moreover, equations defined with the variable K_q instead of K are valid for systems with and without Q -Modification.

The received sequence given by the vector \mathbf{y} , cf. (3.22), yields in the basic MC-CDMA receiver after inverse OFDM the vector \mathbf{r} defined according to (3.18). If either the M -, the Q -, or the $M\&Q$ -Modification is used, an additional frequency deinterleaver is applied after inverse OFDM. At the output of the frequency deinterleaver the vector

$$\mathbf{r} = \mathbf{H}\mathbf{s} + \mathbf{n} = (\underline{R}_1, \underline{R}_2, \dots, \underline{R}_L)^T, \quad (3.43)$$

assigned to one MC-CDMA subsystem, is obtained. The transmitted vector \mathbf{s} , the received vector \mathbf{r} , the channel matrix \mathbf{H} , and the noise vector \mathbf{n} correspond to (3.16), (3.17), (3.19), and (3.20), respectively, except for the subcarrier index n , $n = 1, \dots, N_c$, which is exchanged by the spreading code index l , $l = 1, \dots, L$, since in a modified MC-CDMA system \mathbf{s} is transmitted only on a subset of the N_c subcarriers. The components of the channel matrix \mathbf{H} and of the noise vector \mathbf{n} in (3.43) represent the fading and noise, respectively, of the subcarriers where \mathbf{s} was transmitted on. Hence, if frequency interleaving is applied, it is taken into account in (3.43). The vector \mathbf{r} is processed in the data detector. The purpose of data detection is to get an estimate of the transmitted data symbol $\underline{d}^{(k)}$ of the k th user. The estimate obtained after data detection can be a soft decided value or a hard decided value. This section evaluates SD and MD techniques in an uncoded MC-CDMA system and focuses on hard decided values. In Chapter 4, the optimum soft decided value of $\underline{d}^{(k)}$ is derived for MC-CDMA systems with channel coding exploiting soft decision decoding.

With SD or MD applying IC, a hard decided value $\hat{\underline{d}}^{(k)}$ for the transmitted data symbol $\underline{d}^{(k)}$ of the k th user is obtained at the output of the data detector.

With MD applying JD, additionally the data symbol vector

$$\mathbf{d} = (\underline{d}^{(1)}, \underline{d}^{(2)}, \dots, \underline{d}^{(K_q)})^T \quad (3.44)$$

is introduced, representing the data symbols of the K_q users, simultaneously transmitted per OFDM symbol in one subsystem. Furthermore, the $L \times K_q$ spreading code matrix containing the spreading codes of the K_q users is defined as

$$\mathbf{C} = (\underline{c}^{(1)} \ \underline{c}^{(2)} \ \dots \ \underline{c}^{(K_q)}) = \begin{pmatrix} \underline{C}_1^{(1)} & \underline{C}_1^{(2)} & \dots & \underline{C}_1^{(K_q)} \\ \underline{C}_2^{(1)} & \underline{C}_2^{(2)} & & \underline{C}_2^{(K_q)} \\ \vdots & & \ddots & \vdots \\ \underline{C}_L^{(1)} & \underline{C}_L^{(2)} & \dots & \underline{C}_L^{(K_q)} \end{pmatrix}, \quad (3.45)$$

where in the case of orthogonal spreading codes, K_q is equal to or less than L . The transmission vector \mathbf{s} defined in (3.33) can be rewritten as

$$\mathbf{s} = \mathbf{C}\mathbf{d} = (\underline{S}_1, \underline{S}_2, \dots, \underline{S}_L)^T. \quad (3.46)$$

The K_q hard decided values obtained with JD in one detection step are given by the vector

$$\hat{\mathbf{d}} = (\hat{d}^{(1)}, \hat{d}^{(2)}, \dots, \hat{d}^{(K_q)})^T. \quad (3.47)$$

The average SNR per subcarrier at the input of the receiver is defined as

$$\gamma_c = \frac{\mathbb{E}\{|H_l \underline{S}_l|^2\}}{\sigma^2}, \quad (3.48)$$

where H_l represents the sample of the channel transfer function $H_{n,i}$ according to (2.26) at the subcarrier where \underline{S}_l was transmitted on. The time index i is omitted for brevity, as mentioned in Section 3.1.1. In the case of frequency interleaving, the index l and the index n are related by the interleaving function. In the basic MC-CDMA system without frequency interleaving, l is equal to n . Moreover, σ^2 is the variance of the noise according to (3.14). When assuming that the channel is power normalized, i.e.,

$$\mathbb{E}\{|H_l|^2\} = 1, \quad (3.49)$$

and H_l is statistically independent of \underline{S}_l for all l , the average SNR per subcarrier results in

$$\gamma_c = \frac{\mathbb{E}\{|\underline{S}_l|^2\}}{\sigma^2} \Big|_{\mathbb{E}\{|H_l|^2\}=1}. \quad (3.50)$$

In this thesis, it is assumed that in the downlink the data symbols of all users have the same average energy or, correspondingly, have the same second moment $\mathbb{E}\{|\underline{d}^{(k)}|^2\}$ per user. Hence, the SNR per data symbol γ_s is related to the SNR per subcarrier γ_c by

$$\gamma_s = \frac{L \gamma_c}{K_q} = \frac{\mathbb{E}\{|\underline{d}^{(k)}|^2\}}{\sigma^2} \Big|_{\mathbb{E}\{|H_l|^2\}=1}. \quad (3.51)$$

The average SNR per subcarrier γ_c is the L th fraction of γ_s due to the spreading of $\underline{d}^{(k)}$ over L subcarriers, multiplied with K_q since the signals of K_q users superpose. The average SNR per source bit γ_b is related to the average SNR per data symbol γ_s by

$$\gamma_b = \frac{\gamma_s}{R \log_2 M_d}, \quad (3.52)$$

where R is the channel code rate. The channel code rate R is defined as the ratio

$$R = \frac{L_a}{L_b}, \quad (3.53)$$

where L_a is the number of source bits and L_b is the number of resulting code bits at the output of the channel encoder. In the uncoded case R is equal to 1.

Information about the SNR at the input of the receiver is required for some detection techniques, for the computation of log-likelihood ratios when applying soft decision decoding, and for channel estimation. The SNR can be estimated with the pilot symbols transmitted for channel estimation and synchronization and by transmitting a null-symbol [FKR95], i.e., an OFDM symbol without signal energy, for instance at the beginning of each OFDM frame. In this thesis, the knowledge about the SNR in the receiver is assumed to be perfect.

3.3.2 Single-User Detection

The approach with SD detects the user signal of interest by not taking into account any information about the MAI. A scheme with SD of the data symbols of the k th user is shown in Fig. 3.12. After inverse OFDM and frequency deinterleaving, the received sequence \mathbf{r} , cf. (3.43),

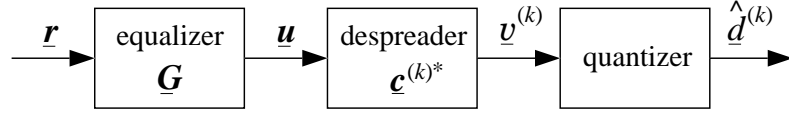


Figure 3.12: SD scheme

is equalized by employing a bank of adaptive one tap equalizers to combat the phase and amplitude distortions caused by the mobile radio channel on the subcarriers. The one tap equalizer is simply realized by one complex-valued multiplication per subcarrier. The term equalizer is generalized in the following, since the processing of the received vector \mathbf{r} according to typical diversity combining techniques is also investigated with the SD scheme shown in Fig. 3.12. The received sequence at the output of the equalizer has the form

$$\mathbf{u} = \mathbf{G} \mathbf{r} = (U_1, U_2, \dots, U_L)^T. \quad (3.54)$$

The diagonal equalizer matrix

$$\mathbf{G} = \begin{pmatrix} G_1 & 0 & \cdots & 0 \\ 0 & G_2 & & 0 \\ \vdots & & \ddots & \vdots \\ 0 & 0 & \cdots & G_L \end{pmatrix} \quad (3.55)$$

of dimension $L \times L$ represents the L complex-valued equalizer coefficients of the subcarriers where \mathbf{s} was transmitted on. The complex-valued output \mathbf{u} of the equalizer is despread by correlating it with the conjugate complex user specific spreading code $\mathbf{c}^{(k)*}$, cf. (3.25). The complex-valued soft decided value at the output of the despreader is

$$\underline{v}^{(k)} = \mathbf{c}^{(k)*} \mathbf{u}^T. \quad (3.56)$$

The hard decided value $\hat{d}^{(k)}$ of the detected data symbol is given by

$$\hat{d}^{(k)} = Q\{\underline{v}^{(k)}\}. \quad (3.57)$$

The quantization operation $Q\{\cdot\}$ assigns to each soft decided value $\underline{v}^{(k)}$ an element of the data symbol alphabet V_d , cf. (3.24).

With the assumptions made in (3.13), the uncoded MC-CDMA system with SD can be represented according to Fig. 3.13. In the case of the basic MC-CDMA implementation, the number

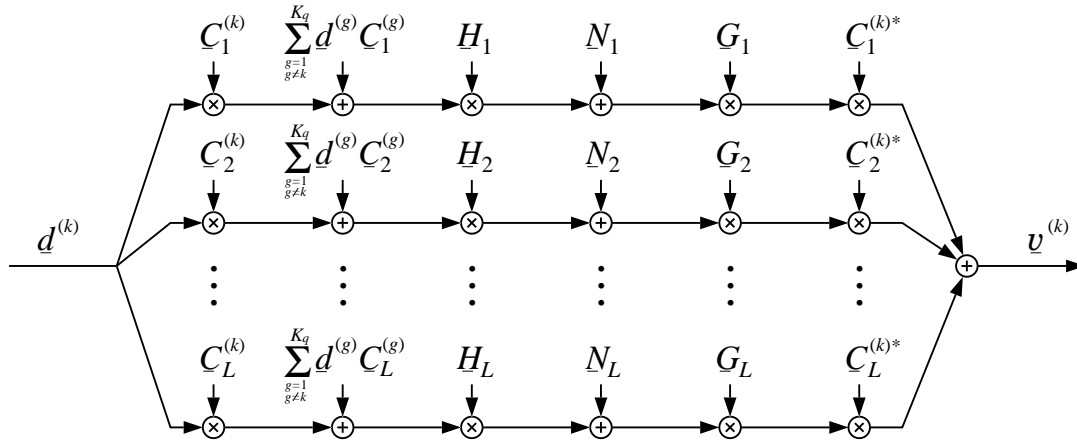


Figure 3.13: Simplified MC-CDMA system

of subcarriers N_c is equal to the spreading code length L in Fig. 3.13. If any of the modifications presented in Section 3.2 is used, only an MC-CDMA subsystem is shown in Fig. 3.13, and the total number of subcarriers N_c is greater than the spreading code length L . In the following, different strategies of selecting the equalizer coefficients G_l , $l = 1, \dots, L$, are presented, where all statements for values and functions with the index l are valid for each l , $l = 1, \dots, L$.

Maximum Ratio Combining (MRC): MRC is the optimum diversity combining technique with respect to the BER, if multiple replicas of the same information bearing signal, received over different diversity branches, are available at the receiver [Pro95, Stü96]. With MRC, the diversity branches are weighted by their respective conjugate complex channel coefficients, leading to

$$G_l = H_l^*. \quad (3.58)$$

The variance σ^2 of the noise per branch is assumed to be the same, cf. (3.14). MRC is only conditionally applicable as an MC-CDMA detection technique. The L components of $\mathbf{s}^{(k)}$ simultaneously transmitted on the L subcarriers contain the information of the same data symbol. However, each component of $\mathbf{s}^{(k)}$ is weighted with the assigned chip of the spreading code before transmission, to achieve orthogonality between the sequences $\mathbf{s}^{(k)}$, $k = 1, \dots, K_q$, which are simultaneously transmitted on the same subcarriers. This orthogonality is lost in the mobile radio channel by affecting the assigned subcarriers with different channel coefficients H_l , $l = 1, \dots, L$. Therefore, by applying MRC according to (3.58), the orthogonality between the spreading codes $\mathbf{c}^{(k)}$, $k = 1, \dots, K_q$, is further destroyed. Thus, MRC applied as MC-CDMA detection technique results in enhanced MAI. However, in the uplink where the user signals do not superimpose in an orthogonal fashion in a multipath channel, MRC is the most promising SD technique for MC-CDMA systems [YLF93].

In the single user case, MRC provides the best performance, since, due to the absence of MAI, the optimal diversity combining scenario is given. Thus, the BER with MRC for K_q equal to 1 is identical to the matched filter (MF) bound, which is the lower bound of the BER P_b of

any data detector [Pro95]. Based on this fact, it is shown in Section 3.3.3 that MRC may be of interest for the second and subsequent stages in a multistage detector based on IC, where after the first IC stage most of the MAI should be cancelled.

Equal Gain Combining (EGC): EGC is a diversity combining technique which, in contrast to MRC, weights all diversity branches, i.e. used subcarriers, with unit amplitude [Stü96]. With EGC, each branch is corrected in its phase by choosing

$$\underline{G}_l = \frac{\underline{H}_l^*}{|\underline{H}_l|}. \quad (3.59)$$

The MAI enhancement caused by (3.58) can be avoided with EGC.

Zero-Forcing (ZF) Equalization: ZF equalization, also known as orthogonality restoring combining (ORC) or channel inversion, can completely eliminate the MAI by restoring the orthogonality between the user specific spreading codes with an equalization coefficient chosen as

$$\underline{G}_l = \frac{1}{\underline{H}_l}, \quad (3.60)$$

corresponding to the inverse of the assigned channel coefficient [Pro95]. The drawback of ZF equalization is that for small amplitudes of \underline{H}_l the equalizer enhances the noise \underline{N}_l in such a way that the SNR γ_c may go to zero on some subcarriers.

Minimum Mean Square Error (MMSE) Equalization: Equalization according to the MMSE criterion minimizes the mean square value of the error

$$\varepsilon_l = \underline{S}_l - \underline{G}_l \underline{R}_l \quad (3.61)$$

between the transmitted signal and the output of the equalizer. The mean square error

$$J_l = \text{E}\{|\varepsilon_l|^2\} \quad (3.62)$$

can be minimized by applying the orthogonality principle [Pap91, PrM96], stating that the mean square error J_l is minimum if the equalizer coefficient \underline{G}_l is selected such that the error ε_l is orthogonal to the received signal \underline{R}_l^* , i.e.,

$$\text{E}\{\varepsilon_l \underline{R}_l^*\} = 0. \quad (3.63)$$

With (3.48), (3.61), and (3.63), the equalization coefficients based on the MMSE criterion result in

$$\underline{G}_l = \frac{\underline{H}_l^*}{|\underline{H}_l|^2 + 1/\gamma_c}. \quad (3.64)$$

The computation of the MMSE equalization coefficients requires an estimation of the actual SNR per subcarrier γ_c , cf. Section 3.3.1. For $\gamma_c \rightarrow \infty$, the MMSE equalizer is identical to the ZF equalizer.

Suboptimal MMSE Equalization: To overcome the additional complexity due to the estimation of γ_c with MMSE equalization, a low-complex suboptimal MMSE equalization can be realized [Kai95b]. With suboptimal MMSE equalization, the equalization coefficients are designed such that they perform optimally only in the most critical case at which successful transmission should be guaranteed. In the other cases, the coefficients are suboptimal since the information about the actual γ_c is not used in the equalizer. Thus, K_q is set equal to the upper bound L , cf. (3.36), and γ_c becomes equal to γ_s , cf. (3.51). The SNR γ_s is set equal to a threshold λ at which the optimal MMSE equalization guarantees the maximum acceptable BER. The equalization coefficient with suboptimal MMSE equalization results in

$$G_l = \frac{H_l^*}{|H_l|^2 + \lambda} \quad (3.65)$$

and requires only information about H_l . The value λ has to be determined by investigations carried out in advance.

Controlled Equalization: Controlled equalization, also referred to as threshold ORC (TORC) or smooth ORC (SORC), applies ZF equalization to avoid MAI only on a subcarrier where the amplitude of the channel coefficient H_l exceeds a predefined threshold a_{thresh} [YeL94a]. A subcarrier with a small fading amplitude, which may be dominated by a noise component, is set to a certain value ξ_l , with the intention of preventing strong noise amplification. Thus, the equalization coefficient is defined as

$$G_l = \begin{cases} \frac{1}{H_l} & \text{if } |H_l| \geq a_{\text{thresh}} \\ \xi_l & \text{if } |H_l| < a_{\text{thresh}} \end{cases} \quad (3.66)$$

In [YeL94a] it is proposed to neglect subcarriers with small amplitudes of the channel coefficients, yielding

$$\xi_l = 0. \quad (3.67)$$

An improvement is achievable when applying EGC on the strong faded subcarriers [Kai95b], so that the information on these subcarriers is not completely neglected, i.e.,

$$\xi_l = \frac{H_l^*}{|H_l|}. \quad (3.68)$$

A further improvement can be achieved by choosing

$$\xi_l = \frac{H_l^*}{|H_l| a_{\text{thresh}}} \quad (3.69)$$

as considered in [RoB96]. Common to all three variants of controlled equalization is that the threshold a_{thresh} depends on both the SNR γ_s and the number of active users K_q and that the optimum a_{thresh} has to be found by investigations carried out in advance.

3.3.3 Interference Cancellation

MD with IC is carried out iteratively in multiple detection stages. Values and functions related to the j th iteration are marked by an index $[j]$, where j may take on the values $1, \dots, J_{\text{it}}$, and J_{it} is the total number of iterations. The initial detection stage is indicated by the index $[0]$. A parallel IC realization is described in the sequel. Successive IC can easily be derived from parallel IC by only cancelling the contribution of the strongest interferer per detection stage.

In the initial detection stage, the data symbols of all K_q active users are detected in parallel by SD. That is,

$$\hat{\underline{d}}^{(k)[0]} = \mathbf{Q} \left\{ \underline{\mathbf{c}}^{(k)*} \underline{\mathbf{G}}^{[0]} \underline{\mathbf{r}}^{\text{T}} \right\}, \quad k = 1, \dots, K_q, \quad (3.70)$$

where $\underline{\mathbf{G}}^{[0]}$ and $\hat{\underline{d}}^{(k)[0]}$ denote the equalization coefficients and the detected data symbol of the k th user, respectively, assigned to the initial stage. The following detection stages work iteratively by using the decisions of the previous stage to reconstruct the interfering contribution in the received signal. The obtained interference is subtracted, i.e, cancelled from the received signal and the data detection is performed again with reduced MAI. Thus, the second and further detection stages apply

$$\hat{\underline{d}}^{(k)[j]} = \mathbf{Q} \left\{ \underline{\mathbf{c}}^{(k)*} \underline{\mathbf{G}}^{[j]} \left(\underline{\mathbf{r}} - \underline{\mathbf{H}} \sum_{\substack{g=1 \\ g \neq k}}^{K_q} \hat{\underline{d}}^{(g)[j-1]} \underline{\mathbf{c}}^{(g)} \right)^{\text{T}} \right\}, \quad j = 1, \dots, J_{\text{it}}, \quad (3.71)$$

where except for the final stage the detection according to (3.71) has to be applied for all K_q users.

The equalization matrix $\underline{\mathbf{G}}^{[j]}$ should be adapted to the detection stages such that in the initial stage an SD technique is employed which can cope with MAI, where in the following stages an SD technique suitable for the quasi MAI-free case should be exploited. Therefore, the performance of an MC-CDMA system first introduced with IC using EGC in all stages [Faz93] is poor compared to IC with equalizers adapted to the detection stages [Kai95c, Kai95b]. Very promising results are obtained with MMSE equalization adapted to the K_q active users in the initial stage, followed by MMSE equalization adapted to the single user case in the previous detection stages [Kai95b].

The application of MRC seems theoretically to be of advantage for the second and further detection stages, since MRC is the best detection technique in the MAI-free, i.e., in the single user case. However, if one or more decision errors are made in one detection stage, MRC performs poorly even with only one wrong decision [Kai95c]. Hence, the average BER with MRC in the second and further stages cannot reach the performance of an MMSE equalizer adapted to the single user case with K_q equal to 1 in the second and further stages, since the latter is less sensitive to decision errors. Other combinations of SD in the different detection stages are proposed in [HLP95] with ZF equalization followed by MRC, and improved in [KaP96b] with controlled equalization followed by MRC. Since IC with adapted MMSE equalization outperforms the other concepts with respect to the BER, the realization of IC with suboptimal

MMSE equalizers adapted to the detection stages seems to be a good compromise between performance and complexity.

3.3.4 Joint Detection with Maximum Likelihood Criterion

The optimum detection technique exploits the maximum a posteriori (MAP) criterion or the maximum likelihood (ML) criterion, respectively, [Pro95] and is based on JD. In this section, two optimum ML detection algorithms are presented, namely the maximum likelihood sequence estimation (MLSE), which optimally estimates the transmitted data sequence \mathbf{d} , and the maximum likelihood symbol-by-symbol estimation (MLSSE), which optimally estimates the transmitted data symbol $d^{(k)}$. It is straightforward, that both algorithms can be extended to a MAP sequence estimator and to a MAP symbol-by-symbol estimator by taking into account the a priori probability of the transmitted sequence and symbol, respectively [Pro95]. However, since within this thesis all possible transmitted sequences and symbols, respectively, are assumed to be equally probable a priori, the estimator based on the MAP criterion and the one based on the ML criterion are equivalent [Pro95]. The possible transmitted data symbol vectors are \mathbf{d}_μ , $\mu = 1, \dots, M_d^{K_q}$, where $M_d^{K_q}$ is the number of possible transmitted data symbol vectors.

The **MLSE** minimizes the sequence error probability, i.e., the data symbol vector error probability, which is equivalent to maximizing the conditional probability $P\{\mathbf{d}_\mu|\mathbf{r}\}$ that \mathbf{d}_μ was transmitted given \mathbf{r} according to (3.43). The estimate of \mathbf{d} obtained with MLSE is

$$\hat{\mathbf{d}} = \arg \max_{\mathbf{d}_\mu} P\{\mathbf{d}_\mu|\mathbf{r}\}, \quad (3.72)$$

with \arg denoting the argument of the function. By using Bayes' rule [Pap91], the conditional probability $P\{\mathbf{d}_\mu|\mathbf{r}\}$ can be written as

$$P\{\mathbf{d}_\mu|\mathbf{r}\} = \frac{p(\mathbf{r}|\mathbf{d}_\mu)P\{\mathbf{d}_\mu\}}{p(\mathbf{r})}, \quad \mu = 1, \dots, M_d^{K_q}. \quad (3.73)$$

When assuming that all vectors \mathbf{d}_μ , $\mu = 1, \dots, M_d^{K_q}$, are equally probable and by noting that the denominator in (3.73) is independent of the transmitted data symbol vector, the decision rule based on finding the sequence that maximizes $P\{\mathbf{d}_\mu|\mathbf{r}\}$ is equivalent to finding the sequence that maximizes $p(\mathbf{r}|\mathbf{d}_\mu)$. The conditional probability density function $p(\mathbf{r}|\mathbf{d}_\mu)$ of the received vector \mathbf{r} given \mathbf{d}_μ is referred to as a likelihood function. With independent noise on the subcarriers, the received values R_l , $l = 1, \dots, L$, cf. (3.43) and (3.12), are statistically independent and $p(\mathbf{r}|\mathbf{d}_\mu)$ may be expressed as [Pap91]

$$p(\mathbf{r}|\mathbf{d}_\mu) = \prod_{l=1}^L p(R_l|\mathbf{d}_\mu), \quad \mu = 1, \dots, M_d^{K_q}. \quad (3.74)$$

With complex-valued AWGN on the subcarriers, $p(R_l|\mathbf{d}_\mu)$ is given by [Pro95]

$$p(R_l|\mathbf{d}_\mu) = \frac{1}{\pi\sigma^2} \exp\left(-\frac{1}{\sigma^2} |R_l - H_l \mathbf{c}_l \mathbf{d}_\mu^\Gamma|^2\right), \quad \mu = 1, \dots, M_d^{K_q}, \quad (3.75)$$

where $\underline{\mathbf{c}}_l$ is the l th row of the spreading code matrix \mathbf{C} defined in (3.45). Substitution of (3.75) into (3.74) leads to the likelihood function

$$p(\mathbf{r}|\underline{\mathbf{d}}_\mu) = \left(\frac{1}{\pi\sigma^2}\right)^L \exp\left(-\frac{1}{\sigma^2} \|\mathbf{r} - \mathbf{H}\underline{\mathbf{C}}\underline{\mathbf{d}}_\mu\|^2\right), \quad \mu = 1, \dots, M_d^{K_q}. \quad (3.76)$$

Since the reciprocal exponential function is a monotonously decreasing function, the maximum of $p(\mathbf{r}|\underline{\mathbf{d}}_\mu)$ over $\underline{\mathbf{d}}_\mu$ is equivalent to finding the data symbol vector $\underline{\mathbf{d}}_\mu$ that minimizes the squared Euclidean distance

$$\Delta^2(\underline{\mathbf{d}}_\mu, \mathbf{r}) = \|\mathbf{r} - \mathbf{H}\underline{\mathbf{C}}\underline{\mathbf{d}}_\mu\|^2, \quad \mu = 1, \dots, M_d^{K_q}, \quad (3.77)$$

between the received and all possible transmitted sequences. The most likely transmitted data vector can be expressed as [Pro95, FaP93]

$$\hat{\underline{\mathbf{d}}} = \arg \min_{\underline{\mathbf{d}}_\mu} \Delta^2(\underline{\mathbf{d}}_\mu, \mathbf{r}). \quad (3.78)$$

Thus, the MLSE requires the evaluation of $M_d^{K_q}$ squared Euclidean distances per estimation step.

The **MLSSE** minimizes the symbol error probability, which is equivalent to maximizing the conditional probability $P\{\underline{d}_\mu^{(k)}|\mathbf{r}\}$ that $\underline{d}_\mu^{(k)}$ was transmitted given \mathbf{r} . The estimate of $\underline{d}^{(k)}$ obtained by MLSSE is

$$\hat{\underline{d}}^{(k)} = \arg \max_{\underline{d}_\mu^{(k)}} P\{\underline{d}_\mu^{(k)}|\mathbf{r}\}. \quad (3.79)$$

The conditional probability $P\{\underline{d}_\mu^{(k)}|\mathbf{r}\}$ is given by

$$P\{\underline{d}_\mu^{(k)}|\mathbf{r}\} = \sum_{\substack{\forall \underline{\mathbf{d}}_\mu \text{ with same} \\ \text{realization of } \underline{d}_\mu^{(k)}}} P\{\underline{\mathbf{d}}_\mu|\mathbf{r}\}, \quad \mu = 1, \dots, M_d^{K_q}, \quad (3.80)$$

where the probability $P\{\underline{d}_\mu^{(k)}|\mathbf{r}\}$ is the union of all mutually exclusive events $P\{\underline{\mathbf{d}}_\mu|\mathbf{r}\}$ with the same realization of $\underline{d}_\mu^{(k)}$ [Pap91, KaP96a]. By using Bayes' rule and assuming that all data symbols $\underline{d}_\mu^{(k)}$ are equally probable and by noting that $p(\mathbf{r})$ is independent of the transmitted data symbol, the decision rule based on finding the symbol that maximizes $P\{\underline{d}_\mu^{(k)}|\mathbf{r}\}$ is equivalent to finding the symbol that maximizes $p(\mathbf{r}|\underline{d}_\mu^{(k)})$. Thus, with (3.79), (3.80), and (3.76), by ignoring the constant factor $1/(\pi\sigma^2)^L$ which is independent of the transmitted data symbol, the most likely transmitted data symbol is

$$\hat{\underline{d}}^{(k)} = \arg \max_{\underline{d}_\mu^{(k)}} \sum_{\substack{\forall \underline{\mathbf{d}}_\mu \text{ with same} \\ \text{realization of } \underline{d}_\mu^{(k)}}} \exp\left(-\frac{1}{\sigma^2} \Delta^2(\underline{\mathbf{d}}_\mu, \mathbf{r})\right). \quad (3.81)$$

The increased complexity with MLSSE compared to MLSE can be observed in the comparison of (3.81) with (3.78), where besides the evaluation of the $M_d^{K_q}$ squared Euclidean distances, the sum over the exponential functions of the squared Euclidean distances for all realizations

of $\underline{d}_\mu^{(k)}$ has to be calculated. Furthermore, knowledge about the variance of the noise σ^2 is required with MLSSE compared to MLSE. Both JD techniques require knowledge about which user is active, i.e., which user specific spreading code is actually in use. An advantage of MLSSE compared to MLSE is that the MLSSE inherently generates a reliability information for a detected data symbols $\hat{\underline{d}}^{(k)}$ which can be exploited in a subsequent soft decision channel decoder, cf. Chapter 4. Since the MLSSE is the optimal symbol detector, the MLSSE reaches a lower symbol error rate compared to the MLSE. However, the improvements with MLSSE are small and often do not justify its additional complexity.

It should be noted that there exist also suboptimal JD techniques for MC-CDMA systems [JBP96b]. Generally, CDMA systems which have to cope with ISI in the detection process are in practice not able to exploit optimum JD with MLSE or MLSSE and require suboptimal approaches [Kle96]. However, due to the avoidance of ISI in the detection process and by employing the Q -Modification in the presented MC-CDMA system, it is possible to implement the optimum JD techniques with reasonable complexity in MC-CDMA systems [FaP93].

3.4 Performance of Uncoded MC-CDMA Systems

In this section, the performance of different MC-CDMA data detection techniques is shown and compared to each other for the downlink. To evaluate the performance, an MC-CDMA reference system is defined in the following. Since the investigations should focus on the performance of the data detection techniques, the MC-CDMA reference system is defined without channel coding and assumes perfect channel estimation. The used spreading codes are orthogonal Walsh-Hadamard codes [Pro95] with the purpose to minimize the MAI. The spreading code length in a subsystem is L equal to 8, which is motivated by the results presented in [Kai96], cf. Section 4.6, and in [ScK96]. Thus, each subsystem can maximally handle $K_{q,\max}$ equal to 8 users. Unless otherwise stated, the case with fully loaded subsystem is considered in the sequel. QPSK with Gray encoding is applied for data symbol mapping [Pro95]. Moreover, the guard interval of the reference system is chosen such that ISI and ICI are completely eliminated. By assuming one of the three modified MC-CDMA systems presented in Figs. 3.8, 3.9, and 3.10, the channel fading on the subcarriers per subsystem is modelled by uncorrelated flat fading due to frequency interleaving. The mobile radio channel is implemented as uncorrelated Rayleigh fading channel, described in detail in Section 2.2.2. Table 3.1 briefly summarizes the parameters of the MC-CDMA reference system used in this section. The performance of the MC-CDMA reference system presented in this section is applicable to any MC-CDMA system with an arbitrary transmission bandwidth B , an arbitrary number of subsystems Q , and an arbitrary number of data symbols M transmitted per user in an OFDM symbol. Only the number of subcarriers within a subsystem has to be 8 and the amplitudes of the channel fading have to be Rayleigh distributed and can be considered as uncorrelated on the subcarriers of a subsystem due to appropriate frequency interleaving. The loss in SNR V_{guard} due to the guard interval, cf. (3.23), is not taken into account in the results presented for the MC-CDMA reference system

Table 3.1: Parameters of the MC-CDMA reference system

spreading code	Walsh-Hadamard code
spreading code length	$L = 8$
maximum number of users per subsystem	$K_{q,\max} = 8$
data symbol mapping	QPSK with Gray encoding
channel coding	no
channel estimation	perfect
channel	uncorrelated Rayleigh fading channel

in Chapters 3 and 4. The intention is that the loss in SNR due to the guard interval can be calculated according to (3.23) individually for each specified guard interval. So, the presented results can generally be modified for any guard interval. Moreover, in contrast to the results presented in Chapter 6, the results presented in Chapters 3 and 4 do not take into account an SNR loss due to the transmission of pilot symbols required for channel estimation.

As reference for the evaluation of the different SD and MD techniques, the MF bound of an MC-CDMA system is used as a lower bound. The MF bound of an uncoded MC-CDMA system with uncorrelated Rayleigh fading on the subcarriers corresponds to the BER P_b obtained from data transmission over L statistically independent Rayleigh fading channels combined with MRC [Pro95], given by

$$P_b = \left(\frac{1}{2} - \frac{1}{2} \sqrt{\frac{\gamma_b}{L + \gamma_b}} \right)^L \sum_{l=0}^{L-1} \binom{L-1+l}{l} \left(\frac{1}{2} + \frac{1}{2} \sqrt{\frac{\gamma_b}{L + \gamma_b}} \right)^l, \quad (3.82)$$

where γ_b is the SNR per bit defined according to (3.52) and L is the spreading code length. If the fading is correlated between the subcarriers of a subsystem and the diversity D offered by the channel is smaller than the spreading code length L , by still having Rayleigh distributed fading amplitudes, (3.82) remains a lower bound. The MF bound of uncoded MC-FDMA and MC-TDMA systems, in the following referred to as the MC-FDMA/MC-TDMA MF bound, is obtained from (3.82) by choosing L equal to 1, since these systems achieve no diversity gain without channel coding.

The theoretically calculated MF bounds of MC-CDMA systems with different spreading code lengths L and for MC-FDMA and MC-TDMA systems in an uncorrelated Rayleigh fading channel are depicted in Fig. 3.14. The MF bounds for the MC-CDMA reference system with L equal to 8 and for MC-FDMA and MC-TDMA systems in an uncorrelated Rayleigh fading channel are included as reference in the following BER curves presented in this section. Furthermore, the performance of the MC-CDMA, MC-FDMA, and MC-TDMA systems in an AWGN channel, also referred to as ideal channel, is illustrated. The performance of the various systems in the AWGN channel is due to the absence of MAI identical and can be calculated

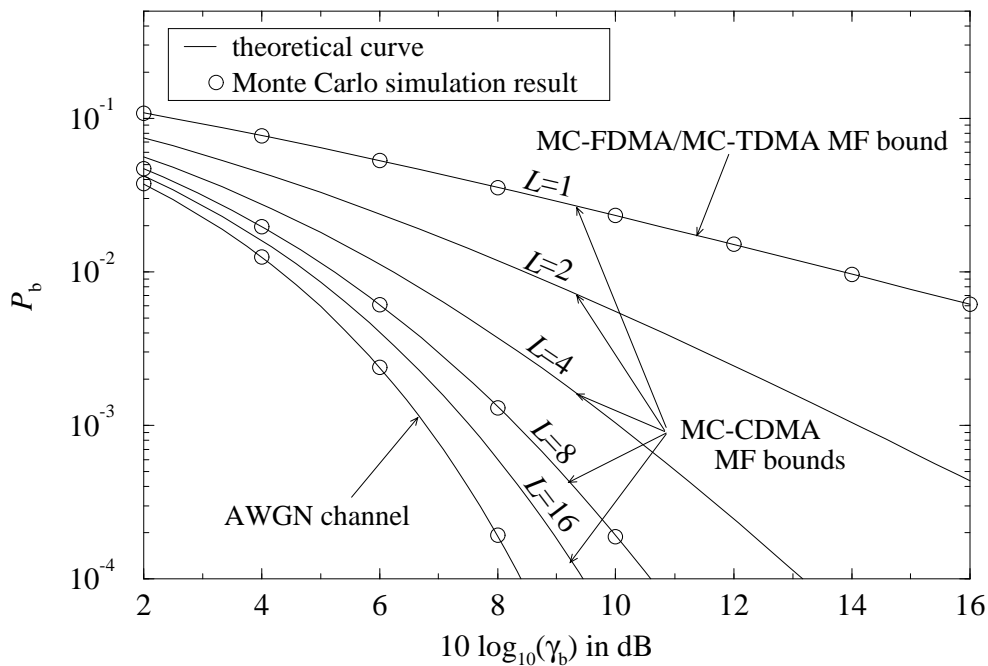


Figure 3.14: MF bounds for uncoded MC-CDMA systems with different spreading code lengths and of MC-FDMA and MC-TDMA systems; uncorrelated Rayleigh fading channel and AWGN channel; QPSK

according to [Pro95]

$$P_b = \frac{1}{2} \operatorname{erfc}(\sqrt{\gamma_b}). \quad (3.83)$$

The theoretical results of the MC-CDMA reference system, of MC-FDMA and MC-TDMA systems for the uncorrelated Rayleigh fading channel and the AWGN channel in Fig. 3.14 are confirmed by Monte Carlo simulation results. The performance curves presented in the following are obtained by Monte Carlo simulations if nothing different is explicitly stated. Since, for instance, in the case of speech transmission an uncoded BER P_b of about 10^{-2} is required which leads to a BER P_b of about 10^{-3} at the output of the channel decoder, the uncoded BER P_b equal to 10^{-2} is focused on in the following considerations.

The average uncoded BER P_b versus the SNR γ_b per bit for the SD techniques MRC, EGC, ZF equalization, and MMSE equalization applied in the MC-CDMA reference system is depicted in Fig. 3.15. The results show that with a fully loaded subsystem the MMSE equalization outperforms the other investigated SD techniques. ZF equalization restores the orthogonality between the user signals and avoids MAI, however, it introduces noise amplification which is especially high at low SNRs. EGC avoids noise amplification but does not counteract the MAI caused by the loss of the orthogonality between the user signals, resulting in a high error floor. The worst performance is obtained with MRC which additionally enhances the MAI, cf. Section 3.3.2. The error floor with MRC and with EGC can be analytically evaluated [YLF93, YeL94a, Kai95c].

In Fig. 3.16, the average uncoded BER P_b versus the SNR γ_b per bit for the SD techniques

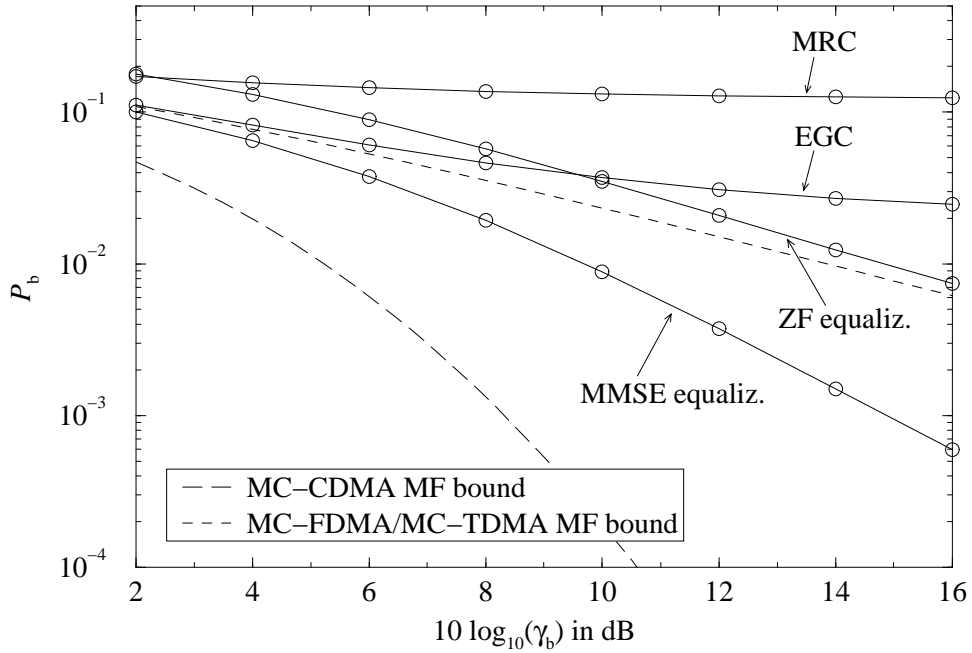


Figure 3.15: Average uncoded BER P_b versus SNR γ_b for SD with MRC, EGC, ZF equalization, and MMSE equalization; uncorrelated Rayleigh fading channel; $L = 8$; $K_q = 8$; QPSK

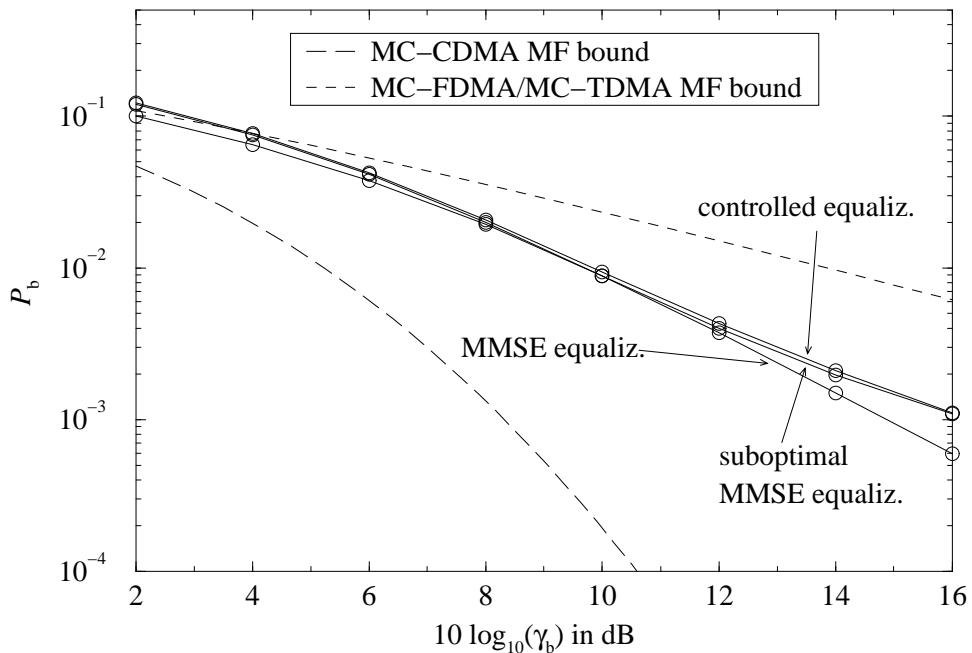


Figure 3.16: Average uncoded BER P_b versus SNR γ_b for SD with MMSE equalization, suboptimal MMSE equalization, and controlled equalization; uncorrelated Rayleigh fading channel; $L = 8$; $K_q = 8$; QPSK

suboptimal MMSE equalization, controlled equalization, and, as reference, for optimal MMSE equalization applied in the MC-CDMA reference system is shown. The parameter λ required for suboptimal MMSE equalization is chosen as the reciprocal of the SNR γ_b at which the BER P_b with optimum MMSE equalization is equal to 10^{-2} . The BER P_b equal to 10^{-2} is obtained with optimum MMSE equalization at $10 \log_{10}(\gamma_b)$ equal to 9.7 dB. Controlled equalization is implemented with ξ_l according (3.69). The optimum threshold which minimizes the SNR γ_b given a BER P_b equal to 10^{-2} for the investigated reference system is found to be a_{thresh} equal to 0.5. The loss in performance with suboptimal MMSE equalization compared to optimal MMSE equalization is small and can be neglected in the SNR range relevant for a mobile radio system at uncoded BERs P_b equal to 10^{-2} . The performance with suboptimal MMSE equalization and with controlled equalization is similar, however, the determination of the parameter λ required for suboptimal MMSE equalization is more straightforward than the search of the optimum threshold a_{thresh} required for controlled equalization.

Analytical approaches to evaluate the performance of MC-CDMA systems with MRC and EGC are given in [YLF93, YeL94a], with ZF equalization in [ToK96c], with controlled equalization in [YeL94a, KaP96b], and with MMSE equalization in [Kai95c]. The derivation of the approach to analytically evaluate the performance of MC-CDMA with the promising MMSE equalization is included in Appendix A1.

Fig. 3.17 shows the average uncoded BER P_b versus the SNR γ_b per bit for the MD techniques parallel IC, MLSE, and MLSSE applied in the MC-CDMA reference system. The performance of parallel IC with adapted MMSE equalization is presented for two detection stages where

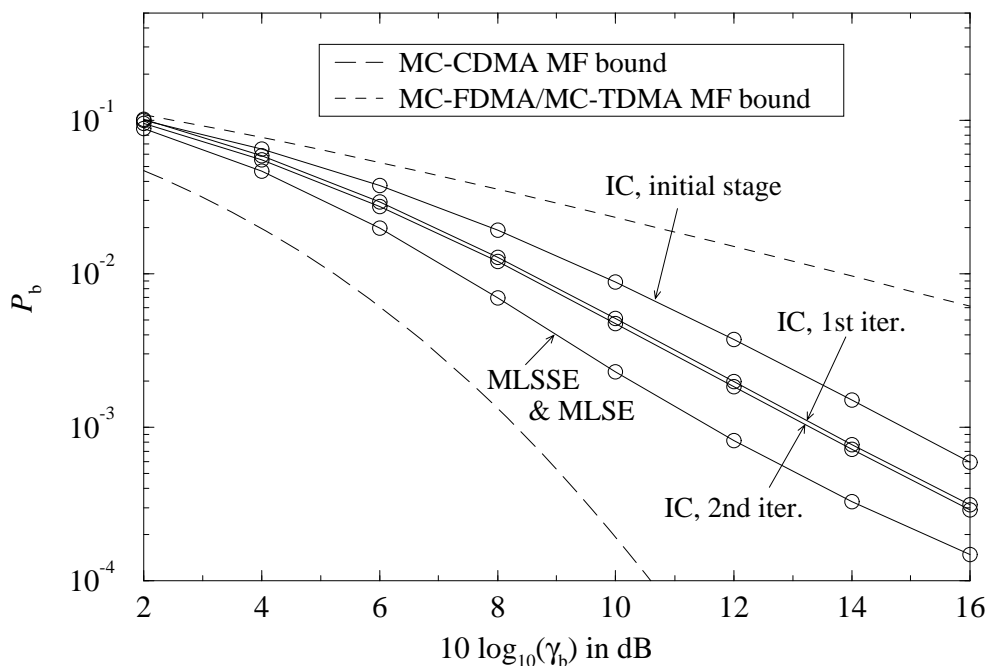


Figure 3.17: Average uncoded BER P_b versus SNR γ_b for MD with parallel IC, MLSE, and MLSSE; uncorrelated Rayleigh fading channel; $L = 8$; $K_q = 8$; QPSK

the performance of the initial stage is identical to the performance of MMSE equalization, cf. Fig. 3.15. It can be shown that relevant performance improvements are obtained only after the first iteration. The optimum JD techniques MLSE and MLSSE perform almost identically. Both JD techniques outperform the investigated SD and IC techniques. For P_b equal to 10^{-2} , the SNR degradation with MLSE and MLSSE relative to the MF bound is 2.1 dB. The SNR degradation with the optimum detection techniques compared to the MF bound is caused by the superposition of orthogonal Walsh-Hadamard codes, resulting in sequences of length L which can contain up to $L - 1$ zeros. Sequences with many zeros perform worse in the fading channel due to the decreased diversity potential than sequences with less zeros. Consequently, the average performance with MLSE or MLSSE is worse than the MF bound. It should be noted that in the uplink the performance of MLSE and MLSSE closely approximates the MF bound since here the Walsh-Hadamard codes do not superpose orthogonally.

The complexity of the MLSE and the MLSSE for QPSK mapping can be reduced by applying MLSE and MLSSE, respectively, separately in the I and the Q quadrature components. Thus, instead of 4^{K_q} only 2×2^{K_q} possible transmitted data sequences have to be evaluated [KaH97a]. This reduces the number of possible transmitted sequences which have to be evaluated in the MC-CDMA receiver of the reference system from 65536 to 512. Since due to the Q -Modification only small numbers of active users have to be taken into account in the ML detector and since ISI can be completely avoided in the detection, an MC-CDMA system can exploit the optimum ML detection algorithm with reasonable complexity. Conventional DS-CDMA systems have to cope with a considerable amount of ISI and cannot exploit the advantages of the Q -Modification. Hence, DS-CDMA systems are in practice not able to exploit optimum JD with MLSE or MLSSE [Kle96].

In Appendix A2, an upper bound on the average BER is derived for MC-CDMA systems applying JD with MLSE and MLSSE for the uncorrelated Rice fading channel [Kai95c] and with K_{Rice} equal to 0, also for the uncorrelated Rayleigh channel [FaP93]. Analytical approaches to determine the performance of MC-CDMA systems with IC are derived in [Kai95c, KaP96b].

The influence of the number of active users on the performance of the MC-CDMA reference system employing SD with MMSE equalization, MD with parallel IC, and MD with MLSSE and MLSE, respectively, is depicted in Fig. 3.18. This figure shows the required SNR γ_b to achieve a BER P_b equal to 10^{-2} versus the loading ratio K_q/L . The parallel IC is implemented with MMSE equalization adapted to the detection stages. In the single user case, the performance with MLSSE and MLSE is equal to the MF bound. With MMSE equalization and IC, a 0.5 dB higher SNR is required to achieve a BER P_b equal to 10^{-2} in the single user case compared to the MF bound. Summarizing, the three detection techniques show an increasing SNR degradation with increasing number of active users K_q . The SNR degradation with increasing K_q is higher for SD with MMSE equalization than for MD with IC, MLSSE, or MLSE.

Due to the absence of MAI in MC-FDMA and MC-TDMA systems, the performance of both is independent of the number of active users. In the uncorrelated Rayleigh fading channel,

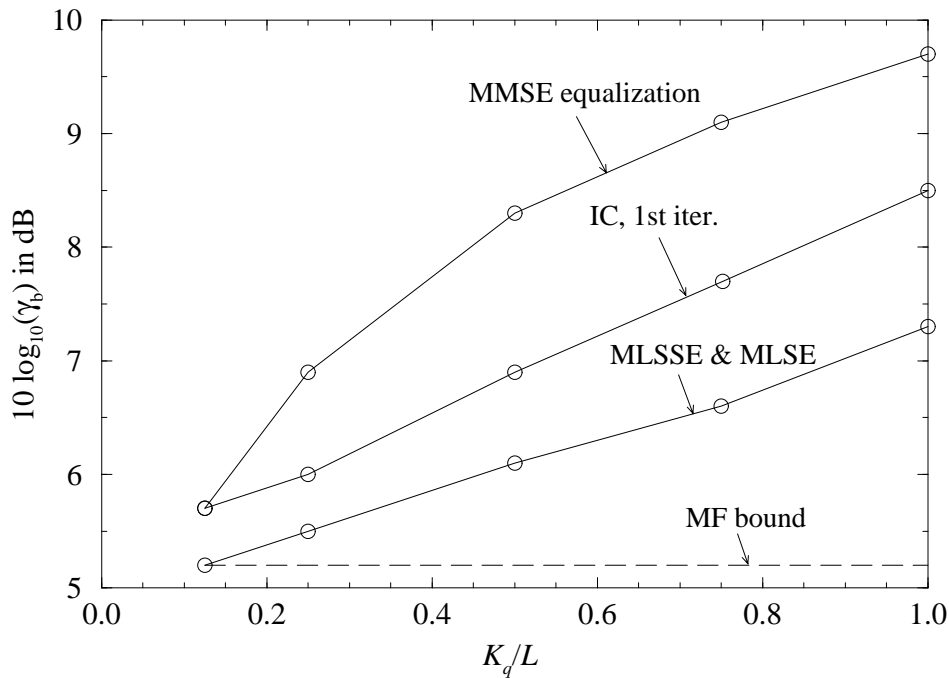


Figure 3.18: SNR γ_b per bit required to achieve a BER of $P_b = 10^{-2}$ versus loading ratio K_q/L ; MMSE equalization, parallel IC after 1st iteration, and MLSSE; uncorrelated Rayleigh fading channel; $L = 8$; QPSK

uncoded MC-FDMA and MC-TDMA systems require an SNR $10 \log_{10}(\gamma_b)$ equal to 13.8 dB to achieve a BER P_b equal to 10^{-2} , $\forall K \in \{1, K_{\max}\}$.

3.5 Equivalence between MC-CDMA and DS-CDMA

In this section, the equivalence between MC-CDMA and DS-CDMA is shown with respect to the spreading code design and with respect to the RAKE receiver implementation.

- Frequency/time domain spreading code:** Each MC-CDMA spreading code with a mapping on frequency slots can be transferred in a DS-CDMA spreading code with a mapping on time slots and vice versa by applying the Fourier transform [FBA94]. The key feature of the Fourier transform is that it preserves the correlation properties of the spreading code [Ach85]. Hence, an MC-CDMA system with a spreading code $\{C_l^{(k)}\}$, $l = 1, \dots, L$, performs identically to a DS-CDMA system with a spreading code $\{c_i^{(k)}\}$, $i = 1, \dots, L$, when both spreading codes are related by the Fourier transform, i.e.,

$$\{C_l^{(k)}\}, l = 1, \dots, L, \quad \bullet \text{---} \circ \quad \{c_i^{(k)}\}, i = 1, \dots, L. \quad (3.84)$$

In (3.84), the symbol $\bullet \text{---} \circ$ denotes the discrete Fourier transformation. When, for instance, applying binary, real-valued, orthogonal MC-CDMA spreading codes, the equivalent DS-CDMA spreading codes are non-binary and complex-valued, but still orthogonal.

Both the MC-CDMA and the equivalent DS-CDMA signals have the same spectral properties. Equation (3.84) is limited to the basic MC-CDMA system presented in Fig. 3.7 where M and Q are equal to 1. The implementation of the M -, the Q -, or the $M&Q$ -Modification with the assigned frequency interleaving as equivalent DS-CDMA signal fails, since the modifications introduce a parallel data symbol transmission which is not possible in conventional DS-CDMA systems without an MC component.

The equivalence between MC-CDMA and DS-CDMA given by the spreading code design enables the implementation of MC-CDMA signals with an OFDM spectrum as equivalent DS-CDMA signals and, hence, enables one to employ receivers developed for conventional DS-CDMA systems [JBP96a, NaS96]. Receivers with conventional DS-CDMA detection algorithms adapted to MC-CDMA signals given as equivalent DS-CDMA signals are in the sequel referred to as equivalent DS-CDMA receivers. Since conventional DS-CDMA receivers are developed to cope with ISI in the detection process, the MC-CDMA mobile radio system exploiting an equivalent DS-CDMA receiver not necessarily require the absence of ISI and, hence, of ICI in the detection process. Thus, the loss in bandwidth efficiency due to the guard interval can be avoided when accepting the higher receiver complexity. The complexity of a conventional DS-CDMA system can also be reduced by inserting a guard interval between adjacent data symbols. Due to the better spectral properties of MC-CDMA signals compared to conventional DS-CDMA signals, the MC-CDMA signal structure introduced in Section 3.2 should be used in any case, either in an MC-CDMA system or in its equivalent implementation as DS-CDMA system.

- **Frequency/time domain RAKE receiver:** The RAKE receiver in a DS-CDMA system resolves and combines multipath components with different time delays [SOS94], whereas the RAKE receiver in an MC-CDMA system resolves and combines multipath components with different Doppler frequencies [FBA94]. The DS-CDMA RAKE receiver, also referred to as time domain RAKE receiver, is suitable for channels with high delay spread and, thus, high ISI, whereas the MC-CDMA RAKE receiver, also referred to as frequency domain RAKE receiver, is suitable for channels with high Doppler shifts and, thus, high ICI. If the delay spread exceeds the reciprocal of the transmission bandwidth, the DS-CDMA RAKE receiver can exploit diversity, whereas the MC-CDMA RAKE receiver can exploit diversity if the maximum Doppler frequency exceeds the reciprocal of the OFDM symbol duration.

When considering the practical implementation of RAKE receivers, the following consideration is important. The MC-CDMA system with an orthogonal spreading code mapped on frequency slots has been introduced to avoid the complexity of a DS-CDMA system with a time domain RAKE receiver in a time dispersive channel [Kai95b]. Consequently, in a frequency dispersive channel, a DS-CDMA system with an orthogonal spreading code mapped on time slots should be applied to avoid the complexity of an MC-CDMA system with a frequency domain RAKE.

Chapter 4

MC-CDMA with Channel Coding

4.1 Introduction

Channel coding with code bit interleaving is an efficient technique to combat the degradations due to fading, noise, interference, and other channel impairments. The basic idea of channel coding is to introduce controlled redundancy into the transmitted data that is exploited at the receiver to correct channel induced errors by means of forward error correction. There are many different types of error correcting codes. Historically, they have been classified into block codes and convolutional codes [LiC83]. Binary convolutional codes are chosen as channel codes in most second generation mobile radio systems and also for the MC-CDMA mobile radio system presented in this thesis, since there exist very simple decoding algorithms that can achieve a soft decision decoding gain. The channel decoding strategies used in the investigated MC-CDMA receiver are based on the Viterbi algorithm which can exploit soft decided values in an optimum manner [For73].

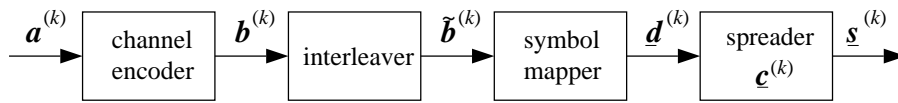
Many of the codes that have been developed for increasing the reliability in the transmission of information are effective when the errors caused by the channel are statistically independent. Signal fading due to time-variant multipath propagation often causes the signal to fall below the noise level, thus, resulting in a large number of errors, called burst errors. An efficient method for dealing with burst error channels is to interleave the code bits in such a way that the bursty channel is transformed into a channel having independent errors. Thus, a code designed for independent errors or short bursts can be used. Code bit interleaving has become an extremely useful technique in all second generation digital cellular systems, and can for example be realized as block, diagonal, or random interleaver [Ste94].

The block diagram of the channel encoding and user specific spreading, cf. (3.28), in the MC-CDMA transmitter assigned to the k th user is shown in Fig. 4.1 a). The block diagram is the same for up- and downlink. The input sequence of the convolutional encoder is represented by the source bit vector

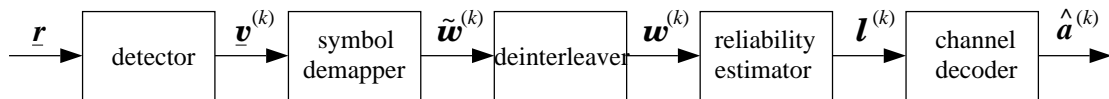
$$\mathbf{a}^{(k)} = (a_1^{(k)}, a_2^{(k)}, \dots, a_{L_a}^{(k)})^T, \quad a_\kappa^{(k)} \in \{-1, +1\}, \quad \kappa = 1, \dots, L_a, \quad (4.1)$$

of length L_a . The code word is the discrete time convolution of $\mathbf{a}^{(k)}$ with the impulse response of the encoder. The memory M_c of the code determines the complexity of the convolutional

a) channel encoding and user specific spreading



b) SD combined with soft decision channel decoding



c) JD combined with soft decision channel decoding

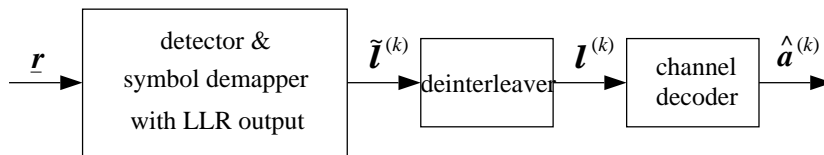


Figure 4.1: Concatenation of the spread spectrum technique with channel coding; a) channel encoding with subsequent data symbol spreading; b) SD and c) JD with optimum soft decision decoding

code, given by 2^{M_c} different memory realizations, also called states, for binary convolutional codes. The states correspond to those of a Mealy automat [Rup93]. The output of the channel encoder is a code bit sequence of length L_b which is represented by the code bit vector

$$\mathbf{b}^{(k)} = (b_1^{(k)}, b_2^{(k)}, \dots, b_{L_b}^{(k)})^T, \quad b_\kappa^{(k)} \in \{-1, +1\}, \quad \kappa = 1, \dots, L_b. \quad (4.2)$$

The interleaved code bit vector $\tilde{\mathbf{b}}^{(k)}$ is passed to a symbol mapper, where $\tilde{\mathbf{b}}^{(k)}$ is mapped into a complex-valued sequence of L_d data symbols taken from the complex data symbol alphabet V_d of size M_d , cf. (3.24), i.e.,

$$\mathbf{d}^{(k)} = (d_1^{(k)}, d_2^{(k)}, \dots, d_{L_d}^{(k)})^T, \quad d_\kappa^{(k)} \in V_d, \quad \kappa = 1, \dots, L_d. \quad (4.3)$$

A data symbol index κ , $\kappa = 1, \dots, L_d$, is introduced to distinguish the different data symbols $d_\kappa^{(k)}$ assigned to $\mathbf{d}^{(k)}$. The spreading of each data symbol $d_\kappa^{(k)}$, $\kappa = 1, \dots, L_d$, with the spreading code $\mathbf{c}^{(k)}$ according to (3.28) yields the vector

$$\mathbf{s}^{(k)} = (\mathbf{s}_1^{(k)T}, \mathbf{s}_2^{(k)T}, \dots, \mathbf{s}_{L_d}^{(k)T})^T \quad (4.4)$$

of length $L_d \cdot L$. The vector $\mathbf{s}^{(k)}$ is superposed with the spread sequences of the other users, cf. (3.33), and MC modulated, cf. (3.10). In the MC-CDMA receiver, the received sequence is MC demodulated according to (3.12). The output of the MC demodulator is the vector

$$\mathbf{r} = (\mathbf{r}_1^T, \mathbf{r}_2^T, \dots, \mathbf{r}_{L_d}^T)^T \quad (4.5)$$

of length $L_d \cdot L$, where each component \mathbf{r}_κ , $\kappa = 1, \dots, L_d$, is defined according to (3.43).

In the case of SD, see Fig. 4.1 b), the L_d soft decided values at the output of the detector are given by the vector

$$\mathbf{v}^{(k)} = (v_1^{(k)}, v_2^{(k)}, \dots, v_{L_d}^{(k)})^T, \quad (4.6)$$

where each component of $\mathbf{v}^{(k)}$ is obtained according to (3.56). The L_d complex-valued, soft decided values of $\mathbf{v}^{(k)}$ assigned to the data symbols of $\mathbf{d}^{(k)}$ are mapped onto L_b real-valued, soft decided values represented by $\tilde{\mathbf{w}}^{(k)}$ assigned to the code bits of $\tilde{\mathbf{b}}^{(k)}$ [ViO79]. The output of the symbol demapper $\tilde{\mathbf{w}}^{(k)}$ after deinterleaving is written as the vector

$$\mathbf{w}^{(k)} = (w_1^{(k)}, w_2^{(k)}, \dots, w_{L_b}^{(k)})^T. \quad (4.7)$$

In the error-free case, $w_\kappa^{(k)}$ is equal to $b_\kappa^{(k)}$ for $\kappa = 1, \dots, L_b$. The vector $\mathbf{w}^{(k)}$ is passed to a reliability estimator which calculates log-likelihood ratios (LLRs) [ViO79, Hag95] of the components of $\mathbf{w}^{(k)}$. LLRs are the optimum soft decided values which can be exploited in a Viterbi decoder [ViO79, Hag95]. The vector

$$\mathbf{l}^{(k)} = (\mathcal{L}_1^{(k)}, \mathcal{L}_2^{(k)}, \dots, \mathcal{L}_{L_b}^{(k)})^T \quad (4.8)$$

of length L_b represents the LLRs assigned to the transmitted code bit vector $\mathbf{b}^{(k)}$, cf. (4.2). Finally, a sequence $\mathbf{l}^{(k)}$ is soft decision decoded by applying the Viterbi algorithm [For73]. At the output of the channel decoder, the detected source bit vector

$$\hat{\mathbf{a}}^{(k)} = (\hat{a}_1^{(k)}, \hat{a}_2^{(k)}, \dots, \hat{a}_{L_a}^{(k)})^T, \quad \hat{a}_\kappa^{(k)} \in \{-1, +1\}, \quad \kappa = 1, \dots, L_a, \quad (4.9)$$

is obtained, consisting of L_a hard decided values.

In the case of JD, see Fig. 4.1 c), the LLRs can inherently be obtained from the detection algorithm, which is also combined with the symbol demapping. After deinterleaving the LLRs given by the vector $\tilde{\mathbf{l}}^{(k)}$, the processing of $\mathbf{l}^{(k)}$ is the same as described above for the scheme with SD.

Before presenting the coding gains of different channel decoding schemes applied in MC-CDMA systems, the calculation of LLRs in fading channels is derived generally for MC modulated transmission systems. Based on this introduction, the LLRs for MC-CDMA systems are derived [KaP96a, Kai96]. The derived LLRs for MC-CDMA systems with SD and with JD are in general applicable for the up- and downlink. In the uplink, only the user index (k) has to be assigned to the individual channel fading coefficients of the corresponding users.

4.2 Soft Decision Decoding in MC-CDMA Systems

4.2.1 Log-Likelihood Ratio

The Viterbi decoding algorithm determines the most likely transmitted code bit sequence $\mathbf{b}^{(k)}$ and, thus, estimates the most likely transmitted source bit sequence $\mathbf{a}^{(k)}$ of the k th user ac-

coding to the ML rule [ViO79]. The ML rule selects the code bit sequence

$$\hat{\mathbf{b}}^{(k)} = (\hat{b}_1^{(k)}, \hat{b}_2^{(k)}, \dots, \hat{b}_{L_b}^{(k)})^T, \quad \hat{b}_\kappa^{(k)} \in \{-1, +1\}, \quad \kappa = 1, \dots, L_b, \quad (4.10)$$

which maximizes the conditioned probability $P\{\mathbf{b}_\nu^{(k)}|\mathbf{w}^{(k)}\}$, i.e.,

$$\hat{\mathbf{b}}^{(k)} = \arg \max_{\mathbf{b}_\nu^{(k)}} P\{\mathbf{b}_\nu^{(k)}|\mathbf{w}^{(k)}\}, \quad (4.11)$$

where $\mathbf{b}_\nu^{(k)}$ is the ν th possible transmitted code bit sequence. By applying Bayes' rule [Pap91] and assuming that all realizations of $\mathbf{b}_\nu^{(k)}$ are equally probable, the decision rule based on finding the sequence that maximizes $P\{\mathbf{b}_\nu^{(k)}|\mathbf{w}^{(k)}\}$ is equivalent of finding the the sequence that maximizes the likelihood function $p(\mathbf{w}^{(k)}|\mathbf{b}_\nu^{(k)})$. It should be noted that the probability density function $p(\mathbf{w}^{(k)})$ which is independent of the possible transmitted code bit vector $\mathbf{b}_\nu^{(k)}$ can be omitted. Due to the interleaving, the channel with memory is ideally transformed into a memoryless channel. Thus, the likelihood function $p(\mathbf{w}^{(k)}|\mathbf{b}_\nu^{(k)})$ is given by

$$p(\mathbf{w}^{(k)}|\mathbf{b}_\nu^{(k)}) = \prod_{\kappa=1}^{L_b} p(w_\kappa^{(k)}|b_{\kappa,\nu}^{(k)}), \quad (4.12)$$

where $b_{\kappa,\nu}^{(k)} \in \{-1, +1\}$ is the κ th bit of the ν th possible transmitted code bit vector $\mathbf{b}_\nu^{(k)}$, and $w_\kappa^{(k)}$ is the κ th soft decided value of the vector $\mathbf{w}^{(k)}$. Equivalently to (4.12), the log-likelihood function

$$\ln(p(\mathbf{w}^{(k)}|\mathbf{b}_\nu^{(k)})) = \sum_{\kappa=1}^{L_b} \ln(p(w_\kappa^{(k)}|b_{\kappa,\nu}^{(k)})) \quad (4.13)$$

can be used since the natural logarithm is a function monotonously increasing with its argument. Thus, the ML rule selects the code bit sequence according to

$$\hat{\mathbf{b}}^{(k)} = \arg \max_{\mathbf{b}_\nu^{(k)}} \sum_{\kappa=1}^{L_b} \ln(p(w_\kappa^{(k)}|b_{\kappa,\nu}^{(k)})). \quad (4.14)$$

Since a bit $b_{\kappa,\nu}^{(k)}$ that maximizes $p(w_\kappa^{(k)}|b_{\kappa,\nu}^{(k)})$ minimizes $p(w_\kappa^{(k)}|-b_{\kappa,\nu}^{(k)})$ for binary codes, (4.14) can be rewritten in the form [ViO79]

$$\begin{aligned} \hat{\mathbf{b}}^{(k)} &= \arg \max_{\mathbf{b}_\nu^{(k)}} \sum_{\kappa=1}^{L_b} \ln\left(\frac{p(w_\kappa^{(k)}|b_{\kappa,\nu}^{(k)})}{p(w_\kappa^{(k)}|-b_{\kappa,\nu}^{(k)})}\right) \\ &= \arg \max_{\mathbf{b}_\nu^{(k)}} \sum_{\kappa=1}^{L_b} b_{\kappa,\nu}^{(k)} \ln\left(\frac{p(w_\kappa^{(k)}|b_{\kappa,\nu}^{(k)} = +1)}{p(w_\kappa^{(k)}|b_{\kappa,\nu}^{(k)} = -1)}\right) \\ &= \arg \max_{\mathbf{b}_\nu^{(k)}} \sum_{\kappa=1}^{L_b} b_{\kappa,\nu}^{(k)} \mathcal{L}_\kappa^{(k)}. \end{aligned} \quad (4.15)$$

The sums in (4.14) and in (4.15) take on different values, however, both terms are equivalent with respect to the argument obtained by maximization of both terms. The term $\mathcal{L}_\kappa^{(k)}$ represents the LLR defined as

$$\mathcal{L}_\kappa^{(k)} = \ln\left(\frac{p(w_\kappa^{(k)}|b_{\kappa,\nu}^{(k)} = +1)}{p(w_\kappa^{(k)}|b_{\kappa,\nu}^{(k)} = -1)}\right) \quad (4.16)$$

and can take on values in the interval $[-\infty, +\infty]$. Since in the following the focus is on the LLR of a single code bit, the index κ is omitted for brevity. The sign of $\mathcal{L}^{(k)}$ is the hard decided value $\hat{b}^{(k)}$ and the magnitude of $\mathcal{L}^{(k)}$ denotes the assigned reliability value of $\hat{b}^{(k)}$.

For the derivation of the LLR in fading channels in this section, an MC transmission system without data spreading, like MC-FDMA or MC-TDMA systems, is considered. A component $w^{(k)}$ is the transmitted bit $b^{(k)}$ affected by flat fading and noise of the subcarrier where the code bit has been transmitted on. Thus, with flat fading on the subcarriers and in the presence of AWGN, the probability density function $p(w^{(k)}|b_\nu^{(k)})$ that $w^{(k)}$ will be received given $b_\nu^{(k)}$ is

$$p(w^{(k)}|b_\nu^{(k)}) = \sqrt{\frac{1}{\pi\sigma^2}} \exp\left(-\frac{1}{\sigma^2} (w^{(k)} - |H_l| b_\nu^{(k)})^2\right). \quad (4.17)$$

It should be noted that the variance σ^2 is defined in (3.14) as the variance of the complex-valued noise. With independent I and Q quadrature components, the variance in each component is $\sigma^2/2$. Substitution of (4.17) into (4.16) leads to the LLR for MC modulated systems without signal spreading in fading channels

$$\begin{aligned} \mathcal{L}^{(k)} &= \ln\left(\frac{\exp\left(-\frac{1}{\sigma^2} (w^{(k)} - |H_l|)^2\right)}{\exp\left(-\frac{1}{\sigma^2} (w^{(k)} + |H_l|)^2\right)}\right) \\ &= \frac{4|H_l|}{\sigma^2} w^{(k)}. \end{aligned} \quad (4.18)$$

In the AWGN channel the fading amplitude $|H_l|$ is equal to 1.

Since in MC-CDMA systems a code bit $b^{(k)}$ is transmitted in parallel on L subcarriers, where each subcarrier may be affected by both independent fading and MAI, (4.18) is not applicable in MC-CDMA systems. The LLR for MC-CDMA systems is derived in the following sections for SD and for JD with MLSSE and MLSE [KaP96a, Kai96].

MC-CDMA receivers using IC without taking into account the channel coding in the iterative process exploit the LLRs derived for SD in each detection stage, where in the second and further stages the term representing the MAI in the LLRs can approximately be set to zero. However, no significant performance improvements can be obtained with this IC scheme, since the gain with IC at the relevant BERs which are greater than 10^{-2} in the uncoded system is negligible. Promising results are obtained when combining the detection and decoding in an iterative manner with soft IC [KaH97b]. The MC-CDMA receiver with optimum soft IC is introduced in Section 4.3.

4.2.2 LLR for MC-CDMA Systems with SD

Fig. 3.13 shows the parallel transmission of a data symbol and, thus, of a code bit on L parallel subcarriers with MC-CDMA. A received data symbol after SD results in the soft decided value

$$\underline{v}^{(k)} = \sum_{l=1}^L C_l^{(k)*} G_l \left(H_l \sum_{g=1}^{K_q} d^{(g)} C_l^{(g)} + N_l \right)$$

$$= \underbrace{\overbrace{d^{(k)} \sum_{l=1}^L |C_l^{(k)}|^2 G_l H_l}_{\vartheta^{(k)}}}_{\text{desired symbol}} + \underbrace{\sum_{\substack{g=1 \\ g \neq k}}^{K_q} d^{(g)} \sum_{l=1}^L G_l H_l C_l^{(g)} C_l^{(k)*}}_{\zeta^{(g,k)}}}_{\text{MAI}} + \underbrace{\sum_{l=1}^L N_l G_l C_l^{(k)*}}_{\eta^{(k)}}}_{\text{noise}}. \quad (4.19)$$

Since a frequency interleaver is applied, the L complex-valued fading factors H_l , $l = 1, \dots, L$, affecting $\underline{d}^{(k)}$ can be assumed to be independent. Thus, for sufficiently long spreading codes, the MAI can be considered as additive zero-mean Gaussian noise according to the central limit theorem [Pap91]. The noise term $\eta^{(k)}$ can also be considered as additive zero-mean Gaussian noise. The attenuation $|\vartheta^{(k)}|$ of the transmitted data symbol $\underline{d}^{(k)}$ is the magnitude of the sum of the equalized channel coefficients $G_l \cdot H_l$ of the L subcarriers used for the transmission of $\underline{d}^{(k)}$ weighted with $|C_l^{(k)}|^2$. The symbol demapper delivers the real-valued soft decided value

$$w^{(k)} = \underbrace{\overbrace{b^{(k)} \vartheta'^{(k)}}}_{\text{desired bit}} + \underbrace{\sum_{\substack{g=1 \\ g \neq k}}^{K_q} b^{(g)} \zeta'^{(g,k)}}_{\text{MAI}} + \underbrace{\overbrace{\eta'^{(k)}}}_{\text{noise}}. \quad (4.20)$$

The desired real-valued soft decided bit $b^{(k)} \vartheta'^{(k)}$ is obtained after symbol demapping the desired complex-valued soft decided data symbol $\underline{d}^{(k)} \vartheta^{(k)}$. Moreover, the real-valued soft decided bit $b^{(g)} \zeta'^{(g,k)}$ is obtained after symbol demapping the complex-valued term $\underline{d}^{(g)} \zeta^{(g,k)}$, and the real-valued noise $\eta'^{(k)}$ is obtained after symbol demapping the complex-value noise $\eta^{(k)}$. The real-valued MAI and the real-valued noise can still be considered as additive zero-mean Gaussian noise with variance σ_{MAI}^2 and σ_{noise}^2 , respectively. With $w^{(k)}$ defined according to (4.20), the LLR can be written according to (4.18) as

$$\mathcal{L}^{(k)} \approx \frac{2 |\vartheta'^{(k)}|}{\sigma_{\text{MAI}}^2 + \sigma_{\text{noise}}^2} w^{(k)}. \quad (4.21)$$

In (4.21), the soft decided value $w^{(k)}$ is multiplied with 2 instead of 4 as in (4.18), since in (4.21) the variance is assigned to real-valued noise, whereas it is assigned to complex-valued noise in (4.18). When applying Walsh Hadamard codes as orthogonal spreading codes [Pro95], the property can be exploited that the product $C_l^{(g)} C_l^{(k)*}$, $l = 1, \dots, L$, in half of the cases equals $-1/L$ and in the other half equals $+1/L$, when g is not equal to k and $C_l^{(k)} \in \{-\sqrt{1/L}, +\sqrt{1/L}\}$, $l = 1, \dots, L$, $k = 1, \dots, K_q$. The chip amplitude $\sqrt{1/L}$ normalizes the energy of a data symbol. Furthermore, by assuming that the realizations $b^{(k)}$ equal to 1 and $b^{(k)}$ equal to -1 are equally probable for all $k = 1, \dots, K_q$, the attenuation $|\vartheta'^{(k)}|$ results in [Kai95c]

$$|\vartheta'^{(k)}| = \frac{1}{L} \left| \sum_{l=1}^L G_l H_l \right|, \quad (4.22)$$

the variance of the MAI becomes

$$\sigma_{\text{MAI}}^2 = \frac{K_q - 1}{L} \left(\mathbb{E}\{|G_l H_l|^2\} - |\mathbb{E}\{G_l H_l\}|^2 \right), \quad (4.23)$$

and the variance of the noise is

$$\sigma_{\text{noise}}^2 = \frac{\sigma^2}{2} \text{E}\{|G_l|^2\}. \quad (4.24)$$

Substitution of (4.22), (4.23), and (4.24) in (4.21) leads to the LLR for MC-CDMA mobile radio systems with SD, given by

$$\mathcal{L}^{(k)} \approx \frac{\frac{2}{L} \left| \sum_{l=1}^L G_l H_l \right|}{\frac{(K_q - 1)}{L} \left(\text{E}\{|G_l H_l|^2\} - |\text{E}\{G_l H_l\}|^2 \right) + \frac{\sigma^2}{2} \text{E}\{|G_l|^2\}} w^{(k)}, \quad (4.25)$$

when Walsh Hadamard codes are used as spreading codes. The implementation of (4.25) is enabled by applying the law of large numbers [Pap91] for evaluation of the expectation values $\text{E}\{.\}$. Thus, the LLR for MC-CDMA mobile radio systems with SD applying Walsh Hadamard codes can be implemented in the form [KaP96a]

$$\mathcal{L}^{(k)} \approx \frac{2 \left| \sum_{l=1}^L G_l H_l \right|}{(K_q - 1) \left(\frac{1}{L} \sum_{l=1}^L |G_l H_l|^2 - \left| \frac{1}{L} \sum_{l=1}^L G_l H_l \right|^2 \right) + \frac{\sigma^2}{2} \sum_{l=1}^L |G_l|^2} w^{(k)}. \quad (4.26)$$

For spreading codes with L much greater than 2, the computation of (4.26) can be simplified to [Kai96]

$$\mathcal{L}^{(k)} \approx w^{(k)}, \quad L \gg 2, \quad (4.27)$$

since with L much greater than 2 the weighting term of $w^{(k)}$ in (4.26) becomes quasi constant and, hence, has no effect on the soft decision decoding process. Thus, (4.25) simplifies to the soft decided value $w^{(k)}$ obtained after detection and symbol demapping. In Section 4.5, the accuracy of the simplified LLR (4.27) versus the spreading code length L is shown.

Since for short spreading codes the simplification (4.27) performs worse than (4.26), an approach yielding similar performance as (4.26) even with short spreading codes when using MMSE equalization was found to be [Kai96]

$$\mathcal{L}^{(k)} = \frac{4}{\sigma^2 L} \sum_{l=1}^L |H_l| w^{(k)}. \quad (4.28)$$

Equation (4.28) has a very similar form as (4.18). In (4.28) a soft decided value $w^{(k)}$ is weighted with the average of all $|H_l|$, $l = 1, \dots, L$, of the subcarriers on which $b^{(k)}$ has been transmitted, and in (4.18) a soft decided value $w^{(k)}$ is weighted with the $|H_l|$ of the one subcarrier on which $b^{(k)}$ has been transmitted. In practice (4.28) is preferable to (4.26) when using SD with MMSE equalization, since it is lower in computational complexity without essential loss in performance. However, it has to be noted that (4.28) performs significantly worse than (4.26) for other SD techniques like MRC or ZF equalization and, thus, is not applicable for all SD techniques.

4.2.3 LLRs for MC-CDMA Systems with MLSSE and MLSE

The LLR for coded MC-CDMA mobile radio systems with JD based on MLSSE is given by

$$\mathcal{L}^{(k)} = \ln \left(\frac{p(\mathbf{r}|b_\nu^{(k)} = +1)}{p(\mathbf{r}|b_\nu^{(k)} = -1)} \right) \quad (4.29)$$

and is inherently delivered in the symbol-by-symbol estimation process presented in Section 3.3.4. The set of all possible transmitted data vectors \mathbf{d}_μ where the considered code bit $b_\nu^{(k)}$ of the k th user is equal to +1 is denoted by $\mathcal{D}_+^{(k)}$. The set of all possible data symbols where $b_\nu^{(k)}$ is equal to -1 is denoted by $\mathcal{D}_-^{(k)}$. Using $\mathcal{D}_+^{(k)}$ and $\mathcal{D}_-^{(k)}$, (4.29) results in

$$\mathcal{L}^{(k)} = \ln \left(\frac{\sum_{\forall \mathbf{d}_\mu \in \mathcal{D}_+^{(k)}} p(\mathbf{r}|\mathbf{d}_\mu)}{\sum_{\forall \mathbf{d}_\mu \in \mathcal{D}_-^{(k)}} p(\mathbf{r}|\mathbf{d}_\mu)} \right). \quad (4.30)$$

With the conditional probability function $p(\mathbf{r}|\mathbf{d}_\mu)$ given in (3.76), the LLR for MC-CDMA systems with MLSSE becomes [KaP96a]

$$\mathcal{L}^{(k)} = \ln \left(\frac{\sum_{\forall \mathbf{d}_\mu \in \mathcal{D}_+^{(k)}} \exp\left(-\frac{1}{\sigma^2} \Delta^2(\mathbf{d}_\mu, \mathbf{r})\right)}{\sum_{\forall \mathbf{d}_\mu \in \mathcal{D}_-^{(k)}} \exp\left(-\frac{1}{\sigma^2} \Delta^2(\mathbf{d}_\mu, \mathbf{r})\right)} \right). \quad (4.31)$$

For coded MC-CDMA systems with JD based on MLSE, the sequence estimation process cannot provide reliability information on the detected code bits. However, an appropriate approximation for the LLR with MLSE is given by [FaP93]

$$\mathcal{L}^{(k)} \approx \frac{1}{\sigma^2} \left(\Delta^2(\mathbf{d}_{\mu_-}, \mathbf{r}) - \Delta^2(\mathbf{d}_{\mu_+}, \mathbf{r}) \right). \quad (4.32)$$

The indices μ_- and μ_+ mark the smallest squared Euclidean distances $\Delta^2(\mathbf{d}_{\mu_-}, \mathbf{r})$ and $\Delta^2(\mathbf{d}_{\mu_+}, \mathbf{r})$ where $b_\nu^{(k)}$ is -1 and $b_\nu^{(k)}$ is +1, respectively. The SNR degradation due to the application of MLSE with approximated LLR (4.32) compared to MLSSE with optimum LLR (4.31) is shown in Section 4.5.

4.3 Iterative Decoding with Soft Interference Cancellation

A coded MC-CDMA system exploiting MD with IC can be realized with two strategies. The first of these is IC performed with the code bits obtained after despreading by not including the channel coding in the iterative process. This strategy performs poorly for the reasons mentioned in Section 4.2.1. A second strategy is to concatenate the IC and decoding in an iterative

scheme [MaO97a, StP97b, KaH97b]. This can be done by re-encoding, re-spreading, and pre-distorting the decoded contributions of the interfering users before cancelling the interference. The optimum IC strategy is obtained when taking reliability information about the detected interference into account so that the decisions with reliability information from the soft-in/soft-out channel decoder are used to reconstruct the interference. This strategy is referred to as soft IC [KaH97b] and outperforms approaches with re-encoding hard decided values and, thus, re-spreading of hard decided values. Soft IC exploits the advantage that the use of soft decided values in the iterative process reduces error propagation compared to the use of hard decided values [KaH97b].

The block diagram of an MC-CDMA receiver with iterative soft IC is illustrated in Fig. 4.2. The data of the desired user k are detected by applying IC with reliability information. Soft IC

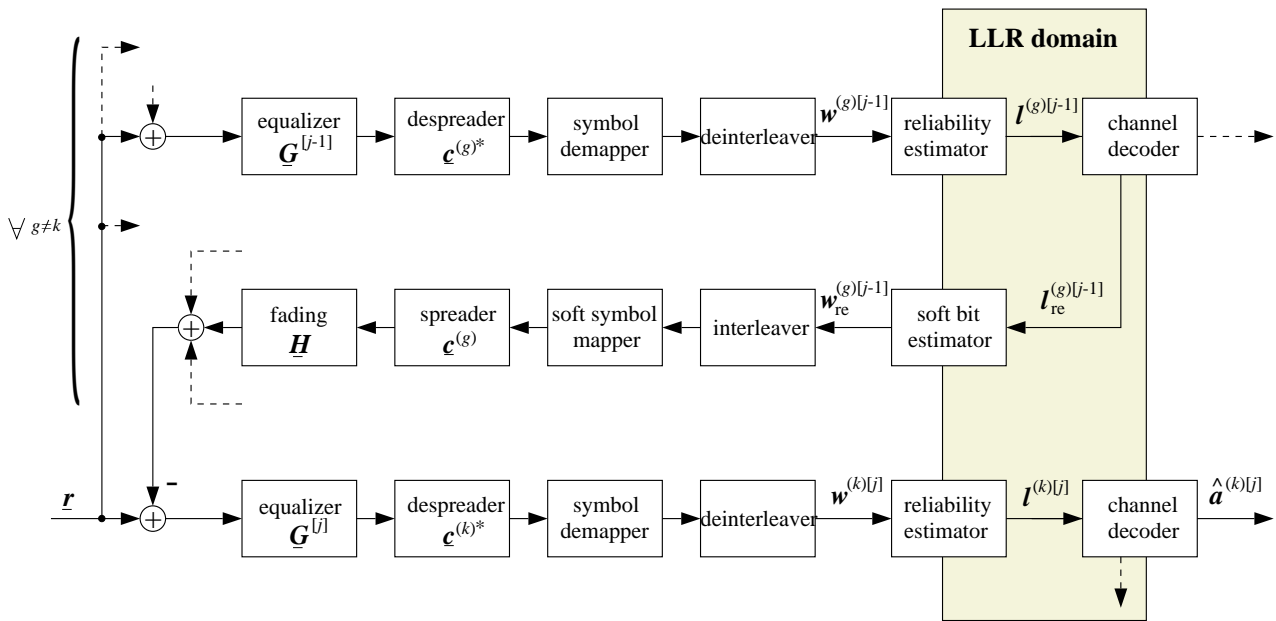


Figure 4.2: Mobile MC-CDMA receiver with soft IC

can be carried out in multiple detection stages. As already introduced in Section 3.3.3, values and functions related to the j th iteration are marked by an index $[j]$, where j may take on the values $j = 1, \dots, J_{it}$, and J_{it} is the total number of iterations. The initial detection stage is indicated by the index $[0]$. Before detection of the data of the k th user in the lowest path of Fig. 4.2 with an appropriate SD technique adapted to the j th iteration, the contribution of the $K_q - 1$ interfering users $g = 1, \dots, K_q$ with g not equal to k is detected with SD adapted to the $(j - 1)$ th detection stage and subtracted from the received signal.

The contribution of the interfering users is detected in the j th detection stage by SD, separately for each user. The soft decided values $w^{(g)[j]}$ of the g th interfering user are obtained after detection, symbol demapping, and deinterleaving. The output of the reliability estimator delivers the LLR vector $\mathbf{l}^{(g)[j]}$. From the subsequent soft-in/soft-out channel decoding, shown

in the uppermost path of Fig. 4.2, besides the output of the decoded source bits, reliability informations in the form of LLRs about the re-encoded bits are obtained. The LLRs of the re-encoded bits are given by the vector

$$\mathbf{l}_{\text{re}}^{(g)[j]} = (\mathcal{L}_{1,\text{re}}^{(g)[j]}, \mathcal{L}_{2,\text{re}}^{(g)[j]}, \dots, \mathcal{L}_{L_b,\text{re}}^{(g)[j]})^T. \quad (4.33)$$

In contrast to (4.16), the LLR of a re-encoded bit

$$\mathcal{L}_{\kappa,\text{re}}^{(g)[j]} = \ln \left(\frac{\text{P}\{b_{\kappa}^{(g)} = +1 | \mathbf{w}^{(g)[j]}\}}{\text{P}\{b_{\kappa}^{(g)} = -1 | \mathbf{w}^{(g)[j]}\}} \right), \quad \kappa = 1, \dots, L_b, \quad (4.34)$$

is the estimate of all the other soft decided values in the sequence $\mathbf{w}^{(g)[j]}$ about this re-encoded bit and not only of one received soft decided value $w_{\kappa}^{(g)[j]}$. For brevity, the index κ is omitted since the focus is on the LLR of one code bit in the sequel. To avoid error propagation, the average value of $b^{(g)}$ which is the so-called soft bit is used [Hag96]. The soft bit is defined as

$$\begin{aligned} w_{\text{re}}^{(g)[j]} &= \text{E}\{b^{(g)} | \mathbf{w}^{(g)[j]}\} \\ &= (+1)\text{P}\{b^{(g)} = +1 | \mathbf{w}^{(g)[j]}\} + (-1)\text{P}\{b^{(g)} = -1 | \mathbf{w}^{(g)[j]}\}. \end{aligned} \quad (4.35)$$

With (4.34), the conditioned probabilities required in (4.35) are

$$\text{P}\{b^{(g)} = +1 | \mathbf{w}^{(g)[j]}\} = \frac{e^{\mathcal{L}_{\text{re}}^{(g)[j]}}}{1 + e^{\mathcal{L}_{\text{re}}^{(g)[j]}}} \quad (4.36)$$

and

$$\text{P}\{b^{(g)} = -1 | \mathbf{w}^{(g)[j]}\} = \frac{1}{1 + e^{\mathcal{L}_{\text{re}}^{(g)[j]}}}. \quad (4.37)$$

Thus, with (4.36) and (4.37), the soft bit $w_{\text{re}}^{(g)[j]}$ is defined as

$$\begin{aligned} w_{\text{re}}^{(g)[j]} &= \frac{e^{\mathcal{L}_{\text{re}}^{(g)[j]}/2} - e^{-\mathcal{L}_{\text{re}}^{(g)[j]}/2}}{e^{\mathcal{L}_{\text{re}}^{(g)[j]}/2} + e^{-\mathcal{L}_{\text{re}}^{(g)[j]}/2}} \\ &= \tanh \left(\mathcal{L}_{\text{re}}^{(g)[j]} / 2 \right). \end{aligned} \quad (4.38)$$

The soft bit $w_{\text{re}}^{(g)[j]}$ can take on values in the interval $[-1, +1]$. After interleaving, the soft bits are soft symbol mapped such that the reliability information included in the soft bits is not lost. The obtained complex-valued data symbols are spread with the user specific spreading code and each chip is predistorted with the channel coefficient assigned to the subcarrier where the chip is transmitted on. After that, the total reconstructed MAI is subtracted from the received signal \mathbf{r} .

The above operation becomes more clear, if one thinks of the channel decoder as a genie soft-in/soft-out decoder as defined in [KaH97b], which supplies

$$\mathcal{L}_{\text{re}}^{(g)[j]} = \begin{cases} \pm\infty & \text{for correctly re-encoded bits} \\ 0 & \text{otherwise} \end{cases} \quad (4.39)$$

or as soft bit

$$w_{\text{re}}^{(g)[j]} = \begin{cases} \pm 1 & \text{for correctly re-encoded bits} \\ 0 & \text{otherwise} \end{cases} . \quad (4.40)$$

Then, the feedback does not use incorrect bits and avoids error propagation. The performance of the genie soft-in/soft-out decoder is a lower bound for MC-CDMA systems with soft IC. A real soft-in/soft-out decoder closely approximates (4.39), as shown in Section 4.5.

After cancelling the interference of the other users, the data of the desired user k are detected with SD. However, in contrast to the initial SD, in the further stages, the equalizer coefficients given by the matrix $\mathbf{G}^{[j]}$ and the LLRs given by the vector $\mathbf{l}^{(k)[j]}$ after soft IC are adapted to the quasi MAI-free case, i.e., K_q is equal to 1.

4.4 Iterative Decoding of Turbo-Codes

Recently, interest has focused on iterative decoding of concatenated codes using soft-in/soft-out decoders with simple component codes in an interleaved scheme. By applying systematic recursive convolutional codes in the iterative scheme and by introducing an interleaver between the two encoders, impressive results can be obtained with so-called Turbo codes [BGT93]. Turbo codes have become of great interest because of their good performance at low SNRs. Fig. 4.3 shows the block diagram of the Turbo encoder. The code structure consists of two

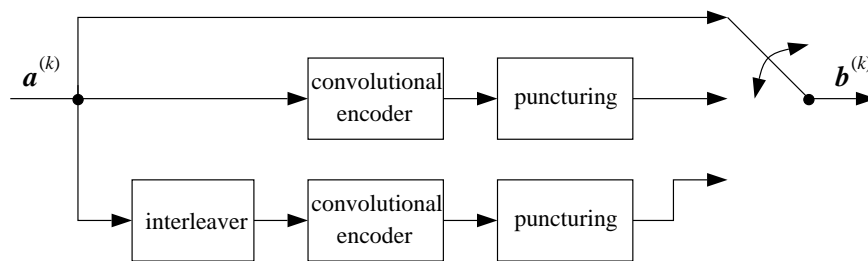


Figure 4.3: Turbo encoder

parallel recursive systematic punctured convolutional codes. A block of encoded bits consists of three parts. The two parity bit parts and the systematic part which is the same in both code bit streams and, hence, has to be transmitted only once. The code bit sequence at the output of the Turbo encoder is given by the vector $\mathbf{b}^{(k)}$, cf. (4.2).

In the receiver, the decoding is performed iteratively. Fig. 4.4 shows the block diagram of the Turbo decoder. The component decoders are soft output decoders providing LLRs of the decoded bits. The basic idea of iterative decoding is to feed forward/backward the soft decoder output in the form of LLRs, improving the next decoding step. In the initial stage, the non-interleaved part of the code $\mathbf{b}^{(k)}$ is decoded. Only the LLRs given by the vector $\mathbf{l}^{(k)}$ at the input

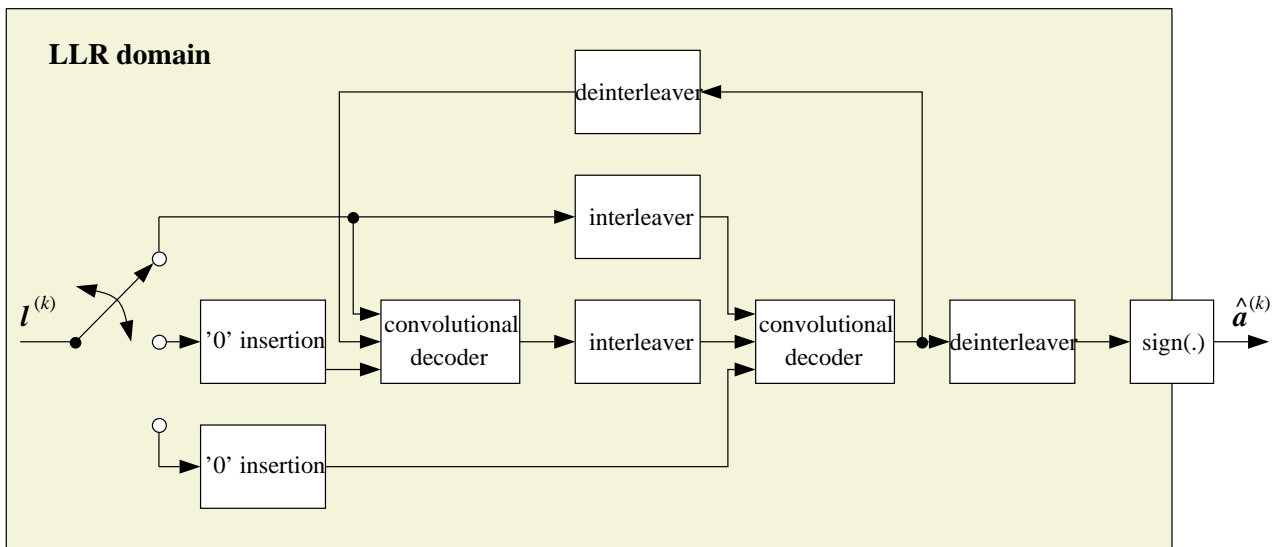


Figure 4.4: Turbo decoder

of the Turbo decoder are used. In the second stage, the interleaved part is decoded. In addition to the LLRs given by $l^{(k)}$, the decoder uses the output of the first decoding step as a priori information about the code bits. This is possible due to the separation of the two codes by the interleaver. In the next iteration cycle, this procedure is repeated, but now the non-interleaved part can be decoded using an a priori information delivered from the last decoding step. Hence, this decoding run has a better performance than the first one and the decoding improves. Since in each individual decoding-step the decoder combines soft information from different sources, the representation of the soft information is crucial. It is shown in [HRP94, HOP96] that the soft value at the decoder input should be a LLR to guarantee that after combining the soft informations at the input of the decoder again LLRs are available. The size of the Turbo code interleaver and the number of iterations essentially determine the performance of the Turbo coding scheme.

4.5 Performance of MC-CDMA Systems with Channel Coding

The performance evaluation of MC-CDMA systems with channel coding and interleaving requires an extension of the MC-CDMA reference system defined in Section 3.4. In the sequel, the channel coding and interleaving of the extended MC-CDMA reference system are defined. The channel coding applies rate compatible punctured convolutional (RCPC) codes [Hag88]. The application of RCPC codes offers a flexible change of code rates by applying the same Viterbi decoder. The RCPC codes are almost as good as the best known general convolutional codes of the respective rates, but are less complex. The mother code rate of the RCPC codes is $1/3$. Unless otherwise stated, non-systematic RCPC codes punctured to rate R equal to $1/2$ with

memory M_c equal to 6 are chosen as channel codes. Blocks of L_a equal to 192 source bits are transmitted. At the output of the channel encoder, the code bits are scrambled in a random interleaver of size I_c equal to 384. When considering speech transmission applications with typical data rate of 9.6 kbit/s, the chosen block size of 384 contains the data of 20 ms speech time, which is an acceptable delay. Table 4.1 briefly summarizes the parameters of the channel coding and interleaving adapted to the MC-CDMA reference system introduced in Section 3.4. Since the focus is on speech transmission applications, the considered BER P_b is equal to 10^{-3} .

Table 4.1: Parameters of the channel coding and interleaving, adapted to the MC-CDMA reference system introduced in Section 3.4

channel code	convolutional code
channel decoder	Viterbi decoder
code rate	$R=1/2$
memory	$M_c=6$
bit interleaver	random interleaver of size $I_c = 384$

Unless otherwise stated, full subsystem load with K_q equal to L is considered. When systems with different spreading code length L are investigated, the maximum number of active users remains constant due to the Q -Modification, cf. (3.38). The performance of coded MC-FDMA and MC-TDMA systems is given as reference. It should be noted that, similar to the uncoded case, the performance of MC-FDMA and MC-TDMA systems is independent of the number of active users K . The curves presented in the following are obtained by Monte Carlo simulations. The circle symbols in the figures explicitly highlight simulation points of the curves where the focus is on.

In Fig. 4.5, the SNR gain due to soft decision decoding exploiting LLRs for MC-CDMA systems compared to hard decision decoding versus the spreading code length L is presented for a BER P_b equal to 10^{-3} . Results are given for SD with MMSE equalization and for JD with MLSSE and with MLSE. It can be observed that with increasing spreading code length the SNR gain due to soft decision decoding decreases. This effect occurs since the spreading can be considered as a kind of averaging of the fading of the subcarriers. Hence, with increasing spreading code length the fading process is more and more averaged and the soft decision decoding gain decreases. However, it has to be mentioned that on the other hand the diversity gain due to data spreading increases.

In the case of SD, the SNR gain with the LLR according to (4.26) and with the approximation (4.27), which simply exploits the soft decided values delivered from the detector by not taking the channel state information into account, is shown. It can be observed that with increasing L the approximation (4.27) becomes more and more accurate. The simplified approach to calculate the LLRs according to (4.28) has approximately the same performance as (4.26) and

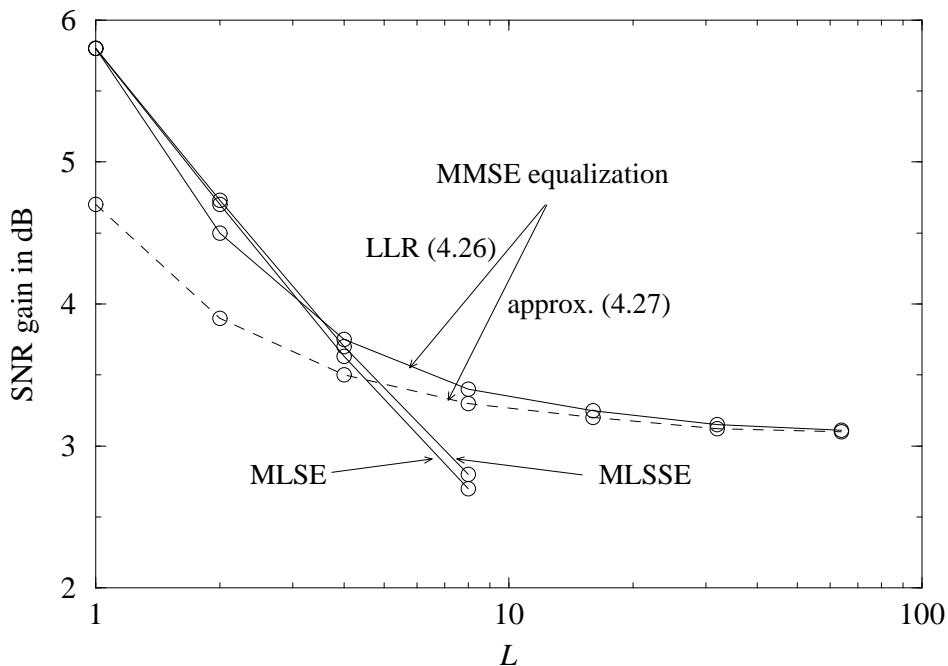


Figure 4.5: SNR gain due to soft decision decoding relative to hard decision decoding versus spreading code length L for different data detection techniques; uncorrelated Rayleigh fading channel; fully loaded subsystem; QPSK; $R = 1/2$; $P_b = 10^{-3}$

is, hence, not shown. In practice, (4.28) may be preferable when using MMSE equalization due to the reduced computational complexity. The results in Fig. 4.5 show that MMSE equalization achieves a soft decision decoding gain of about 3 dB compared to hard decision decoding in the case of large L . For L equal to 1, the LLRs (4.18) and (4.26) are identical and the performance of MC-CDMA, MC-FDMA, and MC-TDMA systems is the same. Both (4.18) and (4.26) are identical in the case of L equal to 1 since $w^{(k)}$ in MC-CDMA is additionally weighted with G_l compared to $w^{(k)}$ in MC-FDMA and MC-TDMA systems. It has to be mentioned that data spreading with L equal to 1 is only relevant in the academic sense. The soft decision decoding gain in the case of L equal to 1 is 5.8 dB with LLRs according to (4.18) and (4.26) and 4.7 dB with the approximation according to (4.27). Thus, with LLRs an additional gain in SNR of 1.1 dB is achievable compared to soft decision decoding without exploiting the channel state information.

The motivation for the use of LLRs in MC-CDMA systems with MMSE equalization is as follows. In the case where the frequency diversity D_f , cf. (2.11), offered by the channel is smaller than the spreading code length L , the achievable soft decision decoding gain depends on the effective spreading code length which is equal to the frequency diversity D_f given by (2.11). Thus, the corresponding soft decision decoding gain is found in Fig. 4.5 at the spreading code length equal to D_f . Typically, the performance in channels where D_f is less than L is worse than in channels where D_f is greater or equal to L . Thus, especially in diversity limited propagation channels where D_f is less than L , the soft decision decoding gain offered by the LLRs (4.26) and (4.28), respectively, compared to (4.27), should be exploited.

In the case of JD, the SNR degradation due to the application of MLSE with approximated LLR according to (4.32) compared to MLSSE with optimum LLR according to (4.31) is shown in Fig. 4.5. Similar to the uncoded case, the SNR degradation with the simpler MLSE compared to the MLSSE can be neglected. Moreover, it can be observed that the SNR gains due to soft decision decoding with MLSSE and MLSE are smaller for large L compared to the SNR gains with SD using MMSE equalization. For the case with L equal to 1, the performance of MC-CDMA systems with MLSSE and with MLSE is equal to the performance of MC-FDMA and MC-TDMA systems using the LLR according to (4.18).

In the following investigations, the LLR according to (4.26) is chosen for SD since it is applicable to all presented SD techniques in contrast to (4.28). In the case of JD, MLSSE with the optimum LLR according to (4.31) is used. Furthermore, the single-user bound for the MC-CDMA reference system with L equal to 8 and the performance for a rate 1/2 coded MC-FDMA and MC-TDMA system in an uncorrelated Rayleigh fading channel is given as a reference in the figures presented in this section.

In Fig. 4.6, the average coded BER P_b versus the SNR γ_b for SD with MRC, ZF equalization, EGC, and MMSE equalization exploiting the optimum LLRs is depicted. In addition, the

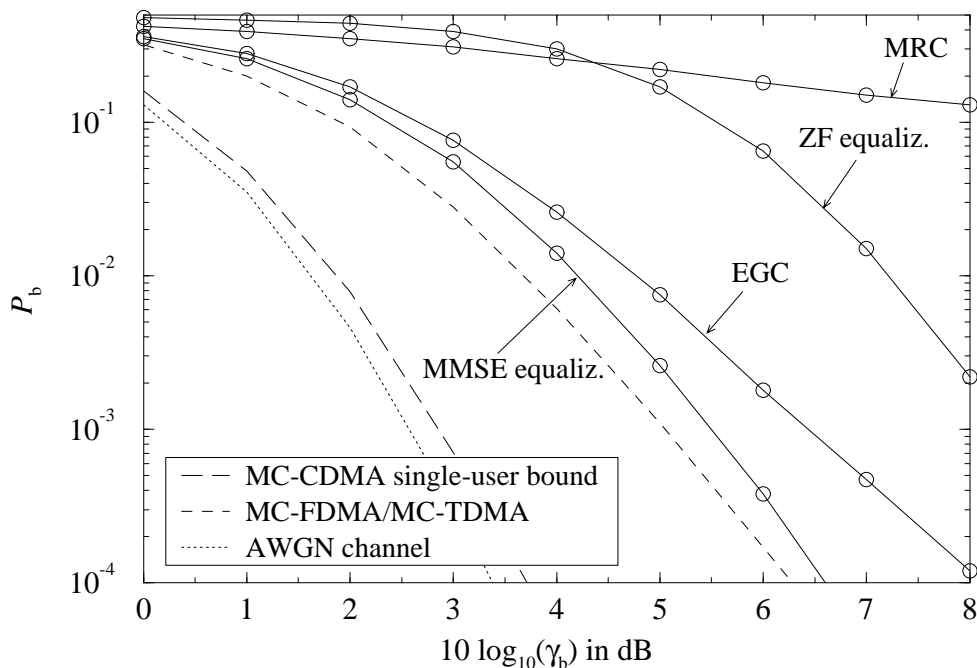


Figure 4.6: Average coded BER P_b versus SNR γ_b for SD with MRC, ZF equalization, EGC, and MMSE equalization; uncorrelated Rayleigh fading channel; $L = 8$; $K_q = 8$; QPSK; $R = 1/2$

performance of the MC-CDMA, MC-FDMA, and MC-TDMA system in the AWGN channel is shown in Fig. 4.6. It is interesting to observe that MC-FDMA and MC-TDMA systems require about 0.5 dB less SNR to reach the average coded BER P_b equal to 10^{-3} than MC-CDMA systems with MMSE equalization when considering the case with full subsystem load.

In contrast to the uncoded performance shown in Fig. 3.15, it can be concluded that MC-CDMA systems exploiting SD with MMSE equalization, MC-FDMA systems, and MC-TDMA systems achieve similar performance with channel coding of rate R equal to $1/2$ and fully loaded subsystem. Furthermore, it should be noted that the performance of coded MC-CDMA systems with simple EGC requires only an about 1 dB higher SNR to reach the average coded BER P_b equal to 10^{-3} compared to the more complex MC-CDMA systems with MMSE equalization. With fully loaded subsystem, the SD techniques MRC and ZF equalization are not of interest in practice.

The average coded BER P_b versus the SNR γ_b for MD with soft IC, MLSSE, and SD with MMSE equalization exploiting the optimum LLRs is presented in Fig. 4.7. The performance

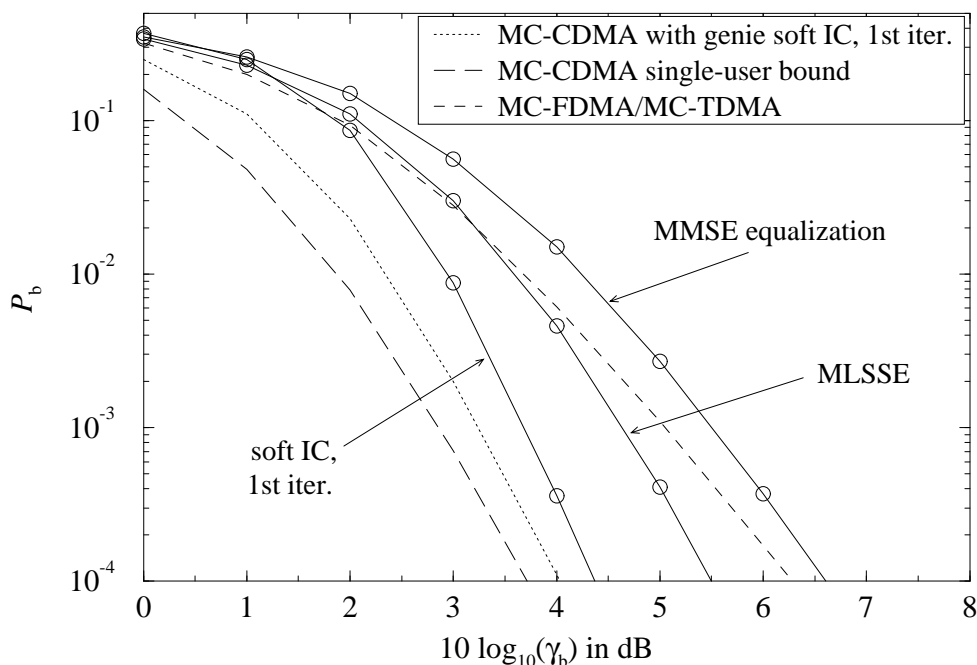


Figure 4.7: Average coded BER P_b versus SNR γ_b for MD with soft IC after 1st iteration, MLSSE, and SD with MMSE equalization; uncorrelated Rayleigh fading channel; $L = 8$; $K_q = 8$; QPSK; $R = 1/2$

of soft IC with genie soft-in/soft-out decoder, cf. (4.39), is shown as reference. MC-CDMA systems with the MD technique soft IC outperform MC-FDMA and MC-TDMA systems and also MC-CDMA systems with MLSSE and with MMSE equalization. The performance with MMSE equalization is the performance obtained after the initial stage with soft IC. Promising results are obtained with soft IC already after the first iteration. The performance with soft IC closely approximates the performance of soft IC with a genie soft-in/soft-out decoder and also the single-user bound and requires already after the first iteration only 0.4 dB and 0.8 dB, respectively, more SNR to reach the average coded BER P_b equal to 10^{-3} . The important result is that when re-encoded bits are used for IC, it is possible to outperform JD with MLSSE followed by soft decision channel decoding. Consequently, it is possible to cancel almost all of

the MAI after only one detection stage. It should be noted that when re-encoded hard decided values are used for IC, the performance degradation in SNR of the MC-CDMA reference system in the uncorrelated Rayleigh fading channel is 0.3 dB compared to soft IC at a coded BER P_b equal to 10^{-3} .

In the following, the influence of the number of active users on the performance of a coded MC-CDMA system is investigated. Fig. 4.8 shows the required SNR γ_b to achieve a BER P_b equal to 10^{-3} versus the loading ratio K_q/L . The considered detection techniques MMSE

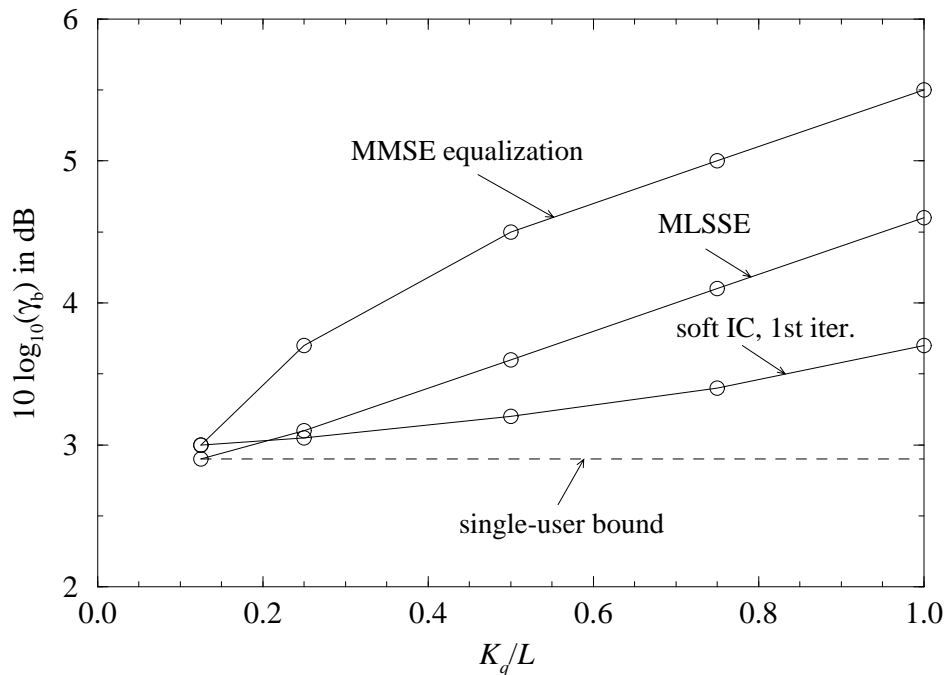


Figure 4.8: SNR γ_b required to achieve a BER of $P_b = 10^{-3}$ versus loading ratio K_q/L ; MMSE equalization, soft IC after 1st iteration, and MLSSE; uncorrelated Rayleigh fading channel; $L = 8$; QPSK; $R=1/2$

equalization, MLSSE, and soft IC after the 1st iteration show, similar to the uncoded case given in Fig. 3.18, an increasing SNR degradation with increasing number of active users K_q . It can be observed that soft IC is the detection technique which best handles MAI compared to MLSSE and MMSE equalization. With soft IC, the SNR degradation compared to the single-user bound is, even with full subsystem load, less than 1 dB at a BER P_b equal to 10^{-3} .

To prove the suitability of Turbo codes as channel codes in MC-CDMA mobile radio systems, the following Turbo coding scheme is chosen. The component codes of the Turbo code are recursive systematic RCP codes, each of rate $2/3$, resulting in an overall Turbo code rate of R equal to $1/2$. Since the performance with Turbo codes in fading channels cannot be improved with a memory M_c greater than 2 for a coded BER P_b equal to 10^{-3} [HRP94], the memory of the used Turbo code is M_c equal to 2 in order to minimize the computational complexity. The component decoders exploit the soft output Viterbi algorithm (SOVA) [HaH89]. The Turbo code interleaver is implemented as a random interleaver [HRP94]. The iterative Turbo

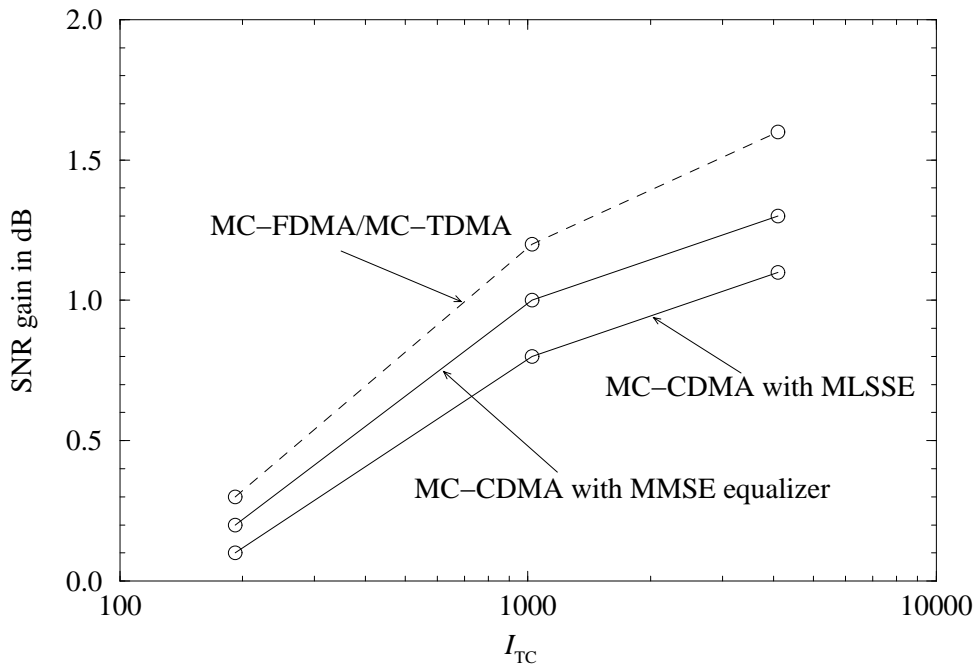


Figure 4.9: SNR gain with Turbo codes relative to conventional convolutional codes versus Turbo code interleaver size I_{TC} ; uncorrelated Rayleigh fading channel; $L = 8$; $K_q = 8$; QPSK; $R = 1/2$; Turbo decoding with 10 iterations; $P_b = 10^{-3}$

decoding in the channel decoder uses 10 iterations. The SNR gain with Turbo codes relative to the convolutional codes presented in Table 4.1 versus the Turbo code interleaver size I_{TC} is given in Fig. 4.9 for the average BER P_b equal to 10^{-3} . The results show that MC-FDMA and MC-TDMA systems most benefit from the application of Turbo codes. It can be observed that the improvements with Turbo codes at interleaver sizes smaller than 1000 are less than 1 dB and, in this case, do not justify the additional complexity and delay due to the iterations with Turbo decoding. Since for speech transmission delays up to 20 ms are tolerable, the Turbo code interleaver size is limited to approximately 200 when assuming data rates of about 10 kbit/s. Thus, MC-CDMA systems developed for speech transmission cannot profit from Turbo decoding. Turbo codes may be of interest, for instance, in data transmission applications which allow greater delays and, thus, greater interleaver sizes.

4.6 Trade-off between Channel Coding and Spreading

In Section 3.4, the achievable SNR gain due to the spread spectrum technique for uncoded MC-CDMA mobile radio systems relative to uncoded MC-FDMA and MC-TDMA systems is demonstrated. In Section 4.5, the potential of channel coding is impressively shown by the significant performance enhancement of MC-FDMA and MC-TDMA systems due to channel coding. Both effects lead to the task of finding a trade-off between channel code rate and spreading code length in MC-CDMA mobile radio systems also with respect to different detection techniques [Kai96]. The following investigations are carried out for MC-CDMA systems

using either SD with MMSE equalization or JD with MLSSE. Unless otherwise stated, the parameters defined for the MC-CDMA reference system are used.

In Fig. 4.10, the average BER P_b for code rates R equal to $2/3$, $1/2$, and $1/3$ versus the SNR γ_b for MC-CDMA systems using SD with MMSE equalization and for MC-FDMA and MC-TDMA systems is presented. The case with fully loaded subsystem is considered, i.e., K_q and L are equal to 8. In Fig. 4.11, the SNR gain achievable with coded MC-CDMA systems using SD with MMSE equalization relative to coded MC-FDMA and MC-TDMA systems versus the spreading code length L is shown. The SNR gains are given for different code rates R at a BER P_b equal to 10^{-3} . The corresponding results for MC-CDMA systems exploiting JD with MLSSE are presented in Figs. 4.12 and 4.13, respectively. However, due to the complexity of the MLSSE, only results with spreading codes of length L up to 8 are given in Fig. 4.13. In Figs. 4.11 and 4.13, the case with fully loaded subsystem and the single-user case is considered. It is important to note that curves in Figs. 4.11 and 4.13 cannot be used to determine SNR gains between any MC-CDMA systems with different code rates R . The reason is that SNR gains presented for different code rates are based on different MC-FDMA and MC-TDMA reference curves. When comparing curves from Fig. 4.11 with curves with the same code rate from Fig. 4.13, the gain of MC-CDMA systems with MLSSE compared to MC-CDMA systems with MMSE equalization is obtained.

From Figs. 4.10 to 4.13 the following important results are obtained:

- In the case with fully loaded subsystem, the performance of MC-CDMA systems is quasi independent of the spreading code length L , except for MC-CDMA systems with MLSSE and high code rates greater than $1/2$. The performance of MC-CDMA, MC-FDMA, and MC-TDMA systems is similar for code rates R lower than $2/3$ in the case of fully loaded subsystem. In not fully loaded systems, which are found most often in practice, MC-CDMA systems can significantly outperform MC-FDMA and MC-TDMA systems. The reason for the good performance of MC-FDMA and MC-TDMA systems with low rate codes is that the high redundancy introduced with low rate codes exploits nearly all the diversity offered by the mobile radio channel.
- The SNR gain achievable with MC-CDMA systems compared to MC-FDMA and MC-TDMA systems does not change essentially with spreading code length L greater than 8. It is important to note that this result is obtained in a mobile radio channel which is not limited in diversity. Thus, MC-CDMA systems using code rates R lower than $2/3$ should use spreading codes of maximum length L equal to 8. Higher spreading code lengths do not improve the performance but only increase the system complexity.
- The SNR gain achievable with MC-CDMA systems compared to MC-FDMA and MC-TDMA systems increases with decreasing subsystem load. This effect becomes more obvious with increasing spreading code length. The reason for this effect lies in the exploitation of the diversity gain due to data symbol spreading, which dominates with decreasing MAI.

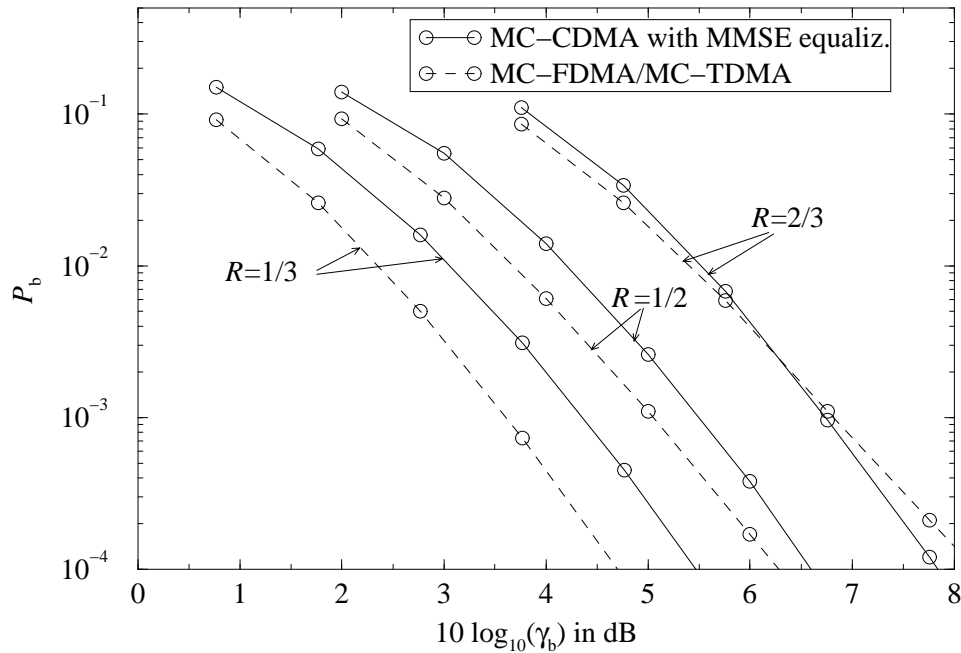


Figure 4.10: Average coded BER P_b versus SNR γ_b for MC-CDMA using SD with MMSE equalization, MC-FDMA, and MC-TDMA; different code rates; uncorrelated Rayleigh fading channel; $L = 8$; $K_q = 8$; QPSK

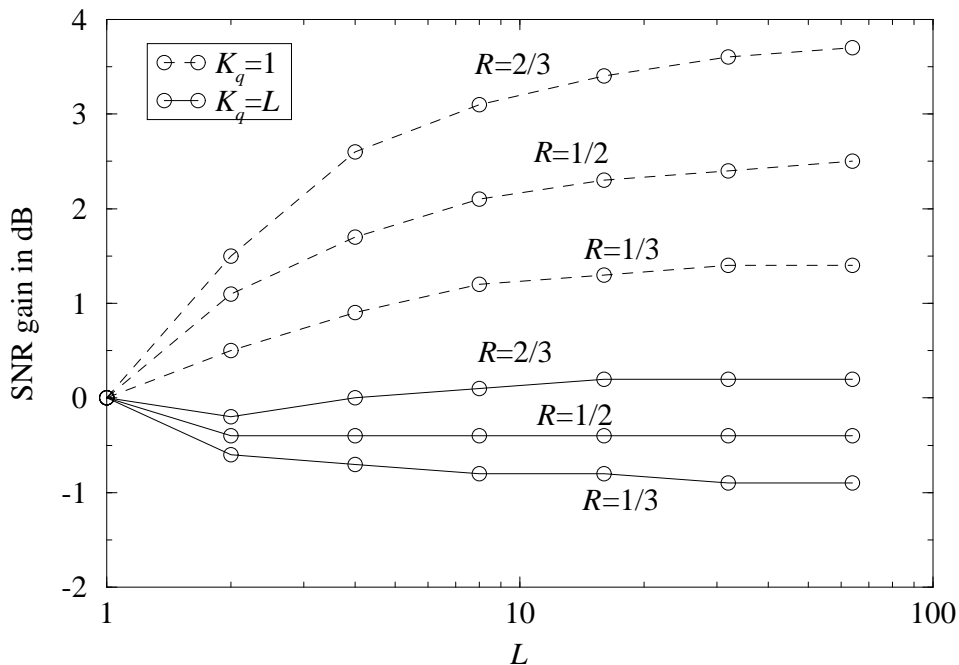


Figure 4.11: SNR gain of MC-CDMA using SD with MMSE equalization relative to MC-FDMA and MC-TDMA versus spreading code length L for different code rates R ; uncorrelated Rayleigh fading channel; fully loaded subsystem and single user case; QPSK; $P_b = 10^{-3}$

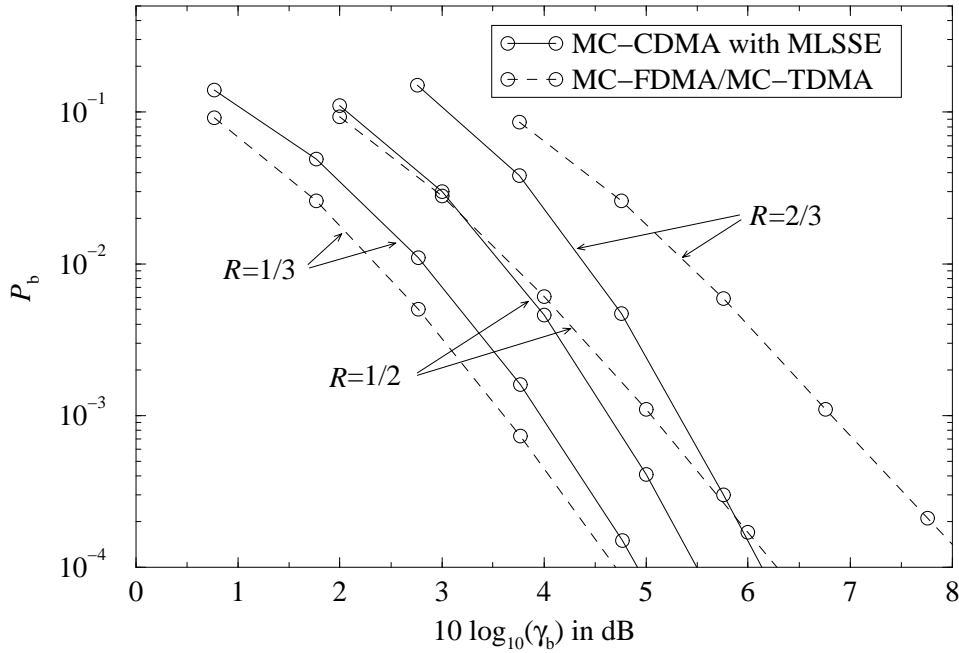


Figure 4.12: Average coded BER P_b versus SNR γ_b for MC-CDMA using JD with MLSSE, MC-FDMA, and MC-TDMA; different code rates; uncorrelated Rayleigh fading channel; $L = 8$; $K_q = 8$; QPSK

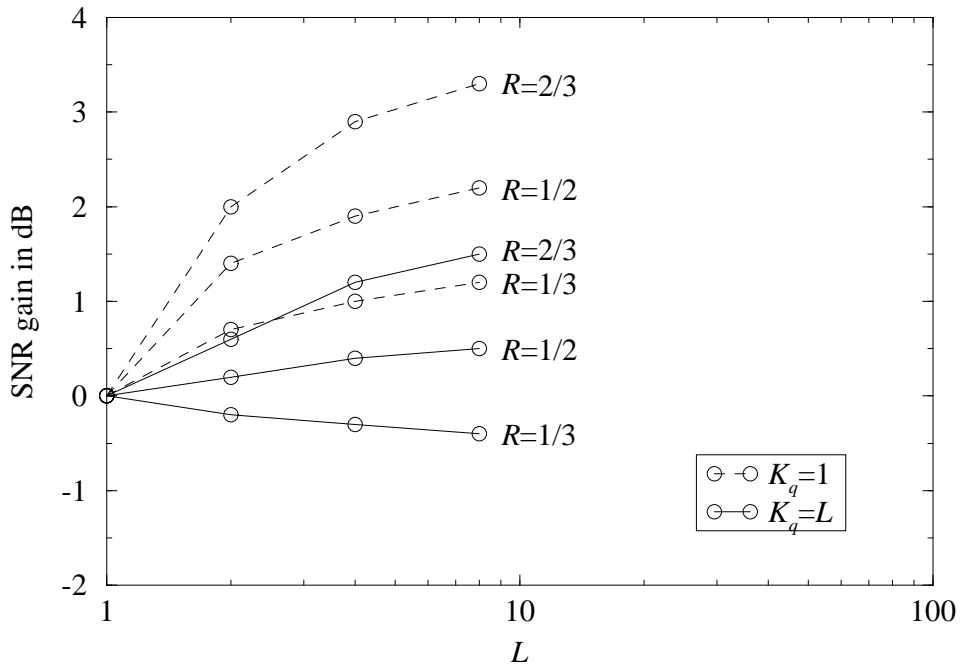


Figure 4.13: SNR gain of MC-CDMA using JD with MLSSE relative to MC-FDMA and MC-TDMA versus spreading code length L for different code rates R ; uncorrelated Rayleigh fading channel; fully loaded subsystem and single user case; QPSK; $P_b = 10^{-3}$

- The SNR gain achievable with MC-CDMA systems compared to MC-FDMA and MC-TDMA systems increases with increasing code rate R . This result could be expected, since in the uncoded case with code rate R equal to 1, MC-CDMA systems significantly outperform MC-FDMA and MC-TDMA systems, cf. Section 3.4.

A useful illustration of the influence of data symbol spreading, channel coding, and system load on the bandwidth efficiency β , cf. (1.1), of a mobile radio system is the so-called bandwidth efficiency plan. The bandwidth efficiency plan depicts the achievable bandwidth efficiency at a certain BER versus the SNR γ_b . Figs. 4.14 and 4.15 present the bandwidth efficiency plan of MC-CDMA systems using JD with MLSSE and of MC-FDMA and MC-TDMA systems. The results are given for the BER P_b equal to 10^{-3} . The JD technique MLSSE has been chosen for data detection in the MC-CDMA receiver since its performance is a good compromise between the enhanced performance achievable with soft IC and the worse performance with simple MMSE equalization, cf. Fig. 4.7. To be more general, the loss in bandwidth efficiency due to the guard interval is not taken into account in both bandwidth efficiency plans for the reason mentioned in Section 3.4. Fig. 4.14 illustrates the influence of channel coding and Fig. 4.15 the influence of data symbol spreading and system load. When comparing both bandwidth efficiency plans, it can be observed that coded MC-CDMA systems outperform coded MC-FDMA and MC-TDMA systems when demanding high bandwidth efficiency at low SNRs, as in the case of UMTS or IMT-2000. It should be noted that in the more probable case with not fully loaded system, the required SNR in MC-FDMA and MC-TDMA systems remains constant given a certain BER, whereas in MC-CDMA system the required SNR decreases, cf. Fig. 4.8.

With the results presented in this section, it can be concluded that for code rates R equal to or greater than $1/2$, a higher bandwidth efficiency can be achieved with MC-CDMA systems compared to MC-FDMA and MC-TDMA systems. Spreading codes of length L up to 8 are sufficient. When using code rates R lower than $1/2$, the additional complexity due to spectrum spreading in MC-CDMA systems cannot significantly improve the system performance compared to the less complex MC-FDMA or MC-TDMA systems and is thus not always justified.

It should be noted that the application of low rate orthogonal convolutional codes [Vit90] as spreading and simultaneously as channel codes has been investigated for MC-CDMA systems in [MaO96, StP97a, MaO97b]. It has been shown that with very low numbers of active users, MC-CDMA systems with low rate orthogonal convolutional codes can outperform MC-CDMA systems with separated channel coding and spreading. However, the application of low rate orthogonal convolutional codes is limited to only a few users [StP97a] since the signals are not necessarily orthogonal between the users, resulting in possibly severe MAI. Thus, the application of low rate orthogonal convolutional codes in MC-CDMA systems as spreading and channel code simultaneously is drastically limited in bandwidth efficiency [StP97a] and cannot reach the high bandwidth efficiency of MC-CDMA systems with separated channel coding and spreading, as considered in this thesis.

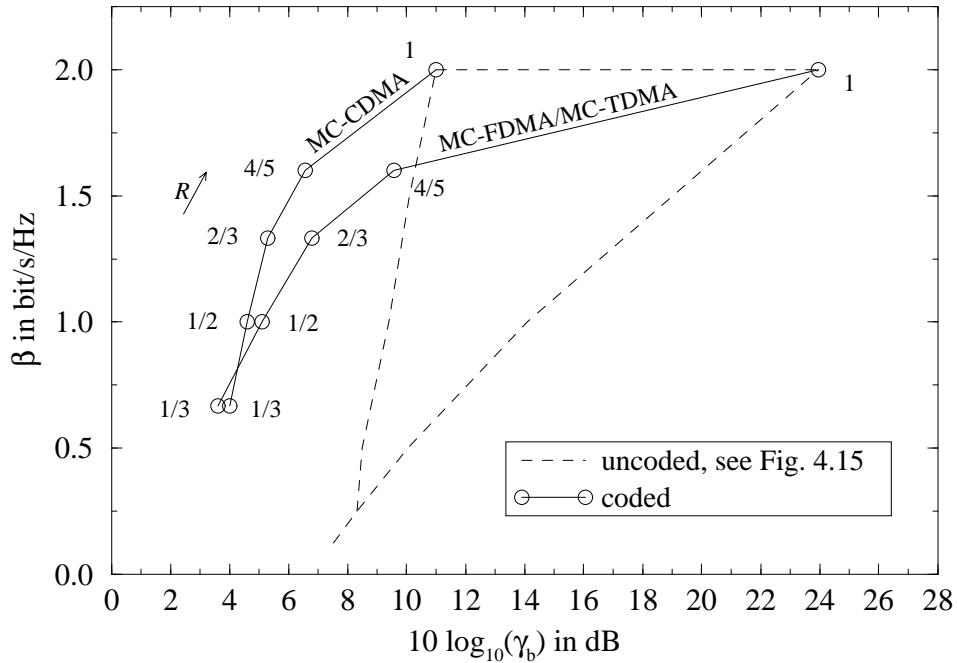


Figure 4.14: Bandwidth efficiency plan for coded MC-CDMA systems with MLSSE, $L = 8$, and $K_q = 8$ and for coded MC-FDMA and MC-TDMA systems; uncorrelated Rayleigh fading channel; QPSK; $P_b = 10^{-3}$; to be more general, a loss due to the guard interval is not taken into account

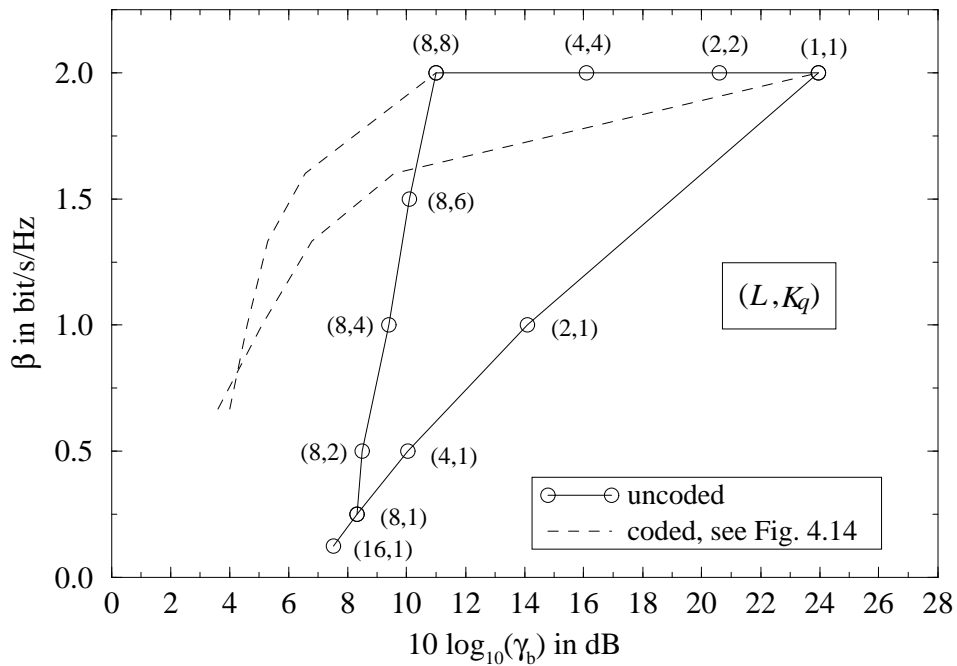


Figure 4.15: Bandwidth efficiency plan for uncoded MC-CDMA systems with MLSSE; uncorrelated Rayleigh fading channel; QPSK; $P_b = 10^{-3}$; to be more general, a loss due to the guard interval is not taken into account

Chapter 5

Channel Estimation for Multi-Carrier Systems

5.1 Pilot Symbol Aided Channel Estimation in Two Dimensions

When applying receivers with coherent detection, cf. Chapter 3, and with soft decision decoding, cf. Chapter 4, in fading channels, information about the channel state is required and has to be estimated by the receiver. The basic principle of pilot symbol aided channel estimation is to multiplex pilot symbols into the data stream. The receiver estimates the channel state information based on the received pilot symbols. In single carrier modulated systems, channel estimation is carried out by inserting pilot symbols or pilot sequences in the serial data stream in time direction to estimate the channel impulse response $\underline{h}(\tau, t)$, as applied in the GSM system [Ste94]. However, particularly transmission systems with MC modulation allow channel estimation in two dimensions by inserting pilot symbols on different subcarriers in frequency direction in addition to the time direction, with the intention to estimate the channel transfer function $\underline{H}(f, t)$ [Höh91, CSM95, San96, HKR97a, HKR97b]. By choosing the distances of the pilot symbols in time and frequency direction sufficiently small with respect to the channel bandwidth, estimates of the channel transfer function can be obtained by interpolation. The channel estimation in two dimensions designed in this chapter is applicable to various MC modulated systems like, for instance, MC-CDMA, MC-FDMA, or MC-TDMA mobile radio systems.

The presented channel estimation operates on OFDM frames where $\underline{H}(f, t)$ is estimated separately for each transmitted OFDM frame, allowing burst transmission based on OFDM frames. The discrete-frequency and -time representation $\underline{H}_{n,i}$ of the channel transfer function introduced in (2.26) is used in the sequel. The values $n = 1, \dots, N_c$ and $i = 1, \dots, N_s$ are the frequency and time indices of the fading process where N_c is the number of subcarriers per OFDM symbol and N_s is the number of OFDM symbols per OFDM frame. The estimates of the discrete channel transfer function are denoted as $\hat{H}_{n,i}$, $n = 1, \dots, N_c$, $i = 1, \dots, N_s$. An OFDM frame consisting of N_s equal to 13 OFDM symbols, each with N_c equal to 11 subcarriers, is shown in Fig. 5.1. The rectangular arrangement of the pilot symbols shown in Fig. 5.1 is

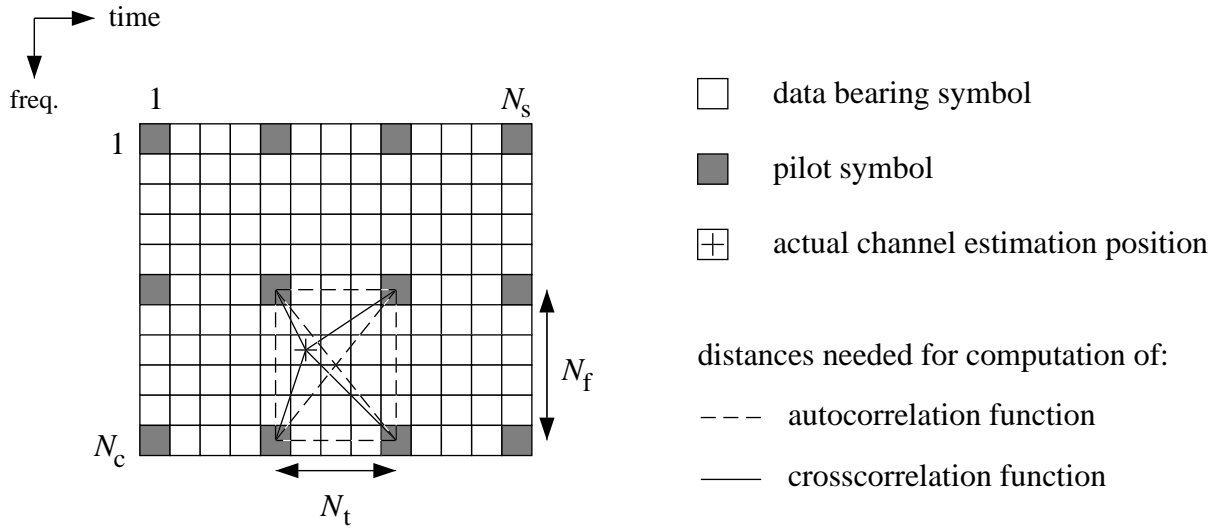


Figure 5.1: OFDM frame with rectangularly distributed pilot symbols; $N_c = 11$; $N_s = 13$; $N_f = 5$; $N_t = 4$; $N_{\text{grid}} = 12$; $N_{\text{tap}} = 4$

referred to as rectangular grid. The distance between two pilot symbols in frequency direction is N_f and in time direction is N_t . In the example given in Fig. 5.1, N_f is equal to 5 and N_t is equal to 4. The choice of a rectangular grid is motivated by the results presented in [HKR97b] where the performance of rectangularly, diagonally, and randomly distributed pilot symbols in an OFDM frame is investigated. A channel estimation either with rectangularly or with diagonally distributed pilot symbols shows similar performance but outperforms channel estimation with randomly distributed pilot symbols [HKR97b].

The received symbols of an OFDM frame are given by

$$R_{n,i} = H_{n,i} S_{n,i} + N_{n,i}, \quad n = 1, \dots, N_c, \quad i = 1, \dots, N_s, \quad (5.1)$$

where $S_{n,i}$ and $N_{n,i}$ are the transmitted symbols and the noise components, respectively, see (3.13). The indices n, i indicate the position of both the symbols and the noise components in time and frequency direction within an OFDM frame.

Assuming that the first pilot symbol in the rectangular grid is located in the first subcarrier of the first OFDM symbol in an OFDM frame, the pilot symbols are given by $S_{(p-1)N_f+1, (q-1)N_t+1}$, $p = 1, \dots, \lceil N_c/N_f \rceil$, $q = 1, \dots, \lceil N_s/N_t \rceil$. For brevity, the pilot symbols are written as $S_{n',i'}$, where the frequency and time indices at locations of pilot symbols are marked as n' and i' , i.e.,

$$n' = (p-1)N_f + 1, \quad p = 1, \dots, \lceil N_c/N_f \rceil \quad (5.2)$$

and

$$i' = (q-1)N_t + 1, \quad q = 1, \dots, \lceil N_s/N_t \rceil. \quad (5.3)$$

The set of pilot positions in an OFDM frame is \mathcal{P} . The number of pilot symbols in an OFDM frame results in

$$N_{\text{grid}} = \left\lceil \frac{N_c}{N_f} \right\rceil \left\lceil \frac{N_s}{N_t} \right\rceil = \|\mathcal{P}\|. \quad (5.4)$$

The two-dimensional (2-D) pilot symbol aided channel estimation operates in two steps:

- In a first step, the initial estimate $\check{H}_{n',i'}$ of the channel transfer function at positions where pilot symbols are located is obtained by dividing the received pilot symbol $R_{n',i'}$ by the originally transmitted pilot symbol $S_{n',i'}$, i.e.,

$$\begin{aligned}\check{H}_{n',i'} &= \frac{R_{n',i'}}{S_{n',i'}} \\ &= \underline{H}_{n',i'} + \frac{N_{n',i'}}{S_{n',i'}}, \quad \forall \{n',i'\} \in \mathcal{P}.\end{aligned}\quad (5.5)$$

- In a second step, the final estimates of the complete channel transfer function belonging to the desired OFDM frame are obtained from the initial estimates $\check{H}_{n',i'}$ by a 2-D interpolation or filtering, respectively. The 2-D filtering is given by

$$\hat{H}_{n,i} = \sum_{\{n',i'\} \in \mathcal{T}_{n,i}} \omega_{n',i',n,i} \check{H}_{n',i'}, \quad \mathcal{T}_{n,i} \in \mathcal{P}, \quad n = 1, \dots, N_c, \quad i = 1, \dots, N_s, \quad (5.6)$$

where $\omega_{n',i',n,i}$ is the shift-variant 2-D impulse response of the filter. The subset $\mathcal{T}_{n,i} \in \mathcal{P}$ is the set of initial estimates $\check{H}_{n',i'}$ that are actually used for estimation of $\hat{H}_{n,i}$. The number of filter coefficients is

$$N_{\text{tap}} = \|\mathcal{T}_{n,i}\| \leq N_{\text{grid}}. \quad (5.7)$$

In the OFDM frame illustrated in Fig. 5.1, N_{grid} is equal to 12 and N_{tap} is equal to 4. In the following, all statements made for values and functions with the index n, i are valid for each $n = 1, \dots, N_c, i = 1, \dots, N_s$.

5.2 Theory of Two-Dimensional Wiener Filtering

The criterion for the evaluation of the channel estimator is the mean square value of the estimation error

$$\varepsilon_{n,i} = H_{n,i} - \hat{H}_{n,i}. \quad (5.8)$$

The mean square error is given by

$$J_{n,i} = \text{E}\{|\varepsilon_{n,i}|^2\}. \quad (5.9)$$

The optimal filter in the sense of minimizing $J_{n,i}$ with the MMSE criterion is the 2-D Wiener filter [Hay86]. The filter coefficients of the 2-D Wiener filter are obtained by applying the orthogonality principle in linear mean square estimation [Hay86, Pap91],

$$\text{E}\{\varepsilon_{n,i} \check{H}_{n'',i''}^*\} = 0, \quad \forall \{n'',i''\} \in \mathcal{T}_{n,i}. \quad (5.10)$$

The orthogonality principle states that the mean square error $J_{n,i}$, is minimum if the filter coefficients $\omega_{n',i',n,i}, \forall \{n',i'\} \in \mathcal{T}_{n,i}$, are selected such that the error $\varepsilon_{n,i}$ is orthogonal to all

initial estimates $\check{H}_{n'',i''}^*$, $\forall \{n'', i''\} \in \mathcal{T}_{n,i}$. The orthogonality principle leads to the Wiener-Hopf equation [Pap91], stating that

$$\mathbb{E}\{\underline{H}_{n,i}\check{H}_{n'',i''}^*\} = \sum_{\{n',i'\} \in \mathcal{T}_{n,i}} \omega_{n',i',n,i} \mathbb{E}\{\check{H}_{n',i'}\check{H}_{n'',i''}^*\}, \quad \forall \{n'', i''\} \in \mathcal{T}_{n,i}. \quad (5.11)$$

The crosscorrelation function $\mathbb{E}\{\underline{H}_{n,i}\check{H}_{n'',i''}^*\}$ is introduced as

$$\underline{\theta}_{n-n'',i-i''} = \mathbb{E}\{\underline{H}_{n,i}\check{H}_{n'',i''}^*\}. \quad (5.12)$$

With (5.5) and by assuming that $\underline{N}_{n'',i''}$ has zero mean and is statistically independent from the pilot symbols $\underline{S}_{n'',i''}$, the crosscorrelation function $\mathbb{E}\{\underline{H}_{n,i}\check{H}_{n'',i''}^*\}$ is equal to the discrete time-frequency correlation function $\mathbb{E}\{\underline{H}_{n,i}\underline{H}_{n'',i''}^*\}$, i.e.,

$$\underline{\theta}_{n-n'',i-i''} = \mathbb{E}\{\underline{H}_{n,i}\underline{H}_{n'',i''}^*\}. \quad (5.13)$$

The time-frequency correlation function is the Fourier transform of the delay cross-power spectral density $\rho(\tau, \Delta t)$, cf. (2.4). The autocorrelation function $\mathbb{E}\{\check{H}_{n',i'}\check{H}_{n'',i''}^*\}$ in (5.11) is given by

$$\underline{\phi}_{n'-n'',i'-i''} = \mathbb{E}\{\check{H}_{n',i'}\check{H}_{n'',i''}^*\} \quad (5.14)$$

and can be written in the form

$$\underline{\phi}_{n'-n'',i'-i''} = \underline{\theta}_{n'-n'',i'-i''} + \frac{\sigma^2}{\mathbb{E}\{|\underline{S}_{n',i'}|^2\}} \delta_{n'-n'',i'-i''}. \quad (5.15)$$

The crosscorrelation function (5.12) depends on the distances between the actual channel estimation position n, i and all pilot positions n'', i'' , whereas the autocorrelation function (5.14) depends only on the distances between the pilot positions and, hence, is independent of the actual channel estimation position n, i . Both relations are illustrated in Fig. 5.1. In this thesis, it is assumed that the second moment $\mathbb{E}\{|\underline{S}_{n,i}|^2\}$, corresponding to the mean energy of the symbols $\underline{S}_{n,i}$, is equal for all transmitted symbols $\underline{S}_{n,i}$, $n = 1, \dots, N_c$, $i = 1, \dots, N_s$, including pilot symbols. With (3.50), the autocorrelation function $\underline{\phi}_{n'-n'',i'-i''}$ for MC-CDMA systems is given by

$$\underline{\phi}_{n'-n'',i'-i''} = \underline{\theta}_{n'-n'',i'-i''} + \frac{1}{\gamma_c} \delta_{n'-n'',i'-i''}, \quad (5.16)$$

assuming that the average SNR γ_c on all subcarriers, i.e., in all subsystems, is equal. It is important to note that in the synchronous downlink of MC-CDMA systems the pilot symbols of the K_q users are transmitted simultaneously on the same positions. Thus, the total available energy of the pilot symbols in an OFDM frame which can be exploited per user increases with increasing number of users. On the other hand, the energy of a pilot symbol per user decreases with increasing spreading code length L . When the channel estimation is applied in MC systems which do not exploit the spread spectrum technique, the SNR γ_c is equal to the SNR γ_s , cf. (3.51).

The pilot symbols $\underline{S}_{n',i'}$ can also be transmitted with higher average energy than the data bearing symbols $\underline{S}_{n,i}$, $n \neq n', i \neq i'$. Pilot symbols with increased energy are called boosted

pilot symbols. The boosting of pilot symbols is for example specified in the European DVB-T standard and achieves better estimates of the channel but reduces the average SNR of the data symbols. The choice of an appropriate boosting level for the pilot symbols is investigated in [HKR97b]. As mentioned before, the pilot symbols used in this thesis are not boosted in energy.

Inserting (5.12) and (5.14) into (5.11) yields in vector notation

$$\boldsymbol{\theta}_{n,i}^T = \boldsymbol{\omega}_{n,i}^T \boldsymbol{\Phi}, \quad (5.17)$$

where $\boldsymbol{\Phi}$ is the $N_{\text{tap}} \times N_{\text{tap}}$ autocorrelation matrix and $\boldsymbol{\theta}_{n,i}$ is the crosscorrelation vector of length N_{tap} . The vector $\boldsymbol{\omega}_{n,i}$ of length N_{tap} represents the filter coefficients $\omega_{n',i',n,i}$ required to obtain the estimate $\hat{H}_{n,i}$. Hence, the filter coefficients of the optimum 2-D Wiener filter are

$$\boldsymbol{\omega}_{n,i}^T = \boldsymbol{\theta}_{n,i}^T \boldsymbol{\Phi}^{-1}, \quad (5.18)$$

when assuming that the auto- and crosscorrelation functions are perfectly known and

$$N_{\text{tap}} = N_{\text{grid}}. \quad (5.19)$$

Since 2-D Wiener filters in general tend to have a large computational complexity, the choice of two cascaded 1-D Wiener filters working sequentially can give a good trade-off between performance and complexity [Höh91, HKR97a, HKR97b]. In the following two sections, the performance of a Wiener filter implemented as a 2-D finite impulse response (FIR) filter and implemented as two one-dimensional (2×1 -D) FIR filters working sequentially is analyzed. The implementation with model mismatch, i.e., the case when the correlation functions used in the filter design and those of the actual channel do not match, is taken into account in the analysis. Hence, the filter coefficients, whether they are optimal or suboptimal with respect to the channel correlation functions, are generally denoted by

$$\tilde{\boldsymbol{\omega}}_{n,i}^T = \tilde{\boldsymbol{\theta}}_{n,i}^T \tilde{\boldsymbol{\Phi}}^{-1} \quad (5.20)$$

in the sequel. When explicitly treating with the optimum correlation functions and filter coefficients, the notation given in (5.18) is used.

5.3 Performance Analysis with Model Mismatch

5.3.1 Two-Dimensional FIR Filter

For a given set of filter coefficients $\tilde{\boldsymbol{\omega}}_{n,i}$ of a 2-D FIR filter, (5.6) can be written in vector notation as

$$\hat{H}_{n,i} = \tilde{\boldsymbol{\omega}}_{n,i}^T \check{\mathbf{h}}. \quad (5.21)$$

The vector $\check{\mathbf{h}}$ of length N_{tap} represents the subset $\mathcal{T}_{n,i} \in \mathcal{P}$ of the initial channel estimates $\check{H}_{n',i'}$ according to (5.5) which are required to obtain the estimate $\hat{H}_{n,i}$. Substitution of (5.21) into (5.9) yields the mean square error

$$\begin{aligned} J_{n,i} &= \text{E}\{(\underline{H}_{n,i} - \tilde{\omega}_{n,i}^T \check{\mathbf{h}})(\underline{H}_{n,i}^* - \check{\mathbf{h}}^H \tilde{\omega}_{n,i}^*)\} \\ &= \text{E}\{|\underline{H}_{n,i}|^2\} - \text{E}\{\underline{H}_{n,i} \check{\mathbf{h}}^H\} \tilde{\omega}_{n,i}^* - \tilde{\omega}_{n,i}^T \text{E}\{\check{\mathbf{h}} \underline{H}_{n,i}^*\} + \tilde{\omega}_{n,i}^T \text{E}\{\check{\mathbf{h}} \check{\mathbf{h}}^H\} \tilde{\omega}_{n,i}^* \\ &= \text{E}\{|\underline{H}_{n,i}|^2\} - \underline{\boldsymbol{\theta}}_{n,i}^T \tilde{\omega}_{n,i}^* - \tilde{\omega}_{n,i}^T \boldsymbol{\theta}_{n,i}^* + \tilde{\omega}_{n,i}^T \boldsymbol{\Phi} \tilde{\omega}_{n,i}^* \end{aligned} \tag{5.22}$$

where $\boldsymbol{\theta}_{n,i}$ and $\boldsymbol{\Phi}$ are the exact cross- and autocorrelation matrices, respectively. The symbol $(\cdot)^H$ denotes the Hermitian transposition which is the conjugate complex transposition $(\cdot)^{*T}$ of a vector or a matrix. Substitution of (5.20) into (5.22) yields the mean square error valid for any FIR filter by taking into account also model mismatch. If the cross- and autocorrelation functions are known perfectly, the MMSE is obtained by inserting (5.18) into (5.22), resulting in

$$J_{n,i} = \text{E}\{|\underline{H}_{n,i}|^2\} - \underline{\boldsymbol{\theta}}_{n,i}^T \boldsymbol{\Phi}^{-1} \boldsymbol{\theta}_{n,i}^* \tag{5.23}$$

5.3.2 Two Cascaded One-Dimensional FIR Filters

The principle of 2×1 -D filtering is depicted in Fig. 5.2. Filtering in the frequency direction on OFDM symbols containing pilot symbols, followed by filtering in time direction on all subcarriers is shown. This ordering is chosen to enable filtering in frequency direction directly

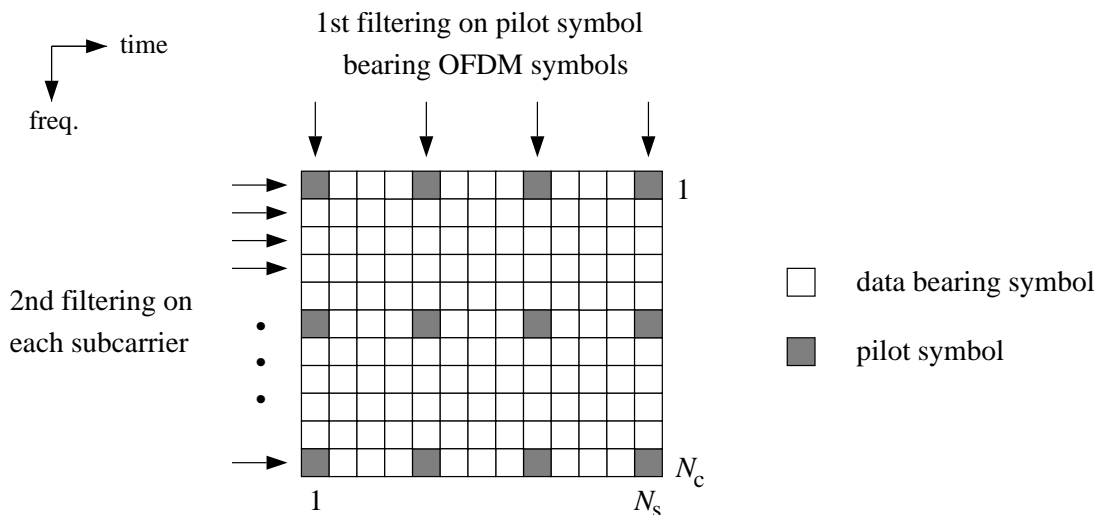


Figure 5.2: Principle of 2×1 -D FIR filtering

after receiving a pilot symbol bearing OFDM symbol and, thus, to reduce the overall filtering delay. However, the opposite ordering would achieve the same performance due to the linearity of the filters. The filter directions of the two FIR filters in frequency and time are orthogonal to each other, see Fig. 5.2. Moreover, in the mobile radio channel, it can be assumed that the

delay power density spectrum $\rho(\tau)$, cf. (2.6), and the Doppler power density spectrum $S_{f_D}(f_D)$, cf. (2.12), are statistically independent. Thus, the time-frequency correlation function can be separated in the frequency correlation function $\theta(\Delta f)$ according to (2.10) which is the Fourier transform of $\rho(\tau)$ and in the time correlation function $\underline{\theta}(\Delta t)$ according to (2.14) which is the inverse Fourier transform of $S_{f_D}(f_D)$. The discrete frequency correlation function $\underline{\theta}_{n-n''}$ is the sampled version of (2.10) and the discrete time correlation function $\underline{\theta}_{i-i''}$ is the sampled version of (2.14). The mean square error of the two cascaded 1-D FIR filters working sequentially is obtained in two steps. Values and functions related to the first filtering are marked with the index ^[1] and values and functions related to the second filtering are marked with the index ^[2].

1. The estimates delivered by the first 1-D FIR filter with coefficients $\tilde{\omega}_n^{[1]}$ are

$$\hat{H}_{n,i'}^{[1]} = \tilde{\omega}_n^{[1]T} \check{\mathbf{h}}_{i'}. \quad (5.24)$$

The filter coefficients given by the vector $\tilde{\omega}_n^{[1]}$ only depend on the frequency index n . The vector $\check{\mathbf{h}}_{i'}$ of length $N_{\text{tap}}^{[1]}$ represents the subset $\mathcal{T}_{n,i'}^{[1]} \in \mathcal{P}$ of the initial estimates $\check{H}_{n',i'}$ according to (5.5) of the i' 'th OFDM symbol used for the estimation of $\hat{H}_{n,i'}^{[1]}$. This operation is performed in all $\lceil N_s/N_t \rceil$ pilot symbol bearing OFDM symbols. Given (5.22), the corresponding mean square error with the first 1-D FIR filter is

$$J_n^{[1]} = \text{E}\{|\underline{H}_{n,i}|^2\} - \underline{\theta}_n^T \tilde{\omega}_n^{[1]*} - \tilde{\omega}_n^{[1]T} \underline{\theta}_n^* + \tilde{\omega}_n^{[1]T} \Phi \tilde{\omega}_n^{[1]*}. \quad (5.25)$$

2. The estimates delivered by the second 1-D FIR filter with coefficients $\tilde{\omega}_i^{[2]}$ are

$$\hat{H}_{n,i} = \hat{H}_{n,i}^{[2]} = \tilde{\omega}_i^{[2]T} \mathbf{h}_n^{[1]}. \quad (5.26)$$

The filter coefficients given by the vector $\tilde{\omega}_i^{[2]}$ only depend on the time index i . The vector $\mathbf{h}_n^{[1]}$ of length $N_{\text{tap}}^{[2]}$ represents the subset $\mathcal{T}_{n,i}^{[2]} \in \mathcal{P}$ of the estimates obtained from the first filtering and used for the second filtering on the n th subcarrier for the estimation of $\hat{H}_{n,i}^{[2]}$. (5.26) is performed for all N_c subcarriers. The mean square error with $2 \times$ 1-D FIR filtering yields [HKR97b]

$$J_{n,i} = J_{n,i}^{[2]} = \text{E}\{|\underline{H}_{n,i}|^2\} - \text{E}\{\underline{H}_{n,i} \mathbf{h}_n^{[1]H}\} \tilde{\omega}_i^{[2]*} - \tilde{\omega}_i^{[2]T} \text{E}\{\mathbf{h}_n^{[1]} \underline{H}_{n,i}^*\} + \tilde{\omega}_i^{[2]T} \text{E}\{\mathbf{h}_n^{[1]} \mathbf{h}_n^{[1]H}\} \tilde{\omega}_i^{[2]*}. \quad (5.27)$$

The crosscorrelation function $\text{E}\{\underline{H}_{n,i} \hat{H}_{n,i'}^{[1]*}\}$ in (5.27) is equal to the discrete time correlation function written as

$$\underline{\theta}_{i-i'}^{[1]} = \text{E}\{\underline{H}_{n,i} \hat{H}_{n,i'}^{[1]*}\}. \quad (5.28)$$

The error

$$\underline{\varepsilon}_{n,i'}^{[1]} = \hat{H}_{n,i'}^{[1]} - \underline{H}_{n,i'} \quad (5.29)$$

between the estimates after the first filtering and the real channel state is a zero mean noise process with variance

$$\text{E}\{|\underline{\varepsilon}_{n,i'}^{[1]}|^2\} = J_n^{[1]}. \quad (5.30)$$

Thus, with (5.28) and (5.30), the autocorrelation function in (5.27) is [HKR97b]

$$E\{\hat{H}_{n,i'}^{[1]}\hat{H}_{n,i''}^{[1]*}\} = J_n^{[1]}\delta_{i'-i''} + \theta_{i'-i''}^{[1]}. \quad (5.31)$$

Inserting (5.28) and (5.31) in (5.27) results in the mean square error obtained with 2×1 -D FIR filtering. A suitable approximation to take into account the SNR improvement after the first iteration is to choose $J_n^{[1]}$ in (5.31) equal to $1/(\gamma_c 10 \log_{10}(N_{\text{tap}}^{[1]}))$ [HKR97b]. This approximation is used in the case of 2×1 -D FIR filtering in the sequel.

5.4 Filter Design

A filter is designed by determining the filter coefficients $\tilde{\omega}_{n,i}$. In the following, the general case of 2-D filtering is considered. The filter coefficients for the of 2×1 -D filters are obtained from the 2-D filter coefficients by omitting the dimension which is not required in the corresponding 1-D filter. With (5.13), (5.16), and (5.20), the 2-D filter coefficients can be calculated, given the discrete time-frequency correlation function of the channel $\underline{\theta}_{n-n'',i-i''}$ and the average SNR γ_c . The discrete time-frequency correlation function $\underline{\theta}_{n-n'',i-i''}$ can be separated into the discrete frequency correlation function $\underline{\theta}_{n-n''}$ and into the discrete time correlation function $\underline{\theta}_{i-i''}$ as described in Section 5.3.2. Hence, the optimum filter has to be adapted to the power density spectra $\rho(\tau)$, cf. (2.6), and $S_{f_D}(f_D)$, cf. (2.12), of the mobile radio channel. However, since in practice $\rho(\tau)$ and $S_{f_D}(f_D)$ are not perfectly known in the receiver, the filters of the channel estimator have to be designed according to the following requirements:

- A great variety of delay power density spectra whether they are exponentially decreasing or not, with different delay spreads should be covered.
- A great variety of Doppler power density spectra like classical, Gaussian, and other power density spectra with different maximum Doppler frequencies should be covered.
- The correlation functions $\tilde{\theta}_{n,i}$ and $\tilde{\Phi}$ should be real-valued functions with the intention of achieving real-valued filter coefficients $\tilde{\omega}_{n,i}$, cf. (5.20), and, thus, to reduce the computational complexity. This corresponds to filtering the quadrature components of $\underline{H}_{n,i}$ by two identical, independent, real-valued filters. Hence, the computational effort is reduced by a factor of approximately two compared to the filter with complex-valued coefficients.

With these requirements, an appropriate solution is to adapt the filters to uniform power density spectra. By choosing the filter parameter τ_{filter} equal to the maximum expected delay of the mobile radio channel τ_{max} , the normalized delay power density spectrum used for the filter design is given by

$$\rho_{\text{filter}}(\tau) = \begin{cases} \frac{1}{\tau_{\text{filter}}} & |\tau| < \frac{\tau_{\text{filter}}}{2} \\ 0 & \text{otherwise} \end{cases}. \quad (5.32)$$

Furthermore, by choosing the filter parameter $f_{D,\text{filter}}$ equal to the maximum expected Doppler frequency of the mobile radio channel $f_{D,\text{max}}$, the normalized Doppler power density spectrum used for the filter design is

$$S_{f_{D,\text{filter}}}(f_D) = \begin{cases} \frac{1}{2f_{D,\text{filter}}} & |f_D| < f_{D,\text{filter}} \\ 0 & \text{otherwise} \end{cases}. \quad (5.33)$$

With the selection of uniform power density spectra, the discrete frequency correlation functions result in

$$\tilde{\theta}_{n-n''} = \frac{\sin(\pi \tau_{\text{filter}} (n - n'') F_s)}{\pi \tau_{\text{filter}} (n - n'') F_s} \quad (5.34)$$

and the discrete time correlation function yields

$$\tilde{\theta}_{i-i''} = \frac{\sin(2\pi f_{D,\text{filter}} (i - i'') T_s')}{2\pi f_{D,\text{filter}} (i - i'') T_s'}. \quad (5.35)$$

Finally, with (5.16), the autocorrelation function is obtained according to

$$\tilde{\phi}_{n'-n'', i'-i''} = \tilde{\theta}_{n'-n''} \tilde{\theta}_{i'-i''} + \frac{1}{\gamma_c} \delta_{n'-n'', i'-i''}. \quad (5.36)$$

The following aspects are of importance with respect to low computational complexity when implementing FIR filters for channel estimation:

- The filter coefficients should be time invariant.
- The autocorrelation matrix $\tilde{\Phi}$ is independent of the actual coordinate (n, i) so that $\tilde{\Phi}^{-1}$ should be precomputed and stored.
- Different sets of the crosscorrelation vector $\tilde{\theta}_{n,i}$ may be precomputed and stored as well, taking symmetries in the pilot symbol grid into account, cf. Fig. 5.1.
- The optimum number of filter coefficients per estimation is N_{tap} equal to N_{grid} . The complexity can be significantly reduced if only a subset $\mathcal{T}_{n,i} \in \mathcal{P}$ of N_{tap} less than N_{grid} pilot symbols is chosen. The trade-off between complexity and performance is adjustable, cf. Section 5.6.

5.5 Pilot Symbol Grid Based on the Two-Dimensional Sampling Theorem

In the previous section, the 2-D filter coefficients are adapted to an appropriate delay power density spectrum and Doppler power density spectrum. In this section, the arrangement of the pilot symbols in an OFDM frame is presented, by applying the 2-D sampling theorem. Given

the normalized filter bandwidths $\tau_{\text{filter}}/2 \cdot F_s$ and $f_{D,\text{filter}} T'_s$, the sampling theorem requires that the distance of the pilot symbols in frequency direction is

$$N_f \leq \frac{1}{\tau_{\text{filter}} F_s} \quad (5.37)$$

and in time direction is

$$N_t \leq \frac{1}{2 f_{D,\text{filter}} T'_s}. \quad (5.38)$$

An optimum sampling of the channel transfer function is given by a balanced design which guarantees that the channel is sampled in time and in frequency with same sampling rate. The balanced design is defined as [HKR97a]

$$f_{D,\text{filter}} T'_s N_t \approx \frac{1}{2} \tau_{\text{filter}} F_s N_f. \quad (5.39)$$

It is verified in the next section that a good choice is the selection of approximately two-times oversampling to achieve a reasonably low complexity with respect to the filter length and performance. With two-times oversampling the pilot distance in frequency direction results in

$$N_f \approx \frac{1}{2 \tau_{\text{filter}} F_s} \quad (5.40)$$

and in time direction in

$$N_t \approx \frac{1}{4 f_{D,\text{filter}} T'_s}. \quad (5.41)$$

Since N_f and N_t are integer variables, (5.40) and (5.41) can in general only be fulfilled approximately. A practical hint concerning the performance of the channel estimation is to design the pilot grid such that the first and the last OFDM symbol and subcarrier, respectively, in an OFDM frame contains pilot symbols, see Fig. 5.2. Otherwise, the channel estimation has to carry out a prediction for the estimates on the edges of the OFDM frame.

Besides the mean square error of a channel estimation, a criterion for the efficiency of a channel estimation is the overhead due to pilot symbols and the loss in SNR due to pilot symbols. The overhead due to pilot symbols is given by

$$\Lambda = \frac{N_{\text{grid}}}{N_c N_s}, \quad (5.42)$$

and the SNR loss in dB due to pilot symbols is defined as

$$V_{\text{pilot}} = 10 \log_{10} \left(\frac{1}{1 - \Lambda} \right). \quad (5.43)$$

5.6 Mean Square Error Performance

In this section, the mean square error performance of the above described channel estimation is investigated. To evaluate and optimize the channel estimation, an MC reference scenario

typical for mobile radio systems is defined. The presented results are valid for any MC system with the same filter choice and pilot symbol grid as the MC reference scenario and are not limited to MC-CDMA systems only. The channel estimation of the MC reference scenario is based on an OFDM frame structure which corresponds to that used in the MC-CDMA mobile radio system investigated in Chapter 6. Therefore, the frequency band and the OFDM frame structure used in Chapter 6 are presented first, before defining the filter parameters and the pilot symbol grid of the channel estimation adapted to that OFDM frame structure.

The frequency band used in the MC reference scenario with channel estimation and also in the MC-CDMA mobile radio system investigated in Chapter 6 has a bandwidth of

$$B = 2 \text{ MHz} \quad (5.44)$$

and is located at a carrier frequency of

$$f_c = 1.8 \text{ GHz}. \quad (5.45)$$

The number of subcarriers per OFDM symbol is chosen to be

$$N_c = 512, \quad (5.46)$$

where the OFDM operation and its inverse is realized with an IFFT and FFT, respectively, of size 512. Thus, a subcarrier spacing of

$$F_s = 3.9 \text{ kHz} \quad (5.47)$$

and an OFDM symbol duration of

$$T_s = 256 \mu\text{s} \quad (5.48)$$

are obtained. To avoid ISI in the data detection, each OFDM symbol is cyclically extended by a guard interval of duration

$$T_g = 20 \mu\text{s}, \quad (5.49)$$

which is equal to or longer than the maximum delay τ_{\max} of the CODIT and COST 207 channel models applied in this thesis. The total OFDM symbol duration including the guard interval duration is

$$T'_s = 276 \mu\text{s}. \quad (5.50)$$

Thus, the coherence bandwidth $(\Delta f)_c$ of the channel, cf. (2.9), has to be greater than 3.9 kHz and the coherence time $(\Delta t)_c$ of the channel, cf. (2.13), has to be greater than $276 \mu\text{s}$ to guarantee time-invariant flat fading per subcarrier and OFDM symbol. When applying (2.9) and (2.13), it can be seen that this conditions are satisfied even for the worst case mobile radio scenarios defined in Section 2.2.1, see Tables 2.3 and 2.4. The considered MC transmission scheme processes one OFDM frame per estimation cycle. An OFDM frame consists of

$$N_s = 24 \quad (5.51)$$

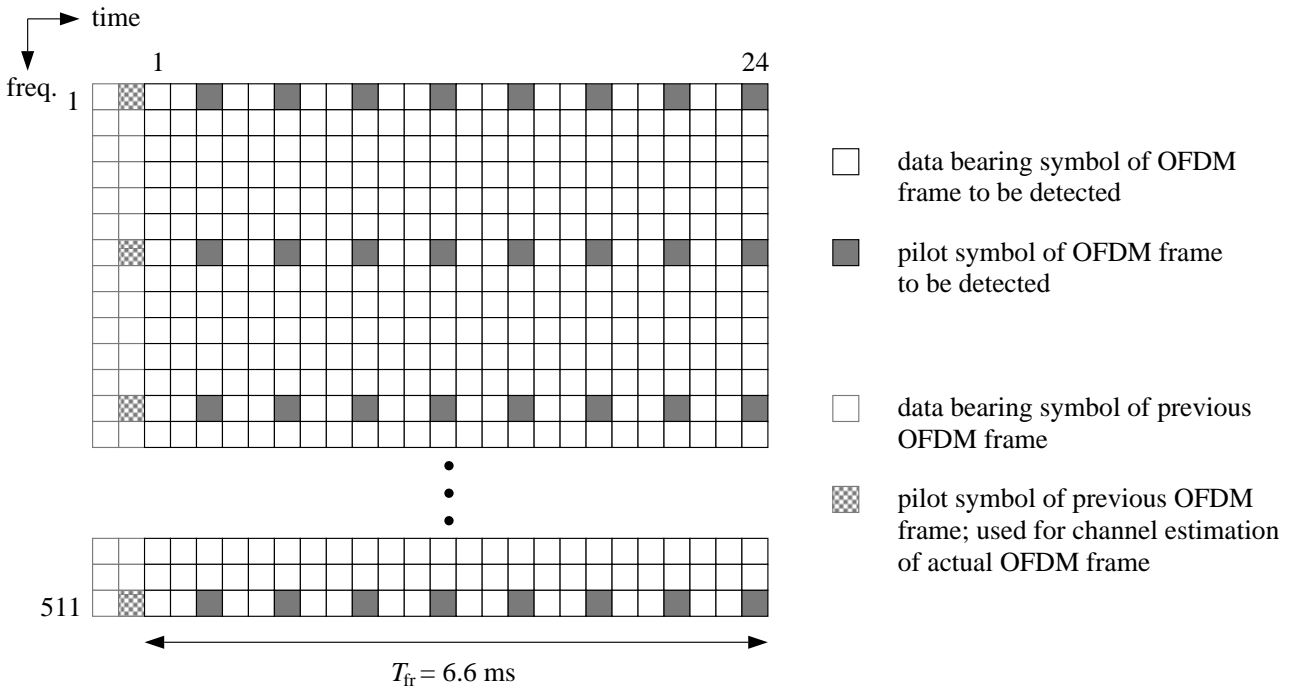


Figure 5.3: OFDM frame defined by the MC reference scenario; $N'_c = 511$; $N_s = 24$; $N_f = 6$; $N_t = 3$; $N_{\text{grid}} = 774$

OFDM symbols as depicted in Fig. 5.3. The OFDM frame duration, cf. (3.15), results in

$$T_{\text{fr}} = 6.6 \text{ ms.} \tag{5.52}$$

The MC-CDMA system under investigation in Chapter 6 should operate in propagation scenarios typical for future mobile radio systems. The highest demands on the channel estimation are given in macrocell scenarios which are characterized by large delay spreads and high Doppler frequencies. Thus, taking into account the propagation scenarios defined in Section 2.2.1, the parameters τ_{filter} and $f_{D,\text{filter}}$ of the channel estimation filter are chosen as

$$\tau_{\text{filter}} = 20 \mu\text{s} \tag{5.53}$$

and

$$f_{D,\text{filter}} = 333.3 \text{ Hz,} \tag{5.54}$$

where $f_{D,\text{filter}}$ is obtained with a velocity of $v = 200 \text{ km/h}$ of the MS, having a path with an angle of incidence of 0 radians.

Given these constraints, the normalized channel bandwidths are

$$\tau_{\text{filter}}/2 \cdot F_s \approx 0.039, \tag{5.55}$$

$$f_{D,\text{filter}} T'_s \approx 0.092. \tag{5.56}$$

With (5.40) and (5.41), a balanced design with approximately two times oversampling is given with a pilot symbol spacing of

$$N_f = 6 \tag{5.57}$$

in frequency direction and of

$$N_t = 3 \quad (5.58)$$

in time direction. The OFDM frame defined for the MC reference scenario and for the MC-CDMA mobile radio system investigated in Chapter 6 is illustrated in Fig. 5.3. As mentioned in the previous section, it is of advantage to design the OFDM frame such that pilot symbols are located on the edges of the OFDM frame. In time direction, the last OFDM symbol with pilot symbols of the previous OFDM frame can be used for filtering, cf. Fig. 5.3, [KaH97a]. With a pilot spacing of N_f equal to 6 in frequency direction, while starting and ending with a subcarrier containing pilot symbols, a number N'_c equal to 511 used subcarriers per OFDM symbol is obtained and is considered in the sequel. The resulting overhead Λ due to pilot symbols, cf. (5.42), is 5.6%. With pilot symbols and data symbols having the same average energy, the loss in SNR V_{pilot} due to pilot symbols, cf. (5.43), is only 0.3 dB in the defined MC reference scenario. Table 5.1 briefly summarizes the parameters of the MC reference scenario with channel estimation.

Table 5.1: Parameters of the MC reference scenario with channel estimation in two dimensions

bandwidth	$B = 2$ MHz
carrier frequency	$f_c = 1.8$ GHz
OFDM frame duration	$T_{\text{fr}} = 6.6$ ms
number of OFDM symbols per OFDM frame	$N_s = 24$
OFDM, inverse OFDM	512 point IFFT, 512 point FFT
OFDM symbol duration including guard interval	$T'_s = 276$ μ s
guard interval duration	$T_g = 20$ μ s
subcarrier spacing	$F_s = 3.9$ kHz
total number of subcarriers used	$N'_c = 511$
pilot symbol distance in frequency	$N_f = 6$
pilot symbol distance in time	$N_t = 3$
delay filter bandwidth	$\tau_{\text{filter}} = 20$ μ s
Doppler filter bandwidth	$f_{D,\text{filter}} = 333.3$ Hz

The performance criterion for the evaluation of the channel estimation is the mean square error

$$J = \frac{1}{N_c N_s} \sum_{n=1}^{N_c} \sum_{i=1}^{N_s} J_{n,i}, \quad (5.59)$$

which is the mean square error $J_{n,i}$, cf. (5.9), averaged over an OFDM frame. Thus, edge effects are also taken into account. The mean square error J is presented for channels which are normalized in the power according to (3.49). The information about the SNR γ_c required

for the calculation of Φ is assumed to be known perfectly at the receiver. In practice, γ_c can be estimated by transmitting a null-symbol without signal energy at the beginning of each OFDM frame as described in Section 3.3.1. Alternatively, similar to the approach taken with suboptimal MMSE equalization, cf. Section 3.3.2, the autocorrelation function can be optimized for the lowest SNR at which successful data transmission should be possible. After that, no information about the actual SNR γ_c is used during channel estimation. The mean square error degradation with this approach is shown at the end of this section.

The mean square error of 2-D FIR filtering and $2 \times$ 1-D FIR filtering without model mismatch applied in the MC reference scenario is presented and compared in the sequel. The used mobile radio channel has a uniform delay power spectrum with $\tau_{\max} = 20 \mu\text{s}$ and a uniform Doppler power density spectrum with $f_{D_{\max}} = 333.3 \text{ Hz}$, modelled according to the COST 207 approach with N_p equal to 100 paths with equal amplitude. In Fig. 5.4, the mean square error J versus the SNR γ_c for 2-D FIR filtering with different numbers of filter taps is shown. The corresponding

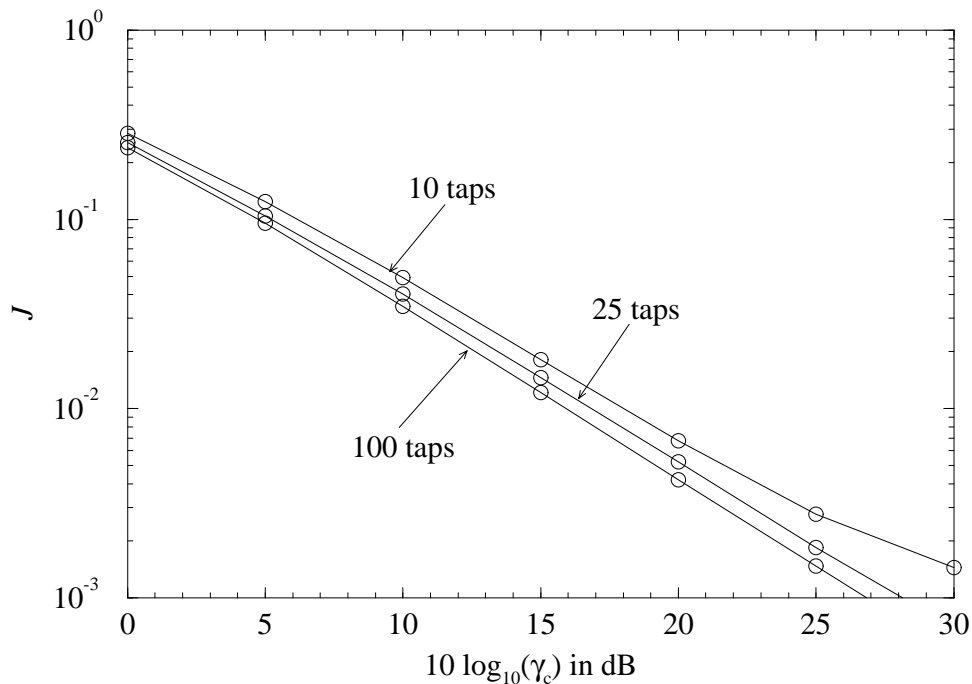


Figure 5.4: Mean square error J versus SNR γ_c for 2-D FIR filtering with different numbers of filter taps; no model mismatch; $v = 200 \text{ km/h}$

results for $2 \times$ 1-D FIR filtering without model mismatch are presented in Fig. 5.5. It can be observed in Figs. 5.4 and 5.5, that the mean square error decreases with increasing numbers of taps. The mean square error presented with 2-D FIR filtering using 100 taps can be considered as a lower bound. In the case of 2-D FIR filtering, 25 taps seems to be reasonable with respect to mean square error performance and complexity. In the case of $2 \times$ 1-D FIR filtering, it can be observed that 2×3 taps, i.e., 3 taps for each FIR filter, performs significantly worse compared to 2×5 taps or more. 2×5 taps is a reasonable choice with respect to mean square error performance and complexity. A further increase of N_{tap} only reduces the mean square error

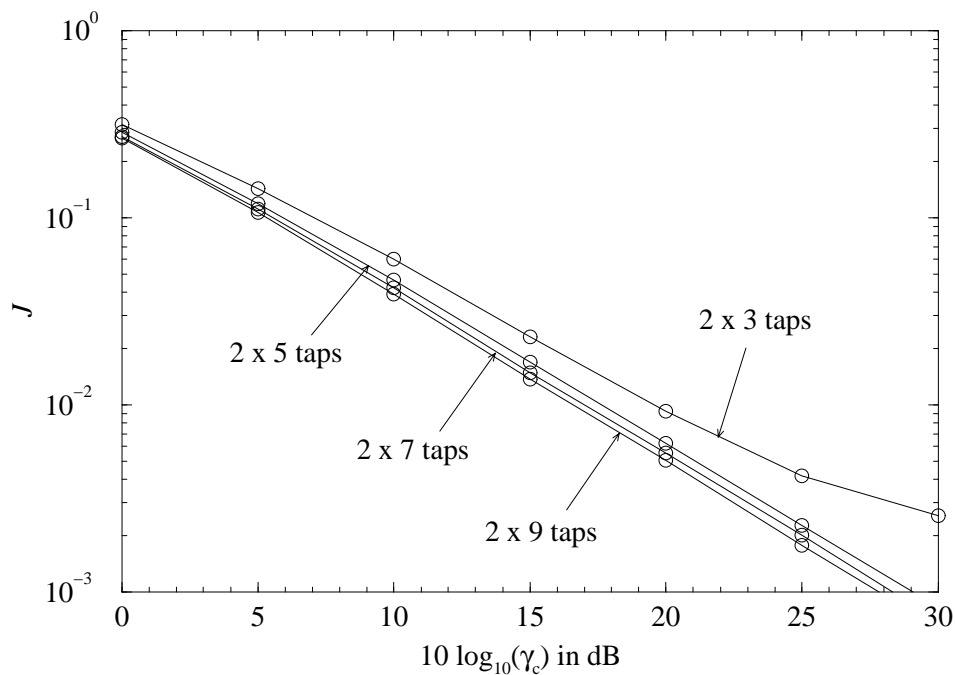


Figure 5.5: Mean square error J versus SNR γ_c for $2 \times$ 1-D FIR filtering with different numbers of filter taps; no model mismatch; $v = 200$ km/h

slightly. Moreover, with 2×5 taps, the performance with $2 \times$ 1-D FIR filtering is similar to the performance with 2-D FIR filtering with 25 taps. Based on this results, $2 \times$ 1-D FIR filtering with 2×5 taps is chosen for channel estimation in the sequel.

After selecting the filter, it is important to know the degradation due to model mismatch, i.e., due to the mismatch of the correlation functions used in the filter design and those of the actual channel. In a first step, the mean square error of the defined channel estimation in different macro-, micro-, and picocell scenarios defined in the CODIT and COST 207 studies, cf. Section 2.2.1, versus the SNR γ_c is shown in Figs. 5.6 and 5.7, respectively. The velocity v of the MS is equal to 3 km/h. As a reference, the mean square error curve without model mismatch for $2 \times$ 1-D FIR filtering with 2×5 taps, cf. Fig. 5.5, is given. It may be surprising that the proposed channel estimation provides a better performance in channels with large delay spread than in channels with low delay spread. The reason for this effect is that a channel with a delay power density spectrum which matches more closely with that chosen for the filter design, also matches more closely with the performance without model mismatch and, thus, shows a better mean square error performance. Summarizing, the degradation in SNR γ_c compared to the case with no model mismatch is in the range of 1 dB up to 3 dB.

In a second step, the influence of different Doppler power density spectra is considered. Furthermore, the effect when the condition of two-times oversampling is hurt in mobile radio channels with Doppler frequencies larger than 333.3 Hz is investigated. Fig. 5.8 shows the mean square error J of the defined channel estimation for different velocities v of the MS in the CODIT channel model SU versus the SNR γ_c . As a reference, the mean square error curve without

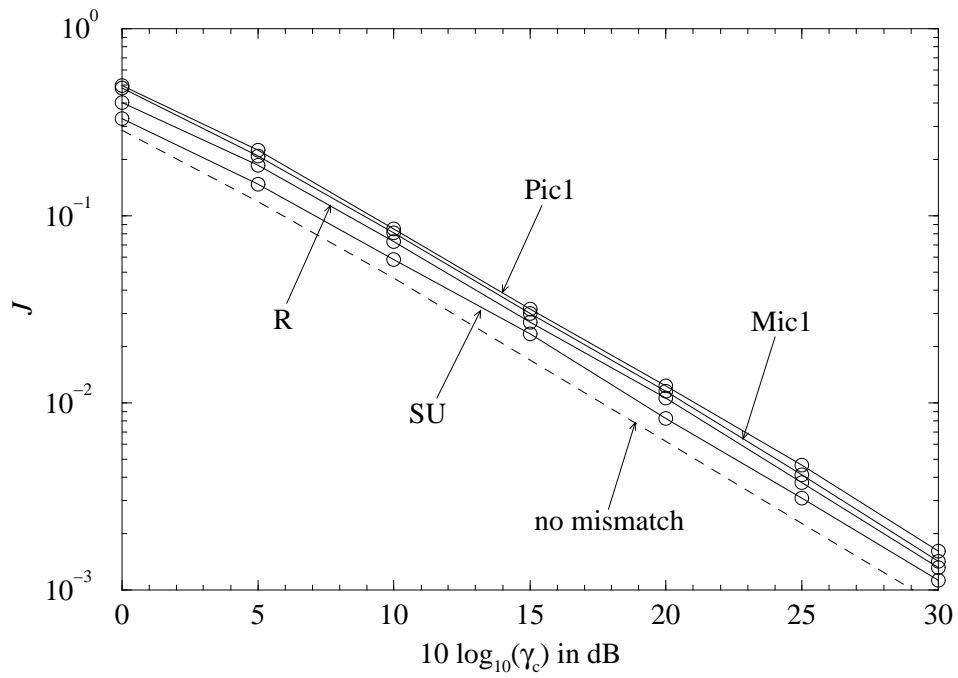


Figure 5.6: Mean square error J versus SNR γ_c for 2×1 -D FIR filtering for different CODIT channel models; 2×5 taps; $v = 3$ km/h

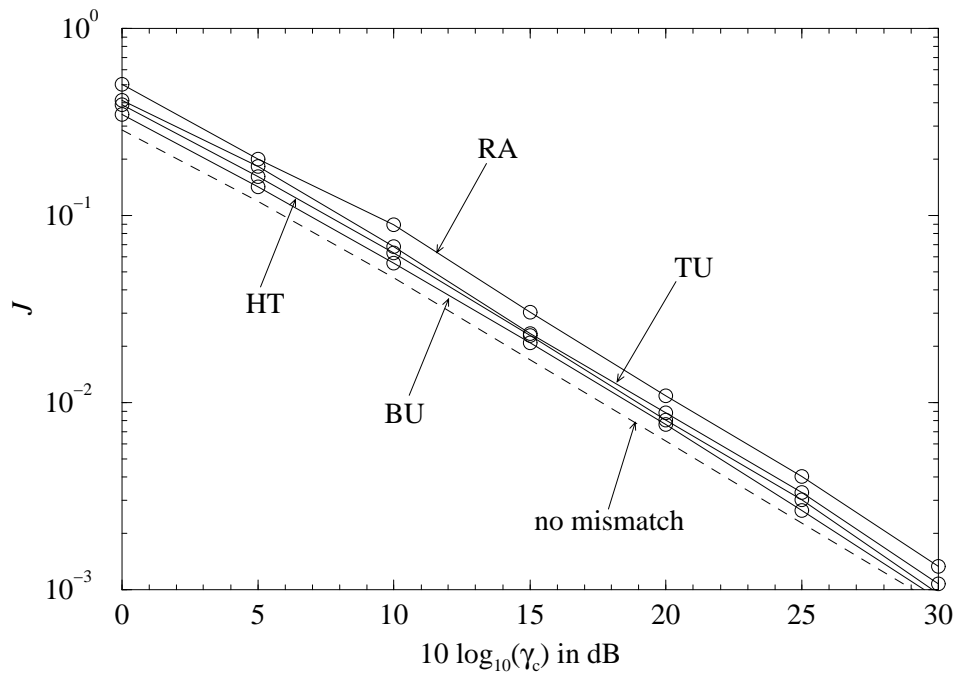


Figure 5.7: Mean square error J versus SNR γ_c for 2×1 -D FIR filtering for different COST 207 channel models; 2×5 taps; $v = 3$ km/h

model mismatch for 2×1 -D FIR filtering with 2×5 taps is given. It is impressive to see that there is approximately no change in the mean square error with different velocities v of the

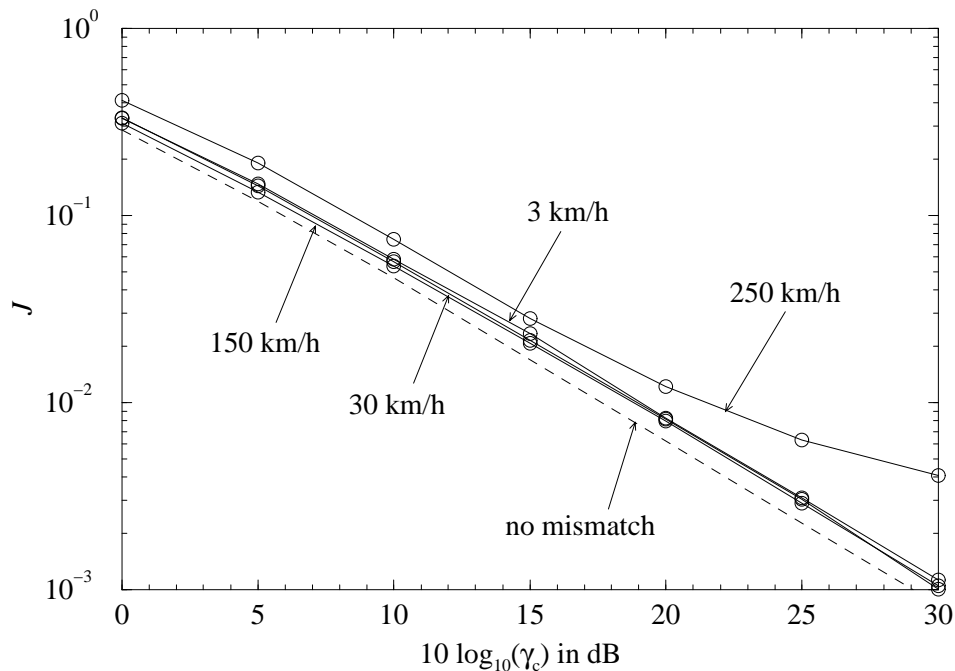


Figure 5.8: Mean square error J versus SNR γ_c for 2×1 -D FIR filtering for different velocities of the MS; CODIT channel model SU; 2×5 taps

MS as long as two-times oversampling of the fading process is guaranteed. For the defined MC reference scenario two-times oversampling is given for a velocity v equal to 200 km/h. As soon as the rule of two-times oversampling is hurt, shown for the case with the velocity of v equal to 250 km/h, the mean square error considerably increases. In the investigated SNR range from 0 dB up to 30 dB, only the curve which hurts the rule of two-times oversampling flattens out. This result is verified in Fig. 5.9 where the mean square error J of the defined channel estimation for different velocities v of the MS in the COST 207 channel model HT versus the SNR γ_c is depicted. The HT propagation area is chosen, since it has a different delay power density spectrum compared to the SU propagation area. The curves presented in Fig. 5.9 confirm the statement that two-times oversampling is an appropriate choice for a filter design. It can be concluded that for different velocities v of the MS the degradation in SNR γ_c compared to the case with no model mismatch is in the range of 1 dB up to 2 dB, as long as the rule of two-times oversampling is fulfilled.

Fig. 5.10 shows the mean square error J obtained with the proposed channel estimation when the autocorrelation matrix Φ is optimized for an SNR $10 \log_{10}(\gamma_c)$ of 10 dB. During the channel estimation no information about the actual SNR γ_c is used to optimally adapt the filter coefficients, otherwise no model mismatch. It can be seen that accurate results are obtained in a span of about 15 dB with mean at 10 dB. For higher SNRs, the mean square error obtained with the simplified channel estimation strongly flattens out. Thus, the application of the simplified channel estimation which requires no estimation of γ_c depends on whether the high error floor is acceptable or not. Otherwise, it depends on the SNR dynamic range at the input of the receiver whether the simplified channel estimation is applicable or not.

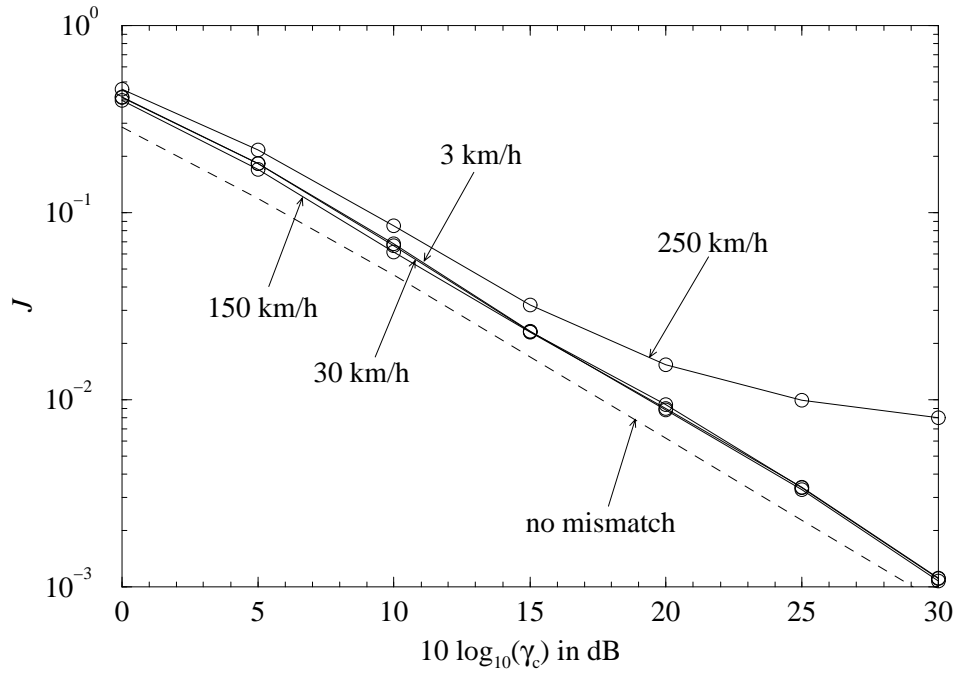


Figure 5.9: Mean square error J versus SNR γ_c for 2×1 -D FIR filtering for different velocities of the MS; COST 207 channel model HT; 2×5 taps

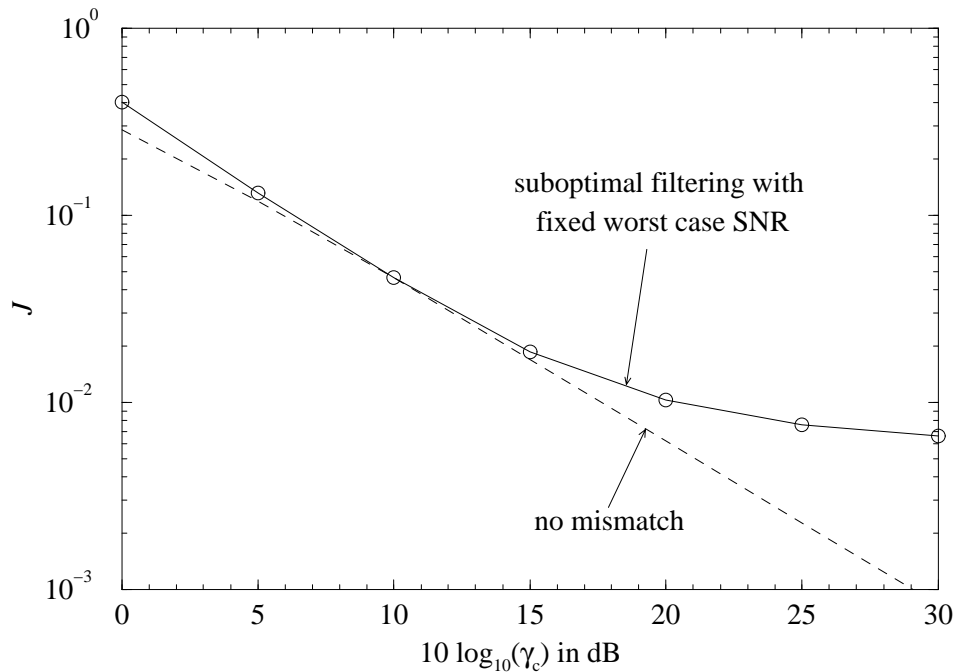


Figure 5.10: Mean square error J versus SNR γ_c for 2×1 -D FIR when the actual SNR γ_c is not used for calculation of the filter coefficients; otherwise no model mismatch; 2×5 taps

The main results are again summarized:

- Two cascaded 1-D FIR filters perform similar at less complexity than a 2-D filter, thus, $2 \times$ 1-D filtering is preferable in practice.
- The rule of two times oversampling of the fading process in time and in frequency direction is a suitable design criterion for the pilot symbol grid.
- A good compromise between mean square error performance and complexity is the choice of 5 filter taps for each of both filters, when two times oversampling of the fading process is guaranteed.
- With the adaptation of the filter to uniform delay and Doppler power density spectra, only knowledge about the maximum occurring Doppler frequency and delay in the mobile radio channel and the SNR is required to design a channel estimation for a given MC system.

Since the focus of this thesis is on MC-CDMA mobile radio systems, a brief overview on research activities concerning channel estimation schemes for MC-CDMA systems follows. Pilot symbol aided channel estimation in two dimensions with $2 \times$ 1-D filtering in MC-CDMA systems has been applied in [MBR96] and in [KaH97a]. In [MBR96], the influence of real channel estimation is approximated by using noisy channel state informations for data detection where the noise has the variance equal to the mean square error J . The channel used for the system evaluation is modelled as uncorrelated Rayleigh fading channel. In [KaH97a] a real $2 \times$ 1-D FIR filtering in mobile radio channels typical for macrocells is investigated and used for the MC-CDMA system evaluation. Both proposed channel estimations were designed for the downlink. 1-D filtering has been investigated for slow fading channels typical for picocell scenarios in [CFG95] for the up- and the downlink and in [ToK96c] for the downlink. For the uplink in larger cells, a pilot tone based channel estimation has been investigated in [Ste97a]. Moreover, an uplink channel estimation approach is given in [BJP97] where the channel estimation for the MC-CDMA receiver is based on a single carrier modulated midamble inserted between the MC modulated, spread data symbols. When roughly comparing the overhead due to pilot symbols and reference sequences between the different concepts, it is not surprising that channel estimation in two dimensions outperforms the other approaches remarkably. However, it has to be mentioned that the advantages of channel estimation in two dimensions can only be exploited in the downlink of an MC-CDMA system. In the uplink, conventional 1-D channel estimation concepts seem to be necessary. In Appendix B, a novel spread spectrum multi-carrier multiple access (SS-MC-MA) scheme suitable for the up- and the downlink with pilot symbol based 1-D channel estimation is presented, which is a very promising concept especially for the uplink [KaF96, KaF97a]. For the sake of completeness, it should be mentioned that MC modulated systems without exploiting the spread spectrum technique, like MC-FDMA and MC-TDMA systems, can also use incoherent detection [RoG97].

Chapter 6

MC-CDMA System Evaluation

6.1 System Design

The MC-CDMA signal generation and the various MC-CDMA receiver components including the key components data detection, soft decision channel decoding, and channel estimation have been presented and investigated individually in Chapters 3 to 5. In this chapter, a complete MC-CDMA system is designed and evaluated. A single cell scenario for the downlink of a mobile radio system is considered. Fig. 6.1 illustrates the structure of the investigated MC-CDMA mobile radio system. The chapter of this thesis where the individual system component is investigated is added to the assigned block.

The basic parameters of the proposed MC-CDMA mobile radio system are chosen according to the results presented in Chapters 3 to 5. The MC-CDMA signal structure exploits the $M&Q$ -Modification. Walsh-Hadamard codes of length L equal to 8 are chosen as spreading codes. The MC-CDMA receiver applies SD with MMSE equalization. Convolutional codes with rate R equal to 1/2, decoded with a Viterbi decoder, are used for the channel coding. QPSK is used for the symbol mapping and 2×1 -D FIR filtering with 2×5 taps is applied for channel estimation. The MC-CDMA mobile radio system is designed for a total bandwidth B equal to 2 MHz and a carrier frequency f_c equal to 1.8 GHz.

It has already been mentioned in Section 3.2 that MC-CDMA systems inherently support an additional TDMA component due to the transmission synchronized on OFDM symbols. This feature is exploited in the proposed MC-CDMA system. Fig. 6.2 illustrates the chosen TDMA frame structure. A TDMA frame consists of

$$N_{\text{fr}} = 3 \quad (6.1)$$

time slots, where each time slot represents an OFDM frame which has the format defined in Section 5.6 and illustrated in Fig. 5.3. The OFDM frame duration T_{fr} is equal to 6.6 ms, resulting in a TDMA frame duration of

$$T_{\text{fr}} = 19.8 \text{ ms.} \quad (6.2)$$

No interleaving of the data beyond a time slot is applied with the intention to keep the transmission delay low. The user capacity of the MC-CDMA mobile radio system with a TDMA

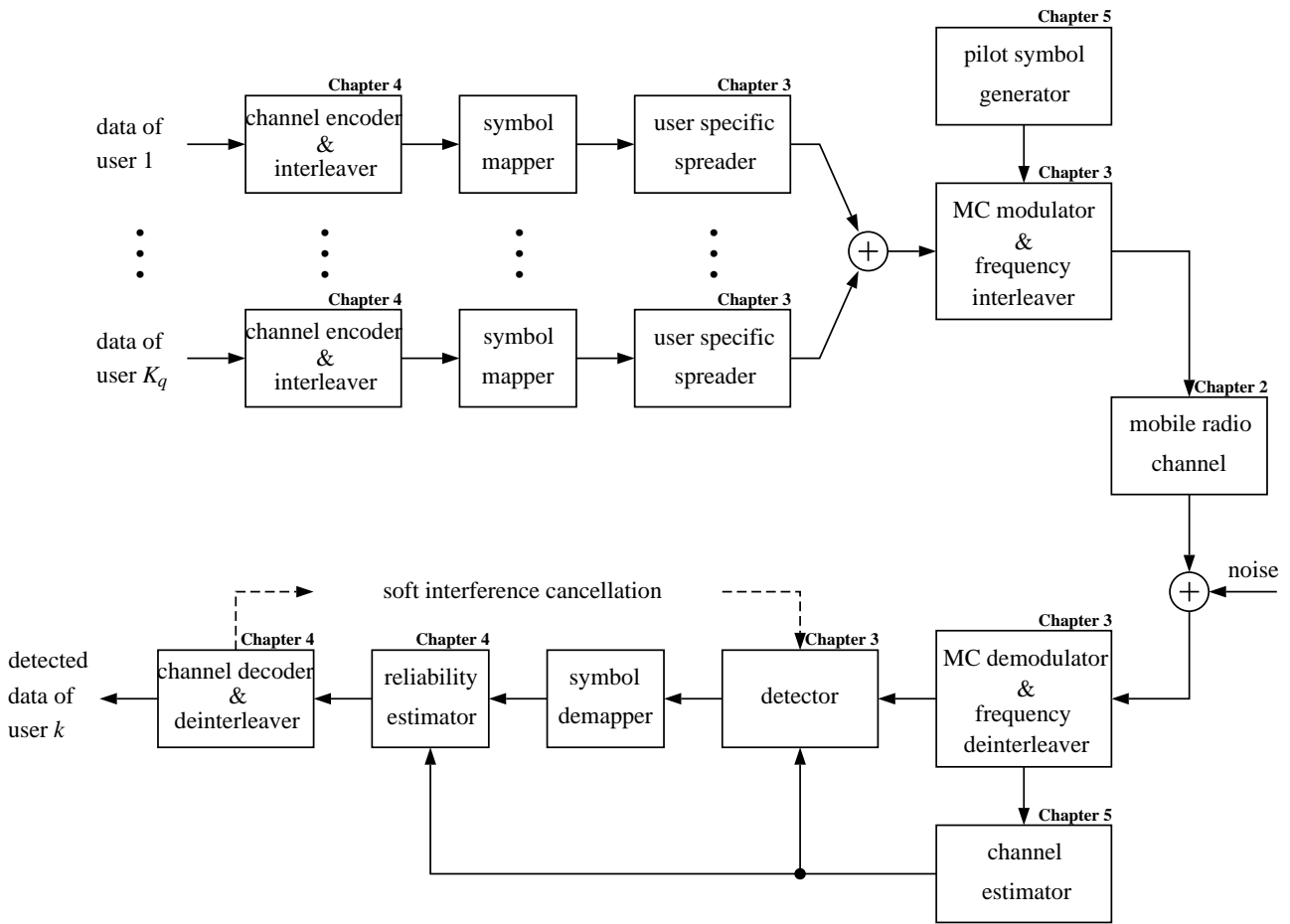


Figure 6.1: MC-CDMA mobile radio system in the downlink

frame consisting of N_{fr} time slots, i.e., OFDM frames, is given by

$$K_{sys} = N_{fr} K_{max}. \tag{6.3}$$

In Table 6.1, the basic parameters of the proposed MC-CDMA mobile radio system are summarized. It has to be noted that the flexible mapping of both data and pilot symbols onto OFDM symbols does not allow to assign distinct values of M and Q for the used $M&Q$ -Modification. However, in the average over all OFDM symbols M equals to 8 and Q equals to 7.

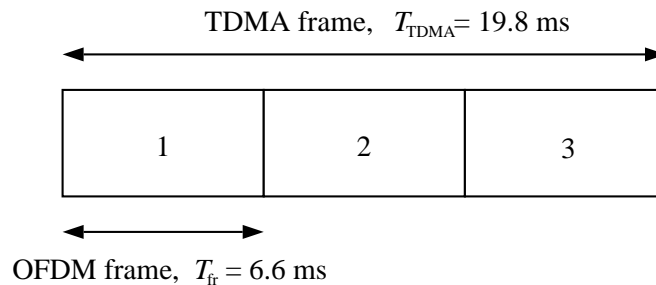


Figure 6.2: TDMA frame with 3 time slots, each time slot represents one OFDM frame

Table 6.1: Basic parameters of the proposed MC-CDMA mobile radio system

bandwidth	$B = 2$ MHz
carrier frequency	$f_c = 1.8$ GHz
TDMA frame duration	$T_{\text{TDMA}} = 19.8$ ms
number of OFDM frames per TDMA frame	$N_{\text{fr}} = 3$
OFDM frame duration	$T_{\text{fr}} = 6.6$ ms
number of OFDM symbols per OFDM frame	$N_s = 24$
OFDM, inverse OFDM	512 point IFFT, 512 point FFT
OFDM symbol duration including guard interval	$T'_s = 276$ μ s
guard interval duration	$T_g = 20$ μ s
subcarrier spacing	$F_s = 3.9$ kHz
total number of subcarriers used	$N'_c = 511$
spreading code	Walsh-Hadamard code
spreading code length	$L = 8$
data detector	MMSE equalizer
data symbol mapping	QPSK with Gray encoding
channel code	convolutional code
code rate	$R = 1/2$
memory	$M_c = 6$
channel decoder	Viterbi decoder
frequency interleaver	pseudo random interleaver
frequency interleaver size	$I_f = 511$
code bit interleaver	pseudo random interleaver
code bit interleaver size	$I_c = 384$
channel estimator	$2 \times$ 1-D FIR filters
filter taps	2×5
delay filter bandwidth	$\tau_{\text{filter}} = 20$ μ s
Doppler filter bandwidth	$f_{\text{D,filter}} = 333.3$ Hz
pilot symbol distance in frequency	$N_f = 6$
pilot symbol distance in time	$N_t = 3$
maximum number of active users per subsystem	$K_{q,\text{max}} = 8$
maximum number of active users per OFDM frame	$K_{\text{max}} = 56$
user capacity	$K_{\text{sys}} = 168$
net bit rate per user	9.7 kbit/s $\leq R_b \leq 1.6$ Mbit/s
bandwidth efficiency	$\beta = 0.81$ bit/s/Hz

The user capacity of a single cell of the investigated MC-CDMA mobile radio system results in

$$K_{\text{sys}} = 168, \quad (6.4)$$

i.e., that 168 users can simultaneously communicate at an acceptable SNR γ_b guaranteeing a coded BER less or equal to 10^{-3} . The user capacity can further be improved when applying, for instance, cell sectorization [Stü96]. Given the system parameters in Table 6.1, each of the 168 active users can transmit with a net bit rate of R_b equal to 9.7 kbit/s, resulting in a bandwidth efficiency β of 0.81 bit/s/Hz at full system load. With respect to UMTS and IMT-2000 requirements, it is possible to assign one user several or all user channels such that a net bit rate up to 1.6 Mbit/s can be assigned to a single user.

The SNR loss V_{guard} due to the guard interval, cf. (3.23), results in

$$V_{\text{guard}} = 0.3 \text{ dB}. \quad (6.5)$$

With an overhead on pilot symbols of

$$\Lambda = 5.6\%, \quad (6.6)$$

cf. (5.42), the SNR loss V_{pilot} due to pilot symbols, cf. (5.43), is

$$V_{\text{pilot}} = 0.3 \text{ dB}. \quad (6.7)$$

Both losses result in a total loss in SNR of only 0.6 dB which is taken into account in the presented simulation results.

6.2 Simulation Results

The simulation results presented in the following are given for fully loaded subsystems, except for investigations focusing on the influence of the loading ratio K_q/L . The various factors of influence on the performance of the MC-CDMA mobile radio system under investigation in this section are shown in Table 6.2. The simulation results are discussed in Section 6.3.

Table 6.2: Factors of influence on the performance of the MC-CDMA mobile radio system

factor of influence	figure/table
propagation area: macro-, micro-, and picocells	Figs. 6.3 and 6.4
velocity v of the MS	Figs. 6.5 and 6.6
loading ratio K_q/L	Figs. 6.7 and 6.8
SNR gain with MLSSE compared to MMSE equalization	Figs. 6.9 and 6.10
bandwidth B in micro- and picocells	Fig. 6.11
SNR degradation due to real channel estimation	Tables 6.3 to 6.5

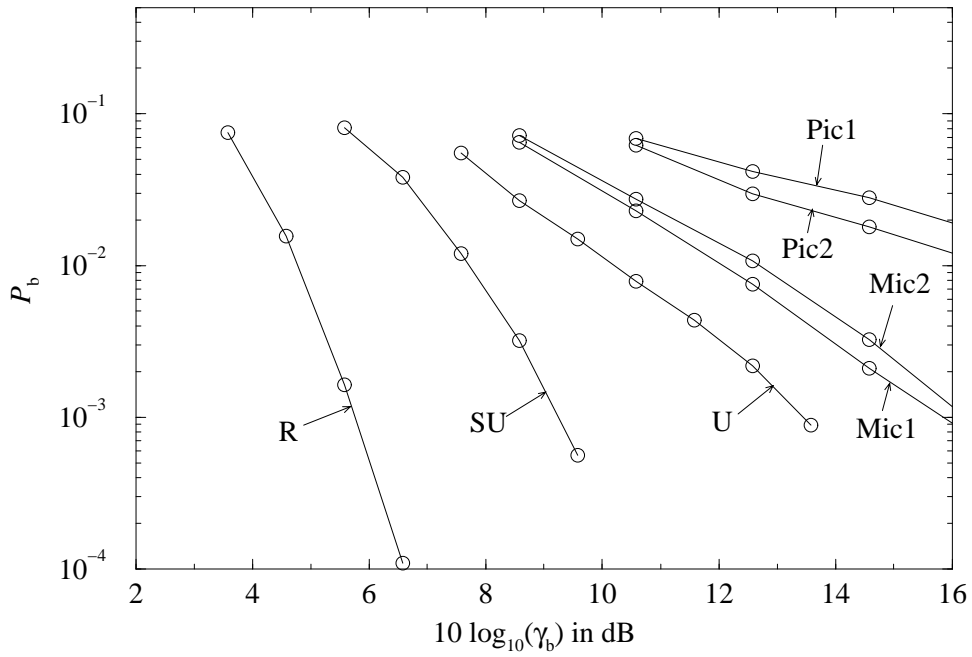


Figure 6.3: Average coded BER P_b versus average SNR γ_b per bit for CODIT channel models; MMSE equalization; 2×1 -D channel estimation; $L = 8$; $K_q = 8$; QPSK; $R = 1/2$; $v = 3$ km/h

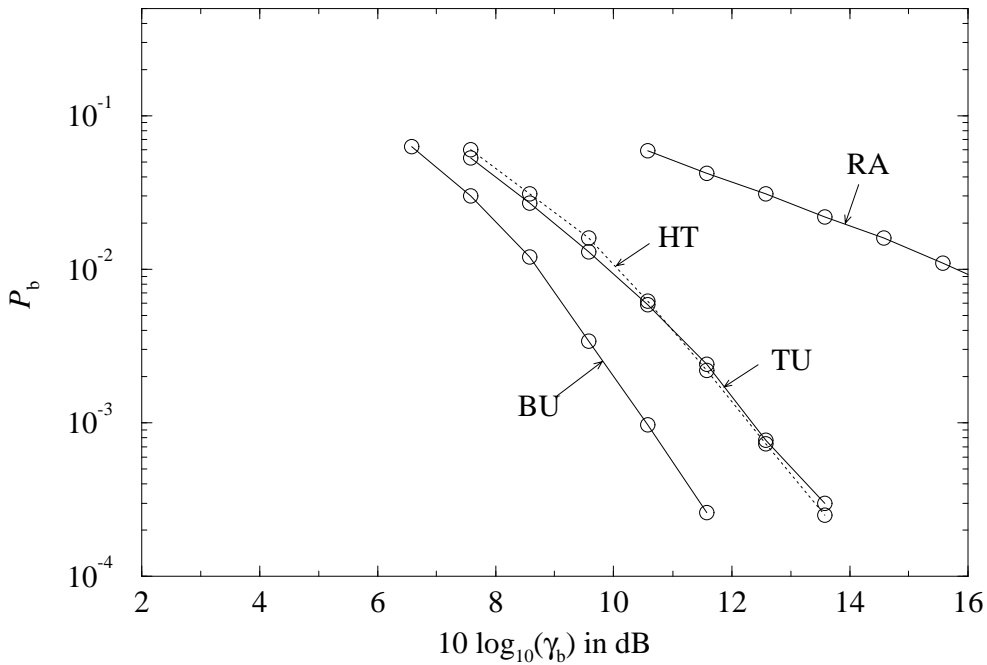


Figure 6.4: Average coded BER P_b versus average SNR γ_b per bit for COST 207 channel models; MMSE equalization; 2×1 -D channel estimation; $L = 8$; $K_q = 8$; QPSK; $R = 1/2$; $v = 3$ km/h

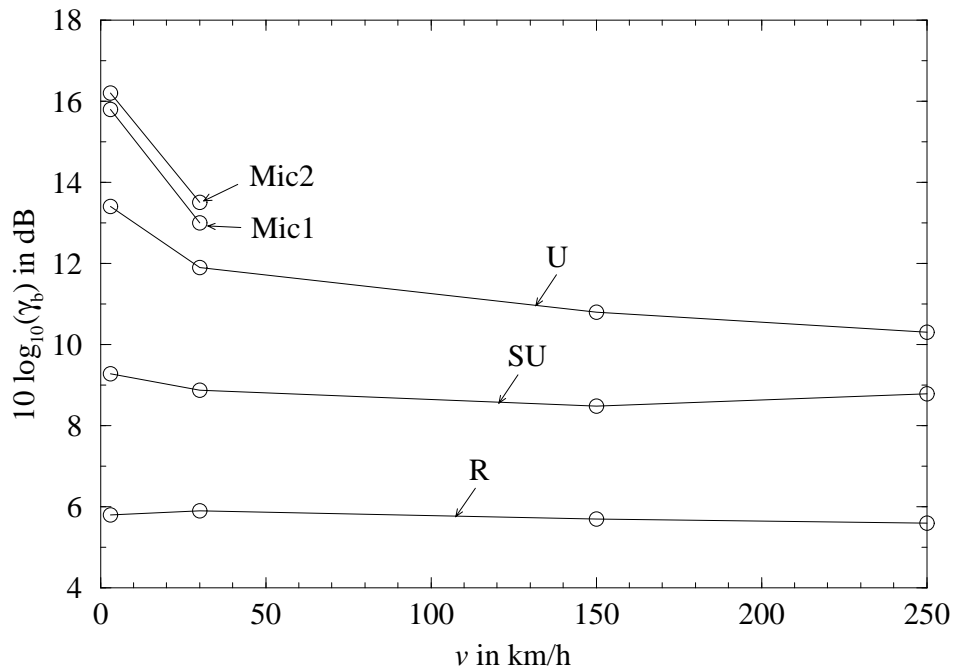


Figure 6.5: Average SNR γ_b per bit required to achieve a BER of $P_b = 10^{-3}$ versus velocity v of the MS for macro- and microcells; CODIT channel models; MMSE equalization; 2×1 -D channel estimation; $L = 8$; $K_q = 8$; QPSK; $R = 1/2$

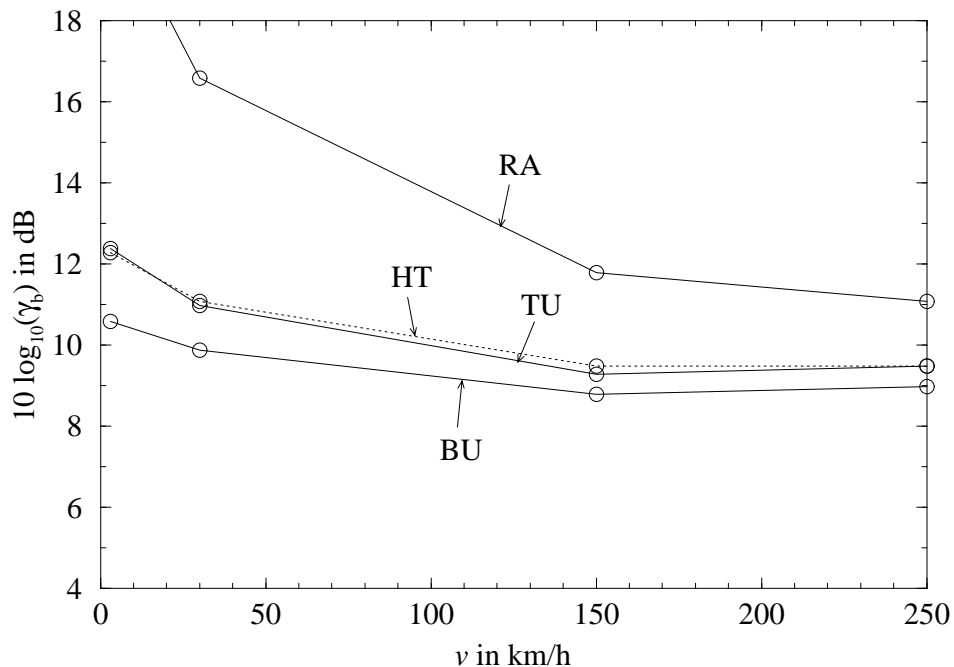


Figure 6.6: Average SNR γ_b per bit required to achieve a BER of $P_b = 10^{-3}$ versus velocity v of the MS for macrocells; COST 207 channel models; MMSE equalization; 2×1 -D channel estimation; $L = 8$; $K_q = 8$; QPSK; $R = 1/2$

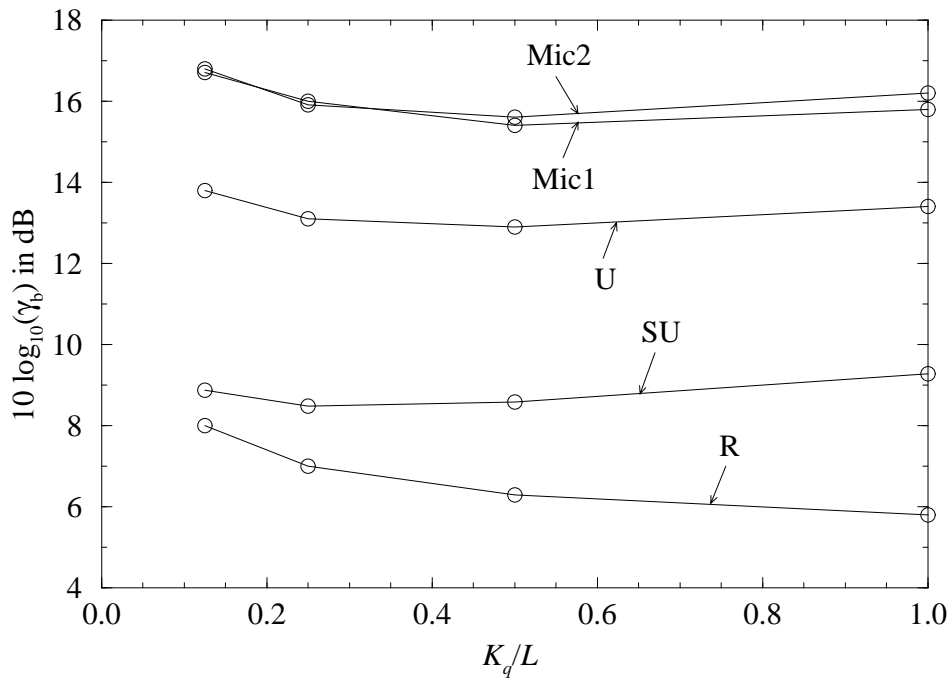


Figure 6.7: Average SNR γ_b per bit required to achieve a BER of $P_b = 10^{-3}$ versus loading ratio K_q/L ; CODIT channel models; MMSE equalization; 2×1 -D channel estimation; $L = 8$; QPSK; $R = 1/2$; $v = 3$ km/h

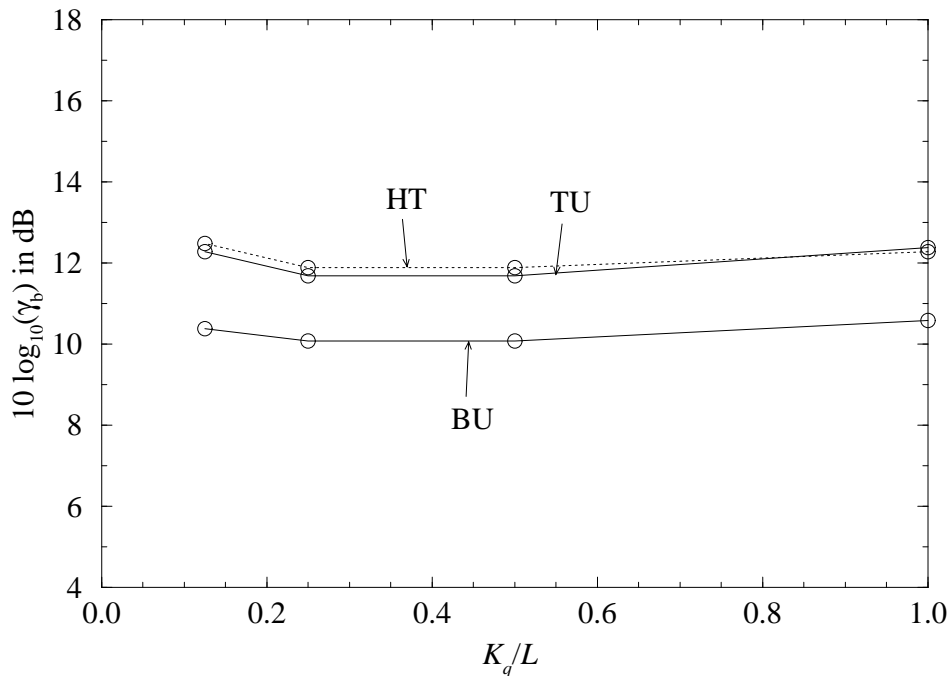


Figure 6.8: Average SNR γ_b per bit required to achieve a BER of $P_b = 10^{-3}$ versus loading ratio K_q/L ; COST 207 channel models; MMSE equalization; 2×1 -D channel estimation; $L = 8$; QPSK; $R = 1/2$; $v = 3$ km/h

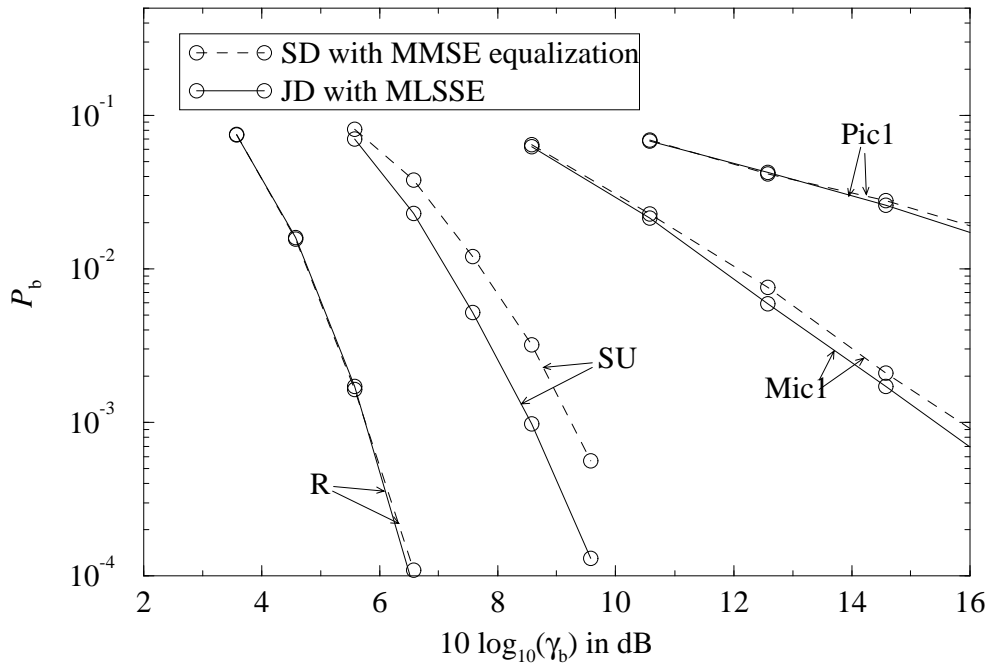


Figure 6.9: Average coded BER P_b versus average SNR γ_b per bit for JD with MLSSE and for SD with MMSE equalization; CODIT channel models; 2×1 -D channel estimation; $L = 8$; $K_q = 8$; QPSK; $R = 1/2$; $v = 3$ km/h

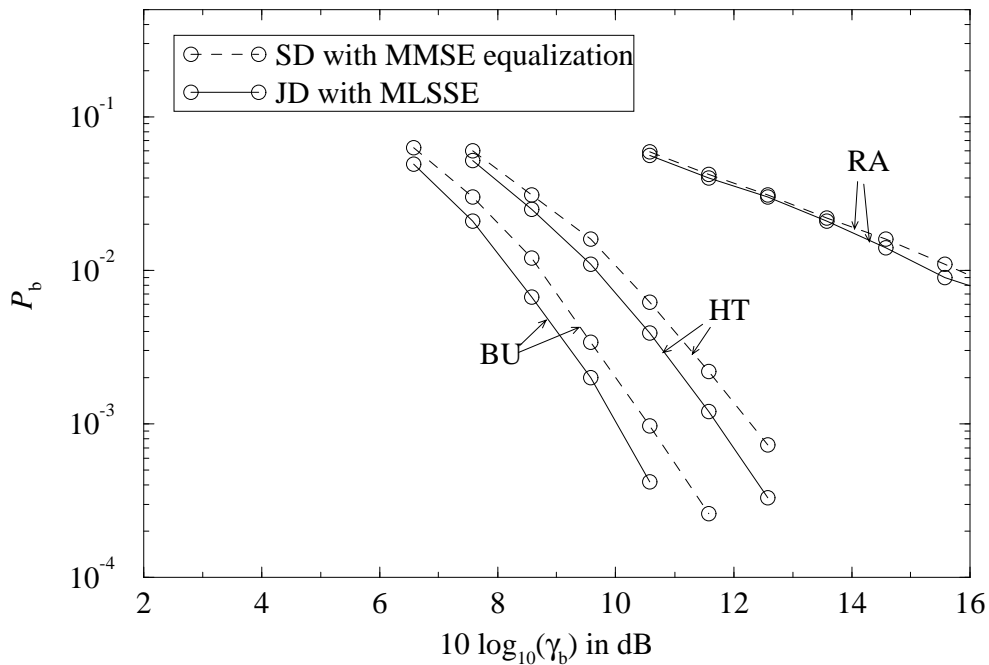


Figure 6.10: Average coded BER P_b versus average SNR γ_b per bit for JD with MLSSE and for SD with MMSE equalization; COST 207 channel models; 2×1 -D channel estimation; $L = 8$; $K_q = 8$; QPSK; $R = 1/2$; $v = 3$ km/h

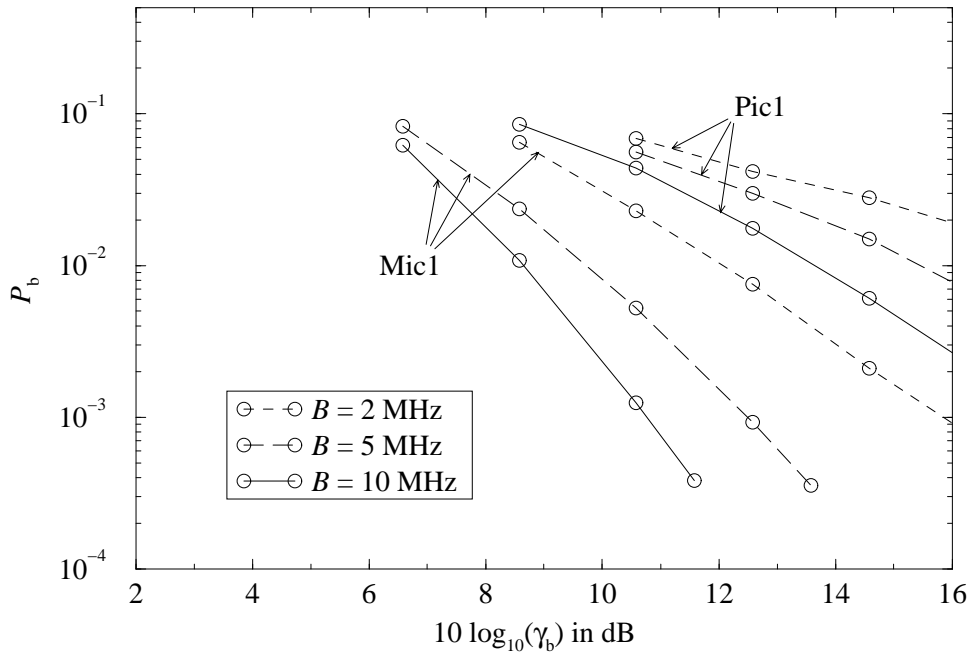


Figure 6.11: Average coded BER P_b versus average SNR γ_b per bit in micro- and picocells for different transmission bandwidths; CODIT channel models; 2×1 -D channel estimation; $L = 8$; $K_q = 8$; QPSK; $R = 1/2$; $v = 3$ km/h

Table 6.3: SNR degradation due to 2×1 -D channel estimation compared to perfect channel estimation for different velocities v of the MS; $K_q = 8$; $P_b = 10^{-3}$

v in km/h	SNR degradation in dB					
	SU	R	Mic1	HT	BU	RA
3	2.6	2.1	2.8	2.5	2.2	2.6
30	2.2	2.2	2.6	2.4	2.2	2.6
150	2.3	2.1	-	2.4	2.2	2.6
250	2.8	2.0	-	2.7	2.6	2.8

Table 6.4: SNR degradation due to 2×1 -D channel estimation compared to perfect channel estimation for different loading ratios K_q/L ; $v = 3$ km/h; $P_b = 10^{-3}$

K_q/L	SNR degradation in dB					
	SU	R	Mic1	HT	BU	RA
1/8	4.4	4.4	5.4	4.8	4.5	5.7
2/8	3.5	3.3	4.4	3.6	3.6	4.4
4/8	2.7	2.6	3.2	2.9	2.7	3.8
8/8	2.6	2.1	2.8	2.5	2.2	2.6

Table 6.5: SNR degradation due to 2×1 -D channel estimation compared to perfect channel estimation for JD with MLSSE and for SD with MMSE equalization; $K_q = 8$; $v = 3$ km/h; $P_b = 10^{-3}$

detection technique	SNR degradation in dB					
	SU	R	Mic1	HT	BU	RA
MMSE equalization	2.6	2.1	2.8	2.5	2.2	2.6
MLSSE	2.5	2.1	2.8	2.5	2.3	2.7

6.3 Discussion of the Simulation Results

From the simulation results presented in the previous section, substantial and comprehensive knowledge about the presented MC-CDMA mobile radio system is obtained. This section discusses the simulation results, focusing on services such as speech transmission which require a coded BER P_b equal to 10^{-3} .

The simulation results in Figs. 6.3 and 6.4 show the influence of different propagation scenarios on the performance of the MC-CDMA system. The BER P_b versus the SNR γ_b is illustrated in this figures. The macro-, micro-, and picocell scenarios defined in the CODIT study and also the macrocell scenarios defined in the COST 207 study have been applied. The velocity v of the MS is equal to 3 km/h in all scenarios. It is shown later that this slow velocity is the most crucial case of all investigated velocities. The slow velocity v does not allow the receiver to exploit time diversity D_t , cf. (2.15), within an OFDM frame but only to exploit frequency diversity D_f , cf. (2.11), offered by the delay spread σ_τ , cf. (2.8). Hence, the frequency diversity potential in the various propagation areas can be shown. As it could have been expected, larger cells which are characterized by larger delay spreads σ_τ offer a higher gain in SNR γ_b due to increased frequency diversity D_f than smaller cells like micro- and picocells. An exception are

macrocell scenarios in rural areas with small delay spread σ_τ and, hence, less frequency diversity potential. The MC-CDMA system performs best in the CODIT channel model rural (R) which has only one scatterer with a strong LOS path. When taking into account the loss in SNR of 2.1 dB due to real channel estimation, see Table 6.3, and the 0.6 dB loss due to the guard interval and the pilot symbols, the coded BER P_b in the propagation area R approaches that of the AWGN channel, cf. Fig. 4.6. The propagation area R produces negligible fading and may serve as a lower bound for the following investigations. In contrast to the rural propagation area defined in the CODIT study, the COST 207 channel model RA shows the worst performance in a macrocell. The propagation area RA has no dominant component, resulting in severe fading which is flat over the whole transmission bandwidth due to the small delay spread σ_τ . It is important to note that it is not possible to achieve a BER P_b equal to 10^{-3} at $10 \log_{10}(\gamma_b)$ less than 20 dB in the investigated picocell scenarios. The reason for this poor performance is that there is almost no frequency and time diversity available within an OFDM frame. Therefore, it is possible that a complete OFDM frame is located in a deep fade. In microcells, this effect can be observed to a reduced extent.

In Figs. 6.5 and 6.6, the influence of the velocity v and, hence, the opportunity to exploit time diversity in the different CODIT and COST 207 channel models is depicted. The simulation results show the required SNR γ_b to achieve a BER P_b equal to 10^{-3} versus the velocity v of the MS. The chosen velocities v are 3 km/h, 30 km/h, 150 km/h, and 250 km/h. It can be observed that with increasing velocity v the performance of the MC-CDMA system improves up to a velocity of 150 km/h. This effect is caused by an increased time diversity gain at higher velocities. In most of the propagation scenarios, the performance with v equal to 250 km/h is slightly worse than with 150 km/h which is originated in the losses due to the channel estimation which is designed for velocities v up to 200 km/h, cf. Figs. 5.8 and 5.9. The performance of the MC-CDMA system improves to the largest extent with time diversity in channels with less frequency diversity. However, in small cells which provide less frequency diversity, the MSs typically moves slowly. In the CODIT propagation area R which approximates the AWGN channel, the performance of the MC-CDMA system is nearly independent from the velocity v in the range from 3 km/h up to 250 km/h.

The influence of the number of active users K_q per MC-CDMA subsystem in the different CODIT and COST 207 channel models is shown in Figs. 6.7 and 6.8. The simulation results show the required SNR γ_b to achieve a BER P_b equal to 10^{-3} versus the loading ratio K_q/L . The velocity v of the MS is equal to 3 km/h in all scenarios. It is interesting to observe that independent from the propagation area, the performance of the investigated MC-CDMA mobile radio system seems to be nearly independent from the number of active users K_q in a cell. This effect results from the proposed channel estimation scheme where the total energy of the pilot symbols in an OFDM frame increases with an increasing number of active users, cf. Section 5.2, improving the accuracy of the channel estimation, where on the other hand, the MAI increases with increasing K_q . Both effects approximately cancel each other out. Only in the CODIT propagation channel R, the MAI is negligible due to the absence of fading, and the performance

improves with K_q due to the improved channel estimation accuracy.

The simulation results in Figs. 6.9 and 6.10 show the performance improvements when applying JD with MLSSE in the MC-CDMA receiver compared to SD with MMSE equalization. Macro-, micro-, and picocell scenarios defined in the CODIT studies and also macrocell scenarios defined in the COST 207 studies have been applied. The velocity v of the MS is equal to 3 km/h in all scenarios and the system is fully loaded. The simulation results show that the performance of the MC-CDMA mobile radio system can be improved with MLSSE compared to MMSE equalization as long as the mobile radio channel offers diversity D , cf. (2.16). Hence, the performance in the investigated micro- and picocell propagation scenarios cannot be improved significantly with MLSSE. In macrocells, the performance improvements in SNR due to MLSSE compared to MMSE equalization are less than 1 dB, and are in the order of the gains shown in Fig. 4.8. The performance in the CODIT propagation area R cannot be further improved with MLSSE, since the performance in the AWGN channel is the same for both detection techniques.

Since the applied micro- and picocells cannot offer frequency diversity at a transmission bandwidth of B equal to 2 MHz, both propagation scenarios have been investigated for larger bandwidths with B equal to 5 MHz and 10 MHz, see Fig. 6.11. The velocity v of the MS is equal to 3 km/h and the system is fully loaded. The results show that the increase of the transmission bandwidth can significantly improve the system performance in small cells. However, in picocells bandwidths larger than 10 MHz are necessary to achieve a BER of P_b equal to 10^{-3} at an $10 \log_{10}(\gamma_b)$ less than 20 dB. As mentioned in Chapter 2, another well known measure to improve the system performance would be the application of antenna diversity [BBS97]. This diversity technique seems to be very important especially for smaller cells as investigated in [ToK96c] for MC-CDMA mobile radio systems in indoor environments.

Finally, the SNR degradation with the proposed 2×1 -D channel estimation compared to perfect channel estimation is considered. Table 6.3 shows the SNR γ_b degradation due to real channel estimation depending on the velocity v of the MS for different propagation areas in the case of a fully loaded subsystem. The results are obtained at a BER P_b equal to 10^{-3} . It can be observed that the SNR degradation is between 2 dB and 3 dB and is nearly independent of the velocity of the MS. A slight increase in the SNR degradation occurs at v equal to 250 km/h which, however, is still below 3 dB and points out that the presented channel estimation can also handle propagation conditions where the rule of two times oversampling of the fading process is not fulfilled, cf. Section 5.5. Table 6.4 shows the SNR γ_b degradation due to real channel estimation depending on the loading ratio K_q/L for different propagation areas. The velocity of the MS is 3 km/h. The results are obtained at a BER P_b equal to 10^{-3} . The SNR degradation increases with decreasing subsystem load since the total energy of the pilot symbols decreases with decreasing K_q/L and, hence, the performance of the channel estimation degrades. This effect can be avoided by boosting the pilot symbols, cf. Section 5.2, such that, for instance, the total energy of the pilot symbols remain constant independent of the loading ratio K_q/L . Table 6.5 shows the SNR γ_b degradation due to real channel estimation for JD with MLSSE in the case of a fully loaded subsystem and v equal to 3 km/h. As reference the assigned results

for SD with MMSE equalization are shown. It can be observed that the SNR degradation with MLSSE is similar compared to MMSE equalization.

It can be summarized that the proposed MC-CDMA mobile radio system is able to handle full system load in the downlink. To guarantee a BER P_b equal to 10^{-3} a value of $10 \log_{10}(\gamma_b)$ between 8 dB and 12 dB is required on the average. Propagation areas typical for smaller cells require additional means to improve the performance, since within this scenario too less diversity is offered by the channel which could be exploited in the MC-CDMA receiver. However, as long as either frequency diversity or time diversity within an OFDM frame is offered by the mobile radio channel, the presented MC-CDMA mobile radio system achieves a high bandwidth efficiency β , cf. (1.1), of

$$\beta = 0.81 \text{ bit/s/Hz.} \quad (6.8)$$

In this thesis, it is shown that MC-CDMA is a very promising multiple access scheme especially for the downlink of future mobile radio systems. MC-CDMA mobile radio systems offer great flexibility and provide high performance at a reasonable complexity. The advantages of MC-CDMA compared to DS-CDMA can also be exploited in the uplink as shown in Appendix B where the already mentioned SS-MC-MA scheme derived from the MC-CDMA scheme is introduced and investigated for the uplink.

Chapter 7

Abstract

Performance and flexibility of mobile radio systems essentially depend on the choice of the multiple access scheme. The novel MC-CDMA scheme which is the topic of this thesis is a promising alternative to conventional FDMA, TDMA, and CDMA schemes. With MC-CDMA, each data modulated chip of the user specific spreading code is mapped onto a separate subcarrier, so that the chips of the spreading code and, hence, the data symbol is transmitted in parallel on multiple subcarriers. The application of OFDM enables one to avoid ISI and ICI in the detection process, resulting in simple SD and MD techniques. In MC-CDMA mobile radio systems, SD can be realized by equalizing each subcarrier individually, yielding only one complex-valued multiplication per subcarrier and OFDM symbol. Due to the M -, Q -, and $M&Q$ -Modification of the MC-CDMA scheme, even the optimum JD techniques MLSSE and MLSE can be applied with reasonable complexity.

After introducing the MC-CDMA signal structure, SD and MD techniques are analyzed, optimized, and compared to each other in this thesis. Taking into account convolutional channel coding with soft decision decoding, the optimum soft decided values which can be delivered to a Viterbi decoder are derived for MC-CDMA receivers with SD and MD. Exploiting the optimum soft decided values, an iterative detection and decoding scheme referred to as soft IC is introduced. With soft IC, reliability information about the reconstructed interference is taken into account in the iterative IC scheme, reducing error propagation. The suitability of the recently proposed Turbo codes as channel codes for MC-CDMA mobile radio systems is also investigated. However, it is shown that Turbo codes are only of limited use in MC-CDMA mobile radio systems when considering speech transmission applications. The trade-off between channel coding and spreading is determined and a bandwidth efficiency plan for MC-CDMA, MC-FDMA, and MC-TDMA mobile radio systems is presented, which reveals that amongst these, MC-CDMA systems are the most bandwidth efficient systems. To enable coherent detection, channel estimation with filtering in frequency and time is investigated for an MC modulated system. A 2×1 -D channel estimation is analyzed and optimized by taking into account model mismatch between the correlation functions of the channel and those used for the filter design. The performance of the presented 2×1 -D FIR filtering closely approximates the performance of optimum 2-D Wiener filtering. It is shown that the proposed MC-CDMA mobile radio system can handle high velocities of the mobile user in various propagation areas. Guaranteeing a good transmission quality with a BER P_b equal to 10^{-3} , the presented MC-CDMA mobile radio system achieves the high bandwidth efficiency of 0.81 bit/s/Hz at a value of $10 \log_{10}(\gamma_b)$ between 8 dB and 12 dB on the average.

Kurzfassung

100 Jahre nach den ersten Experimenten des italienischen Funktechniklers und späteren Nobelpreisträgers G. Marconi mit drahtloser Nachrichtenübertragung ist der Mobilfunksektor einer der am schnellsten wachsenden Märkte der Welt. Bereits nach der Einführung der ersten Generation von Mobilfunksystemen in den 80er Jahren war bald abzusehen, daß die Kapazität dieser überwiegend analogen Systeme nicht ausreichen würde, um die steigende Nachfrage an mobiler Kommunikation abzudecken. Dieser Engpaß konnte Anfang der 90er Jahre durch die Einführung der zweiten Generation von Mobilfunksystemen überwunden werden, wobei die Kapazität durch die Verwendung vollständig digitaler Systeme erheblich verbessert werden konnte. Der in Europa entwickelte GSM (Global System for Mobile Communications) Standard für Mobilfunksysteme der zweiten Generation hat sich weltweit am stärksten durchgesetzt. Doch bereits heute weiß man, daß die zweite Generation den Bedürfnissen an mobiler Kommunikation des 21. Jahrhunderts nicht gerecht werden kann. Die Anforderungen an die zukünftigen Mobilfunksysteme der dritten Generation sind hohe Bandbreiteneffizienz bedingt durch einen beschränkt verfügbaren Frequenzbereich und hohe Flexibilität. Von Bedeutung sind hierbei Multimedienienste mit Sprach-, Bild- und Datenübertragung, welche unter anderem verschiedene und variable Datenraten erfordern und in verschiedensten Umgebungen und Zellstrukturen verfügbar sein sollen.

Beim Entwurf von Mobilfunksystemen der dritten Generation ist das Verfahren, mit dem die einzelnen Teilnehmer auf den Kanal zugreifen, ausschlaggebend für die Bandbreiteneffizienz und Flexibilität des Systems. Anwendung finden hier die elementaren Vielfachzugriffsverfahren Frequenzmultiplex (engl. frequency division multiple access, FDMA), Zeitmultiplex (engl. time division multiple access, TDMA) und Codemultiplex (engl. code division multiple access, CDMA). Von den unterschiedlichen CDMA-Vielfachzugriffsverfahren hat sich dasjenige mit DS-Spreizung (engl. direct sequence spreading) am meisten durchgesetzt. Bei DS-CDMA werden die Teilnehmerdaten mit hochratigen Spreizcodes multipliziert und somit in der Übertragungsbandbreite gespreizt. Die einzelnen Teilnehmer senden ihre gespreizten Daten im gleichen Frequenzband, wobei durch geeignete Wahl der teilnehmerspezifischen Spreizcodes gewährleistet werden kann, daß die Interferenzen zwischen den Teilnehmern (engl. multiple access interference, MAI) minimal sind. Umfangreiche Untersuchungen haben gezeigt, daß keines der elementaren Vielfachzugriffsverfahren alleine den Anforderungen der Mobilfunksysteme der dritten Generation gerecht werden kann und weitere Untersuchungen mit hybriden Vielfachzugriffsverfahren notwendig sind. Hybride Vielfachzugriffsverfahren sind Kombinationen aus den elementaren Vielfachzugriffsverfahren, die es ermöglichen, die Vorteile der elementaren Vielfachzugriffsverfahren in geeigneter Weise miteinander zu kombinieren. Darüberhinaus ist es wichtig, jüngste Entwicklungen in der Nachrichtentechnik, wie z.B. auf dem Gebiet der

Mehrträgermodulation, mitzuverfolgen, da diese möglicherweise die elementaren und hybriden Vielfachzugriffsverfahren verbessern können.

Die Mehrträgermodulation hat in jüngster Zeit stark an Bedeutung gewonnen, da die Entwicklung in der Halbleitertechnik es ermöglicht hat, unter Verwendung der schnellen Fourier-Transformation (engl. fast Fourier transform, FFT) digitale Mehrträgermodems mit geringer Komplexität basierend auf mehreren tausend Unterträgern zu implementieren. Durch die Mehrträgermodulation werden hochratige, serielle Datenströme, die in typischen Mobilfunkkanälen mit Mehrwegeausbreitung starker Intersymbolinterferenz (engl. inter symbol interference, ISI) unterliegen, in niederratige, parallele Teilströme mit reduzierter ISI umgewandelt und auf unterschiedliche Unterträger moduliert. Verbleibende ISI kann durch Einfügen eines Schutzintervalls, bestehend aus einer zyklischen Verlängerung des Symbols, im Empfänger eliminiert werden. Um die verfügbare Übertragungsbandbreite möglichst effizient zu nutzen, werden die Frequenzspektren der Teilströme überlappt, wobei die Signale auf den einzelnen Unterträgern orthogonal zueinander sind und Interkanalinterferenz (engl. inter channel interference, ICI) vermieden werden kann, wenn der Unterträgerabstand gleich der Datenrate gewählt ist. Dieses orthogonale Frequenzmultiplexverfahren wird als OFDM (engl. orthogonal frequency division multiplexing) bezeichnet, und die parallel übertragenen Datensymbole bilden ein OFDM-Symbol. Der große Durchbruch der Mehrträgermodulation gelang in den 90er Jahren, als OFDM für den europäischen, digitalen Hörfunkstandard (engl. Digital Audio Broadcasting standard, DAB standard) und den europäischen, digitalen, terrestrischen Fernsehstandard (engl. terrestrial Digital Video Broadcasting standard, DVB-T standard) gewählt wurde. Seit 1993 gibt es intensive Forschungsaktivitäten, die sich mit dem Einsatz der Mehrträgermodulation in Mobilfunksystemen beschäftigen. Die meiste Aufmerksamkeit wurde dabei der Verbindung von Mehrträgermodulation mit CDMA geschenkt, wobei zwei unterschiedliche Konzepte eingeführt wurden. Das erste Konzept wird als MC-CDMA (engl. multi-carrier CDMA) oder auch OFDM-CDMA bezeichnet und ist Inhalt der vorliegenden Arbeit. Das zweite Konzept wurde in zwei Varianten eingeführt, wobei die erste als MC-DS-CDMA (engl. multi-carrier direct sequence CDMA) und die zweite als MT-CDMA (engl. multi-tone CDMA) bezeichnet wird.

Beim Vielfachzugriffsverfahren MC-CDMA wird jedes Chip des CDMA-Spreizcodes einem Unterträger zugeordnet, so daß ein Datensymbol gleichzeitig über mehrere Unterträger gespreizt übertragen wird. Um ICI zu vermeiden, haben die Unterträger einen Abstand, der dem Kehrwert der OFDM-Symboldauer entspricht. Wenn durch geeignete Dimensionierung des MC-CDMA-Mobilfunksystems der Kanalschwund auf den einzelnen Unterträgern als nicht frequenzselektiv und für die Dauer eines OFDM-Symbols als zeitinvariant angesehen werden kann und ferner ISI eliminiert wird, ist es möglich, effiziente Empfänger mit geringer Komplexität zu realisieren. Im Gegensatz zu konventionellen CDMA-Mobilfunksystemen können in MC-CDMA-Mobilfunksystemen orthogonale, teilnehmerspezifische Spreizcodes optimal eingesetzt werden, da ISI und ICI bei der Datendetektion vermieden werden können.

Mit MC-DS-CDMA und MT-CDMA werden die Datensymbole eines Teilnehmers in parallele,

niederratige Teilströme gewandelt, bevor jeder Teildatenstrom mit einem teilnehmerspezifischen Spreizcode multipliziert und somit gespreizt wird. Beim Vielfachzugriffsverfahren MC-DS-CDMA sind die Signale auf den Unterträgern nach der Spreizung orthogonal, während sie bei MT-CDMA vor der Spreizung orthogonal zueinander sind. Bei MC-DS-CDMA werden die Daten eines Teilnehmers nicht mehr über den gesamten Frequenzbereich gespreizt, sondern nur noch über den eines Unterträgers, wodurch der erzielbare Frequenzdiversitätsgewinn des Systems mit zunehmender Unterträgerzahl abnimmt. MC-DS-CDMA eignet sich eher zur Ausnutzung von Zeitdiversität, wobei größere Verzögerungen bei der Datenübertragung auftreten. MT-CDMA kann etwa die gleichen Frequenzdiversitätsgewinne wie DS-CDMA oder MC-CDMA erzielen, da ein Datensymbol fast über den gesamten Frequenzbereich gespreizt wird. Bei MT-CDMA geht aber durch die DS-Spreizung der Daten die Orthogonalität der Signale auf den Unterträgern verloren, so daß ICI auftritt.

In mehreren Untersuchungen wurde die Leistungsfähigkeit der Vielfachzugriffsverfahren MC-CDMA, DS-CDMA, MC-DS-CDMA und MT-CDMA bezüglich der Bitfehlerrate und der Bandbreiteneffizienz miteinander verglichen. In der Abwärtsstrecke eines Mobilfunksystems zeigten die Untersuchungsergebnisse klare Vorteile für MC-CDMA gegenüber den anderen Vielfachzugriffsverfahren, wobei mit MC-CDMA eine bis zu viermal höhere Bandbreiteneffizienz erzielt werden konnte. Vergleiche zwischen MC-CDMA und DS-CDMA in der Aufwärtsstrecke eines Mobilfunksystems zeigten auch hier Vorteile für MC-CDMA.

Parallel zu den Aktivitäten auf dem Gebiet MC-CDMA gibt es auch Untersuchungen mit den mehrträgermodulierten Vielfachzugriffsverfahren MC-FDMA und MC-TDMA. Beide neuartigen Vielfachzugriffsverfahren werden in der vorliegenden Arbeit beschrieben und ihre Leistungsfähigkeit wird mit derjenigen von MC-CDMA-Mobilfunksystemen verglichen.

Die vorliegende Arbeit verfolgt zwei wesentliche Ziele. Das erste Ziel ist die Entwicklung und Optimierung der einzelnen MC-CDMA-Systemkomponenten Datendetektion, Kanaldecodierung mit Zuverlässigkeitsinformation und Kanalschätzung. Das zweite Ziel ist eine Gesamtsystembetrachtung, bei der ein MC-CDMA-Mobilfunksystem entwickelt und analysiert wird. Wichtig bei der Gesamtsystembetrachtung ist es, daß die verwendeten Mobilfunkkanalmodelle, mit denen das vorgestellte MC-CDMA-Mobilfunksystem getestet wird, den Anforderungen zukünftiger Mobilfunksysteme gerecht werden. So werden bei den Untersuchungen Ausbreitungsszenarien nachgebildet, die typisch für Makro-, Mikro- und Picozellen sind. Hierfür werden die Kanalmodelle der CODIT (Code Division Testbed) Studie wie auch der COST (European Cooperation in the Field of Scientific and Technical Research) 207 Studie herangezogen.

Ausgehend von der Beschreibung der Mehrträgermodulation basierend auf OFDM wird in dieser Arbeit die MC-CDMA-Signalstruktur hergeleitet und ihre Flexibilität bezüglich der Datenrate und der Teilnehmerkapazität durch das Einführen geeigneter Systemmodifikationen und dem Einsatz von Frequenzinterleaving gezeigt. Ein zeit- und frequenzdiskretes MC-CDMA-Übertragungsmodell wird hergeleitet, für dessen mathematische Beschreibung die Matrix-Vektor-Notation verwendet wird. Basierend auf dem zeit- und frequenzdiskreten MC-CDMA-

Übertragungsmodell werden optimale und suboptimale MC-CDMA-Datendetektionstechniken mathematisch beschrieben und bezüglich ihrer Leistungsfähigkeit miteinander verglichen. In MC-CDMA-Mobilfunksystemen wird die einfache Einzeldetektion (engl. single-user detection, SD), die kein Vorwissen über die MAI in der Datendetektion berücksichtigt, durch eine separate Entzerrung auf jedem Unterträger realisiert, die pro OFDM-Symbol einer komplexwertigen Multiplikation pro Unterträger entspricht. Danach erfolgt eine Rückspreizung der Daten mit dem teilnehmerspezifischen Spreizcode. Untersucht werden die SD-Techniken MMSE-Entzerrung (engl. minimum mean square error equalization) und ZF-Entzerrung (engl. zero-forcing equalization). Ferner werden auch Diversitätstechniken wie MRC (engl. maximum ratio combining) und EGC (engl. equal gain combining) als SD-Techniken eingesetzt. Die MMSE-Entzerrung minimiert den mittleren quadratischen Fehler zwischen dem gesendeten und dem im Empfänger entzerrten Signal und zeigt in Mobilfunkkanälen mit MAI die geringsten Bitfehlerraten verglichen zu den anderen SD-Techniken bei gleichem mittlerem Signal-Stör-Verhältnis (engl. signal-to-noise ratio, SNR). Da die MMSE-Entzerrung Wissen über das mittlere SNR pro Unterträger benötigt, wird eine suboptimale MMSE-Entzerrung vorgestellt, die kein Zusatzwissen über das aktuelle SNR benötigt, jedoch an die Leistungsfähigkeit der optimalen MMSE-Entzerrung herankommt. Darüber hinaus wird die aufwendigere, aber leistungsstärkere Mehrteilnehmer-Detektion (engl. multi-user detection, MD) untersucht, bei der Vorwissen über die MAI bei der Datendetektion ausgenutzt wird. Bei der MD unterscheidet man Detektionstechniken nach den Prinzipien der Interferenzeliminierung (engl. interference cancellation, IC) und der gemeinsamen Detektion (engl. joint detection, JD). Das Prinzip der IC ist es, die Information der interferierenden Teilnehmer zu detektieren und damit die MAI zu rekonstruieren und vom empfangenen Signal abzuziehen, bevor die Information des betrachteten Teilnehmers detektiert wird. Die IC kann in mehreren Iterationen durchgeführt werden, woraus sich eine Mehrstufendetektion ergibt. In dieser Arbeit wird ein Mehrstufendetektionsverfahren mit IC vorgestellt, bei dem die einzelnen Detektionsstufen mit einer an die jeweils verbleibende MAI angepaßten MMSE-Entzerrung arbeiten. Der optimale Datendetektor verwendet JD mit Maximum-Likelihood-Kriterium. Es werden die optimale MLSE (engl. maximum likelihood sequence estimation) und die optimale MLSSE (engl. maximum likelihood symbol-by-symbol estimation) für MC-CDMA-Mobilfunksysteme beschrieben und analysiert. Durch die Vermeidung von ISI und ICI im Detektionsprozeß und mit Hilfe von geeigneten Systemmodifikationen, die sich durch die Mehrträgermodulation ergeben, können in MC-CDMA-Mobilfunksystemen die optimalen Datendetektoren mit akzeptabler Komplexität realisiert werden. Der Einsatz von optimalen Datendetektoren ist in konventionellen DS-CDMA-Mobilfunksystemen bedingt durch den höheren Realisierungsaufwand praktisch nicht möglich.

Kanalcodierung ist eine effiziente Technik, um den Störungen durch den Mobilfunkkanal entgegenzuwirken. In der vorliegenden Arbeit wird ein MC-CDMA-Mobilfunksystem mit Faltungscodierung und Viterbi-Decodierung untersucht. Der Viterbi-Algorithmus ist ein einfacher Decodieralgorithmus, der in optimaler Weise Entscheidungen mit Zuverlässigkeitsinformation verarbeiten kann und gemäß dem Maximum-Likelihood-Kriterium die am wahrscheinlichsten gesendete Sequenz ermittelt. Die optimalen Entscheidungen mit Zuverlässigkeitsinformation

sind Log-Likelihood-Verhältnisse (engl. log-likelihood ratios, LLRs). In dieser Arbeit werden die LLRs für MC-CDMA-Mobilfunksystem mit SD und mit MD hergeleitet und geeignete Vereinfachungen der optimalen LLRs vorgestellt. Ferner wird eine sogenannte Soft-IC vorgestellt, bei der die Datendetektion und die Kanaldecodierung in einer Weise iterativ miteinander verknüpft sind, die es bei der IC ermöglicht, zusätzlich Zuverlässigkeitsinformationen über die rekonstruierte MAI auszunutzen. Hierdurch wird die Fehlerfortpflanzung im Vergleich zur konventionellen IC verringert. Es wird gezeigt, daß mit Soft-IC niedrigere Bitfehlerraten als mit MLSSE und Kanalcodierung bei gleichem SNR erreicht werden. Der MAI-freie Fall (engl. single-user bound), der eine untere Grenze für die Bitfehlerrate darstellt, kann mit Soft-IC sehr gut angenähert werden. Die in der vorliegenden Arbeit hergeleiteten LLRs ermöglichen es, die 1993 vorgeschlagenen Turbo-Codes mit iterativer Turbo-Decodierung in optimaler Weise in MC-CDMA-Mobilfunksystemen einzusetzen. Bei der Turbo-Decodierung sind die Interleavergröße und die Anzahl der Iterationen ausschlaggebend für den Codiergewinn. Es wird gezeigt, daß Turbo-Codes in MC-CDMA-Mobilfunksystemen bei Sprachübertragung nur geringe Codiergewinne erzielen und daß ihre höhere Komplexität verglichen mit einfachen Faltungscodes ihren Einsatz nicht rechtfertigen. Ausschlaggebend hierfür ist, daß bei der Sprachübertragung nur geringe Verzögerungen zulässig sind und daher nur kleine Interleavergrößen eingesetzt werden können. Für MC-CDMA-Mobilfunksysteme mit Faltungscodierung wird das optimale Verhältnis zwischen Kanalcode rate und Spreizcode länge ermittelt. Anhand eines Bandbreiteneffizienzplans wird gezeigt, daß MC-CDMA-Mobilfunksysteme eine höhere Bandbreiteneffizienz verglichen mit MC-FDMA- und MC-TDMA-Mobilfunksystemen erzielen.

Empfänger mit kohärenter Datendetektion und Kanaldecodierung mit Zuverlässigkeitsinformation benötigen Wissen über die Übertragungsfunktion des Mobilfunkkanals, welches daher im Empfänger geschätzt werden muß. Bei Nachrichtensystemen mit Mehrträgermodulation eignet sich eine zweidimensionale (2-D) Kanalschätzung basierend auf Pilotsymbolen. Werden die Pilotsymbole mit ausreichender Dichte in Frequenz- und Zeitrichtung über die OFDM-Symbole verteilt, so kann die Übertragungsfunktion des Kanals durch Interpolation bzw. Filterung ermittelt werden. Das optimale 2-D-Filter nach dem MMSE-Kriterium ist das 2-D-Wiener-Filter. Ausgehend von der Beschreibung der Theorie der optimalen 2-D-Wiener-Filterung wird in dieser Arbeit eine Kanalschätzung mit Filterung in zwei Dimensionen für ein MC-CDMA-Mobilfunksystem entwickelt, wobei die Abwärtsstrecke betrachtet wird. Da dem optimalen 2-D-Wiener-Filter die Korrelationsfunktionen des Mobilfunkkanals bekannt sein müssen, werden zwei weniger komplexe, kaskadierte eindimensionale (1-D) FIR-Filter eingesetzt, die für die kritischsten Bedingungen, die im betrachteten Mobilfunkkanal auftreten können, optimiert sind. Wie gezeigt wird, entspricht die Leistungsfähigkeit von zwei kaskadierten 1-D-FIR-Filtern derjenigen eines 2-D-FIR-Filters. Da die Datenübertragung beim untersuchten MC-CDMA-Mobilfunksystem in einzelnen OFDM-Rahmen erfolgt, wird die Übertragungsfunktion des Mobilfunkkanals nur über einen OFDM-Rahmen gefiltert. Ein OFDM-Rahmen besteht aus einer endlichen Anzahl von aufeinanderfolgenden OFDM-Symbolen. Die gewählte Anordnung der Pilotsymbole in einem OFDM-Rahmen erfüllt das 2-D-Abtasttheorem, wobei sich zweifache Überabtastung

in Zeit- und in Frequenzrichtung als geeignet erweist. In Untersuchungen wird anhand des mittleren quadratischen Schätzfehlers gezeigt, daß die entwickelte Kanalschätzung in unterschiedlichen Ausbreitungsgebieten, die typisch für Makro-, Mikro- und Picozellen sind, und bei Dopplerfrequenzen von über 400 Hz noch vernünftig arbeitet.

Im Rahmen einer Gesamtsystembetrachtung wird ein MC-CDMA-Mobilfunksystem in der Abwärtsstrecke mit realer Kanalschätzung und Kanalcodierung entworfen und untersucht. Hierzu werden die CODIT- und COST-207-Kanalmodelle verwendet. Es wird gezeigt, daß das betrachtete MC-CDMA-Mobilfunksystem in der Lage ist, bei unterschiedlichsten Ausbreitungsbedingungen eine gute Übertragungsqualität mit voller Systemauslastung zu garantieren. So reicht in den meisten Fällen ein SNR von 8 dB bis 12 dB aus, um eine mittlere Bitfehlerrate von 10^{-3} zu garantieren. Das vorgestellte MC-CDMA-Mobilfunksystem erreicht die hohe Bandbreiteneffizienz von 0.81 bit/s/Hz. Ferner zeigen die Untersuchungen, daß Ausbreitungsbedingungen, die typisch für kleine Mobilfunkzellen wie Mikro- und Picozellen sind, generell kritisch sind, da sie wenig Frequenz- und Zeitdiversität bieten und eine ausreichende Übertragungsqualität nur durch Maßnahmen wie z.B. größere Übertragungsbandbreiten erzielt werden kann.

Im Anhang zu dieser Arbeit wird die Leistungsfähigkeit von MC-CDMA-Mobilfunksystemen mit SD basierend auf MMSE-Entzerrung und von JD basierend auf MLSSE und MLSE in Mobilfunkkanälen analytisch hergeleitet. Ferner wird ein neuartiges Vielfachzugriffsverfahren vorgestellt, das in ähnlicher Weise wie MC-CDMA die Vorteile der Mehrträgermodulation und der Bandspreiztechnik geeignet verbindet, jedoch nicht auf CDMA sondern auf FDMA auf der Ebene von Unterträgern beruht. Das Vielfachzugriffsverfahren wird als SS-MC-MA (engl. spread spectrum multi-carrier multiple access) bezeichnet und läßt sich direkt aus dem Vielfachzugriffsverfahren MC-CDMA ableiten. In SS-MC-MA-Mobilfunksystemen kann die Kanalschätzung für die Aufwärtsstrecke aufwandsgünstig realisiert werden. Es wird gezeigt, daß SS-MC-MA-Mobilfunksysteme eine gute Übertragungsqualität bei voller Systemauslastung in der Aufwärtsstrecke ermöglichen. In der Abwärtsstrecke benötigen sie jedoch ein etwa 1 dB höheres SNR gegenüber MC-CDMA-Mobilfunksystemen mit gleicher Übertragungsqualität.

Appendix A

Analytical Performance Evaluation

A.1 SD with MMSE Equalization

Since MMSE equalization is the most promising SD technique which has been investigated in this thesis, the analytical derivation of the performance of uncoded MC-CDMA systems with MMSE equalization presented in [Kai95c] is also included in this thesis.

A soft decided value after SD, symbol demapping, and deinterleaving can be written according to (4.20). Assuming perfect frequency interleaving and sufficiently long spreading codes, cf. Section 4.2.2, the MAI and the modified noise in (4.20) can be considered as additive zero mean Gaussian noise according to the central limit theorem. Furthermore, when assuming that the code bit $b^{(k)}$ and the real-valued fading factor $\vartheta^{(k)}$ are statistically independent and $E\{|b^{(k)}|^2\}$ is equal to 1, the BER can be calculated according to [Kai95c]

$$P_b = \frac{1}{2} \operatorname{erfc} \left(\sqrt{\frac{E\{\vartheta^{(k)2}\}}{2(\sigma_{\text{MAI}}^2 + \sigma_{\text{noise}}^2)}} \right). \quad (\text{A.1})$$

Employing Walsh Hadamard codes as orthogonal, user specific spreading codes, cf. Section 4.2.2, and assuming perfect channel estimation, the application of the law of large numbers [Pap91] together with (4.22) yields

$$E\{\vartheta^{(k)2}\} = |E\{G_l \underline{H}_l\}|^2. \quad (\text{A.2})$$

The variance of the MAI σ_{MAI}^2 and the variance of the noise σ_{noise}^2 are defined according to (4.23) and (4.24), respectively. When applying MMSE equalization according to (3.64), the expectation values in (A.2), (4.23), and (4.24) result for the uncorrelated Rayleigh fading channel with (2.18) in

$$\begin{aligned} E\{G_l \underline{H}_l\} &= E \left\{ \frac{|\underline{H}_l|^2}{|\underline{H}_l|^2 + 1/\gamma_c} \right\} \Big|_{|\underline{H}_l| \text{ is Rayleigh distributed}} \\ &= 1 + \frac{e^{1/\gamma_c}}{\gamma_c} \operatorname{Ei} \left(-\frac{1}{\gamma_c} \right), \\ E\{|G_l \underline{H}_l|^2\} &= E \left\{ \left| \frac{|\underline{H}_l|^2}{|\underline{H}_l|^2 + 1/\gamma_c} \right|^2 \right\} \Big|_{|\underline{H}_l| \text{ is Rayleigh distributed}} \end{aligned} \quad (\text{A.3})$$

$$= 1 + \frac{1}{\gamma_c} + \left(\frac{1}{\gamma_c^2} + \frac{2}{\gamma_c} \right) e^{1/\gamma_c} \text{Ei} \left(-\frac{1}{\gamma_c} \right), \quad (\text{A.4})$$

$$\begin{aligned} \text{E}\{|G_l|^2\} &= \text{E} \left\{ \left| \frac{H_l^*}{|H_l|^2 + 1/\gamma_c} \right|^2 \right\} \Big|_{|H_l| \text{ is Rayleigh distributed}} \\ &= -1 - \left(1 + \frac{1}{\gamma_c} \right) e^{1/\gamma_c} \text{Ei} \left(-\frac{1}{\gamma_c} \right), \end{aligned} \quad (\text{A.5})$$

where the required integrals can be found in [RyG63] and $\text{Ei}(-1/\gamma_c)$ is the exponential integral defined as

$$\text{Ei} \left(-\frac{1}{\gamma_c} \right) = - \int_{1/\gamma_c}^{\infty} \frac{e^{-x}}{x} dx. \quad (\text{A.6})$$

The exponential integral converges for $1/\gamma_c$ greater than 0 [AbS64]. By insertion of (A.3), (A.4), and (A.5) in (A.2), (4.23), and (4.24), the values $\text{E}\{\vartheta^{(k)2}\}$, σ_{MAI}^2 , and σ_{noise}^2 result for MC-CDMA receivers using SD with MMSE equalization in [Kai95c]

$$\text{E}\{\vartheta^{(k)2}\} = \left[1 + \frac{e^{1/\gamma_c}}{\gamma_c} \text{Ei} \left(-\frac{1}{\gamma_c} \right) \right]^2, \quad (\text{A.7})$$

$$\sigma_{\text{MAI}}^2 = \frac{K_q - 1}{L} \left[\frac{1}{\gamma_c} + \frac{e^{1/\gamma_c}}{\gamma_c^2} \text{Ei} \left(-\frac{1}{\gamma_c} \right) - \frac{e^{2/\gamma_c}}{\gamma_c^2} \text{Ei}^2 \left(-\frac{1}{\gamma_c} \right) \right], \quad (\text{A.8})$$

$$\sigma_{\text{noise}}^2 = \frac{\sigma^2}{2} \left[-1 - \left(1 + \frac{1}{\gamma_c} \right) e^{1/\gamma_c} \text{Ei} \left(-\frac{1}{\gamma_c} \right) \right]. \quad (\text{A.9})$$

Insertion of (A.7), (A.8), and (A.9) in (A.1) and given (3.51), a function which only depends on K_q , L , and γ_s or γ_b according to (3.52), respectively, is obtained. Since the presented analytical approach is based on the central limit theorem, its accuracy increases with increasing spreading code length L . Thus, assuming sufficiently long spreading codes, the performance of MC-CDMA mobile radio systems using SD with MMSE equalization can analytically be evaluated. In Fig. A.1, the deviation between the analytical and the simulation results due to the assumption with the central limit theorem is shown. The deviation is given in terms of the required SNR γ_b to achieve the uncoded BER P_b equal to 10^{-2} for the uncorrelated Rayleigh fading channel versus the spreading code length L . The results are obtained with fully loaded subsystem. It can be observed that for spreading code lengths L equal to or greater than 8, the SNR deviation between the analytical and the simulation results is equal to or less than 1 dB. Hence, the analytical approach provides useful results for a spreading code length of L equal to or greater than 8. It should be noted that the analytical results tend to be too optimistic.

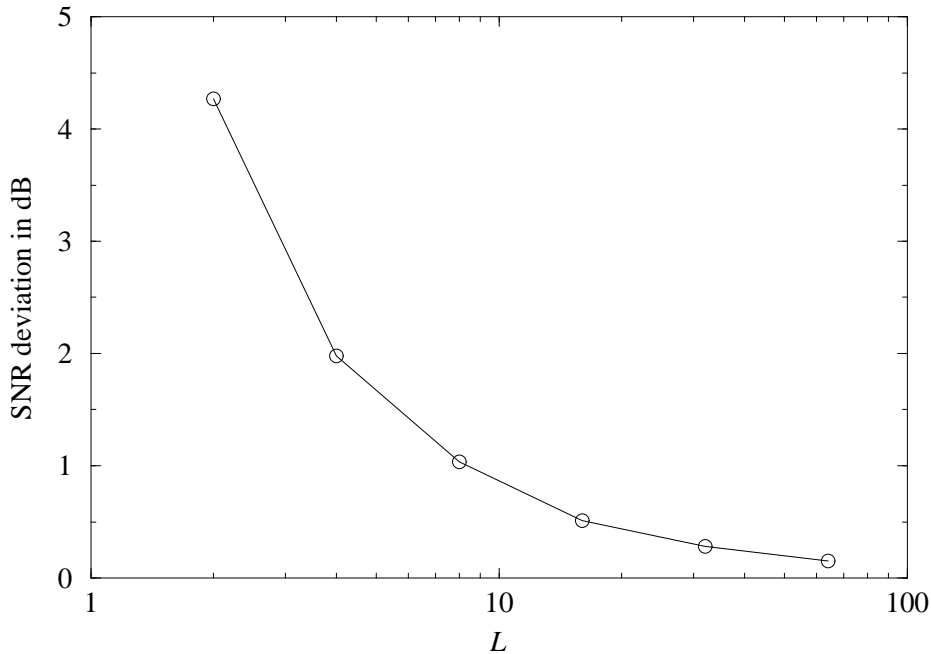


Figure A.1: SNR deviation between the analytical and the simulation results versus spreading code length L ; uncorrelated Rayleigh fading channel; QPSK; fully loaded subsystem, $K_q = L$; $P_b = 10^{-2}$

A.2 JD with MLSSE and MLSE

The BER obtained with MC-CDMA receivers using JD with MLSE and MLSSE can be upper bounded for the uncorrelated Ricean fading channel [Kai95c] and with K_{Rice} equal to 0, also for the uncorrelated Rayleigh fading channel [Faz93]. The BER P_b for any detector or decoder based on MLSE can be upper bounded by [DiS88, MMB91]

$$P_b \leq \frac{1}{2} \sum_{\mu=1}^{M_d^{K_q}} \sum_{\nu=1}^{M_d^{K_q}} e(\mathbf{s}_\nu, \hat{\mathbf{s}}_\mu) P\{\mathbf{s}_\nu\} P\{\hat{\mathbf{s}}_\mu | \mathbf{s}_\nu\}, \quad (\text{A.10})$$

where \mathbf{s}_ν , $\nu = 1, \dots, M_d^{K_q}$, is the set of all possible transmitted sequences, $\hat{\mathbf{s}}_\mu$, $\mu = 1, \dots, M_d^{K_q}$, is the set of all possible detected sequences, and $e(\mathbf{s}_\nu, \hat{\mathbf{s}}_\mu)$ is the number of bit errors that occur when the sequence \mathbf{s}_ν is transmitted and $\hat{\mathbf{s}}_\mu$ is chosen in the detector. $P\{\mathbf{s}_\nu\}$ is the probability that the sequence \mathbf{s}_ν has been transmitted. Since there are $M_d^{K_q}$ possible sequences per block which are assumed to be equal likely, the sequence probability is

$$P\{\mathbf{s}_\nu\} = \frac{1}{M_d^{K_q}}. \quad (\text{A.11})$$

$P\{\hat{\mathbf{s}}_\mu | \mathbf{s}_\nu\}$ represents the conditioned error probability that the decoder chooses $\hat{\mathbf{s}}_\mu$ when \mathbf{s}_ν was transmitted. The conditioned error probability $P\{\hat{\mathbf{s}}_\mu | \mathbf{s}_\nu\}$ using the Chernoff bound is given by

[DiS88, Kai95c]

$$P\{\hat{\mathbf{s}}_\mu|\mathbf{s}_\nu\} \leq \prod_{l=1}^L \left[\frac{1 + K_{\text{Rice}}}{1 + K_{\text{Rice}} + \frac{\gamma_s}{4L} |S_{\nu,l} - \hat{S}_{\mu,l}|^2} \exp\left(\frac{-K_{\text{Rice}} \frac{\gamma_s}{4L} |S_{\nu,l} - \hat{S}_{\mu,l}|^2}{1 + K_{\text{Rice}} + \frac{\gamma_s}{4L} |S_{\nu,l} - \hat{S}_{\mu,l}|^2}\right) \right] \quad (\text{A.12})$$

for the uncorrelated Ricean fading channel, and simplifies to [DiS88, Faz93]

$$P\{\hat{\mathbf{s}}_\mu|\mathbf{s}_\nu\} \leq \prod_{l=1}^L \left(1 + \frac{\gamma_s}{4L} |S_{\nu,l} - \hat{S}_{\mu,l}|^2\right)^{-1} \quad (\text{A.13})$$

for the uncorrelated Rayleigh fading channel. Hence, with (A.10), (A.11), (A.12), and (A.13), the BER of MC-CDMA receivers using JD with MLSE can be upper bounded for the uncorrelated Ricean and Rayleigh fading channel. Since MLSSE theoretically achieves lower BERs than MLSE, the derived upper bound for MLSE is also an upper bound for MLSSE. In Section 3.3.4, it is shown that the performance of an uncoded MC-CDMA system with MLSSE is almost the same as with MLSE. Fig. A.2 shows the derived upper bounds for an MC-CDMA system with MLSSE in an uncorrelated Rayleigh fading channel and in an uncorrelated Ricean fading channel with K_{Rice} equal to 5. The length of the Walsh Hadamard spreading codes L is 8 and the subsystem is fully loaded. It can be seen from Fig. A.2 that the upper bounds for the uncorrelated Ricean and the uncorrelated Rayleigh fading channel are only 1 dB to 2 dB above the simulation results for BERs P_b less than 10^{-2} .

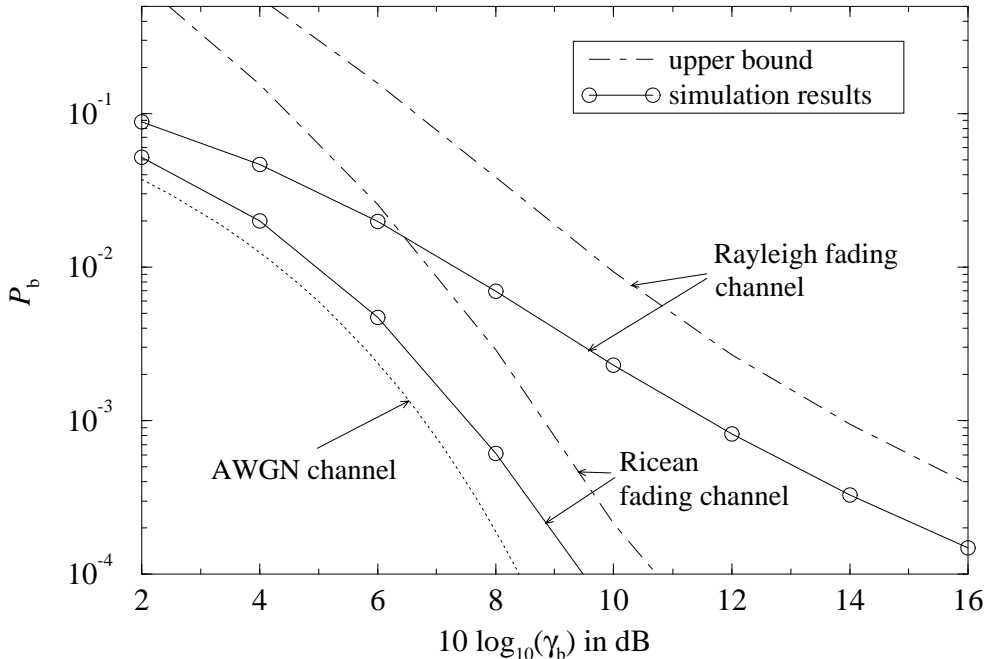


Figure A.2: Average uncoded BER P_b versus SNR γ_b for JD with MLSSE and the assigned upper bounds; uncorrelated Rayleigh and Ricean fading channel, $K_{\text{Rice}} = 5$; $L = 8$; $K_q = 8$; QPSK

Appendix B

Multiple Access Scheme SS-MC-MA

B.1 SS-MC-MA Signal Structure

This section presents a novel multiple access scheme which is referred to as spread spectrum multi-carrier multiple access (SS-MC-MA). Similar to MC-CDMA, SS-MC-MA exploits the advantages given by the combination of the spread spectrum technique with MC modulation [KaF96, KaF97a]. An SS-MC-MA system is superior compared to an MC-CDMA system in the uplink of a mobile radio system due to a simple channel estimation and a low-complex data detection. Whereas, an MC-CDMA system outperforms an SS-MC-MA system in the downlink, as it will be shown at the end of this section. Before presenting the SS-MC-MA signal structure and its uplink performance, the basic similarities and differences between SS-MC-MA and MC-CDMA systems are pointed out. This can preferably be done by comparing the SS-MC-MA and the MC-CDMA transmitter for the downlink. Fig. B.1 shows the SS-MC-MA transmitter for the downlink. The counterpart is the MC-CDMA transmitter with M -Modification shown

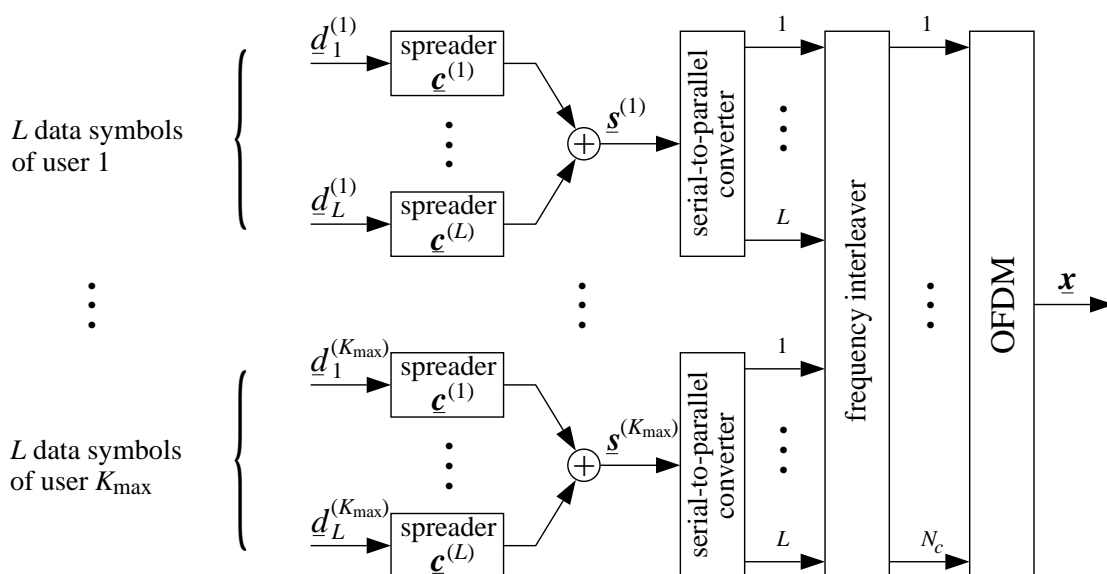


Figure B.1: Principle of SS-MC-MA illustrated for the transmitter in the downlink to enable a comparison with MC-CDMA shown in Fig. 3.8

in Fig. 3.8. For convenience, the case with M equal to L and K_{\max} equal to L is considered in this comparison. It can be observed that both transmitters are identical except for the mapping of the user data to the subsystems. In SS-MC-MA systems, one user maps L data symbols to one subsystem which this user exclusively uses for transmission. Consequently, different users use different subsystems in SS-MC-MA systems. In MC-CDMA systems, M data symbols per user are mapped to M different subsystems where each subsystem is shared by different users.

Between SS-MC-MA and MC-CDMA systems exist the following similarities:

- SS-MC-MA and MC-CDMA systems exploit frequency diversity by spreading each data symbol over L subcarriers.
- Per subsystem, the same data detection techniques can be applied with both SS-MC-MA and MC-CDMA systems.
- ISI and ICI can be avoided in SS-MC-MA and MC-CDMA systems, resulting in simple data detection techniques.

Between SS-MC-MA and MC-CDMA systems exist the following differences:

- In SS-MC-MA systems, the code division is used for the simultaneous transmission of the data of one user on the same subcarriers, whereas in the case of MC-CDMA systems, the code division is used for the transmission of the data of different users on the same subcarriers. Therefore, SS-MC-MA is an FDMA scheme on subcarrier level, whereas MC-CDMA is a CDMA scheme.
- MC-CDMA systems have to cope with MAI, which is not present in SS-MC-MA systems. Instead of MAI, the SS-MC-MA system has to cope with self interference caused by the superposition of signals from the same user.
- In SS-MC-MA systems, each subcarrier is exclusively used by one user, enabling low complex channel estimation especially for the uplink. In MC-CDMA systems, the channel estimation in the uplink has to cope with the superposition of signals from different users which are faded independently on the same subcarriers, increasing significantly the complexity of the uplink channel estimation.
- In an MC-CDMA system, M data symbols are spread over $M \cdot L$ subcarriers, whereas in an SS-MC-MA system, L data symbols are spread over the same L subcarriers. Hence, MC-CDMA is able to exploit more frequency diversity.

After this comparative introduction of SS-MC-MA, the uplink transmitter and the assigned receiver are described in detail in the sequel.

SS-MC-MA Transmitter: Fig. B.2 shows an SS-MC-MA transmitter with channel coding for the data of the k th user, $k = 1 \dots K$, for the uplink. The components channel encoding,

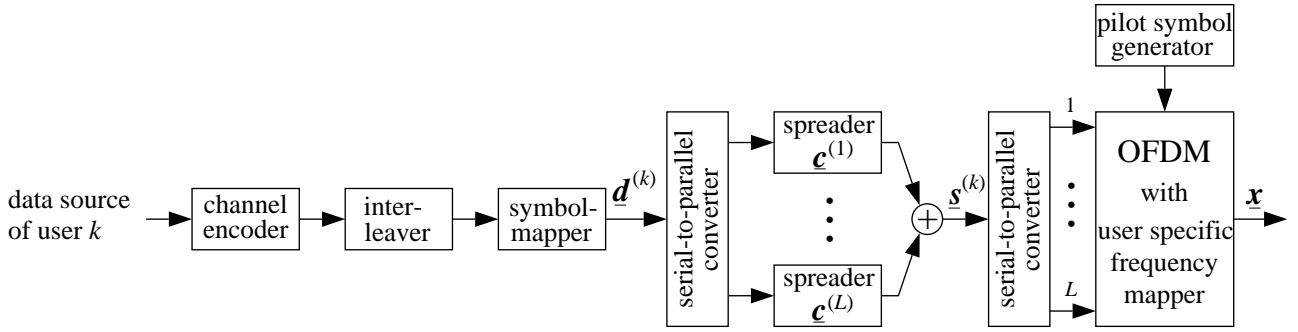


Figure B.2: SS-MC-MA transmitter of the k th user for the uplink

interleaving, and symbol mapping are identical to those described in Chapter 4 for MC-CDMA systems. In SS-MC-MA systems, L subsequent complex-valued data symbols $\underline{d}_l^{(k)}, l = 1 \dots L$, of user k are serial-to-parallel converted. The vector

$$\underline{\mathbf{d}}^{(k)} = (\underline{d}_1^{(k)}, \underline{d}_2^{(k)}, \dots, \underline{d}_L^{(k)})^T \quad (\text{B.1})$$

represents one block of L parallel converted data symbols of the k th user. Each of the L data symbols is multiplied with another orthogonal spreading code of length L . The $L \times L$ matrix

$$\mathbf{C} = (\underline{\mathbf{c}}_1 \ \underline{\mathbf{c}}_2 \ \dots \ \underline{\mathbf{c}}_L) = \begin{pmatrix} C_{1,1} & C_{2,1} & \dots & C_{L,1} \\ C_{1,2} & C_{2,2} & & C_{L,2} \\ \vdots & & \ddots & \vdots \\ C_{1,L} & C_{2,L} & \dots & C_{L,L} \end{pmatrix} \quad (\text{B.2})$$

represents the L different spreading codes $\underline{\mathbf{c}}_l, l = 1, \dots, L$, used by user k . The matrix \mathbf{C} is the same for all users. The modulated spreading codes are data symbol and, thus, chip synchronously added, resulting in the transmission vector

$$\underline{\mathbf{s}}^{(k)} = \mathbf{C} \underline{\mathbf{d}}^{(k)} = (\underline{s}_1^{(k)}, \underline{s}_2^{(k)}, \dots, \underline{s}_L^{(k)})^T \quad (\text{B.3})$$

consisting of L components. To increase the robustness of SS-MC-MA systems e.g. against inter cell interference, less than L data modulated spreading codes can be added to one transmission vector $\underline{\mathbf{s}}^{(k)}$.

Comparable to the frequency interleaving in MC-CDMA systems, the SS-MC-MA transmitter performs a user specific frequency mapping [KaF97b] such that subsequent components of $\underline{\mathbf{s}}^{(k)}$ are interleaved and mapped to subcarriers with maximum distance. The subcarriers of the different subsystems are chosen such that each subsystem exploits the whole transmission bandwidth. The user specific frequency mapping assigns each subsystem and, hence, each user exclusively its L subcarriers, avoiding MAI. The Q -Modification introduced in Section 3.2 for MC-CDMA systems is inherent in SS-MC-MA systems. The M -Modification can similar as for MC-CDMA systems be applied to SS-MC-MA systems by assigning a user more than one subsystem.

OFDM with guard interval is applied in SS-MC-MA systems in the same way as in MC-CDMA systems, cf. Section 3.1.1. In order to perform coherent data detection at the receiver and to guarantee robust time and frequency synchronization, pilot symbols are multiplexed in the transmitted data.

SS-MC-MA Receiver: An SS-MC-MA receiver with coherent detection of the data of the k th user is shown in Fig. B.3. After inverse OFDM with user specific frequency demapping and

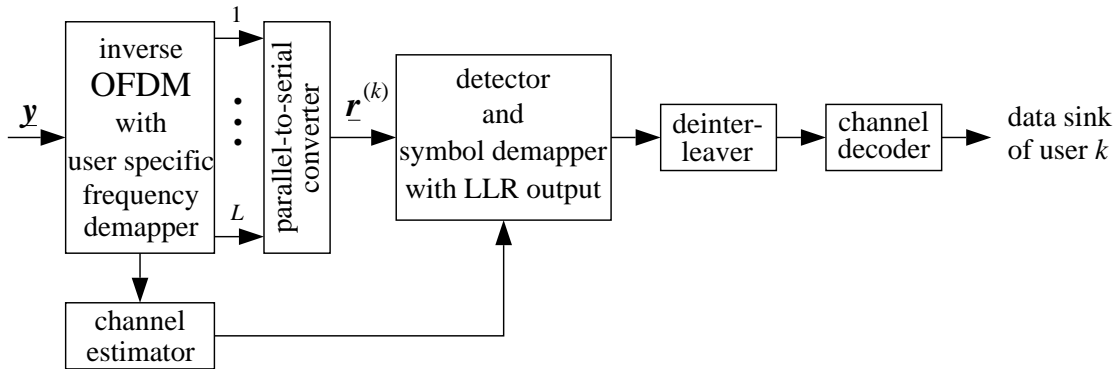


Figure B.3: SS-MC-MA receiver of the k th user

extraction of the pilot symbols from the symbols with user data, the MC demodulated vector

$$\underline{r}^{(k)} = \underline{H}^{(k)} \underline{s}^{(k)} + \underline{n}^{(k)} = (R_1^{(k)}, R_2^{(k)}, \dots, R_L^{(k)})^T \quad (\text{B.4})$$

with the data of the k th user is obtained, where the $L \times L$ diagonal matrix $\underline{H}^{(k)}$ and the vector $\underline{n}^{(k)}$ of length L describe the channel fading and noise, respectively, on the subcarriers exclusively used by the k th user.

Any of the SD or MD data detection techniques presented for MC-CDMA systems in Section 3.3 can be applied for the detection of the data of a single user per subsystem in SS-MC-MA systems. However, SS-MC-MA systems offer especially in the downlink the advantage that with JD in one estimation step simultaneously L data symbols of a single user are estimated. Compared to MC-CDMA systems, the complexity of JD per data symbol in SS-MC-MA systems reduces by a factor of L in the downlink. With JD, LLRs can inherently be obtained from the detection algorithm which may also include the symbol demapping, cf. Chapter 4. After deinterleaving and decoding of the LLRs, the detected source bits of the k th user are obtained.

B.2 Performance

In the following, the performance of an SS-MC-MA mobile radio system in the uplink is presented. Table B.1 shows the SS-MC-MA system parameters used in the uplink. These parameters are chosen such that they correspond as far as possible with the MC-CDMA system

Table B.1: Basic parameters of the proposed SS-MC-MA mobile radio system

bandwidth	$B = 2$ MHz
carrier frequency	$f_c = 1.8$ GHz
TDMA frame duration	$T_{\text{TDMA}} = 18.4$ ms
number of OFDM frames per TDMA frame	$N_{\text{fr}} = 4$
OFDM frame duration	$T_{\text{fr}} = 4.6$ ms
number of OFDM symbols per OFDM frame	$N_s = 31$
OFDM, inverse OFDM	256 point IFFT, 256 point FFT
OFDM symbol duration including guard interval	$T'_s = 148$ μ s
guard interval duration	$T_g = 20$ μ s
subcarrier spacing	$F_s = 7.8$ kHz
total number of subcarriers used per user	$N'_c = 8$
spreading code	Walsh Hadamard code
spreading code length	$L = 8$
data detector	MLSSE
data symbol mapping	QPSK with Gray encoding
channel code	convolutional code
code rate	$R = 1/2$
memory	$M_c = 6$
channel decoder	Viterbi decoder
code bit interleaver	pseudo random interleaver
code bit interleaver size	$I_c = 384$
channel estimator	1-D FIR filters
filter taps	$N_{\text{tap}} = 5$
Doppler filter bandwidth	$f_{\text{D,filter}} = 333.3$ Hz
pilot symbol distance in time	$N_t = 5$
maximum number of active users per OFDM frame	$K_{\text{max}} = 32$
user capacity	$K_{\text{sys}} = 128$
net bit rate per user	10.5 kbit/s $\leq R_b \leq 1.3$ Mbit/s
bandwidth efficiency	$\beta = 0.67$ bit/s/Hz

parameters for the downlink presented in Table 6.1. The SS-MC-MA system parameters described in the following differ from those of the MC-CDMA system presented in Chapter 6. The SS-MC-MA system transmits only on 256 subcarriers. Since the channel estimation in the considered SS-MC-MA system is based on a 1-D filtering in time direction which should fulfill two-times oversampling of the time-variant fading process, the overhead due to pilot symbols

can be reduced with decreasing OFDM symbol durations. However, it has to be taken into account that with decreasing OFDM symbol duration the loss in bandwidth efficiency due to the guard interval increases. The used TDMA frame structure consisting of 4 time slots. A time slot corresponds to an OFDM frame consisting of 31 OFDM symbols as illustrated in Fig. B.4. Each user exclusively transmits on 8 subcarriers, where 3 of the 8 subcarriers used by

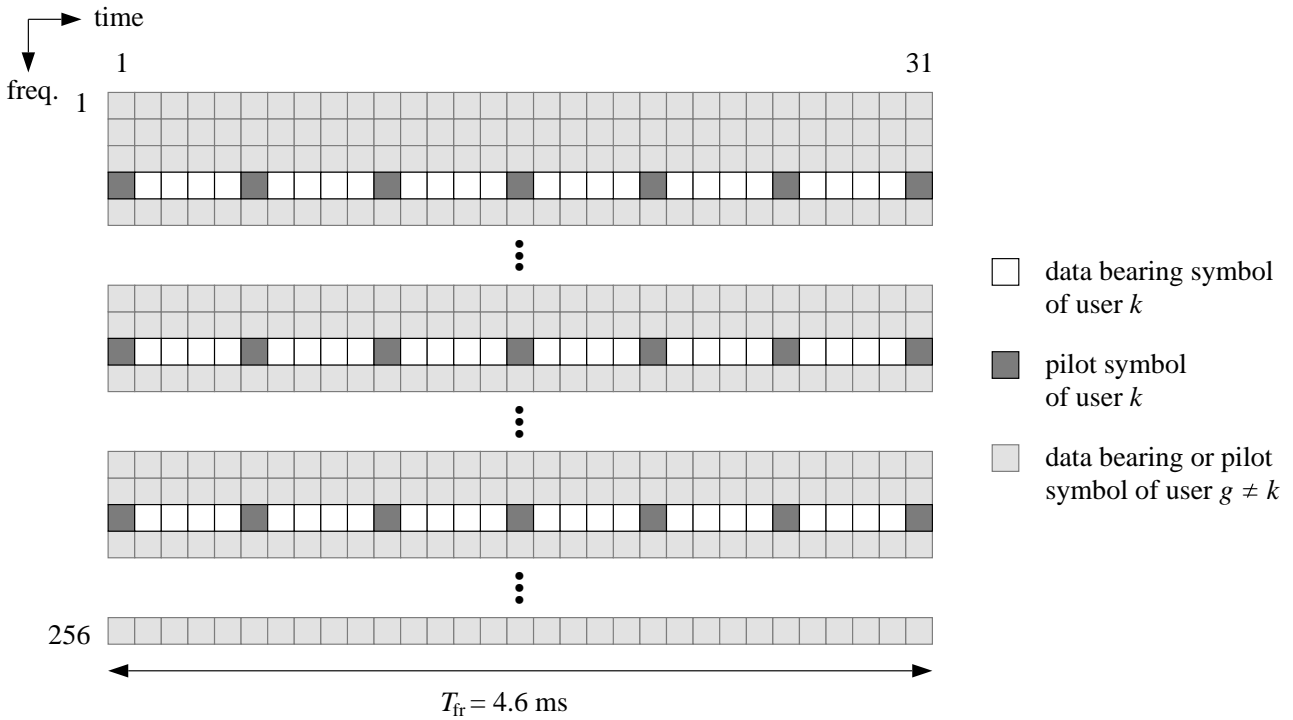


Figure B.4: OFDM frame of the proposed SS-MC-MA mobile radio system; $N_c = 256$; $N_s = 31$; $N_t = 5$; $N_{grid} = 1792$

the k th user are depicted. Hence, per user, a block of 8 serial data symbols is parallel converted and spread with orthogonal Walsh Hadamard codes of length L equal to 8, resulting after superposition in the transmission sequence $\mathbf{s}^{(k)}$, cf. (B.3). Note that in contrast to Fig. B.2, an additional interleaver is applied which scrambles 192 components of 24 transmission sequences $\mathbf{s}^{(k)}$ with the intention to increase the diversity potential of the system. Per OFDM symbol, 8 randomly interleaved components are mapped on 8 subcarriers exclusively used by the k th user. The 8 user specific subcarriers are distributed over the whole bandwidth. The receiver applies an MLSSE for data detection. The channel coding part is identical to that of the MC-CDMA system presented in Chapter 6.

For the uplink channel estimation, a simple 1-D filtering in time direction is used per subcarrier. The 1-D FIR filter is designed as 1-D Wiener filter for a rectangular Doppler power spectrum where $f_{D,filter} = 333.3$ Hz is chosen as worst case condition. The pilot symbol spacing in time direction N_t is chosen equal to 5 to two-times oversample the dynamics of the fading in time direction, given $f_{D,max} = 333.3$ Hz. The 1-D FIR filter is realized with 5 taps, which is a good compromise between performance and complexity [HKR97a].

The average coded BER P_b versus the SNR γ_b for the presented SS-MC-MA system in the uplink is shown in Fig. B.5. The COST 207 channel models, each with different velocities v of the MS, are considered. It should be noted that the performance of the SS-MC-MA system is independent of the number of active users due to the avoidance of MAI, i.e., the presented performance is valid for a fully loaded system and also for a system with only one active user. The total SNR loss due to the guard interval and the pilot symbols is 1.6 dB and is taken into

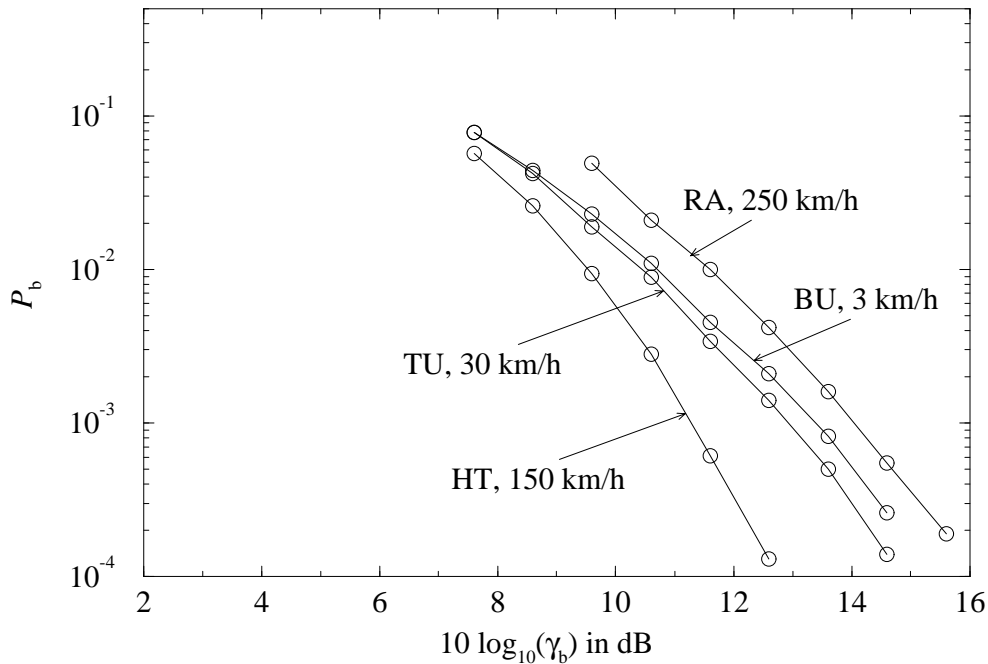


Figure B.5: Average coded BER P_b versus average SNR γ_b per bit for the SS-MC-MA system in the uplink; COST 207 channel models: different velocities v of the MS; MLSSE; 1-D channel estimation; $L = 8$; QPSK; $R = 1/2$

account in the results of Fig. B.5. It can be observed that even in a scenario with velocity of 250 km/h in a rural area, an SNR of 14 dB is sufficient to guarantee a BER P_b less than 10^{-3} . The proposed SS-MC-MA system achieves for the uplink the bandwidth efficiency of

$$\beta = 0.67 \text{ bit/s/Hz.} \quad (\text{B.5})$$

In the downlink, an SS-MC-MA system can achieve the same high bandwidth efficiency as the MC-CDMA system presented in Chapter 6, when also applying channel estimation in two dimensions. To fair compare the performance of the MC-CDMA system proposed in Chapter 6 with the performance of the SS-MC-MA system proposed in this section, the influence due to the different channel estimation concepts is avoided by comparing the performance under the assumption of perfect channel estimation. In Table B.2, the SNR γ_b degradation of the SS-MC-MA system compared to the MC-CDMA system is given for the four propagation scenarios under investigation at a BER P_b of 10^{-3} . The MC-CDMA system shows a significant performance improvement compared to the SS-MC-MA system in the propagation scenario BU,

Table B.2: SNR degradation of the presented SS-MC-MA mobile radio system compared to the MC-CDMA mobile radio system investigated in Chapter 6; perfect channel estimation

	BU	TU	HT	RA
	$v=3$ km/h	$v=30$ km/h	$v=150$ km/h	$v=250$ km/h
SNR degradation in dB	1.6	0.8	1.0	1.1

v equal to 3 km/h, which has less time diversity. As already mentioned, MC-CDMA systems can better exploit frequency diversity compared to SS-MC-MA systems. If the propagation scenario offers time diversity, the SNR degradation with the SS-MC-MA system compared to the MC-CDMA system is about 1 dB. For more details about the performance and flexibility of SS-MC-MA mobile radio systems, the reader is referred to [KaF97a, KaF97b].

It can be concluded that a promising future mobile radio system may use in the downlink the MC-CDMA system proposed in Chapter 6, and in the uplink the SS-MC-MA system proposed in this section. This combination achieves for both links a high bandwidth efficiency and great flexibility. Furthermore, in both links the same hardware can be used, only the user data have to be mapped differently.

Notations

Symbols

$a(f, t)$	magnitude of $H(f, t)$
$\arg \max_x y(x)$	value of x which maximizes the function $y(x)$
$a_{\kappa}^{(k)}$	κ th source bit of $\mathbf{a}^{(k)}$ of the k th user
$\hat{a}_{\kappa}^{(k)}$	hard decided value of $a_{\kappa}^{(k)}$
$a_{n,i}$	amplitude of $H_{n,i}$
a_p	amplitude of the p th path
a_{thresh}	threshold determining the controlled equalization
$\mathbf{a}^{(k)}$	source bit vector of the k th user
$\hat{\mathbf{a}}^{(k)}$	hard decided value of $\mathbf{a}^{(k)}$
$b^{(k)}$	code bit of the k th user
$b_{\kappa}^{(k)}$	κ th code bit of $\mathbf{b}^{(k)}$ of the k th user
$\hat{b}_{\kappa}^{(k)}$	hard decided value of $b_{\kappa}^{(k)}$
$\mathbf{b}^{(k)}$	code bit vector of the k th user
$\hat{\mathbf{b}}^{(k)}$	hard decided value of $\mathbf{b}^{(k)}$
B	bandwidth
c	speed of light
$\underline{\mathbf{c}}^{(k)}$	MC-CDMA spreading code vector of the k^{th} user
$\underline{C}_l^{(k)}$	l th chip of the MC-CDMA spreading code vector $\underline{\mathbf{c}}^{(k)}$
$\underline{\mathbf{C}}$	spreading code matrix
$\underline{d}^{(k)}$	data symbol of the k th user
$\underline{d}_{\kappa}^{(k)}$	κ th data symbol of $\underline{\mathbf{d}}^{(k)}$ of the k th user
$\hat{\underline{d}}^{(k)[j]}$	hard decided value with IC after j th iteration
$\hat{\underline{d}}^{(k)}$	hard decided value of $\underline{d}^{(k)}$
$\hat{\underline{d}}_{\kappa}^{(k)}$	hard decided value of $\underline{d}_{\kappa}^{(k)}$
$\underline{\mathbf{d}}$	data symbol vector representing the K_q data symbols $\underline{d}^{(k)}$
$\underline{\mathbf{d}}^{(k)}$	data symbol vector of the k th user
$\hat{\underline{\mathbf{d}}}$	hard decided value of $\underline{\mathbf{d}}$
$\hat{\underline{\mathbf{d}}}^{(k)}$	hard decided value of $\underline{\mathbf{d}}^{(k)}$
D	diversity
D_f	frequency diversity
D_t	time diversity

$E\{\cdot\}$	expectation
$Ei(\cdot)$	exponential integral
f	frequency
Δf	frequency difference
f_c	carrier frequency
f_D	Doppler frequency
$f_{D,\text{filter}}$	maximum Doppler frequency permitted in the filter design
$f_{D,\text{max}}$	maximum Doppler frequency
$f_{D,p}$	Doppler frequency of the p th path
f_n	n th subcarrier frequency
$(\Delta f)_c$	coherence bandwidth
F_s	subcarrier spacing
G_l	l th diagonal element of the equalizer matrix \mathbf{G}
\mathbf{G}	equalizer matrix
$\mathbf{G}^{[j]}$	equalizer matrix used for IC in the j th iteration
$\underline{h}(\tau)$	time-invariant channel impulse response
$\underline{h}(\tau, t)$	time-variant channel impulse response
$\underline{H}(f, t)$	time-variant channel transfer function
$\underline{H}_{n,i}$	discrete-time/-frequency time-variant channel transfer function
$\check{\underline{H}}_{n',i'}$	initial estimate of $\underline{H}_{n',i'}$ at pilot symbol positions
$\hat{\underline{H}}_{n,i}$	final estimate of $\underline{H}_{n,i}$
\underline{H}_l	l^{th} diagonal element of the channel matrix \mathbf{H}
\mathbf{H}	channel matrix
$I_0(\cdot)$	zero-order modified Bessel function of first kind
I_c	size of the bit interleaver
I_{TC}	size of the Turbo code interleaver
j	$\sqrt{-1}$
J	average mean square error
J_{it}	number of iterations in the multistage detector
J_l	mean square error of the equalizer used for SD
$J_{n,i}$	mean square error of the channel estimation
K	number of active users
K_{max}	maximum number of active users
K_q	number of active users of the q th user group
$K_{q,\text{max}}$	maximum number of active users of the q th user group
K_{Rice}	Rice factor
K_{sys}	user capacity
$\mathbf{l}^{(k)}$	log-likelihood ratios of $\mathbf{b}^{(k)}$
$\mathbf{l}_{\text{re}}^{(g)[j]}$	log-likelihood ratio vector representing the L_b log-likelihood ratios $\mathcal{L}_{\text{re}}^{(g)[j]}$
L	spreading code length
L_a	length of the source bit vector $\mathbf{a}^{(k)}$

L_b	length of the code bit vector $\mathbf{b}^{(k)}$
L_d	length of the data symbol vector $\underline{\mathbf{d}}^{(k)}$
L_g	length of guard interval
$\mathcal{L}^{(k)}$	log-likelihood ratio assigned to $b^{(k)}$
$\mathcal{L}_{re}^{(g)[j]}$	log-likelihood ratio ratios after re-encoding for soft IC, j th iteration
$\mathcal{L}_\kappa^{(k)}$	log-likelihood ratio assigned to $b_\kappa^{(k)}$
m	parameter of the Nakagami- m distribution
m_p	parameter of the Nakagami- m distribution assigned to the p th path
M	number of data symbols transmitted per user and OFDM symbol
M_c	memory of channel code
M_d	maximum number of different realizations of a data symbol $\underline{\mathbf{d}}^{(k)}$
M_s	maximum number of different realizations of a chip $C_l^{(k)}$
$\underline{\mathbf{n}}(t)$	additive noise signal
\mathbf{n}	noise vector
N_c	number of subcarriers
N_l	l th element of the noise vector \mathbf{n}
N_f	pilot symbol distance in frequency direction
N_{fr}	number of time slots per TDMA frame
N_{grid}	number pilot symbols per OFDM frame
N_p	number of path
N_s	number of OFDM symbols per OFDM frame
N_t	pilot symbol distance in time direction
N_{tap}	number of filter taps
N_w	number of waves assigned to one scatterer
$p(\cdot)$	probability density function
$P\{\cdot\}$	probability
P_b	average BER
\mathcal{P}	set of pilot positions in an OFDM frame
Q	number of user groups
$Q\{\cdot\}$	quantization operation
\mathbf{r}	received vector after inverse OFDM
$\mathbf{r}^{(k)}$	received vector of the k th user after inverse OFDM
R	code rate
$R(\tau_1, \tau_2, \Delta t)$	autocorrelation function of a WSS channel impulse response
R_b	bit rate
R_l	l th element of the received vector \mathbf{r}
$\underline{\mathbf{s}}$	source vector before OFDM
$\underline{\mathbf{s}}^{(k)}$	source vector of the k th user before OFDM
$\underline{\mathbf{s}}_m$	source vector containing the m th transmitted data symbol before OFDM
$\underline{\mathbf{s}}_q$	source vector of the q th user group before OFDM
$S(\tau, f_D)$	scattering function

$S_{f_D}(f_D)$	Doppler power density spectrum
$S_{f_D, \text{filter}}(f_D)$	Doppler power density spectrum used for filter design
\underline{s}_l	l th element of the vector \underline{s}
t	time
Δt	time difference
$(\Delta t)_c$	coherence time
T	source symbol duration
T_c	chip duration
T_d	data symbol duration
T_{fr}	OFDM frame duration
T_g	duration of guard interval
T_s	OFDM symbol duration without guard interval
T'_s	OFDM symbol duration with guard interval
T_{TDMA}	TDMA frame duration
$\mathcal{T}_{n,i}$	set of filter coefficients used for estimation of $\hat{H}_{n,i}$
\underline{u}	equalized vector
\underline{U}_l	l th element of the equalized vector \underline{u}
v	velocity
$\underline{v}^{(k)}$	soft decided value of $\underline{d}^{(k)}$
$\underline{v}_\kappa^{(k)}$	soft decided value of $\underline{d}_\kappa^{(k)}$
$\underline{\mathbf{v}}^{(k)}$	soft decided value of $\underline{\mathbf{d}}^{(k)}$
V_c	chip alphabet
V_d	data symbol alphabet
V_{guard}	loss in SNR due to the guard interval
V_{pilot}	loss in SNR due to the pilot symbols
$w^{(k)}$	soft decided value of $b^{(k)}$
$w_\kappa^{(k)}$	soft decided value of $b_\kappa^{(k)}$
$w_{\text{re}}^{(g)[j]}$	soft decided value after re-encoding for soft IC, j th iteration
$\mathbf{w}^{(k)}$	soft decided value of $\mathbf{b}^{(k)}$
$\mathbf{w}_{\text{re}}^{(g)[j]}$	soft decided value vector representing the L_b soft decided values $w_{\kappa, \text{re}}^{(g)[j]}$
$\underline{x}(t)$	transmitted signal
x_ν	ν th element of the transmitted vector $\underline{\mathbf{x}}$
$\underline{\mathbf{x}}$	transmitted vector
$\underline{X}(f)$	frequency spectrum of the transmitted signal $\underline{x}(t)$
$\underline{y}(t)$	received signal
y_ν	ν th element of the received vector $\underline{\mathbf{y}}$
$\underline{\mathbf{y}}$	received vector
α_p	angle of incidence of a wave assigned to the p th path
β	bandwidth efficiency
γ_b	average SNR per bit at the input of the data detector

γ_c	average SNR per subcarrier at the input of the data detector
γ_s	average SNR per data symbol at the input of the data detector
$\Gamma(\cdot)$	Gamma function
$\delta(t)$	Dirac delta function
δ_i	Kronecker delta
$\Delta^2(\cdot, \cdot)$	squared Euclidean distance
ε_l	error between transmitted and equalized element on the l th subcarrier
$\varepsilon_{n,i}$	estimation error of the channel estimation
$\zeta^{(g,k)}$	weighting factor of the MAI after detection
$\zeta'^{(g,k)}$	weighting factor of the MAI after symbol demapping
$\eta^{(k)}$	noise after detection
$\eta'^{(k)}$	noise after symbol demapping
$\theta(\Delta f)$	frequency correlation function
$\theta(\Delta t)$	time correlation function
$\theta_{i-i''}$	discrete time correlation function
$\theta_{n-n''}$	discrete frequency correlation function
$\theta_{n-n'',i-i''}$	crosscorrelation function
$\boldsymbol{\theta}_{n,i}$	crosscorrelation vector
$\varrho^{(k)}$	modified fading factor after detection
$\varrho'^{(k)}$	modified fading factor after symbol demapping
λ	parameter used for suboptimum MMSE equalization
Λ	overhead due to pilot symbols
ξ_l	parameter used for controlled equalization
$\rho(\tau)$	delay power density spectrum
$\rho(\tau, \Delta t)$	delay cross-power spectral density
$\rho_{\text{filter}}(\tau)$	delay power density spectrum used for the filter design
σ^2	variance of the noise
$\sigma_{a_{p,w}}^2$	variance of the wave amplitudes in the CODIT channel models
σ_{MAI}	variance of the MAI
σ_{noise}	variance of the noise after detection
σ_τ	delay spread
τ	delay
τ_{filter}	maximum delay permitted in the filter design
τ_{max}	maximum delay
$\bar{\tau}$	mean delay
τ_p	delay of the p th path
$\phi_{n'-n'',i'-i''}$	autocorrelation function
$\boldsymbol{\Phi}$	autocorrelation matrix
$\varphi_{n,i}$	phase offset of $H_{n,i}$
φ_p	phase offset of the p th path
$\omega_{n',i',n,i}$	filter coefficient

$\underline{\omega}_{n,i}$	filter coefficient vector
$\tilde{\omega}_{n,i}$	filter coefficient vector with model mismatch
Ω	average power
Ω_p	average power of the p th path
$(\cdot)^H$	Hermitian transposition of a vector or a matrix
$(\cdot)^T$	transposition of a vector or a matrix
$(\cdot)^{-1}$	inversion
$(\cdot)^*$	complex conjugation
$ \cdot $	absolute value
$\ \cdot\ $	norm of a vector
$\lceil x \rceil$	smallest integer larger or equal to x
∞	infinity

Abbreviations

AWGN	additive white Gaussian noise
BER	bit error rate
BPSK	binary phase shift keying
BS	base station
CDMA	code division multiple access
CODIT	Code Division Testbed
COST	European Cooperation in the Field of Scientific and Technical Research
DAB	Digital Audio Broadcasting
DFT	discrete Fourier transform
DS	direct sequence
DVB-T	terrestrial Digital Video Broadcasting
EGC	equal gain combining
FDMA	frequency division multiple access
FFT	fast Fourier transform
FH	frequency hopped
FIR	finite impulse response
FPLMTS	Future Public Land Mobile Telecommunications Systems
GSM	Global System for Mobile Communications
IC	interference cancellation
ICI	intersubchannel interference
IDFT	inverse discrete Fourier transform
IFFT	inverse fast Fourier transform

IMT-2000	International Mobile Telecommunications 2000
ISI	intersymbol interference
JD	joint detection
LLR	log-likelihood ratio
LOS	line of sight
MAI	multiple access interference
MAP	maximum a posteriori
MC	multi-carrier
MD	multi-user detection
MF	matched filter
ML	maximum likelihood
MLSE	maximum likelihood sequence estimation
MLSSE	maximum likelihood symbol-by-symbol estimation
MMSE	minimum mean square error
MRC	maximum ratio combining
MS	mobile station
MT	multi-tone
OFDM	orthogonal frequency division multiplexing
ORC	orthogonality restoring combining
QPSK	quaternary phase shift keying
RCPC code	rate compatible punctured convolutional code
SD	single-user detection
SNR	single-to-noise ratio
SORC	smooth orthogonality restoring combining
SOVA	soft output Viterbi algorithm
SS-MC-MA	spread spectrum multi-carrier multiple access
TDMA	time division multiple access
TH	time hopped
TORC	threshold orthogonality restoring combining
UMTS	Universal Mobile Telecommunications Systems
US	uncorrelated scattering
WSS	wide sense stationary
WSSUS	wide sense stationary uncorrelated scattering
ZF	zero-forcing

Bibliography

- [AbS64] M. Abramowitz and I. A. Stegun, *Handbook of Mathematical Functions*. New York: Dover Publications, 1964.
- [Ach85] D. Achilles, *Die Fourier-Transformation in der Signalverarbeitung*. Berlin: Springer, 1985.
- [Agh96] A. H. Aghvami, "Spread spectrum techniques & applications in Europe," in *Proceedings IEEE Fourth International Symposium on Spread Spectrum Techniques & Applications (ISSSTA '96)*, Mainz, Germany, p. 9, Sept. 1996.
- [AIL87] M. Alard and R. Lassalle, "Principles of modulation and channel coding for digital broadcasting for mobile receivers," *EBU Review*, Technical No. 224, pp. 47-69, Aug. 1987.
- [AuF96] V. Aue and G. P. Fettweis, "Multi-carrier spread spectrum modulation with reduced dynamic range," in *Proceedings IEEE Vehicular Technology Conference (VTC'96)*, Atlanta, USA, pp. 914-917, Apr./May 1996.
- [Bai94] P. W. Baier, "CDMA or TDMA? CDMA for GSM?," in *Proceedings IEEE International Symposium on Personal, Indoor and Mobile Radio Communications (PIMRC'94)*, The Hague, The Netherlands, pp. 1280-1284, Sept. 1994.
- [Bai96] P. W. Baier, "A critical review of CDMA," in *Proceedings IEEE Vehicular Technology Conference (VTC'96)*, Atlanta, USA, pp. 6-10, Apr./May 1996.
- [BBS97] P. W. Baier, J. J. Blanz, and R. Schmalenberger, "Fundamentals of smart antennas for mobile radio applications," in *Wireless Communications: TDMA versus CDMA*, S. G. Glisic and P. A. Leppänen (eds.), pp. 345-376. Boston: Kluwer Academic Publishers, 1997.
- [BCF96] P. Banelli, S. Cacopardi, F. Frescura, and G. Reali, "OM-DS-SS wireless LAN radio system: Performance in clipping environment using measured channel delay profiles," in *Proceedings IEEE Global Telecommunications Conference (GLOBECOM'96)*, London, UK, pp. 1897-1903, Nov. 1996.
- [Bel63] P. A. Bello, "Characterization of randomly time-variant linear channels," *IEEE Transactions on Communications Systems*, vol. 11, pp. 360-393, Dec. 1963.

- [BFG94] A. Baier, U.-C. Fiebig, W. Granzow, W. Koch, P. Teder, and J. Thielecke, "Design study for a CDMA-based third-generation mobile radio system," *IEEE Journal on Selected Areas in Communications*, vol. 12, pp. 733-743, May 1994.
- [BGP84] P. W. Baier, G. Grünberger, and M. Pandit, *Störunterdrückende Funkübertragungstechnik*. München: Oldenbourg, 1984.
- [BGT93] C. Berrou, A. Glavieux, and P. Thitimajshima, "Near Shannon limit error-correcting coding and decoding: Turbo-codes (1)," in *Proceedings IEEE International Conference on Communications (ICC'93)*, Geneva, Switzerland, pp. 1064-1070, May 1993.
- [Bin90] J. A. C. Bingham, "Multicarrier modulation for data transmission: An idea whose time has come," *IEEE Communications Magazine*, vol. 28, pp. 5-14, May 1990.
- [BJK96] P. W. Baier, P. Jung, and A. Klein, "Taking the challenge of multiple access for third-generation cellular mobile radio systems - a European view," *IEEE Communications Magazine*, vol. 34, pp. 82-89, Feb. 1996.
- [BJP97] F. Berens, P. Jung, J. Plechinger, and P. W. Baier, "Multicarrier joint detection CDMA mobile communications," in *Proceedings IEEE Vehicular Technology Conference (VTC'97)*, Phoenix, USA, pp. 1897-1901, May 1997.
- [BKN94] J. Blanz, A. Klein, M. Nasshan, and A. Steil, "Performance of a cellular hybrid C/TDMA mobile radio system applying joint detection and coherent receiver antenna diversity," *IEEE Journal on Selected Areas in Communications*, vol. 12, pp. 568-579, May 1994.
- [BrD91] W. R. Braun and U. Dersch, "A physical mobile radio channel model," *IEEE Transactions on Vehicular Technology*, vol. 40, pp. 472-482, May 1991.
- [CBJ93] A. Chouly, A. Brajal, and S. Jourdan, "Orthogonal multicarrier techniques applied to direct sequence spread spectrum CDMA systems," in *Proceedings IEEE Global Telecommunications Conference (GLOBECOM'93)*, Houston, USA, pp. 1723-1728, Nov./Dez. 1993.
- [CDE94] D. Cygan, F. David, H. J. Eul, J. Hoffmann, N. Metzner, and W. Mohr, "RACE-II advanced TDMA mobile access project - An approach for UMTS," in *Proceedings International Zurich Seminar on Digital Communications*, Zurich, Switzerland, pp. 428-439, Mar. 1994.
- [CFG95] S. Cacopardi, F. Frescura, F. Gatti, and G. Reali, "A frequency division duplex configuration for indoor wireless multicarrier DS-CDMA systems," in *Proceedings First European Personal and Mobile Communications Conference (EPMCC'95)*, Bologna, Italy, pp. 237-244, Nov. 1995.

- [CFR96] S. Cacopardi, F. Frescura, and G. Reali, "An orthogonal multicarrier DS-SS radio access scheme for wireless LAN," in *Proceedings IEEE Fourth International Symposium on Spread Spectrum Techniques & Applications (ISSSTA '96)*, Mainz, Germany, pp. 1325-1329, Sept. 1996.
- [Cha66] R. W. Chang, "Synthesis of band-limited orthogonal signals for multichannel data transmission," *Bell System Technical Journal*, vol. 45, pp. 1775-1796, Dec. 1966.
- [Cim85] L. J. Cimini, "Analysis and simulation of a digital mobile channel using orthogonal frequency division multiplexing," *IEEE Transactions on Communications*, vol. 33, pp. 665-675, July 1985.
- [CIM94] F. Classen and H. Meyr, "Synchronization algorithms for an OFDM system for mobile communication," in *Proceedings ITG Conference on Source and Channel Coding*, Munich, Germany, pp. 105-113, Oct. 1994.
- [COD95] CODIT, *Final Propagation Model*. Report R2020/TDE/PS/DS/P/040/b1, 1994.
- [COS89] COST 207, *Digital Land Mobile Radio Communications*. Final Report, Luxembourg: Office for Official Publications of the European Communities, 1989.
- [CSM95] F. Classen, M. Speth, and H. Meyr, "Channel estimation units for an OFDM system suitable for mobile communication," in *Proceedings ITG Conference on Mobile Radio*, Neu-Ulm, Germany, Sept. 1995.
- [CSP95a] Q. Chen, E. S. Sousa, and S. Pasupathy, "Performance of a coded multi-carrier DS-CDMA system in multi-path fading channels," *Wireless Personal Communications*, vol. 2, pp. 167-183, 1995.
- [CSP95b] Q. Chen, E. S. Sousa, and S. Pasupathy, "Multi-carrier DS-CDMA with adaptive sub-carrier hopping for fading channels," in *Proceedings IEEE International Symposium on Personal, Indoor and Mobile Radio Communications (PIMRC'95)*, Toronto, Canada, pp. 76-80, Sept. 1995.
- [DaS93] V. DaSilva and E. S. Sousa, "Performance of orthogonal CDMA codes for quasi-synchronous communication systems," in *Proceedings IEEE International Conference on Universal Personal Communications (ICUPC'93)*, Ottawa, Canada, pp. 995-999, Oct. 1993.
- [DaS94] V. DaSilva and E. S. Sousa, "Multicarrier orthogonal CDMA signals for quasi-synchronous communication systems," *IEEE Journal on Selected Areas in Communications*, vol. 12, pp. 842-852, June 1994.
- [DeK97] A. Dekorsy and K.-D. Kammeyer, "M-ary orthogonal modulation for MC-CDMA systems in indoor wireless radio networks," in *Proceedings First International Workshop on Multi-Carrier Spread-Spectrum*, Oberpfaffenhofen, Germany, pp. 69-76, Apr. 1997.

- [DHM57] M. L. Doelz, E. T. Heald, and D. L. Martin, "Binary data transmission techniques for linear systems," *Proceedings of the IRE*, vol. 45, pp. 656-661, May 1957.
- [DiS88] D. Divsalar and M. K. Simon, "The design of trellis coded MPSK for fading channels: Performance criteria," *IEEE Transactions on Communications*, vol. 36, pp. 1004-1012, Sept. 1988.
- [Dix94] R. C. Dixon, *Spread Spectrum Systems with Commercial Applications*. New York: John Wiley & Sons, 1994.
- [FaP93] K. Fazel and L. Papke, "On the performance of convolutionally-coded CDMA/OFDM for mobile communication system," in *Proceedings IEEE International Symposium on Personal, Indoor and Mobile Radio Communications (PIMRC'93)*, Yokohama, Japan, pp. 468-472, Sept. 1993.
- [Faz93] K. Fazel, "Performance of CDMA/OFDM for mobile communication system," in *Proceedings IEEE International Conference on Universal Personal Communications (ICUPC'93)*, Ottawa, Canada, pp. 975-979, Oct. 1993.
- [FBA94] G. Fettweis, A. S. Bahai, and K. Anvari, "On multi-carrier code division multiple access (MC-CDMA) modem design," in *Proceedings IEEE Vehicular Technology Conference (VTC'94)*, Stockholm, Sweden, pp. 1670-1674, June 1994.
- [FKR95] K. Fazel, S. Kaiser, P. Robertson, and M. J. Ruf, "A concept of digital terrestrial television broadcasting," *Wireless Personal Communications*, vol. 2, pp. 9-27, 1995.
- [FKR96] K. Fazel, S. Kaiser, and P. Robertson, "OFDM: A key component for terrestrial broadcasting and cellular mobile radio," in *Proceedings International Conference on Telecommunications (ICT'96)*, Istanbul, Turkey, pp. 576-583, Apr. 1996.
- [FKS95] K. Fazel, S. Kaiser, and M. Schnell, "A flexible and high performance cellular mobile communications system based on orthogonal multi-carrier SSMA," *Wireless Personal Communications*, vol. 2, pp. 121-144, 1995.
- [FIL96] B. H. Fleury and P. E. Leuthold, "Radiowave propagation in mobile communications: An overview of European research," *IEEE Communications Magazine*, vol. 34, pp. 70-81, Feb. 1996.
- [For73] G. D. Forney, "The Viterbi algorithm," *Proceedings of the IEEE*, vol. 61, pp. 268-278, Mar. 1973.
- [Hag88] J. Hagenauer, "Rate-compatible punctured convolutional codes (RCPC codes) and their applications," *IEEE Transactions on Communications*, vol. 36, pp. 389-400, Apr. 1988.
- [Hag95] J. Hagenauer, "Source-controlled channel decoding," *IEEE Transactions on Communications*, vol. 43, pp. 2449-2457, Sept. 1995.

- [Hag96] J. Hagenauer, "Forward error correcting for CDMA systems," in *Proceedings IEEE Fourth International Symposium on Spread Spectrum Techniques & Applications (ISSSTA '96)*, Mainz, Germany, pp. 566-569, Sept. 1996.
- [HaH89] J. Hagenauer and P. Höher, "A Viterbi algorithm with soft-decision outputs and its applications," in *Proceedings IEEE Global Telecommunications Conference (GLOBECOM'89)*, Dallas, USA, pp. 1680-1686, Nov. 1989.
- [HaP96] S. Hara and R. Prasad, "DS-CDMA, MC-CDMA and MT-CDMA for mobile multimedia communications," in *Proceedings IEEE Vehicular Technology Conference (VTC'96)*, Atlanta, USA, pp. 1106-1110, Apr./May 1996.
- [Hay86] S. Haykin, *Adaptive Filter Theory*. Englewood Cliffs, NJ: Prentice-Hall, 1986.
- [Hir81] B. Hirosaki, "An orthogonally multiplexed QAM system using the discrete Fourier transform," *IEEE Transactions on Communications*, vol. 29, pp. 982-989, July 1981.
- [HKR97a] P. Höher, S. Kaiser, and P. Robertson, "Two-dimensional pilot-symbol-aided channel estimation by Wiener filtering," in *Proceedings IEEE International Conference on Acoustics, Speech and Signal Processing (ICASSP'97)*, Munich, Germany, pp. 1845-1848, Apr. 1997.
- [HKR97b] P. Höher, S. Kaiser, and P. Robertson, "Pilot-symbol-aided channel estimation in time and frequency," in *Proceedings IEEE Global Telecommunications Conference (GLOBECOM'97), Communication Theory Mini-Conference*, Phoenix, USA, pp. 90-96, Nov. 1997.
- [HLP95] S. Hara, T.-H. Lee, and R. Prasad, "BER comparison of DS-CDMA and MC-CDMA for frequency selective fading channels," in *Proceedings 7th Tyrrhenian International Workshop on Digital Communications*, Viareggio, Italy, pp. 3-14, Sept. 1995.
- [Höh91] P. Höher, "TCM on frequency-selective land-mobile fading channels," in *Proceedings 5th Tirrenia International Workshop on Digital Communications*, Tirrenia, Italy, pp. 317-328, Sept. 1991.
- [Höh92] P. Höher, "A statistical discrete-time model for the WSSUS multipath channel," *IEEE Transactions on Vehicular Technology*, vol. 41, pp. 461-468, Nov. 1992.
- [HOP96] J. Hagenauer, E. Offer, and L. Papke, "Iterative decoding of binary block and convolutional codes," *IEEE Transactions on Information Theory*, vol. 42, pp. 429-445, Mar. 1996.
- [HRP94] J. Hagenauer, R. Robertson, and L. Papke, "Iterative ("turbo") decoding of systematic convolutional codes with the MAP and SOVA algorithms," in *Proceedings ITG Conference on Source and Channel Coding*, Munich, Germany, pp. 21-29, Oct. 1994.

- [Jak74] W. C. Jakes, *Microwave Mobile Communications*. New York: John Wiley & Sons, 1974.
- [JBB97] P. Jung, F. Berens, J. Blanz, and J. Plechinger, "Performance of multicarrier joint detection CDMA mobile communications systems," in *Proceedings IEEE Vehicular Technology Conference (VTC'97)*, Phoenix, USA, pp. 1892-1896, May 1997.
- [JBP96a] P. Jung, F. Berens, and J. Plechinger, "Joint detection for multicarrier CDMA mobile radio systems - Part I: System model," in *Proceedings IEEE Fourth International Symposium on Spread Spectrum Techniques & Applications (ISSSTA'96)*, Mainz, Germany, pp. 991-995, Sept. 1996.
- [JBP96b] P. Jung, F. Berens, and J. Plechinger, "Joint detection for multicarrier CDMA mobile radio systems - Part II: Detection techniques," in *Proceedings IEEE Fourth International Symposium on Spread Spectrum Techniques & Applications (ISSSTA'96)*, Mainz, Germany, pp. 996-1000, Sept. 1996.
- [JBS93] P. Jung, P. W. Baier, and A. Steil, "Advantages of CDMA and spread spectrum techniques over FDMA and TDMA in cellular mobile radio applications," *IEEE Transactions on Vehicular Technology*, vol. 42, pp. 357-364, Aug. 1993.
- [JuB95] P. Jung and J. Blanz, "Joint detection with coherent receiver antenna diversity in CDMA mobile radio systems," *IEEE Transactions on Vehicular Technology*, vol. 44, pp. 76-88, Feb. 1995.
- [Jun95] P. Jung, *Digitale zellulare Mobilkommunikation, Grundlagen und Beispiele*. Thesis for the certificate of habilitation, University of Kaiserslautern, Kaiserslautern, Sept. 1995.
- [KaF96] S. Kaiser and K. Fazel, "Verfahren zur gleichzeitigen Funkübertragung digitaler Daten zwischen mehreren Teilnehmerstationen und einer Basisstation," *German Patent Application 196 47 833.2*, Nov. 1996.
- [KaF97a] S. Kaiser and K. Fazel, "A spread-spectrum multi-carrier multiple-access system for mobile communications," in *Proceedings First International Workshop on Multi-Carrier Spread-Spectrum*, Oberpfaffenhofen, Germany, pp. 49-56, Apr. 1997.
- [KaF97b] S. Kaiser and K. Fazel, "A flexible spread-spectrum multi-carrier multiple-access system for multi-media applications," in *Proceedings IEEE International Symposium on Personal, Indoor and Mobile Radio Communications (PIMRC'97)*, Helsinki, Finland, pp. 100-104, Sept. 1997.
- [KaH97a] S. Kaiser and P. Höher, "Performance of multi-carrier CDMA systems with channel estimation in two dimensions," in *Proceedings IEEE International Symposium on Personal, Indoor and Mobile Radio Communications (PIMRC'97)*, Helsinki, Finland, pp. 115-119, Sept. 1997.

- [KaH97b] S. Kaiser and J. Hagenauer, "Multi-carrier CDMA with iterative decoding and soft-interference cancellation," in *Proceedings IEEE Global Telecommunications Conference (GLOBECOM'97)*, Phoenix, USA, pp. 6-10, Nov. 1997.
- [Kai95a] S. Kaiser, "OFDM-CDMA versus DS-CDMA: Performance evaluation for fading channels," in *Proceedings IEEE International Conference on Communications (ICC'95)*, Seattle, USA, pp. 1722-1726, June 1995.
- [Kai95b] S. Kaiser, "On the performance of different detection techniques for OFDM-CDMA in fading channels," in *Proceedings IEEE Global Telecommunications Conference (GLOBECOM'95)*, Singapore, pp. 2059-2063, Nov. 1995.
- [Kai95c] S. Kaiser, "Analytical performance evaluation of OFDM-CDMA mobile radio systems," in *Proceedings First European Personal and Mobile Communications Conference (EPMCC'95)*, Bologna, Italy, pp. 215-220, Nov. 1995.
- [Kai96] S. Kaiser, "Trade-off between channel coding and spreading in multi-carrier CDMA systems," in *Proceedings IEEE Fourth International Symposium on Spread Spectrum Techniques & Applications (ISSSTA'96)*, Mainz, Germany, pp. 1366-1370, Sept. 1996.
- [KaP96a] S. Kaiser and L. Papke, "Optimal detection when combining OFDM-CDMA with convolutional and Turbo channel coding," in *Proceedings IEEE International Conference on Communications (ICC'96)*, Dallas, USA, pp. 343-348, June 1996.
- [KaP96b] D.N. Kalofonos and J.G. Proakis, "Performance of the multi-stage detector for a MC-CDMA system in a Rayleigh fading channel," in *Proceedings IEEE Global Telecommunications Conference (GLOBECOM'96)*, London, UK, pp. 1784-1788, Nov. 1996.
- [KKB94] A. Klein, G.K. Kaleh, and P.W. Baier, "Equalizers for multi-user detection in code division multiple access mobile radio systems," in *Proceedings IEEE Vehicular Technology Conference (VTC'94)*, Stockholm, Sweden, pp. 762-766, June 1994.
- [KIB93] A. Klein and P.W. Baier, "Linear unbiased data estimation in mobile radio systems applying CDMA," *IEEE Journal on Selected Areas in Communications*, vol. 11, pp. 1058-1066, Sept. 1993.
- [Kle96] A. Klein, *Multi-user detection of CDMA signals - algorithms and their application to cellular mobile radio*. Düsseldorf: VDI-Verlag, Fortschrittberichte VDI, series 10, no. 423, 1996.
- [KoM93] S. Kondo and L.B. Milstein, "On the use of multicarrier direct sequence spread spectrum systems," in *Proceedings IEEE Military Communications Conference (MILCOM'93)*, Boston, USA, pp. 52-56, Oct. 1993.

- [KoM96] S. Kondo and L. B. Milstein, "Performance of multicarrier DS CDMA systems," *IEEE Transactions on Communications*, vol. 44, pp. 238-246, Feb. 1996.
- [Lee93] W. C. Y. Lee, *Mobile Communications Design Fundamentals*. New York: John Wiley & Sons, 1993.
- [LiC83] S. Lin and D. J. Costello, Jr., *Error Control Coding: Fundamentals and Applications*. Englewood Cliffs: Prentice-Hall, 1983.
- [MaO96] J. J. Maxey and R. F. Ormondroyd, "Low-rate orthogonal convolutional coded DS-CDMA using non-coherent multi-carrier modulation over the AWGN and Rayleigh faded channel," in *Proceedings IEEE Fourth International Symposium on Spread Spectrum Techniques & Applications (ISSSTA'96)*, Mainz, Germany, pp. 575-579, Sept. 1996.
- [MaO97a] J. J. Maxey and R. F. Ormondroyd, "Multi-carrier CDMA using convolutional coding and interference cancellation over fading channels," in *Proceedings First International Workshop on Multi-Carrier Spread-Spectrum*, Oberpfaffenhofen, Germany, pp. 89-96, Apr. 1997.
- [MaO97b] J. J. Maxey and R. F. Ormondroyd, "Non-coherent differential encoded multi-carrier SS modulation schemes using low-rate orthogonal convolutional coding in frequency selective Rayleigh fading," in *Proceedings IEEE Vehicular Technology Conference (VTC'97)*, Phoenix, USA, pp. 2045-2046, May 1997.
- [MBR96] T. Müller, K. Brüninghaus, and H. Rohling, "Performance of coherent OFDM-CDMA for broadband mobile communications," *Wireless Personal Communications*, vol. 2, pp. 295-305, 1996.
- [MMB91] R. G. McKay, P. J. McLane, and E. Biglieri, "Error bounds for trellis-coded MPSK on a fading mobile satellite channel," *IEEE Transactions on Communications*, vol. 39, pp. 1750-1761, Dec. 1991.
- [MRG95] T. Müller, H. Rohling, and R. Grünheid, "Comparison of different detection algorithms for OFDM-CDMA in broadband Rayleigh fading," in *Proceedings IEEE Vehicular Technology Conference (VTC'95)*, Chicago, USA, pp. 835-838, July 1995.
- [NaF97] A. Nahler and G.P. Fettweis, "An approach for a multi-carrier spread spectrum system with RAKE receiver," in *Proceedings First International Workshop on Multi-Carrier Spread-Spectrum*, Oberpfaffenhofen, Germany, pp. 97-104, Apr. 1997.
- [Nak60] M. Nakagami, "The m-distribution - A general formula of intensity distribution of rapid fading," in *Statistical Methods of Radio Wave Propagation*, W. C. Hoffman (ed.), pp. 3-36. New York: Pergamon Press, 1960.

- [NaS96] S. Nahm and W. Sung, "Time-domain equalization of the orthogonal multi-carrier CDMA system," in *Proceedings IEEE Global Telecommunications Conference (GLOBECOM'96)*, London, UK, pp. 1583-1587, Nov. 1996.
- [OrM97] R. F. Ormondroyd and J. J. Maxey, "Comparison of time guard-band and coding strategies for OFDM digital cellular radio in multipath fading," in *Proceedings IEEE Vehicular Technology Conference (VTC'97)*, Phoenix, USA, pp. 850-854, May 1997.
- [Pap91] A. Papoulis, *Probability, Random Variables, and Stochastic Processes*. New York: McGraw-Hill, 1991.
- [Par92] D. Parsons, *The Mobile Radio Propagation Channel*. London: Pentech Press, 1992.
- [PGH95] J. E. Padgett, C. G. Günther, and T. Hattori, "Overview of wireless personal communications," *IEEE Communications Magazine*, vol. 33, pp. 28-41, Jan. 1995.
- [Pra96] R. Prasad, *CDMA for Wireless Personal Communications*. Boston: Artech House, 1996.
- [PoM95] T. Pollet and M. Moeneclaey, "Synchronizability of OFDM signals," in *Proceedings IEEE Global Telecommunications Conference (GLOBECOM'95)*, Singapore, pp. 2054-2058, Nov. 1995.
- [PrH96] R. Prasad and S. Hara, "An overview of multi-carrier CDMA," in *Proceedings IEEE Fourth International Symposium on Spread Spectrum Techniques & Applications (ISSSTA '96)*, Mainz, Germany, pp. 107-114, Sept. 1996.
- [PrM96] J. G. Proakis and D. G. Manolakis, *Digital Signal Processing: Principles, Algorithms, and Applications*. Upper Saddle River: Prentice-Hall, 1996.
- [Pro95] J. G. Proakis, *Digital Communications*. New York: McGraw-Hill, 1995.
- [Rap96] T. S. Rappaport, *Wireless Communications: Principles & Practice*. Upper Saddle River: Prentice-Hall, 1996.
- [ReR94] C. Reiners and H. Rohling, "Multicarrier transmission techniques in cellular mobile communications systems," in *Proceedings IEEE Vehicular Technology Conference (VTC'94)*, Stockholm, Sweden, pp. 1645-1649, June 1994.
- [RoB96] H. Rohling and K. Brüninghaus, "Performance of an ORC-based detection scheme for multi-carrier CDMA," in *Proceedings International Conference on Telecommunications (ICT'96)*, Istanbul, Turkey, pp. 572-575, Apr. 1996.
- [Rob97] P. Robertson, "Close-to-optimal one-shot frequency synchronization for OFDM using pilot carriers," in *Proceedings IEEE Global Telecommunications Conference (GLOBECOM'97), Communication Theory Mini-Conference*, Phoenix, USA, pp. 97-102, Nov. 1997.

- [RoG96a] H. Rohling and R. Grünheid, "OFDM transmission technique with flexible sub-carrier allocation," in *Proceedings International Conference on Telecommunications (ICT'96)*, Istanbul, Turkey, pp. 567-571, Apr. 1996.
- [RoG96b] H. Rohling and R. Grünheid, "Performance of an OFDM-TDMA mobile communication system," in *Proceedings IEEE Vehicular Technology Conference (VTC'96)*, Atlanta, USA, pp. 1589-1593, Apr./May 1996.
- [RoG97] H. Rohling and R. Grünheid, "Performance comparison of different multiple access schemes for the downlink of an OFDM communication system," in *Proceedings IEEE Vehicular Technology Conference (VTC'97)*, Phoenix, USA, pp. 1365-1369, May 1997.
- [RoK95] P. Robertson and S. Kaiser, "Analysis of the effects of phase-noise in orthogonal frequency division multiplex (OFDM) systems," in *Proceedings IEEE International Conference on Communications (ICC'95)*, Seattle, USA, pp. 1652-1657, June 1995.
- [Rup93] W. Rupperecht, *Signale und Übertragungssysteme*. Berlin: Springer, 1993.
- [RyG63] I. M. Ryshik and I. S. Gradstein, *Tables of Series, Products, and Integrals*. Berlin: VEB Deutscher Verlag der Wissenschaften, 1963.
- [Sal67] B. R. Saltzberg, "Performance of an efficient parallel data transmission system," *IEEE Transactions on Communication Technology*, vol. 15, pp. 805-811, Dec. 1967.
- [San96] M. Sandell, *Design and Analysis of Estimators for Multicarrier Modulation and Ultrasonic Imaging*. Ph.D. Thesis, Luleå University of Technology, Luleå, Sweden, 1996.
- [Sch82] R. A. Scholtz, "The origins of spread-spectrum communications," *IEEE Transactions on Communications*, vol. 30, pp. 822-854, May 1982.
- [Sch89] H. Schulze, "Stochastische Modelle und digitale Simulation von Mobilfunkkanälen," *Kleinheubacher Berichte*, vol. 32, pp. 473-483, 1989.
- [ScK96] M. Schnell and S. Kaiser, "Diversity considerations for MC-CDMA systems in mobile communications," in *Proceedings IEEE Fourth International Symposium on Spread Spectrum Techniques & Applications (ISSSTA'96)*, Mainz, Germany, pp. 131-135, Sept. 1996.
- [Sk197a] B. Sklar, "Rayleigh fading channels in mobile digital communication systems Part I: Characterization," *IEEE Communications Magazine*, vol. 35, pp. 90-100, July 1997.
- [SoN94] E. A. Sourour and M. Nakagawa, "Performance of orthogonal multi-carrier CDMA in nonfading and nonselective fading channels," in *Proceedings IEEE Fourth International Symposium on Spread Spectrum Techniques & Applications (ISSSTA'94)*, Oulu, Finland, pp. 203-207, July 1994.

- [SoN96] E. A. Sourour and M. Nakagawa, "Performance of orthogonal multi-carrier CDMA in a multipath fading channel," *IEEE Transactions on Communications*, vol. 44, pp. 356-367, Mar. 1996.
- [SOS94] M. K. Simon, J. K. Omura, R. A. Scholz, and B. K. Lavitt, *Spread Spectrum Communications Handbook*. New York: McGraw-Hill, 1994.
- [SSR95] M. Schilpp, W. Sauer-Greff, W. Rupprecht, and E. Bogenfeld, "Influence of oscillator phase noise and clipping on OFDM for terrestrial broadcasting of digital HDTV," in *Proceedings IEEE International Conference on Communications (ICC'95)*, Seattle, USA, pp. 1678-1682, June 1995.
- [Ste94] R. Steele, *Mobile Radio Communications*. London: Pentech Press, 1994.
- [Ste96] A. Steil, *Spektrale Effizienz digitaler zellularer CDMA-Mobilfunksysteme mit gemeinsamer Detektion*. Düsseldorf: VDI-Verlag, Fortschrittberichte VDI, series 10, no. 437, 1996.
- [Ste97a] B. Steiner, "Time domain uplink channel estimation in multicarrier-CDMA mobile radio system concepts," in *Proceedings First International Workshop on Multi-Carrier Spread-Spectrum*, Oberpfaffenhofen, Germany, pp. 153-160, Apr. 1997.
- [Ste97b] B. Steiner, "Uplink performance of a multicarrier-CDMA mobile radio system concept," in *Proceedings IEEE Vehicular Technology Conference (VTC'97)*, Phoenix, USA, pp. 1902-1906, May 1997.
- [StM97] H. Steendam and M. Moeneclaey, "Sensitivity of OFDM/CDMA to carrier phase jitter," in *Proceedings First International Workshop on Multi-Carrier Spread-Spectrum*, Oberpfaffenhofen, Germany, pp. 145-152, Apr. 1997.
- [StP97a] R. A. Stirling-Gallacher and G. J. R. Povey, "Different channel coding strategies for OFDM-CDMA," in *Proceedings IEEE Vehicular Technology Conference (VTC'97)*, Phoenix, USA, pp. 845-849, May 1997.
- [StP97b] R. A. Stirling-Gallacher and G. J. R. Povey, "Performance of a OFDM-CDMA system with orthogonal convolutional coding and interference cancellation," in *Proceedings IEEE Vehicular Technology Conference (VTC'97)*, Phoenix, USA, pp. 860-864, May 1997.
- [Stü96] G. L. Stüber, *Principles of Mobile Communications*. Boston: Kluwer Academic Publishers, 1996.
- [TCC97] A. Toskala, J. Castro, L. Chalard, S. Hämmäläinen, and K. Kalliojärvi, "Cellular OFDM/CDMA downlink performance in the link and system levels," in *Proceedings IEEE Vehicular Technology Conference (VTC'97)*, Phoenix, USA, pp. 855-859, May 1997.

- [TER97] W. G. Teich, J. Egle, M. Reinhardt, and J. Lindner, "Detection method for MC-CDMA based on a recurrent neural network structure," in *Proceedings First International Workshop on Multi-Carrier Spread-Spectrum*, Oberpfaffenhofen, Germany, pp. 135-142, Apr. 1997.
- [ToK96a] L. Tomba and W. A. Krzymien, "Effect of carrier phase noise and frequency offset on the performance of multicarrier CDMA systems," in *Proceedings IEEE International Conference on Communications (ICC'96)*, Dallas, USA, pp. 1513-1517, June 1996.
- [ToK96b] L. Tomba and W. A. Krzymien, "Performance enhancement of multicarrier CDMA systems impaired by chip timing jitter," in *Proceedings IEEE Fourth International Symposium on Spread Spectrum Techniques & Applications (ISSSTA'96)*, Mainz, Germany, pp. 136-140, Sept. 1996.
- [ToK96c] L. Tomba and W. A. Krzymien, "Downlink detection schemes for MC-CDMA systems in indoor environments," *IEICE Transactions on Communications*, vol. E79-B, pp. 1351-1360, Sept. 1996.
- [VaA90] M. K. Varanasi and B. Aazhang, "Multistage detection in asynchronous code-division multiple-access communications," *IEEE Transactions on Communications*, vol. 38, pp. 509-519, Apr. 1990.
- [Van93] L. Vandendorpe, "Multitone direct sequence CDMA system in an indoor wireless environment," in *Proceedings IEEE First Symposium of Communications and Vehicular Technology*, Delft, The Netherlands, pp. 4.1.1-4.1.8, Oct. 1993.
- [Van95] L. Vandendorpe, "Multitone spread spectrum multiple access communications systems in a multipath Rician fading channel," *IEEE Transactions on Vehicular Technology*, vol. 44, pp. 327-337, May 1995.
- [Van97] L. Vandendorpe, "Overview of the results about multitone CDMA detection," in *Proceedings First International Workshop on Multi-Carrier Spread-Spectrum*, Oberpfaffenhofen, Germany, pp. 13-21, Apr. 1997.
- [ViF95] E. Viterbo and K. Fazel, "How to combat long echoes in OFDM transmission schemes: Sub-channel equalization or more powerful channel coding," in *Proceedings IEEE Global Telecommunications Conference (GLOBECOM'95)*, Singapore, pp. 2069-2074, Nov. 1995.
- [ViO79] A. J. Viterbi and J. K. Omura, *Principles of Digital Communication and Coding*. New York: McGraw-Hill, 1979.
- [Vit90] A. J. Viterbi, "Very low rate convolutional codes for maximum theoretical performance of spread-spectrum multiple-access channels," *IEEE Journal on Selected Areas in Communications*, vol. 8, pp. 641-649, May 1990.

- [Vit95] A. J. Viterbi, *CDMA Principles of Spread Spectrum Communication*. Reading: Addison-Wesley, 1995.
- [WeE71] S.B. Weinstein and P.M. Ebert, "Data transmission by frequency-division multiplexing using the discrete Fourier transform," *IEEE Transactions on Communication Technology*, vol. 19, pp. 628-634, Oct. 1971.
- [YeL94a] N. Yee and J.-P. Linnarz, "Controlled equalization of multi-carrier CDMA in an indoor Rician fading channel," in *Proceedings IEEE Vehicular Technology Conference (VTC'94)*, Stockholm, Sweden, pp. 1665-1669, June 1994.
- [YeL94b] N. Yee and J.-P. Linnarz, "Wiener filtering of multi-carrier CDMA in Rayleigh fading channel," in *Proceedings IEEE International Symposium on Personal, Indoor and Mobile Radio Communications (PIMRC'94)*, The Hague, The Netherlands, pp. 1344-1347, Sept. 1994.
- [YLF93] N. Yee, J.-P. Linnarz, and G. Fettweis, "Multi-carrier CDMA in indoor wireless radio networks," in *Proceedings IEEE International Symposium on Personal, Indoor and Mobile Radio Communications (PIMRC'93)*, Yokohama, Japan, pp. 109-113, Sept. 1993.